NEW GENERATION ADSORBENTS FOR GAS SEPARATION: FROM MODELING TO INDUSTRIAL APPLICATION

Authored by

DANIEL BAHAMÓN GARCÍA

A dissertation submitted in partial fulfillment of the requirements for the degree of

DOCTOR OF PHILOSOPHY

PRESENTED TO

Universitat Autònoma de Barcelona

PhD Program in Environmental Science and Technology

DIRECTOR: Dr. Lourdes F. Vega

Bellaterra   September 2015

Dr. Lourdes Vega Fernández,

CERTIFIES THAT:

Daniel Bahamón García, Bachelor in Chemical Engineering and MSc in Engineering from the "Universidad Pontificia Bolivariana", Colombia, has undertaken this thesis entitled "New generation adsorbents for gas separation: from modeling to industry application" under her direction, and the main results are presented in this memory as partial fulfillment for the degree of Doctor

For the record, this certificate is signed by

_____   _____

Dr. Lourdes F. Vega   Dr. Javier Lafuente
Director   UAB Tutor

_____

Daniel Bahamón García
PhD candidate

Bellaterra, September 2015

Summary

As defined by the Brundtland Commission, sustainable development is the advance that "meets the needs of the present without compromising the ability of future generations to meet their own needs". Sustainable development is of special relevance in the present situation, in which an explosive growth in energy consumption as a consequence of the great inventions and developments related to transportation and technology is observed, along with a rapid increase in population worldwide. Most of these technologies are related to an increased amount of greenhouse gases emitted to the atmosphere. In this context, sustainable development would suggest searching for ways to mitigate these emissions, including carbon capture and storage (or utilization, CCSU), energy efficiency, alternative sources of energy and energy saving, as already suggested by the Kyoto's protocol and the IPCC reports. Hence, much effort has been devoted in recent years to capture and storage of CO_2 from concentrated sources of emission such of power plants and others.

Apart from establishing new technologies for CO_2 capture and separation, the exploration of advanced adsorbent materials with high separation performance and low capital cost is very significant for various gas-separation- related issues. Over the last three decades, the science of porous solid materials has become one of the most intense areas of research and development for chemists, physicists, and materials scientists. These materials have found a large number of applications in many fields, such as adsorption, separation and purification, as well as catalysis for different processes. Exploration of advanced porous materials is therefore an intense subject of scientific research and practical applications.

In fact, considerable progress has been made in recent years on the development of novel adsorbents. For instance, Metal Organic Frameworks (MOFs) have been gaining considerable attention as promising nanoporous materials for gas storage and gas separation applications due to their exceptional physical and chemical properties. The rational design and synthesis of various types of MOFs have been achieved by tailoring the combination of different organic linkers and metal-ions. MOFs have already been demonstrated to be promising materials in the separation of different gases, however, a molecular level understanding of gas adsorption in the pores is crucial to accelerate the design and development of these and other

applications. It is also fundamental to know their behavior under moisture conditions and impurities content, as normally found at specific industrial applications.

The overall objective of this PhD Thesis is to advance in the field of materials for CO_2 capture and separation at process conditions. New tools are proposed for assessing and optimizing capture systems at industrial conditions, based on molecular simulations. Although several adsorbents are considered, particular attention is paid to zeolites and MOFs, given their promising *a-priori* properties for this separation. The influence of water vapor and impurities is explicitly considered, both, in the light of the fundamentals of adsorption and in the application for post-combustion carbon dioxide capture by swing adsorption cycles.

A brief description of the fundamentals of adsorption and molecular simulations is first presented, followed by generalities on CO_2 capture and separation, including the processes and the conditions at which it should occur. A novel throughout review on recent studies of materials for CO_2 capture and separation is presented, including few studies of impurities, thus providing valuable information to assess their industrial application. Based on this review, some of the most promising materials for CO_2 separation in a Temperature Swing Adsorption (TSA) process are studied in detail by using molecular simulations (compared to experimental data when available). A new procedure for assessing and optimizing capture systems at real conditions, based on molecular simulations, is proposed in this work. Given the great influence of water as a trace compound on the separation, CuBTC (one of the most studied MOFs, stable in water and with potential for industrial application) is investigated in comparison to the benchmark zeolite 13X, already used in some industrial processes. The effect of the coexisting species as well as the influence of water and SO_2 in flue gas is examined in detail in order to reach a better understanding of the adsorption capacity, selectivity, adsorption density location and isosteric heat distributions.

And finally, detailed parametric studies have been carried out for a comparative computational investigation for separating of multi-component mixtures of flue gas by using other representative zeolites such as kaolinite and chabazite. Additional work, related to another environmental problem, the separation of a pollutant (ibuprofen) in water, by using activated carbons, is also presented here, demonstrating the versatility of the tools for these types of systems.

In summary, the work developed in this Thesis highlights the use of molecular simulation techniques for optimizing environmental related processes, with special focus on CO_2 capture and separation. It provides new procedures to assess the use of these materials from their fundamental knowledge until their applications at industrial conditions.

Resum

Segons la definició de la Comissió Brundtland, el desenvolupament sostenible és l'avanç que "satisfà les necessitats del present sense comprometre la capacitat de les generacions futures per satisfer les seves pròpies necessitats". El desenvolupament sostenible és d'especial rellevància en la situació actual, en què s'observa un creixement explosiu en el consum d'energia com a conseqüència de grans invents i desenvolupaments en transport i tecnologia, juntament amb un ràpid augment de la població arreu del món. Les tecnologies esmentades estan relacionades amb una major quantitat de gasos d'efecte hivernacle emesos a l'atmosfera. En aquest context, el desenvolupament sostenible suggereix la cerca de formes de mitigar aquestes emissions, incloent la captura i emmagatzematge de diòxid de carboni (o la seva utilització, *Carbon Capture Storage and Utilization, CCSU*), l'eficiència energètica, fonts alternatives d'energia i estalvi d'energia, com ja s'ha suggerit al protocol de Kyoto i als informes de l'IPCC. Com a conseqüència, molt esforç s'han dedicat en els últims anys a cerca tecnologies de CCSU a partir de fonts concentrades d'emissió.

Apart d'establir noves tecnologies per a la captura de CO_2, hi ha hagut un gran avanç en l'exploració de materials adsorbents avançats amb un alt rendiment i un baix cost de capital per a diversos processos de separació. Durant les últimes tres dècades, la ciència de materials sòlids porosos s'ha convertit en una de les àrees més intenses de recerca i desenvolupament per als químics, físics i científics de materials. Aquests materials han trobat un gran nombre d'aplicacions en molts camps, com ara l'adsorció, la separació i purificació, així com la catàlisi per diferents processos industrials. Per tant, la cerca de materials porosos avançats per a la captura de CO_2 i la seva separació d'altres gasos és un tema d'intensa investigació científica i d'aplicacions pràctiques.

De fet, en els darrers anys s'ha avançat considerablement en el desenvolupament de nous adsorbents. Per exemple, les estructures òrgan-metàl·liques (*Metal-Organic Frameworks, MOFs*) han anat guanyant considerable atenció com materials nanoporosos prometedors per a aplicacions d'emmagatzematge i separació de gasos, per les seves propietats físiques i químiques excepcionals. El disseny racional i la síntesi de diversos tipus d'MOFs es fa mitjançant l'adaptació de la combinació de diferents ions metàl·lics i enllaçants orgànics. Els MOFs ja han demostrat ser materials prometedors en la separació de diferents gasos, però encara manca una comprensió a

nivell molecular de l'adsorció de gas en els porus és crucial per accelerar el disseny i desenvolupament d'aquests materials *fets a mida*. També és fonamental conèixer el seu comportament sota condicions d'humitat i impureses, condicions sota les quals es troben en aplicacions industrials específiques.

L'objectiu general d'aquesta tesi doctoral és avançar en el camp dels materials per a la captura i separació de CO_2 a condicions del procés. A partir de simulacions moleculars es proposen noves eines per a l'avaluació i optimització dels sistemes de captura en condicions reals. Encara que es consideren diversos adsorbents, el treball es centra sobretot en zeolites i MOFs, donades les seves propietats prometedores *a-priori* per a aquesta separació. Com a novetat es considera de manera explicita la influència del vapor d'aigua i impureses, tant des del punt de vista fonamental com en l'aplicació per a la captura de CO_2 per post-combustió mitjançant cicles d'adsorció per oscil·lació (*Swing Adsorption Cycles*).

En primer lloc, es presenta una breu descripció dels fonaments de l'adsorció i de les simulacions moleculars, seguit per generalitats en la captura de CO_2, incloent processos i condicions d'operació. Es presenta una revisió exhaustiva d'estudis recents de materials per a la captura i separació de CO_2, proporcionant així informació valuosa per optimitzar la seva aplicació industrial. Basats en aquesta revisió, es van estudiar en detall alguns dels materials més prometedors per a la separació de CO_2 en un procés d'adsorció per canvi de temperatura (*TSA*) utilitzant simulacions moleculars (comparant amb dades experimentals disponibles). Es proposa en aquesta tesi un nou procediment per a l'avaluació i optimització dels sistemes de captura en condicions reals, basats en simulacions moleculars. Donada la gran influència de l'aigua com un compost traça en la separació, es va investigar el CuBTC (un dels MOF més estudiats i estables en aigua) en comparació amb la zeolita de referència 13X, que ja s'utilitza en alguns processos industrials. S'examina en detall l'efecte de les espècies coexistents, així com la influència de l'aigua i el SO_2 en els gasos de combustió, per tal d'arribar a una millor comprensió de la capacitat d'adsorció, la selectivitat, la ubicació de les molècules al material i les distribucions de calor isotèrics. Finalment, s'han dut a terme estudis paramètrics detallats per a una investigació computacional comparativa de la separació de mescles multi-components de gasos de combustió mitjançant l'ús d'altres zeolites com ara caolinita i chabazita. També es presenta un treball addicional, d'un altre problema mediambiental, la separació d'un contaminant (ibuprofèn) en aigua, mitjançant l'ús de carbons activats, emprant les mateixes eines de simulació.

En resum, el treball desenvolupat en aquesta tesi destaca l'ús de tècniques de simulació molecular per a l'optimització de processos relacionats amb el medi ambient, amb especial atenció a la captura i separació de CO_2. Es proporcionen nous procediments per avaluar l'ús d'aquests materials a partir del seu coneixement fonamental fins a la seva aplicació en condicions industrials.

Resumen

Según la definición de la Comisión Brundtland, el desarrollo sostenible es aquel que "satisface las necesidades del presente sin comprometer la capacidad de las generaciones futuras para satisfacer sus propias necesidades". El desarrollo sostenible es de especial relevancia en la situación actual, en la que se observa un crecimiento explosivo en el consumo de energía como consecuencia de grandes inventos y desarrollos en transporte y tecnología, junto con un rápido aumento de la población en todo el mundo. La mayoría de estas tecnologías están relacionadas con una mayor cantidad de gases de efecto invernadero emitidos a la atmósfera. En este contexto, el desarrollo sostenible sugiere la búsqueda de formas de mitigar estas emisiones, incluyendo la captura y almacenamiento de carbono (o utilización, *Carbon Capture and Storage and Utilization CCSU*), la eficiencia energética, fuentes alternativas de energía y ahorro de energía, como ya se ha sugerido por el protocolo de Kioto y los informes del IPCC. De ahí que en los últimos años se haya dedicado un esfuerzo considerable a desarrollar tecnologías para la captura y almacenamiento de CO_2 a partir de fuentes concentradas de emisión.

Además de establecer nuevas tecnologías para la captura de CO_2, en los últimos años se ha intensificado la búsqueda de materiales adsorbentes avanzados con un alto rendimiento en la separación y un bajo costo de capital para diversos procesos de separación. Así, durante las últimas tres décadas, la ciencia de materiales sólidos porosos se ha convertido en una de la áreas más intensas de investigación y desarrollo para químicos, físicos y científicos de materiales. Estos materiales han encontrado un gran número de aplicaciones en campos, tales como la adsorción, la separación y purificación, así como la catálisis para diferentes procesos.

De hecho, se ha avanzado considerablemente en los últimos años en el desarrollo de nuevos adsorbentes. Por ejemplo, las estructuras órgano-metálicas (*Metal Organic Frameworks, MOFs*) han ido ganando considerable atención como materiales nanoporosos prometedores para aplicaciones de almacenamiento y separación de gases, debido a sus propiedades físicas y químicas excepcionales. Los MOFs ya han demostrado ser materiales prometedores en la separación de diferentes gases, sin embargo, se necesita la comprensión a nivel molecular de la adsorción de gases para acelerar el diseño y desarrollo de aplicaciones *a la carta*. También es fundamental

conocer su comportamiento bajo condiciones de humedad e impurezas, como se tiene normalmente en aplicaciones industriales específicas.

El objetivo general de esta Tesis Doctoral es avanzar en el campo de materiales para la captura y separación de CO_2 a condiciones del proceso. Se proponen nuevas herramientas para la evaluación y optimización de los sistemas de captura en condiciones reales, basadas en simulaciones moleculares. Aunque se consideran varios adsorbentes, el trabajo se centra en zeolitas y MOFs, dadas sus propiedades prometedoras *a-priori* para esta separación. Por primera vez se considera de manera explícita la influencia del vapor de agua e impurezas, tanto a la luz de los fundamentos de la adsorción como en la aplicación para la captura de CO_2 por post-combustión mediante ciclos de adsorción por oscilación (*Swing Adsorption Cycles*).

En primer lugar, se presenta una breve descripción de los fundamentos de la adsorción y de las simulaciones moleculares, seguido por generalidades en la captura de CO_2, incluyendo procesos y condiciones de operación. Se presenta una revisión exhaustiva de estudios recientes de materiales para captura y separación de CO_2, proporcionando así información valiosa para su aplicación industrial. Basados en esta revisión, se han estudiado en detalle algunos de los materiales más prometedores para la separación de CO_2 en un proceso de adsorción por cambio de temperatura (*TSA*) utilizando simulaciones moleculares (comparando con datos experimentales de la literatura). Se propone un nuevo procedimiento para la evaluación y optimización de los sistemas de captura en condiciones reales, basados en simulaciones moleculares. Dada la gran influencia de trazas de agua en la separación, se investiga el CuBTC (uno de los MOF más estudiados y estables en agua) en comparación con la zeolita de referencia 13X, utilizada en algunos procesos industriales. Se examina en detalle el efecto de las especies coexistentes, así como la influencia del agua y SO_2 en los gases de combustión, con el fin de llegar a una mejor comprensión de la capacidad de adsorción, la selectividad, la localización de las moléculas en el material, las distribuciones de calor isostérico y su relación con el proceso. Se han llevado a cabo estudios paramétricos detallados para una investigación comparativa de la separación de mezclas multi-componentes de gases de combustión mediante el uso de otras zeolitas como caolinita y chabacita. También se presenta un trabajo adicional, relacionado con otro problema medioambiental, la separación de un contaminante (ibuprofeno) en agua, mediante el uso de carbones activados, usando las mismas técnicas computacionales.

En resumen, el trabajo desarrollado en esta tesis destaca el uso de técnicas de simulación molecular para la optimización de procesos relacionados con el medio ambiente, con especial atención a la captura y separación de CO_2. Se proporcionan nuevos procedimientos para evaluar el uso de estos materiales a partir de su conocimiento fundamental hasta su aplicación en condiciones industriales.

Acknowledgments

I want to express my sincere gratitude to my director, Dr. Lourdes Vega, from which I learned and appreciated every minute addressed to me. Her tenacity, patience and wise counsel led me to take her as an example of life. In few words, without her it would have been impossible to conduct this research.

Special thanks to all the people I met in MATGAS, for their company, help and disinterested friendship. The last three years have been quite an adventure, and would not have been as enjoyable as it was without a great group of colleagues.

To my father, mother and grandparents, who have been always with me and are a source of inspiration and desire to move forward. To my sister, to whom I dedicate this Thesis. To my friends, who never let me decline and helped me in the darkest moments. And to Luis and Carmen for their hospitality since I came to Spain.

Particular gratefulness to the professor Dr. Pablo Gamallo from the University of Barcelona for his invaluable scientific discussions and suggestions in some chapters of this Thesis.

And to all those who somehow participated in the development of this thesis. Thanks for the support!

Content

List of acronyms and symbols

4A/5A Zeolite: molecular sieve (alkali metal alumino-silicate) whose aperture are 4Å and 5Å respectively. Is a kind of alkali metal silica acid salt, and can absorb water and other materials whose critical diameter are not more than 5Å, such as NH_3, H_2S, SO_2, CO_2. Widely used in dry gas, liquid, gas or liquid refining and.

AC MAXSORB R: Activated Carbon (with commercial conditions, it can be type I, II or III).

Amino-MIL-53(Al): type of MOF exhibiting either small or large pores. The first series included the rigid (M) VIV, where MIL stands for Materiaux Institut Lavoisier).

BET: Brunauer, Emmett and Teller.

BTC: 1,3,5-BenzeneTriCarboxylic acid.

BTT: Benzene-1,3,5-Tris(1H-Tetrazole).

COF: Covalent Organic Framework. COFs are porous and crystalline, and are made entirely from light elements (H, B, C, N, and O) that are known to form strong covalent bonds in well-established and useful materials such as diamond, graphite, and boron nitride.

DUT-9: $NiO(BTB)(DMF)(H_2O)$. Highly Porous Metal-Organic Framework.

GCMC: Grand Canonical Monte Carlo

H-KUST-1: MOF material developed by the Hong Kong University of Science and Technology. Also known as CuBTC, $Cu_3(BTC)_2$.

HMS: hexagonal Mesoporous Silicas (HMS) and related structures (MCM-41, SBA-15, etc) which have long-range periodicity, yet poorly defined short-range order, possess very high surface areas and well hydroxylated surfaces that are amenable to functionalization.

IRMOF-1: equivalent to MOF-5. The IRMOF-1 crystal structure is a cubic array of Zn_4O units bridged by benzenedicarboxylate.

IUPAC: International Union of Pure and Applied Chemistry

LJ: Lennard Jones.

MC: Monte Carlo.

MD: Molecular Dynamics.

K_H: Henry's constants ($kmol/m^3$-kPa)

PCN-61: is a MOF composed of 5,5,5"-benzene-1,3,5-triyltris(1-ethynyl-2-isophthalate) (btei) linkers coordinated to copper ions in the 2^+ oxidation state. PCN stands for Porous Coordination Network.

PE-MCM-41: Pore Expanded; Mobil Composition of Matter - initial name given for a series of mesoporous materials that were first synthesized by Mobil's researchers in 1992.

PSA: Pressure Swing Adsorption.

q: amount adsorbed per mass (mol/kg) or per volume of adsorbent ($kmol/m^3$)

Q_{ST}: isosteric heat of adsorption (kJ/mol).

SBA-15: Santa Barbara Amorphous silica. Non zeolitic material.

SNU-50/SNU-31: MOF which name stands for Seoul National University.

SWNTS/SWCN: Single Walled Carbon Nanotubes.

TraPPE: Transferable Potential for Phase Equilibria.

TSA: Temperature Swing Adsorption.

x_i: mole fraction of component i in the adsorbed phase

y_i: mole fraction of component i in the gas phase

ZSM-5: Zeolite Socony Mobil–5.

Greek symbols

ε: voidage of bed

$\pi_{i1,2}$: equilibrium pressure at any adsorption point (kPa)

List of Figures

List of Tables

Para tatica.

"Life is not easy for any of us. But what of that? We must have perseverance and above all confidence in ourselves"

Marie Curie (1867-1934).

1

INTRODUCTION

The new environmental constraints, the required intensification of processes and the search of the society for sustainable resources and products are becoming a paradigm for designing new processes and refining existing ones. Carbon dioxide is the most abundant greenhouse gas emitted to the atmosphere by anthropogenic processes (as seen in Figure 1.1), and although it is used in many applications, it is often associated with the problem of climate change. In this sense, a great effort has been devoted in recent years to develop sustainable processes, or to improve existing ones, searching for a net positive impact in the environment or, at least, better environmental performance than the processes currently used.

Figure 1.1. Anthropogenic emissions of carbon dioxide

Hence, one of the most important methods proposed to mitigate anthropogenic CO_2 emissions is to adsorb and separate CO_2 from diluted sources, such as gases emitted from fossil fuel combustion, usually known as Carbon Capture and Storage (CCS), together with the search for alternative, cleaner, sources of energy and energy efficiency.

Several approaches have been proposed for CO_2 capture including cryogenic distillation, amine scrubbing, membrane separation and sorbent adsorption. Because of the occurrence of phase transition, cryogenic distillation is energetically intensive. Furthermore, chemical absorption using aqueous alkanolamine solutions is proposed to be the most applicable technology for CO_2 capture. However, this technology possesses some drawbacks such as high equipment corrosion rate, high energy consumption in regeneration, solvent regeneration and a large absorber volume required. As a result, solid adsorption processes are suggested and studied to overcome those inherent problems. Upon comparison, adsorption in porous materials

has considerably high energy efficiency, low capital cost, large separation capability and ease for scaling-up, providing advantages particularly at low to moderate throughput. So far, the economic viability of adsorptive processes is largely due to the versatility of zeolites.

Considerable progress has been made in recent years on the development of novel adsorbents for CO_2. A variety of promising types such as activated carbonaceous materials, functionalized materials, microporous/mesoporous silica and cation-exchanged zeolites have been studied by different authors due to their specific properties. Moreover, Metal–Organic Frameworks (MOFs) have recently attracted significant attention due to their impressive high surface areas and versatile crystalline structures that allow a "materials by design" approach, causing them to try to find their way into industrial applications.

Nevertheless, in spite of the increasing interest for efficient materials, most of the published work focuses on adsorption isotherms and characteristics of the pure substances, and few measurements are related to mixtures, providing limited data to be used for the industrial conditions. Besides, for practical applications, the effect of coexisting components or impurities such as water, oxygen, sulfur and nitrogen compounds and other molecules present has been less explored. The necessary understanding about the influence of the main components still needs further investigation.

In this sense, molecular simulations play a crucial role, since apart from giving a deep understanding of the physical phenomenon, allow us to obtain unique and exclusive information of the material properties and operation, which cannot be deduced by experimental macroscopic techniques, as well as be a screening method to explore a vast amount of materials and conditions in less time.

1.1. Thesis objectives

The work is mainly focused on the computational study for application of advanced materials such as cation-exchanged zeolites and MOFs to carry out a detailed and comprehensive study of the adsorption process. The scope of this Thesis is to study molecular aspects that are important for understanding of carbon dioxide capture and the effect that impurities have on this.

The main novelty is to combine basic science with applied engineering, in order to obtain a fundamental understanding and optimize specific processes at real industrial conditions. For this case, accurately and transferable force fields were used

in order to reproduce experimental values of adsorption of gases, allowing the use of more complex models that describe the system more realistically.

1.2. Thesis outline

The outline of this thesis is as follows:

In Chapter 2, some of the most important features about the adsorption process are introduced. Emphasis has been put on the different computational techniques used for the simulations. Special importance has been given to those features and peculiarities which make these techniques suitable tools to obtain unique and valuable information. Similarly, in Chapter 3, the technologies for CO_2 capture, current uses, as well as computational approaches for CO_2 adsorption and separation are briefly discussed.

In Chapter 4, a deep review of the most used and promising materials found in literature for carbon dioxide capture and separation is presented, regarding: 1) pure adsorption, 2) mixture behavior, and 3) impurities effect. Care has been taken to put all results in the same units for a fair comparison

In Chapter 5, the separation between carbon dioxide and nitrogen in different crystallographic families is studied in detail for a typical industrial TSA process. The binary mixture behavior and the influence of water traces is also investigated. A new procedure for assessing and optimizing capture systems at real conditions, based on molecular simulations, is proposed in this work

Chapter 6 is devoted to the study of the effect of impurities such as water and SO_2 in the post-combustion carbon dioxide separation on two different materials: CuBTC (well known and studied MOF that is stable upon adsorption of water at standard conditions and has potential for industrial applications), and the traditionally used zeolite 13X. The adsorption isotherms, selectivities, isosteric heats and location of the preferential adsorption sites for the main gasses contained in a multi-component exhaust gas are computed, in order to reach a better understanding of the competition of the different molecules for be adsorbed inside the frameworks, and hence, the true influence of these impurities at real operating conditions.

Chapter 7 presents a detailed computational investigation of the effect of multi-component mixtures of flue gas for gas separation in representative zeolites such as kaolinite and chabazite.

A final conclusion chapter summarizes the most important results showed in the previous chapters, and highlights some possible future directions of this work

Additional work, based on the application of the same simulation techniques to the study of adsorption properties of ibuprofen on activated carbon is presented in an Appendix. This is also an environmental related problem, in this case focused on the removal of pollutants in water. With this, we show the versatility of the computational tools used in this Thesis, compared to experimental data found in literature, and related to different environmental problems.

2

FUNDAMENTALS

2.1. Adsorption

Adsorption is a process in which a supporting medium, usually a porous material, is required for separation. The process is considered one of the natural phenomena most relevant area of human activity, since through it, one can selectively capture species, thus controlling emissions of pollutants into the environment. It also allows separating a high added value product from subproducts or waste.

The term adsorption is used to denote the enrichment or accumulation of one or more components, whether molecules, atoms or ions, in an interfacial layer between two bulk phases. In dealing with adsorption at gas/porous solid interfaces, it is customary to call the components in the adsorbed state the adsorbate, and to refer to the same species in the bulk gas phase as the adsorptive. Additionally, the adsorbing solid is called adsorbent. Adsorption is distinguished from absorption, which involves bulk penetration of the gas into a mass of the adsorbing solid or liquid [Dabrowski, 2001; Sing et al., 1985].

The essential requirement of an adsorption separation processes is to have an adsorbent that preferentially adsorbs/retain a family of related components from a mixed feed. The forces acting in an adsorption process can be categorized into two main groups: (i) van der Waals forces directly correlated with adsorbate molecular polarizability and (ii) electrostatic forces such as polarization forces, surface field–molecular dipole interactions and surface field gradient–molecular quadrupole interactions. Adsorption is usually promoted by synergies among these different kinds of interactions.

When a gas is introduced into a solid, an adsorbed phase bonded to adsorbent surfaces may form. When the conditions are changed, gas molecules may desorb. Adsorption of a gas on a porous solid is a spontaneous process, which means that it involves a decrease in free energy (ΔG) due to the passing of the free gas to the adsorbed film. There is also a decrease in entropy (ΔS), because the gas adsorbed on the surface of the adsorbent is more ordered than in the gas phase.

There are two broad types of adsorption processes: physical adsorption and chemical adsorption. These are both characterized by the strength and nature of the bond between the adsorbate and substrate [Sing et al., 1985]. The distinction between physical and chemical adsorption is very important as the process and the behavior of the adsorbed layers are quite different.

2.1.1. Physical and chemical adsorption

The adsorption process can be divided into two: the chemical adsorption (or irreversible chemisorption) and physical (physisorption), due to the bonds that are formed between the adsorbate and the adsorbent surface (see Figure 2.1).

The physisorption is characterized by weak bonds (van der Waals force and dipolar forces) and low heats of adsorption. Furthermore adsorbate molecules are not restricted to specific sites but, instead, are free to cover the entire surface of the adsorbent caused by the attraction between permanent dipoles and induced dipoles, without altering the atomic or molecular orbitals of the species involved.

Chemisorption involves the exchange or sharing of electrons between the adsorbate and the substrate. As the links between the adsorbate/adsorbent are strong (ionic or covalent) due to an interaction of chemical type, the bonding electrons between the gas and the solid undergo a rearrangement and respective orbital change shape or degree occupancy of such a chemical reaction mode [Lowell et al., 1984; Rouquerol et al., 1999].
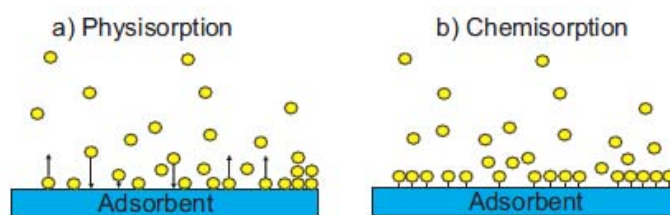
Figure 2.1*. Solid-gas interactions: physisorption (reversible) and chemisorption (strong and irreversible bond formed with the solid surface).*

It is evident that the enthalpy of adsorption of gases on porous solids is always an exothermic process for physisorption. In physisorption, the uptake is generally favored at low temperature while the uptake caused by chemisorption is favored at high temperature. Chemisorption is typically characterized by the formation of a single layer of adsorbate on the surface of porous materials; contrarily in physisorption, multiple layers of the adsorbate can form on the porous materials.

Some significant differences between physisorption and chemisorption are summarized in Table 1.1 [adapted from Young and Crowell, 1962; Adamson and Gast, 1997; Rouquerol et al., 1999; Atkins, 1998; Attard and Barnes, 2008]

Table 1.1. Comparison between physical and chemical adsorption.

	Physical adsorption	Chemical adsorption
Rate of adsorption	Fast	Slow (normally has to overcome the activation energy for breaking chemical bonds)
Monolayer coverage	Monolayer and multilayer formation depending on environment	Limited to mono layer coverage
Origin of interactions force and specificity	van der Waals forces, non-specific adsorption, easy for desorption	Chemical bond forces, highly specific adsorption, difficult for desorption due to the need to break bonds
Dependence of the temperature	Decrease with increasing temperature	Increase with increasing temperature
Reversibility	Reversible (the adsorbate will desorb when the temperature is raised or the pressure is lowered)	Usually not reversible
Specificity	Non-specific and does not result in the dissociation of adsorbed molecules	Very specific due to chemical reactions between gas molecules and surface groups. Often results in dissociation of molecules during the process

2.1.2. Adsorption isotherms

One of the most common ways of representing adsorption equilibrium is by the relationship between adsorbed amount and pressure for a given temperature. This relationship is known as adsorption isotherm for a given adsorbate-adsorbent system.

The adsorption phenomena are characterized by measuring adsorption isotherms which represent the amount of adsorbed molecules in the adsorbate as a function of gas pressure or liquid outside. This graph is usually expressed as the amount of adsorbate per gram (or volume) of adsorbent to each equilibrium pressure of the gas (at a constant temperature). When a porous material is exposed in a closed space with some definite pressure of gas, it begins to adsorb the gas. The quantity of gas taken up by a sample of solid is proportional to the mass of the sample, the temperature, the pressure of the gas and the nature of both, the solid and the gas.

By studying the adsorption isotherms, one can: 1) estimate the surface area/pore volumes, 2) estimate the pore size distribution, 3) assess the surface

chemistry of the adsorbents, and 4) determine the fundamentals of the adsorption process, among others.

There are different correlations in the literature for adjusting the experimental equations typical values such as Langmuir, Freundlich, BET, among others.

2.1.3. Isotherms Types

The adsorption isotherms can be classified in six ways as shown in Figure 2.2. This classification was first proposed by Brunauer [Brunauer et al., 1938] and his colleagues in 1938, and completed later by Sing et al. [Gregg and Sing, 1982; Sing et al., 1985]. Currently this classification is recommended by the International Union of Pure and Applied Chemistry (IUPAC).
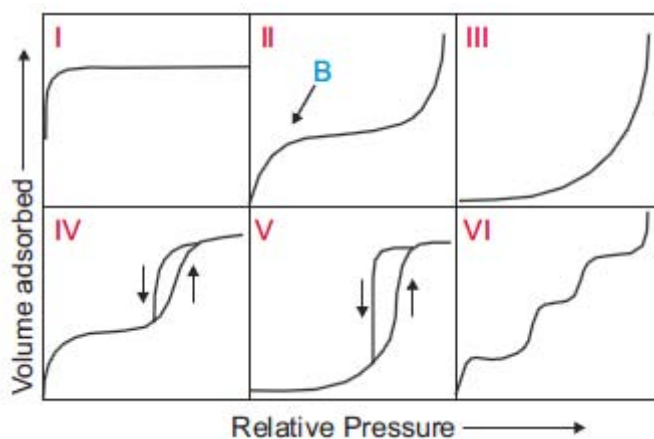
Figure 2.2. Isotherms classification according to IUPAC.

Depending on the shape of the curve, different information can be inferred about the distribution of pores of the material and/or interactions between the adsorbate and the adsorbent, classified as follows:

- The type I isotherm shows a rapid increase in the amount of gas adsorbed over the low relative pressure range and then reaches a plateau in the high pressure range. This is sometimes referred to as Langmuir isotherm and is often obtained when adsorption is restricted to a monolayer. Therefore, chemisorption isotherms and physisorption in microporous materials (very narrow or slit pore structures, e.g. activated carbons, molecular sieve zeolites) usually show to this shape. The plateau indicates that the micropores are filled and no further adsorption will take place, so the limiting uptake is governed by the accessible micropore volume rather than by internal surface area.

- The Type II isotherms are typically produced by solids which are non-porous or macroporous and the isotherms represent unrestricted monolayer-multilayer

adsorption on a heterogeneous adsorbent. The point B indicates the value of the relative pressure where adsorption monolayer is completed and initiates multilayer adsorption. Consequently, multilayer adsorption increases progressively with rising pressure.

- Type III: this type of isotherm is shown by non-porous or macroporous materials when there is little affinity between the adsorbate and the adsorbent. This is distinguished from Type II isotherms by a convexity towards the relative pressure axis in the entire range of the isotherm and do not exhibit a point B. Therefore, at low pressures relative effect force field (a low slope) is not observed due to the weak interactions between the adsorptive partners. In other words, the adsorbate-adsorbate interactions are stronger than adsorbate-adsorbent interactions. However, the uptake at high relative pressure is much higher due to the adsorbate-adsorbate interactions being much stronger inside the pore and this increases the driving force of the adsorption process.

- The Type IV is presented by mesoporous adsorbents. The isotherm shows a hysteresis loop, which is associated with capillary condensation in adsorption/desorption mesopores, and a limit on the amount adsorbed to the upper range of relative pressure. The initial part of the isotherm is attributed to adsorption monolayer, because it coincides with the first region of the isotherm of type II. At this initial state, adsorption of molecules on to the walls of porous material occurs at a very low relative pressure until a monolayer is formed. Hence, the multilayer adsorption occurs as pressure increases and follows capillary condensation at high relative pressure. In the capillary condensation process, gas molecules tend to form a liquid-like layer with a curved meniscus at pore entrances. As pressure decreases, the angle of the curve of the meniscus also changes. The liquid meniscus blocks the liquid condensed in pores from evaporating, thus resulting in a high mass of adsorbate remaining in the porous material which then creates the hysteretic loop.

- Type V: presented by mesoporous materials because of the presence of hysteresis in the process. There is little affinity between the adsorbate and the adsorbent. Unlike Type III, there is a hysteresis loop and it exhibits a point of inflection at a higher relative pressure. Subsequently, Type V isotherms reach a plateau in the multilayer region of the isotherm where the capillary condensation occurs. This isotherm is rare.

- The Type VI isotherm represents the step-like nature of the adsorption process in some materials. The steps result from sequential multilayer adsorption on an uniform non-porous surface. Each of the steps corresponds to having an adsorbed layer (represents the monolayer capacity for each adsorbed layer). The adsorption process should be ideally reversible, however, some deviations can occur.

2.1.4. Heat of adsorption

The concept of adsorption equilibrium is deeply involved in the evaluation of adsorbent specific capacity, selectivity and regenerability. Equilibrium adsorption isotherms and heat of adsorption represent essential input data for a process modeling. Heat of adsorption is a measure of the strength of interactions between adsorbate and adsorbent (adsorption is an exothermal phenomenon). For adsorbents characterized by energetically heterogeneous surfaces (e.g. most zeolites), heat of adsorption is higher at low loadings, describing interactions on strongest sites. Thus, it is properly referred as isosteric (i.e. at a definite loading) heat of adsorption, q_{ST}.

From the process engineering point of view, the heat of adsorption is a measure of the energy required for adsorbent regeneration and it provides an indication of temperature variations that can be expected on the bed during adsorption (and desorption) under adiabatic conditions. It appears that the heat of adsorption should, ideally, have an intermediate value. If it is too high, the sorbent will be difficult to regenerate economically, and if it is too low the capacity for adsorbing a specific molecule (i.e. CO_2) and the selectivity will be too small for practical applications.

Hence, since the isosteric heat of adsorption is the energy dissipated during adsorption [Ackley et al., 2003; Martin et al., 2010], this can be calculated from the equilibrium established between the condensed phase and gas phase, reduced to the Clapeyron equation for adsorption equilibrium.

$$Q_{isost} = -R \frac{\partial \ln P}{\partial \left(\frac{1}{T} \right)} \Bigg]_N = RT^2 \frac{\partial \ln P}{\partial T} \Bigg]_N \tag{2.1}$$

The isosteric heat from the Clapeyron equation is independent of temperature and pressure, and it is calculated based on the slope of a straight line built when relating "ln P" vs. "$1/T$". From a set of isosteres (at the same concentration) or experimental data for a phase equilibrium between a solid and a gas phase (T, P, N_{ads}) one can fully describe the adsorption equilibrium and evaluate the isosteric heat of adsorption.

The magnitude of the heat of adsorption is often used to distinguish between chemisorption and physisorption. It is recognized as physisorption when the heat of adsorption is typically in the range of 20-70 kJ/mol (and is larger than the enthalpy of condensation). Enthalpy of chemisorption, in general, is much larger than enthalpy of physical adsorption and generally higher than 80 kJ/mol. In the intermediate zone identification is uncertain [Rouquerol et al., 1999].

The nature of both, the adsorbent and the adsorbate, governs the strength of the interaction. Strong forces between the fluid and the surface lead to chemisorption, which is characterized by the formation of a monolayer on the surface of the adsorbent

[Rouquerol et al., 1998]. Small adsorption enthalpies occur in physical adsorption or physisorption when only weak forces like van der Waals interactions appear between the phases. The formation of multilayers is common in this case.

2.1.5. Adsorbent selectivity

Equilibrium selectivity is the key parameter to evaluate adsorbent separation ability. It is based on differences in affinities of the adsorbent for the different species constituting the fluid phase. The preferential adsorption of components from a gas mixture can be achieved by one, or a combination, of the following mechanisms: (1) differences in the adsorbate–surface interactions and/or adsorbate packing interactions when the system reaches equilibrium (thermodynamic equilibrium mechanism), (2) differences in the size and/or shape of gas molecules leading to exclusion of molecules with a critical diameter too large to enter the adsorbent pores) and (3) differences in the diffusion rates of molecules through the adsorbent pores (kinetic mechanism).

For mixtures, the selectivity of preferential adsorption of component 1 over component 2, can be formally defined as:

$$S_{ads} = \frac{x_1/y_1}{x_2/y_2} \tag{2.2}$$

where x and y denotes composition of each component at the adsorbed and at the bulk phases, respectively.

This definition of S_{ij} serves as a useful tool to screen potential adsorbents. However, to adequately design an adsorption-based separation process, the selectivity of the adsorbent for components from a real gas mixture must be confirmed and the capacity of the adsorbent needs to be evaluated [Rochelle et al., 2009].

In order to determine the amount adsorbed, correlations and techniques are often used due to the complex of measure mixture streams. The Ideal Adsorbed Solution Theory (IAST) [Myers and Prausnitz, 1965], one of the most known methods, provides at estimation of the composition values at the adsorbent surface based only on the knowledge of the pure component isotherms. This is an incredibly useful method, since one only have to run calculations or experiments for pure adsorption isotherms, and then predict any combination of the gases.

It is represented as follows:

$$\pi_i = \frac{RT}{A} \int_{P=0}^{P_i^0} q_i \, dLnP = \frac{RT}{A} \int_{P=0}^{P_j^0} q_j \, dLnP = \pi_j \tag{2.3}$$

$$\pi_i x_i = P y_i \tag{2.4}$$

being π and P the equilibrium and bulk pressure respectively.

The accuracy of the IAST calculations for estimation of the component loadings for several binary mixtures in a wide variety of materials has been well established by comparison with the Configurational-Bias Monte Carlo simulations of mixture adsorption [Krishna and Baur, 2003]. These predicted selectivities from IAST are typically accurate at low loadings because the method is exact in the Henry law limit [Challa et al., 2002]: for example, Babarao and Jiang [Babarao and Jiang, 2008] found good agreement between IAST predicted isotherms and mixture simulation isotherms for silicalite, C168 Schwarzite and IRMOF-1 at low pressures. However, IAST assumes an ideal solution and it is inaccurate at higher loadings when there is inhomogeneous adsorption of the mixed-gas components in the framework, either underestimating or overestimating the adsorption compared with mixture simulation results.

2.1.6. Breakthrough Curves

The adsorption selectivity of the material for one component of the mixture versus the other is most commonly used to screen adsorbent materials for separation purposes, especially at the early stages of the investigation. However, the performance of an adsorbent is governed by both, selectivity and capacity factors. The proper combination of these two factors is obtained by using breakthrough calculations [Xiang et al., 2012].

To formulate the model for a dynamic column breakthrough process, the following mathematical model is the main used and is based on the following assumptions: 1) the flow pattern is described by the axially dispersed plug flow model. 2) The system operates under isothermal conditions and column wall temperature was constant and equal to the water bath temperature. 3) the frictional pressure drop through the column is negligible. 4) the adsorbent particles are spherical and homogenous in size and density. 6) The velocity of the gas is constant. The driving force is the concentration gradient of the adsorbed phase and the diffusion coefficient is constant. Under the above assumptions, a set of governing scaled equations and appropriate scaled initial and boundary conditions can be established [Krishna and Baur, 2002]:

The mass balance equation for a single component system, subjected to the above assumptions, is presented below.

Component mass balance and boundary conditions:

$$\frac{\partial c}{\partial t} = -\frac{\partial N}{\partial z} - \left(\frac{1-\varepsilon}{\varepsilon}\right)\frac{\partial q}{\partial \tau} \tag{2.5}$$

Where

$$N = -CD_L\frac{\partial y}{\partial z} + yN \tag{2.6}$$

Substituting:

$$-D_L\frac{\partial^2 c}{\partial z^2} + \frac{\partial(vc)}{\partial z} + \frac{(1-\varepsilon)}{\varepsilon}\frac{\partial \bar{q}}{\partial t} = -\frac{\partial c}{\partial t} \tag{2.7}$$

In the above equations, N is the flux of the adsorbates, q is the average adsorbate concentration in the solid phase at any location along the column length. D_L is the axial dispersion coefficient, z is axial distance measured from the column inlet, and t represents time. C is the total concentration (or density, ρ_g) of the feed gas, which can be obtained from the ideal gas law, ε is the bed voidage and u is the superficial gas velocity (see Figure 2.3).

The left hand side of Eq. represent the concentration of component i in the gas due to convection, the axial dispersion, the accumulation in the packing, and sorption onto the solid sorbent, while the right hand side represents the rate of diffusion of the component.
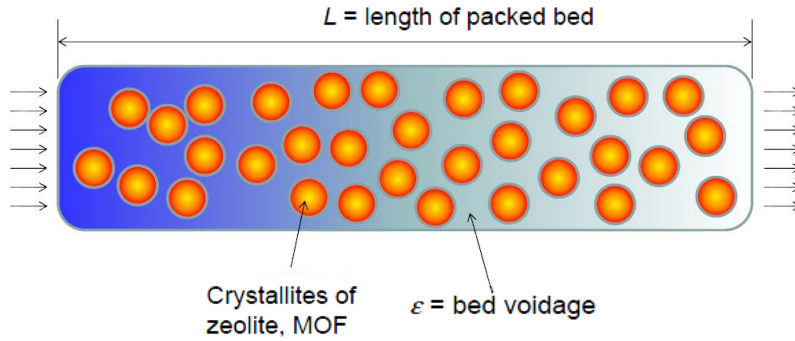
Figure 2.3. Packed bed scheme.

The initial and boundary conditions:

$$t = 0; \; q_{i(0,z)} = 0$$

$$t \geq 0; \; p_{i(t,0)} = p_{i0}; \; v_{(t,0)} = u_0/\varepsilon \tag{2.8}$$

$$t \geq 0; \; p_{i(t,L)} = p_{i0}; \; dx_i/dz = 0$$

The set of equations can be solved numerically, by introducing appropriate scaling factors and applying the finite difference technique. The finite difference method discretized the space derivatives and converted the partial differential equations to ordinary differential equations and the ordinary differential equation (overall mass balance) to algebraic equation at each node point. Thus, the algebraic equations give explicit expressions for calculating dimensionless interstitial fluid velocity at every node. Mole fraction of the adsorbable component at the column exit are then used to analyze the experimental breakthrough responses.

2.2. Molecular Simulations

The term "**molecular simulation**" refers to computational methods in which the molecular properties are explicitly taken into account. These methods play an important role in the study of the behavior of microscopic and macroscopic processes such as adsorption, since they provide a unified theoretical framework, based on statistical mechanics, to model the thermodynamic properties of a substance.

A well-designed computer simulation can be a complement for experiments. Molecular simulation can also provide data that is inaccessible through experimental methods or when the experiment has components that are too dangerous or too expensive. At the same time, they offer the possibility to create hypothetical scenarios and to test theories, while help to provide a molecular understanding of why the observed events occur.

The molecular mechanical methods are based on classical mechanics. These methods allow the study of materials at atomic level and determine the bulk properties through force fields, which are a set of potential functions and parameters. The potential functions define the interactions in a molecular system. These functions can be parameterized in a variety of analytical forms to give the correct energies and forces in order to describe how the molecules interact as a function of their positions. The parameters encompass optimal values of balance, such as distances, bond angles and force constants.

2.2.1. Statistical Mechanics

Statistical mechanics is the area of physics that, using probability theory, studies the macroscopic behavior of a system using the microscopic properties of its constituents. This theory allows to study a large number of molecules (around 10^{24}), by examining the statistical properties of a much smaller system (i.e. 10^4 particles). It

provides a molecular level interpretation of thermodynamic quantities like free energy, entropy, heat or work.

There are two fundamental postulates in statistical mechanics:

- Postulate of equal *a-priori* probabilities: this one states that given an isolated system in equilibrium, each accessible microstate corresponding to the same total energy can be found with equal probability, *i.e.* a system in equilibrium does not have any preference for any of its microstates.
- The other postulate is so-called the Ergodic Hypothesis. This hypothesis, fundamental in statistical mechanics, postulates that if a system is in equilibrium, at any point in time the average thermodynamic properties remain constant. This hypothesis, supported by experimental evidence, enables the use of the statistical thermodynamics and, therefore, molecular simulation methods.

The aim of molecular simulations is to describe a system using a molecular model in order to predict its properties. For example, with molecular simulations it could be easily observed the orientation and arrangement of molecules inside a structure. To connect the simulation with the real world and make useful predictions, it is crucial to compare the result of the calculations with macroscopic properties of the system which can be measured experimentally, such as temperature, pressure, etc. This connection between the microscopic and macroscopic view of the system can be achieved using statistical mechanics.

To address the calculation of thermophysical properties, two molecular simulation techniques are the most common: Monte Carlo and Molecular Dynamics. For a detailed description of these techniques the reader is referred to the text books by Allen and Tildesley [Allen and Tildesley, 1989], and Frenkel and Smit [Frenkel and Smit, 2002].

The workhorse of statistical mechanics is the **partition function** or in other words "the sum over all microstates". This refers to a mathematical formula which expresses the statistical weight of all the phase space configurations of the system. The classical expression of the partition function Q for a N-particle system is defined as

$$Q = \frac{1}{N!\, h^{3N}} \int exp[-\beta H(r^N, p^N)]\, dr^N dp^N \qquad (2.9)$$

where r^N and p^N denote the positions and momenta, respectively, and h is Planck's constant [Frenkel and Smit, 2002]. The function $H(r^N, p^N)$ is the Hamiltonian of the system, which is the total energy as a function of the coordinates and momenta of the particles.

If the partition function is known exactly, then all thermodynamic properties, such as the energy of the system, the chemical potential, the pressure, or the entropy, etc., can be determined from it. Usually, the partition function cannot be computed. Instead it can be computed averages corresponding to a certain statistical ensemble.

If consider a very large system of N classical particles (not relativistic, no quantum effects), this system is dynamically described by $3N$ spatial coordinates q, and $3N$ velocity (or linear momentum) coordinates v. This means that every microstate, or microscopic state of the system, is uniquely described by $6N$ variables. In a $6N$-dimensional coordinate system this microstate can be plotted as a point. Such $6N$-dimensional coordinate system is called *phase space*.

The system can also be described in terms of its number of molecules N, its energy E and its volume V. From the microstate we can easily calculate the macrostate, or macroscopic state of the system, in terms of number of N, V and E. If the system is isolated and in thermodynamic equilibrium, the macrostate will have constant values of N, V, and E while the system can change between different microstates with the same values for N, V and E. There is a large number of microstates that describe the same macrostate of the system. In the phase space, the microstates that are compatible with the macrostate NVE will define a (hyper)volume described by a density function (q,v). And, as mentioned before, the crucial postulate of statistical mechanics is that all these microstates are equally likely:

$$N(q,v) = \delta(H(q,v) - E) \tag{2.10}$$

$\delta(x)$ is the Dirac's delta function, which is zero for every x except when x=0, with $\delta(0)=\infty$. The integral of Dirac's delta function equals the unity. This microstate density is called *microcanonical ensemble*.

Under these NVE conditions, the only possible distribution is the one that places each system at the energy level E. This level will generally have degeneracy, so the system can be found in any of the states of identical energy.

The thermodynamic properties of the system can be obtained from the properties of the microstates. If Ω is the number of microstates compatible with one single macrostate, then:

$$S = k_B.Ln \tag{2.11}$$

where k_B is the *Boltzmann's constant* (1.3806503_x10^{-23} m² kg s⁻² K⁻¹) and S the entropy of the system. Usually is not only wished to describe isolated systems, but systems in thermal equilibrium where N, V and the T are constant as they are closer to experimental situations. In that case, following a similar formulation, a different microstate density can be obtained called *canonical ensemble*. In absence of electromagnetic fields, the velocities of the particles can be integrated to obtain:

$$N(q) = \frac{exp\,(-\beta E_1)}{\sum_j exp\,(-\beta E_1)} = \frac{exp\,(-\beta E_1)}{Q(N,V,T)} \quad , \quad \beta = \frac{1}{k_B T} \tag{2.12}$$

were $N(q)$ is the probability that the system is in the microstate i with energy E_i. The numerator is called Boltzmann factor and the summation in the denominator is the normalization factor called the partition function of the system: $Q(N,V,T)$. From the partition function all the thermodynamic information on the system can be obtained, as the Helmholtz free energy can be directly computed as a function of N, V and T [Pathria, 1996]:

$$A(N,V,T) = -k_B.LnQ(N,V,T) \tag{2.13}$$

However, $Q(N,V,T)$ can only be calculated exactly for a limited number of systems such as the ideal gas.

Similarly, the microstate density in other ensembles can also be calculated. For example, in the *Grand-canonical*, or *μVT ensemble*, where the volume, temperature and chemical potential μ are constant, the density of microstates is, in absence of electromagnetic fields:

$$N(q,N) = \frac{V^N}{3^N N!} \frac{exp\,(\beta\mu N_1 - \beta E_1)}{\sum_j exp\,(\beta\mu N_1 - \beta E_1)} \tag{2.14}$$

where Λ is the thermal de Broglie wavelength:

$$= \frac{h}{\sqrt{2\pi.mkT}} \tag{2.15}$$

Being h the Plank's constant ($6.626_x 10^{-34}$ J s).

Here the number of particles, N, can fluctuate but the chemical potential μ, remains constant as well as the volume, V, and the temperature, T. To study the adsorption properties the grand-canonical ensemble is a natural choice. By varying the chemical potential, which is related to the system pressure by an equation of state [Valderrama and Vargas, 2003; Wagner and Pruss, 2002], one can obtain a local adsorption isotherm for a given structure. The interactions between the particles of the adsorbate in the pore model, and between the gas and particle pore wall can be evaluated by long and short range potentials [Frenkel and Smit, 2002; Prausnitz et al., 2000]. To compute this property the use non-physical trial moves, such as the insertion and deletion of particles is needed in order to change the number of particles in the system.

To calculate a property of the system it is necessary to average the value of that property over all the possible microstates. For example, if A is the property we would like to measure in a canonical ensemble and <A> its average value, we need to calculate:

$$\langle A \rangle = \frac{\int A(X^N) exp\left(\frac{v(r_{ij})}{kT}\right) dX^N}{\int exp\left(\frac{v(r_{ij})}{kT}\right) dX^N} = \frac{\sum_i A.\,exp\,(-\beta E_1)}{\sum_i exp\,(-\beta E_1)} \tag{2.16}$$

The ergodic hypothesis states that this time averaging equals the previous ensemble averaging [Pathria, 1996]:

$$\langle A \rangle = \lim_{t \to \infty} \frac{1}{t} \int A(q, v).\,dt \tag{2.17}$$

Time averages corresponds to Molecular Dynamic methods (integration of Newton's equations of motion,). Instead, averages over microstates can be computed efficiently using Monte Carlo methods.

2.2.2. Monte Carlo

The Monte Carlo (MC) method is a technique for computing ensemble averages of macroscopic system properties, such as pressure, volume, temperature, etc. These techniques rely upon stochastic methods, in particular on importance sampling methods [Leach, 2001]. One attractive aspect is that only energies rather than forces are evaluated during configurational sampling. In the MC method, system configurations are generated with a probability proportional to their statistical weight, and the weight of a configuration is proportional to Boltzmann factor, in turns. Based on repeated random samplings, the methods are able to generate states of low energy (thus most probable), enabling properties to be calculated correctly.

MC methods are extensively used for complex molecules constructions, in systems where the temporal evolution is not significant for properties calculation, or in all cases where molecular dynamics could fail due to the complexity of the system, or to prohibit long required calculations.

The main problem is that the number of microstates is usually too large to be computed (it would take beyond the lifetime of the universe using all computers in the world). In addition, for most systems only a small fraction of the microstates has a Boltzmann factor different from zero [Frenkel and Smit, 2002]. Molecular simulations can only describe a limited number of atoms, usually in the order of a few thousand, or hundreds of thousands with highly optimized codes and supercomputers, within the limit of a reasonable simulation time. To avoid these inconveniences, *periodic boundary conditions* are used. With this method, the volume containing the system is infinitely replicated in each direction of space depending on the dimensionality of the problem (see Figure 2.4).
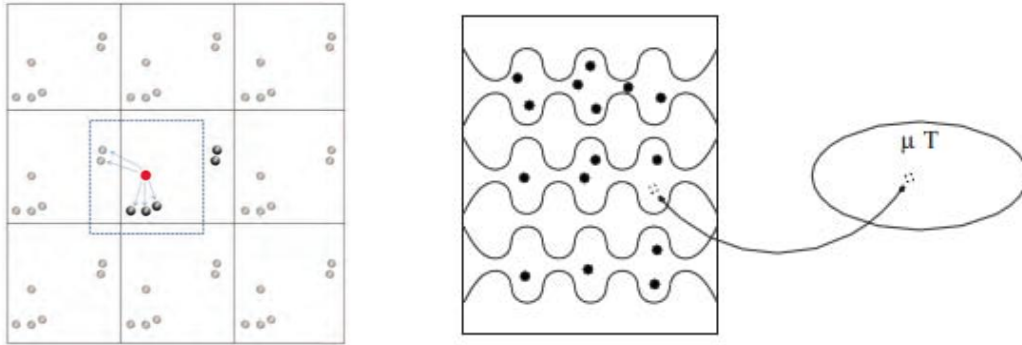
Figure 2.4. Schematic representation of the periodic boundary conditions and the Grand Canonical ensemble (the framework is in contact with a particle at a fixed temperature and chemical potential; guest molecules are exchanged between the crystal framework and the reservoir).

It is important to start a Monte Carlo simulation from a representative equilibrium configuration. However, a randomly selected or arbitrary configuration may be far away from typical configurations at equilibrium. Therefore, one should neglect the first part of the simulation and not consider these configurations for computing averages.

To effectively considerate significant states only, in the Metropolis method [Metropolis et.al., 1953], a Markov chain is generated. This satisfies these two conditions [Leach, 2001]:

1. The outcome of each trial depends only upon the preceding trial and not upon the previous trials;

2. Each trial belongs to a finite set of possible (acceptable) configurations.

Metropolis

The algorithm introduced by Metropolis [Rosenbluth and Teller, 1953], allows to generate the set of configurations according to a Markovian stochastic process.

The Metropolis MC Method is a process in which a random walk is constructed in such a way that the probability of visiting a particular system state is proportional to the Boltzmann factor *exp[−βUi]*. For such a sequence, the average property is still possible to estimate and becomes

$$\langle A \rangle = \lim_{n \to \infty} \frac{1}{n} \sum_{i=1}^{n} A(q(i), v(i)) \tag{2.18}$$

Starting from a certain configuration, a so-called trial move that changes the system state is performed. Depending on the energy difference and a random number, the new state is either rejected or accepted. The acceptance rule is constructed such as

the probability that the system is in a certain configuration is proportional to its statistical weight.

As seen in Figure 2.5, a typical simulation consists of the following, randomly selected, trial moves [Frenkel and Smit, 2002]:

• _Translation_. In this move, the position of the center of mass of a randomly selected molecule i in the system is displaced by a random vector:

$$x_i(n) = x_i(o) + \Delta(Random - 0.5)$$
$$y_i(n) = y_i(o) + \Delta(Random - 0.5) \tag{2.19}$$
$$z_i(n) = z_i(o) + \Delta(Random - 0.5)$$

where Δ is the maximum displacement and Random is a uniformly distributed random number between 0 and 1. The value of Δ has to be chosen to have a reasonable fraction of accepted moves. If Δ is very small, most displacements will be accepted, but this will lead to a very inefficient sampling of the phase space. If Δ is very large, most of the trial moves will be rejected. The optimum value of Δ depends on the characteristics of the interaction potential [Frenkel and Smit, 2002].

• _Rotation_. For molecules consisting of more than one interaction center, the rotational degrees of freedom of the molecule can be sampled by a random rotation. Either the x, y or z axis of the coordinate system can be selected as a rotation axis. For example, for a rotation around the z axis we will have:

$$r' = \begin{pmatrix} cos\Delta\theta & -sin\Delta\theta & 0 \\ sin\Delta\theta & cos\Delta\theta & 0 \\ 0 & 0 & 1 \end{pmatrix} . r \tag{2.20}$$

where r is the vector that contains the coordinates of a molecule, r' the coordinates after the rotation, and $\Delta\theta$ the rotated angle in a counterclockwise direction. The maximum rotation angle is chosen such that on average a 50% of rotations are accepted [Frenkel and Smit, 2002].

• _Insertion and deletion of molecules_. In the grand-canonical ensemble, the number of guest molecules present in the system is not constant. This ensemble is useful when we want to calculate adsorption isotherms in a porous material.

To obey detailed balance, the same procedure has to be applied to derive the acceptance rule for insert/removing a guest molecule. The difference is that the old configuration is now a randomly selected molecule of the system.

Once the movement has been made, intermolecular potential energy $v(X^N)$ is calculated along with the change in potential, $\Delta v = v(X^N) - v(X^M)$. If Δv is negative, then the move is accepted. If Δv is positive, then the move is accepted with probability.

The decision to accept or reject the motion in this case is to assign a random number ζ with a value in the range 0 to 1. If $\zeta \leq exp(v(r_{ij})/kT)$, the motion is accepted;

otherwise it is rejected [Frenkel and Smit, 2002]. If the status n is rejected, then the former state m is again taken as the new configuration of the series. This condition usually is summarized writing the probability of acceptance of a trial.

To be specific, from the state old o, m different new state n are accessible. The probability of leaving state o must be equal to that of entering state o. This leads to the detailed balance equation:

$$N(o) \sum_m |\alpha(o \rightarrow n) P_{acc}(o \rightarrow n)| = \sum_m |N(n)\alpha(n \rightarrow o)P_{acc}(n \rightarrow o)| \tag{2.21}$$

In the Metropolis Method, α is chosen to be a symmetric matrix, namely $a(o{\rightarrow}n){=}a(n{\rightarrow}o)$. As a result, the acceptance rule follows

$$\frac{P_{acc}(o \rightarrow n)}{P_{acc}(n \rightarrow o)} = \frac{N(n)}{N(o)} = exp\{-\beta[U(n) - U(o)]\} = exp\,(-\beta\Delta U) \tag{2.22}$$
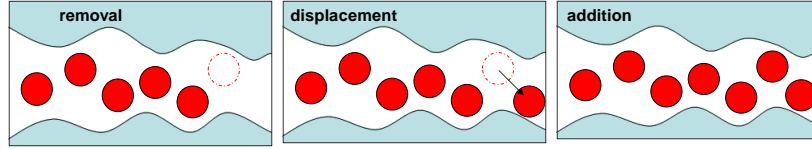
Figure 2.5. *Metropolis Monte Carlo movements*

In summary, the Metropolis Method works as follows:

1. Start from an initial configuration. For example, random positions can be generated for all N particles in the system.

2. Compute the total energy *U(o)* of the old state.

3. Make a trial move to a new configuration n by, for example, displacing one of the particles at random.

4. Compute the total energy *U(n)* of the new state.

5. Accept this trial move with the probability.

6. Sample ensemble averages.

7. Repeat this procedure from step 2 many times until the system reaches equilibrium.

The strength of the MC method lies in its capability to calculate statistical averages without explicitly sampling the entire partition function. The capability to deal with complex variation in spatial and energetic variables is what makes MC such an attractive method.

2.2.3.   Molecular Dynamics

Molecular Dynamics (MD) is a method for computing equilibrium and transport properties of a classical many-body system. MD simulates the time evolution of molecules by solving Newton's equation of motion, allowing calculating structural and thermodynamics properties. Since the calculations are interested in the time evolution of the particle, the equation can be expressed in terms of displacement r with respect to time t.

$$\frac{F_i}{m_i} = \frac{d^2 r_i}{dt^2} \tag{2.23}$$

The trajectory of the system can be obtained by integrating over several finite difference schemes. In particular, the Verlet algorithm is probably most widely. Using a Taylor expansion, the velocity Verlet algorithm can be easily derived:

$$r(t + \Delta t) = r(t) + v(t)\Delta t + a(t)\Delta^2 t \tag{2.24}$$

The time step Δt is chosen such a way that the integration is accurate enough and the total energy of the system is conserved. The average properties of the system can be determined from the trajectory obtained over a sufficient period of time.

This method can be used to study the diffusion of guest molecules inside adsorbent materials. In general, transport diffusion is the process in which an initial non-uniform concentration profile is smoothed by molecular motion. The typical diffusion coefficients calculated with MD are the transport diffusivity and the self-diffusivity: the first one describes the diffusive motion of single molecules, while the transport diffusivity describes the transport of mass and the decay of concentration fluctuations.

The advantages of this algorithm is that it is very simple to implement, the error in the calculation of the positions is of order four in Δt, and it is time reversible just as Newton's equations.

2.2.4.   Molecular interaction potentials (Force Fields)

Both MD and MC techniques use interaction potentials for the calculation of the energy. The term force field refers to the functional form and parameterization used to describe this energy U of a system of interacting molecules.

Force fields are usually derived from experiments and quantum mechanical calculations [Vlugt et al., 1998]. There are many different force fields available in the literature. They differ in (i) the functional forms used to describe the interaction and (ii)

the parameters used to describe the functional forms. In the majority of cases, the parameters values are specific for a certain system, instead of being suitable for many different systems. So in this case is necessary to have transferable force fields that can be extended to different phases or configurations.

The particular expression depends on the model used to represent the atoms in the system. The total energy of the system U^{total} is separated in two parts, bonded interactions between linked atoms, and non-bonded interactions between non-linked atoms.

In a classical force field based approach, the atoms interact through a series of forces like bond stretching, bond bend and dihedral torsion, and through interactions between non-bonded atoms such as van der Waals and electrostatic interactions. Those forces can be written in term of potential energy functions.

The sum of the different contributions to the potential energy is the potential function:

$$U^{total} = U^{bonded} + U^{non-bonded} \qquad (2.25)$$

$$U^{bonded} = U^{bond} + U^{bend} + U^{torsion} \qquad (2.26)$$

$$U^{non-bonded} = U^{LJ} + U^{elect} \qquad (2.27)$$

Sometimes, more sophisticated functions such as improper torsions, hydrogen bonds, polarizability and cross terms are used.

There are three main components of intramolecular interactions: angle bending, is the interaction of two atoms which are bonded to a common atom; bond stretching, describes a bond between two atoms; and dihedral angle, describes the interaction arising from torsional forces in molecules

Obtaining adequate values for the parameters of these equations can be achieved by two different means: by adjusting the parameter to experimental data such as liquid and vapor densities, heats of adsorption, dipole moment, or heat of vaporization; or by using parameters derived by quantum mechanical studies fitted to different conformations of a structure.

Non-bonded interactions: The non-bonded interaction term describe how the molecules and atoms interrelate with each other through forces that are not due to chemical bonds. These interactions play an important role in determining the structure of adsorbed molecules and evaluation of their energies.

Usually these expressions are distance dependent equations with parameters to model the behavior of the specific interaction between pairs of atoms. The potentials generally consist of two parts, a contribution of electrostatic origin and another contribution corresponding to the dispersive interactions between molecules, i.e. a Lennard-Jones (LJ) potential.

i) van der Waals interactions

The force of attraction between adsorbate and solid adsorbent is due to instantaneously fluctuating electric dipole moments in the adsorbate and the surface of the adsorbent, while the repulsive force arises from the penetration or overlap of the electron cloud between adjacent molecules and surfaces.

Both attractive dispersive and repulsive forces of the two isolated atoms are frequently combined to give the total potential energy or Lennard-Jones [Rouquerol et al., 1998].

$$U(r_{ij}) = B_{ij} \sum_j r_{ij}^{-12} - C_{ij} \sum_j r_{ij}^{-6} \tag{2.28}$$

In Eq. (2.34), the attractive r^{-6} part of the LJ potential corresponds to dispersive van der Waals interactions, while the repulsive part r^{-12} represents the repulsion of two atoms at short distances. From the surface plane; r_{ij} is the distance between i and an atom j, in the solid and B_{ij} and C_{ij} are characteristic repulsion and attraction constants for the gas-solid system. Figure 2.6 shows that the potential energy of a physisorbed atom varies as a function of the distance z from the surface of the adsorbent. With a larger z, the potential energy reduces as the attractive force decreases. With a smaller z, the potential energy increases rapidly due to the adsorbate-adsorbent force becoming repulsive. Once the atom moves closer to the surface of the adsorbent, the balance between the attractive and repulsive forces may be established at distance z_e. At this distance z_e the potential energy of the atom or ion is at a minimum.

The most common form to express de LJ interactions is by using the 12-6 model, as follows:

$$U_{LJ}(r_{ij}) = 4\varepsilon_{ij} \left[\left(\frac{\sigma_{ij}}{r_{ij}} \right)^{12} - \left(\frac{\sigma_{ij}}{r_{ij}} \right)^{6} \right] \tag{2.29}$$

where σ is the LJ size parameter, and ε is the potential well depth at a separation distance of $r_{min} = 2^{1/6}\sigma$, so $U(r_{min}) = -\varepsilon$. The parameters ε and σ are specific for every kind of atom and they must be known to carry out a molecular mechanic calculation.
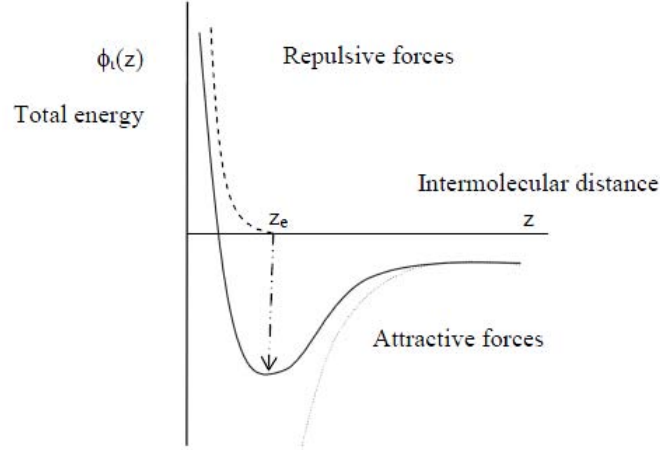
Figure 2.6. *Lennard-Jones potential as a function of the distance of the molecule to the solid surface (contribution of repulsive and attractive forces).*

The interactions between same atoms species (framework-framework, adsorbate-adsorbate or cation-cation interactions), are often defined by reproducing the critical values and adsorption isotherm. For the interactions between different atoms (adsorbent-adsorbate), the Lorentz-Berthelot mixing rules [Ungerer et al., 2005] are usually computed:

$$\varepsilon_{ij} = \sqrt{\varepsilon_{ii}\varepsilon_{jj}} \quad and \quad \sigma_{ij} = \frac{\sigma_{ii} + \sigma_{jj}}{2} \tag{2.30}$$

Moreover, as the potential rapidly vanishes for large distances, it is usually truncated and shifted at a certain *cutoff radius* r_{cutoff}. This will significantly increase the computational efficiency.

$$U^{LJ}_{shift}(rij) = \begin{cases} U^{LJ}(rij) - U^{LJ}(r_{cutoff}) & r_{ij} \leq r_{cutoff} \\ 0 & r_{ij} > r_{cutoff} \end{cases} \tag{2.31}$$

The typical cut-off distance of the LJ potential is usually chosen as $r_c \geq 2.5\sigma$. Thus, the length of the simulation box needs to be at least twice as large as the cut-off distance.

ii) Electrostatics

The electrostatic interactions are written using the classical Coulomb potential:

$$U_{elec}(r_{ij}) = \frac{1}{4\pi\varepsilon_r\varepsilon_0}\frac{q_i q_j}{r_{ij}} \tag{2.32}$$

where ε_r is the electric constant of the medium where the charges are placed, ε_0 is the permittivity in the vacuum (8.85_x10^{-12} C^2 s^2 kg^{-1} m^{-3}), q_i and q_j are the charges of the interacting atoms and r_{ij} the distance between the atoms i and j.

As the polarization effects are often neglected, the partial charge on a certain atom is constant. The magnitude and distribution of the partial charges in a molecule are chosen such that the dipole or higher order moments of the molecule taken from quantum mechanical calculations are reproduced.

Compared to the LJ potential (r^{-6}), the range of the electrostatic interaction (r^{-1}) is much larger. Due to the long-ranged nature of electrostatic interactions, simple truncation cannot be used [Allen and Tildesley, 1989; Frenkel and Smit, 2002]. Electrostatic interactions are more difficult to calculate than the van der Waals interaction because the integral of the interaction potential over volume is diverging. The coulombic interactions are usually calculated using the Ewald sum method [Allen and Tildesley, 1989; Frenkel and Smit, 2002]. This methodology was introduced in 1921 as a technique to add long-range interactions between particles and their infinite periodic images [Ewald, 1921]. This method is a very accurate way to calculate the electrostatic potential in the system with periodic boundary conditions [Frenkel and Smit, 2002], however, a considerable computation time is consumed in calculating the Fourier-space part of the Ewald summation.

The van der Waals term and the electrostatic terms must be calculated carefully. The real-space part of the Ewald summation and the conventional Lennard-Jones interactions can be calculated simultaneously using the same cut-off radius.

Note that these interactions terms are zero only when the distance between atoms is infinite. As a consequence, all atoms in a finite system interact with each other, which has a large computational cost. The easiest way to solve this problem in the van der Waals interactions is to shift and integrate them beyond a certain distance between a pair of atoms, only considering the particles whose distance to the interaction center is less than the cutoff radius r_{cutoff}, therefore it is only necessary to consider the nearest periodic image of *j* to *i*. This is called the *nearest image convention* [Allen and Tildesley, 1989; Frenkel and Smit, 2002].

2.2.5. Molecular Models

Structures

Crystalline structures such as zeolite and MOFs, are completely described in terms of their unit cell and their space group. Their atomic structures can be resolved from different diffraction techniques, X-ray absorption near edge structure (XANES) or

nuclear magnetic resonance (NMR), being the X-ray diffraction the most common technique.

The structure is often modeled using the periodic boundary conditions (see Figure 2.4). The original simulation box is replicated throughout space, and during the simulation, the molecules in all periodic images move in the same way as the ones in the central box. If a molecule leaves the central box, it will enter the central box from the opposite side.

In molecular simulations, it is often assumed that the materials are rigid. In this case, the positions of the framework atoms are fixed at their crystallographic positions during simulations. In this way, the computation of the interaction between the framework and the guest molecules can be considerately simplified by using grid interpolation techniques. However, in some cases, the flexibility may be of importance. For example, the diffusion of molecules in zeolites may depend strongly on framework flexibility, while for adsorption of small molecules flexibility is not important.

The model to describe flexible structures consist on different bonded potentials between the atoms and the framework, as well as non-bonded interaction (as already mentioned). The most common bonded potentials considered are: bond stretching, bond bending, bond bending coupling, torsion and switching function to avoid discontinuities. In our study we only consider rigid structures. Although some flexible models have been proposed for some types of MOFs, developing such models is very time consuming and is beyond the scope of this work.

Adsorbed guest molecules

The molecules are represented as a set of spheres of different sizes and masses, connected by springs of different lengths continuously. In the classical approach, polyatomic molecules can be described by either the all-atom model or the united-atom model. In the all-atom model, each atom is considered as an interaction site. In the united-atom model, a group of atoms are represented by a single interaction site. For example, the united-atom model is often used for CH_2, CH_3 and CH_4 groups of alkanes where the hydrogen atoms are usually not modeled as separate interaction sites. The all-atom approach takes into account the molecular geometry and structure more realistically. However, as the number of interaction sites can be much larger, simulations could be computationally more intensive.

In this work we only use atomistic, classical models of atoms and molecules. In these models, one atom or set of atoms is represented by a single interaction center called *pseudo atom* (the center of dispersive interaction) and may carry a partial charge. Pseudo atoms are linked by rigid or flexible bonds in such a way that their geometry

resembles the geometry of the molecule. In some cases, models may include pseudo atoms that do not correspond to actual atoms in order to better describe some properties of the real molecules, such as the quadrupole moment. The bonded interactions are easily fitted from quantum chemistry calculations, while the non-bonded interactions between guest molecules are fitted to reproduce specific properties, such as the vapor-liquid equilibrium curve (VLE), the liquid density, or the location of the triple point.

3

GENERAL CONSIDERATIONS ON CO₂ CAPTURE AND SEPARATION

3.1. Introduction

The sharply rising level of atmospheric carbon dioxide resulting from anthropogenic emissions is one of the greatest environmental concerns facing our civilization today. These emissions, which stem predominantly from the combustion of coal, oil, and natural gas are projected to continue to increase in the future due to economic growth and industrial development. Although the transition of the existing infrastructure from carbon-based sources to cleaner alternatives would be ideal in this regard, such a change requires considerable modifications to the current energy framework, and many of the proposed technologies are not yet sufficiently developed to facilitate large scale industrial implementation.

Thus, CCS technologies that efficiently capture CO_2 from existing emission sources will play a vital role until more significant modifications to the energy infrastructure can be realized. Nevertheless, these systems must capture CO_2 from flue gas in an efficient, reversible fashion, and as will be discussed, the use of novel materials exhibiting the right properties for performing CO_2 capture is an area requiring urgent development.

In this regard, the most significant challenge for CO_2 capture at present is the large energy penalty associated with the capture process. With current technologies, approximately 70% of the cost of CCS is associated with the selective capture of CO_2 from the power plant flue gas, being the high cost primarily emerged from the large energy input required for regeneration of the capture material.

Other scenarios of CO_2 capture, such as natural gas processing (CO_2/CH_4 separation), capture from transportation emissions, or direct air capture, are also highly important areas of research.

3.1.1. Current uses of CO_2

It is well known in the oil industry that carbon dioxide can be applied to reservoir as a tertiary oil recovery method. However, besides the CCS technologies, whether gas, liquid or solid ("dry ice"), CO_2 has a vast number of applications in very different industries, such as [Vega, 2010]:

- Food and beverage: CO_2 is used as a key cryogenic agent in cooling, chilling and freezing applications −protecting the taste and texture of the food products by maintaining proper temperature control. CO_2 also reduces the need for preservatives in packaged products, and is an essential ingredient in carbonated soft drinks and soda water.

- Solvent: Liquid CO_2 is considered as a good dissolving agent for many organic compounds. For instance, it can be used to remove caffeine from coffee.

- Healthcare: used for insufflations and is often combined with oxygen or air as a respiratory stimulant to promote deep breathing (in order to stabilize the O_2/CO_2 balance in blood).

- Pressured Gas: It is used as the cheapest noncombustible pressurized gas. Compressed CO_2 gas is used in paintball markers, air guns, for ballooning bicycle tires, fire extinguishers, etc.

- Fumigation: Used as a fumigant to increase shelf life and remove infestations

- Pulp & Paper: used to control pH levels, enhance pulp yield and wash brownstock and bleached stock.

- Water & Wastewater Treatment: A safe alternative to mineral acids, carbon dioxide replaces chemicals used in pH reduction, lowering costs and improving plant safety and flexibility.

- Welding & Metal Fabrication: Carbon dioxide is most often mixed with argon as a shielding gas used to prevent atmospheric contamination of molten metal in electric arc welding processes. It is also used in the manufacture of casting influences so as to enhance their hardness.

- Chemical Industry: It is used as a raw material, especially for the production of urea and methanol.

3.2. Technologies for CO₂ capture

Exploring cost-effective and scalable technologies and methods for CO_2 capture from power generation and industrial operation where CO_2 is produced on the combustion of fossil fuels is regarded as the most effective strategy in controlling anthropogenic CO_2 emission. Depending on the generation of CO_2, several capture options and tendentious technologies have been suggested and implemented. Generally, based on the fundamental chemical process involved in the combustion of fossil fuels, three basic CO_2 separation and capture options were adopted: (1) post-combustion capture; (2) pre-combustion capture; and (3) oxy-fuel combustion. In this context, there are three main scenarios under which new materials could serve to reduce the energy requirements of capture, as illustrated in Figure 3.1.

Post-combustion:
(CO_2/N_2, low pressure)
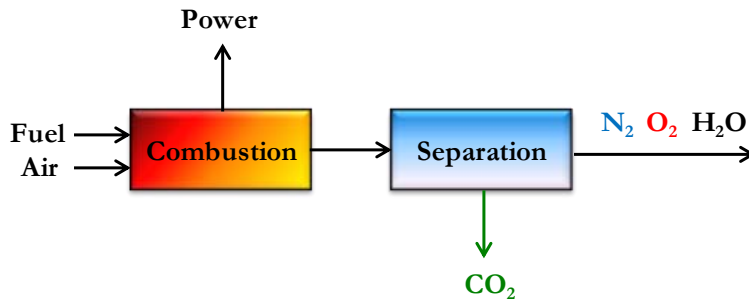
Pre-combustion:
(CO_2/H_2, high pressure)
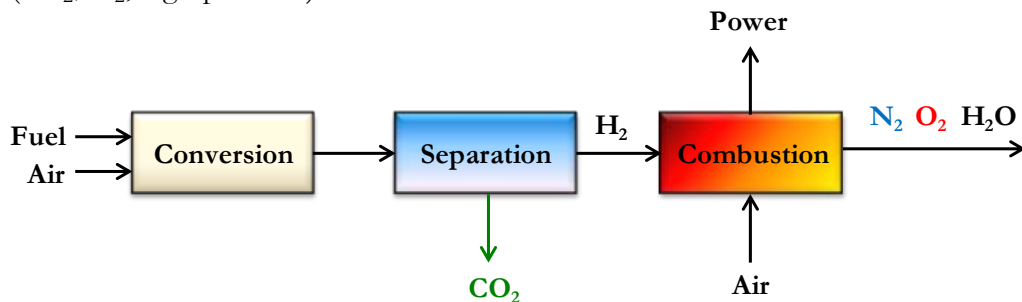
Oxy-fuel combustion:
(O_2/N_2, low pressure)
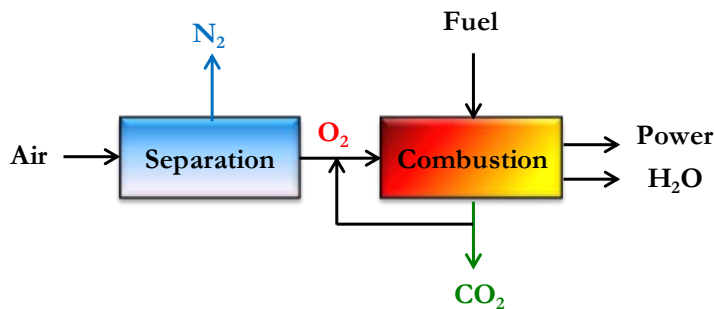
Figure 3.1. Scheme of three types/options for CO_2 capture.

- In post-combustion capture, CO_2 is removed from the flue gas that results after combustion of the fuel in air. This is predominantly a CO_2/N_2 gas separation owing to the high content of N_2 in the air used for combustion and has been the most explored strategy to date since a post-combustion CO_2 capture system could be readily retrofitted to existing power plants. An additional advantage of post-combustion capture is that even if when the CO_2 capture unit is shut down for an emergency, one can still generate electricity, which is not possible with the other more integrated capture methods. A further advantage of developing CO_2 separation techniques is their application in the purification of natural gas (mainly CH_4), which is typically soured with over 40% CO_2 and N_2 and is only useable at low concentrations of CO_2.

- Alternatively, pre-combustion capture can be performed following gasification of the coal prior to combustion, producing a high-pressure flue gas ("syngas") containing H_2 and CO_2. This carries the advantage of being an easier separation than the CO_2/N_2 separation required for post-combustion CO_2 capture, owing to the greater differences in the polarizability and quadrupole moment of the molecules. Once the CO_2 is removed from the gas mixture, the H_2 is then used for electricity generation, resulting in only H_2O as the byproduct. With regard to industrial applications, pre-combustion CO_2 capture systems based upon CO_2-absorbing solvents are the closest to being realized, and a number of power plants incorporating such systems are being constructed.

- Another possible method of reducing CO_2 emissions would be to perform oxy-fuel combustion, in which pure O_2 is utilized for the combustion of coal or natural gas. Oxy-fuel combustion refers to the ignition of pulverized coal or other carbon-based fuels in a nearly pure O_2 environment and represents a relatively new process for mitigating CO_2 emissions compared with pre-combustion and post-combustion CO_2 capture. In this case, an O_2/N_2 separation from air is performed, and the O_2 is diluted with CO_2 prior to combustion, leading to a flue gas that is a mixture of CO_2 and H_2O, which can be efficiently separated using existing technologies. The significant advantages of this process stem from the fact that the flue gas (following removal of particulates, water, and trace impurity gases) is almost entirely CO_2, which greatly simplifies the capture step, and that most existing power plants could be readily retrofitted. The main drawback for this option is in the large-scale generation of pure O_2 from air, since the purification is still challenging.

It can be noted that each of the three processes requires a different gas separation, and there is a need for an entirely different set of materials properties for each separation due to the different physical properties of the gases. This serves to highlight the importance of materials optimization, which will be essential in the development of next-generation separation materials.

Figure 3.2 schematically illustrates the technologies and method usually used in CO_2 separation; in each case, except for cryogenic separation, different materials are required as the carriers. Absorption (i.e. solvent scrubbing) is a well-established CO_2 separation approach used in the chemical and petroleum industries today. Absorption falls into two categories: (1) physical, which is temperature and pressure dependent (absorption occurs at high pressures and low temperatures) and (2) chemical, where absorption of CO_2 depends on the acid–base neutralization reaction (in this case caustic solvents are required). Some of the preferred solvents are amines (such as monoethanolamine), ammonia solutions and fluorinated solvents. The most recent

addition is ionic liquids, which have exhibited great potential in absorption of CO_2 and are also environmentally benign.
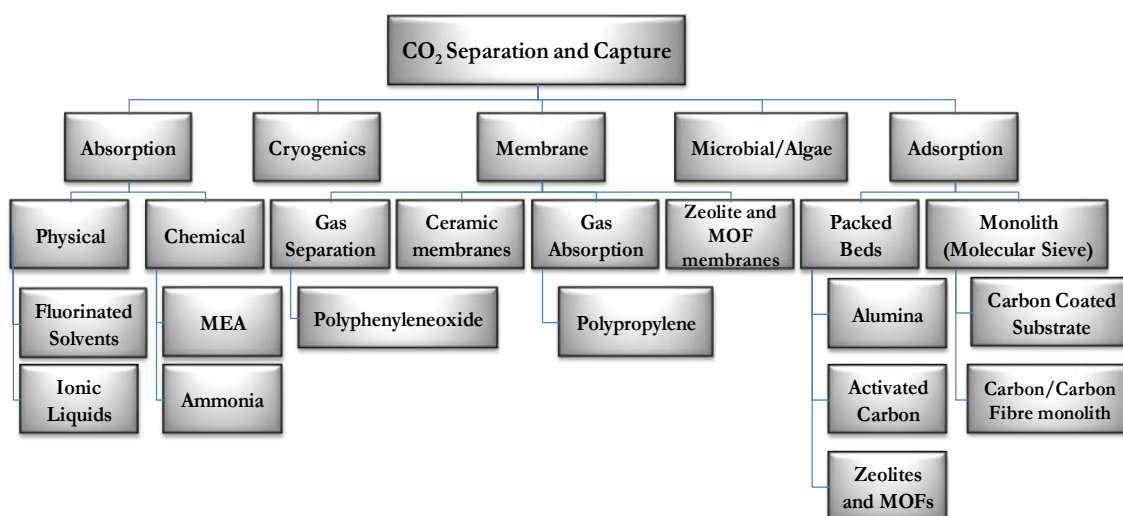
Figure 3.2. *Different technologies and associated materials for CO_2 capture.*

Cryogenic distillation uses a principle of separation based on cooling and condensation, and has been used in liquid separations for a long time. This technique is theoretically sound for CO_2 separation, however, the considerable energy demand deems it unreasonable for practical application. This method is more effective when the gas stream contains high CO_2 concentration and it can be adopted in oxygen production for oxyfuel combustion. It is presently the most widely used system for the large-scale production of O_2 from the separation of air.

Excellent separation performance can be achieved using MEA and other amines but the respective regeneration step is energy intensive. Due to the strong binding of CO_2 to the amines, the amine solutions have to be boiled to remove the CO_2 and regenerate the solvent. At a maximum amine concentration of about 30%, most of the energy is used to boil the water. In addition, the oxygen in the flue gas causes the amines to degenerate. At present, however, amine scrubbing is the only technology that is sufficiently advanced to be applied in CCS. Finding alternative technologies aimed at mitigating some of the disadvantages of these amine solutions is an active area of research which focuses on membrane and adsorption technologies.

Gas separation based on adsorption has been well developed, in which the selection of a fine adsorbent is the key for specific separation. Although materials for gas adsorptive separation have been established and a diverse range of useful adsorbents are available for CO_2 separation, there is still plenty of room to optimize the performance of these materials and investigate a wider range of new adsorbents. These

materials can then be combined with a broad range of process options yielding to the optimization of the separation performance.

3.2.1. Swing Adsorption Processes

In any CO_2 capture process, the adsorbent must be regenerated after each adsorption cycle. Regeneration of a solid adsorbent is typically accomplished by Temperature Swing Adsorption (TSA), Pressure Swing Adsorption (PSA), Vacuum Swing Adsorption (VSA), or some combination of these processes. In all cases, the solid adsorbent will likely be packed into a large fixed-bed column, and the adsorbate would be desorbed from the material by increasing the temperature (for TSA) or reducing the pressure (for PSA and VSA) of the bed.

Figure 3.3 illustrates the basic steps in an adsorption process. The starting point is a clean, regenerated bed. During the adsorption step flue gas flows through the bed and the CO_2 selectively adsorbs, leaving a N_2 rich exhaust stream. Once the bed is saturated the bed needs to be regenerated. This can be done by applying a vacuum and/or by increasing the temperature to conditions where the CO_2 desorbs resulting in a CO_2 rich stream for subsequent sequestration.
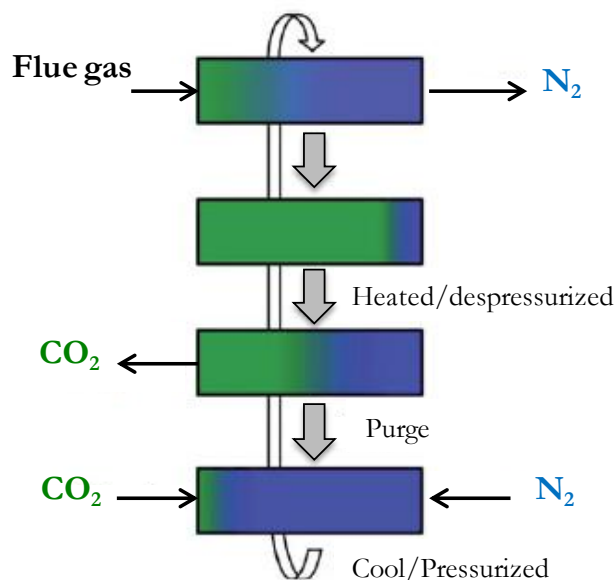
Figure 3.3. *Swing Adsorption Cycle scheme.*

In PSA, adsorption is typically performed at pressures higher than atmospheric pressure, while desorption is performed at atmospheric pressure. In VSA, adsorption operates at atmospheric pressure and near-room temperature and desorption operates

at lower pressures. Both PSA and VSA are performed by altering the pressures. Generally, the adsorbents with high adsorption capacity and high selectivity toward CO_2 are preferred.

In practice, several columns are operated in a swing-mode to make the process continuous and additional steps are added to the basic cycle, in order to maximize productivity and energy saving (as shown in Figure 3.4).
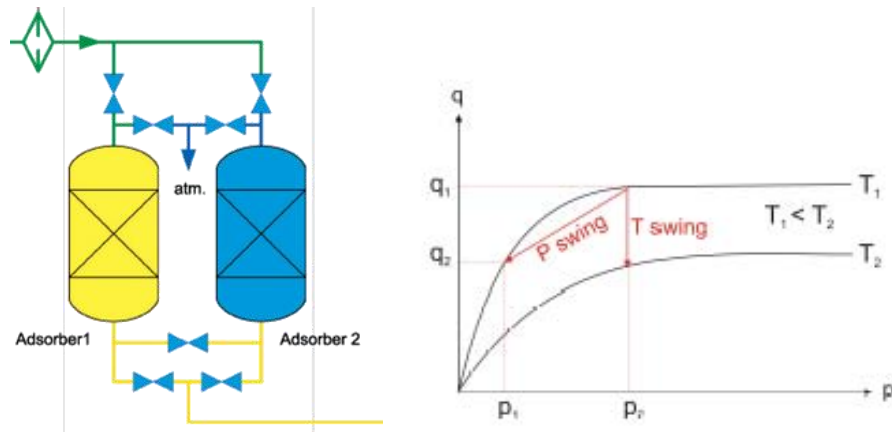
Figure 3.4. *The concept of PSA and TSA processes, related to the working capacity.*

Due to the possibility of using low-grade heat from the power plant as a source of energy for regeneration, TSA is particularly promising. Conversely, for pre-combustion capture, the gas stream is inherently pressurized after the conversion reactions, and a PSA cycle is expected to be most appropriate.

The CO_2 within the flue gas is selectively adsorbed along with other minor impurities of the mixture, and following a series of concurrent and countercurrent pressurization and depressurization steps, the adsorbed gases can be removed, and the capture material can be regenerated for subsequent CO_2 capture cycles.

In summary, a few technologies have already reached the deployment stage, but most require further improvements to the technical capabilities and reduction in the associated costs. The most mature technology, post-combustion amine absorption, has been employed in industry for a long time. Simultaneously, a number of materials are available for different technologies and some new materials are emerging. However, the commercialization of any one these technologies still faces substantial challenges not only in the final technological and processes aspects but also in the capabilities of the capture materials themselves.

3.2.2. Other considerations

- **Raw materials cost:** The low cost of natural materials such as zeolites is often cited as a major incentive for their use. Although the raw material cost is "low," the adsorbent is shipped to a processing site where it must be at least calcined, sized and packaged prior to use in any gas separation application. The useable adsorbent yield from the mined material may be only 50–75% due to water evaporation and over/under-sized waste. Thus, the final cost of these adsorbents will be 60% higher than 13X and more than 10 times higher than the original raw material cost.

Although each application must be judged on its own merits, this example shows that the "low" cost of natural zeolites does not necessarily result in a lower adsorbent cost for a gas separation [Wenning, 1996].

- **Human risk:** Finally, the potential human health risk from the inhalation may discourage the use of novel adsorbents. That is the case of fibrous erionite and mordenite [Doskocil and Davis, 1999; Siriwardane et al., 2003], which generally have greater thermal stability and better resistance to acid environments than many common commercial synthetic ones [Khelifa et al., 2001; Coughlan and Kilmartin, 1975; Gallei and Stumpf, 1976].

3.3. Computational Approaches for CO₂ Adsorption and Separation

Another important component to this area of research are the computational simulations, which have been widely used to evaluate CO_2 capture and have produced a vast amount of publications including several reviews [Li et al., 2012; Jiang et al., 2011; Guillem et al., 2014; Dogru et al., 2011; Han et al., 2008]. Compared with experiments, molecular simulations are much faster to be used to explore some materials for their optimized performances, such as in CO_2 uptake, selective adsorption and separation. Computational studies related to the adsorption of CO_2 within adsorbent materials [Moellmer et al., 2010; Cheon et al., 2009; Zelenak et al., 2010; Wu et al., 2012; Yazaydin et al., 2009; Bae et al. 2009; Dubbeldam et al., 2007] are an important endeavor in supporting the experimental work performed in the area. In this regard, GCMC simulations have been especially employed in predicting the single and mixed-component adsorption isotherms [Torrisi et al., 2010; Babarao et al., 2010; Wu et al., 2010].

The underlying information required in simulation are molecular interactions, which determine the reliability and accuracy of the simulation results. Together with a

robust code and an appropriate force field for molecular interactions, simulation can be performed using either the MC or MD method [Liu and Smit, 2010; Valenzano et al., 2011; Grajciar et al., 2011].

In particular, GCMC has been recognized as one of the most extensively used techniques to study gas adsorption properties, being well-suited to calculate thermodynamic properties for adsorption in nanoporous materials [Babarao et al., 2011; Frost et al., 2006; Han and Goddard, 2008; Deng et al., 2004; Frenkel and Smit, 2002; Ramsahye et al., 2007; Iwai et al., 1997], as well as Henry's constant, isosteric heat and binding energies. With a series of simulations at different pressures, the adsorption isotherms can be obtained by relating the chemical potential and gas phase pressure through an equation of state (see chapter 5 in this dissertation).

GCMC simulations can be used not only to evaluate the adsorption properties of simple gas; in the case of gas mixtures, but also to predict the selectivity. Since the selectivity is not easily accessible from experiments, GCMC simulations show a clear advantage to predict gas mixture separations.

To date, many GCMC simulations of gas adsorption on adsorbent materials have employed general-purpose force fields, including the universal force field (UFF) [Rappé et al., 1992] and DREIDING [Pottoff and Siepmann, 2001], which include the force field parameters for the atoms in most of the periodic table. Specifically for zeolites, both Watanabe and Calero's group have taken the lead on developing force fields to different structures, different Si/Al ratios and using different cations. [Watanabe et al., 1995; Garcia-Perez et al., 2008], In addition, because a wide range of possible inorganic (inorganic-organic) fragments are involved in novel MOFs, the force field parameters for these new fragments are not available or inaccurate in some cases, which limits the investigations in the screening and design for specific applications. For this, first-principle-based force fields are proposed to describe the interactions between adsorbate and adsorbent [Han and Goddard, 2008; Deng et al., 2004].

Conversely, MD has been employed to investigate the kinetic properties of gas molecules [Salles et al., 2010; Yang et al., 2008]. The kinetic properties, together with adsorption equilibrium properties are crucial to evaluate the overall performance of a material. Following Newton's second law, MD simulation imitates the natural pathway of molecular motion to sample successive configurations. The initial velocities of molecules at a given temperature are assigned by the Maxwell–Boltzmann distribution. At each time, the forces between molecules are calculated, then the equations of motion are solved numerically with a time step, and finally the velocities and positions are updated. In addition to thermodynamic properties that can be simulated, transport properties such as diffusivity and conductivity can be determined from the trajectory [Kulkarni et al., 2012; Fisher II et al., 2009]. In characterizing the diffusion of a single adsorbate, two most common quantities are the self-diffusion coefficient and transport

diffusion coefficient. The self-diffusion coefficient describes the displacement of individual gas molecules, while the transport diffusion coefficient quantifies the mass transport induced by a concentration gradient in the adsorbed species [Papadopoulos et al., 2004; Keskin et al., 2009].

One of the challenges in understanding the diffusion behavior is the little experimental information available in regard with molecular transport. Moreover, experimental measurement of mixture diffusion is extremely challenging, so these simulations can provide some precious information about transport properties of gas mixtures, which is very helpful in screening and designing materials for CO_2/N_2 separation [Haldoupis et al., 2010; Rasahye et al., 2008].

Another main molecular simulation techniques used for the investigation of CO_2 adsorption and separation are *ab initio* and density functional theory (DFT) calculations. These quantum mechanical modeling methods are normally implemented when detailed information regarding chemical and physical interactions is required (for instance, to describe molecular behaviors of atoms and molecules, where electrons are explicitly represented in the calculation, or to obtain accurate ground-state properties for real materials such as total energies and energy barriers) them [Ghoniem et.al., 2003]. During the past years, ab initio and DFT calculations have been employed extensively to study, for example, specific adsorption sites, interaction mechanisms, and interaction energies between a material and small molecules [Xu et al., 2010; Torrisi et al., 2010; Dubbeldam et al., 2007; Huang et al., 2007]. Furthermore, a number of DFT studies have emerged recently, [Wells and Chaffee, 2011; Walton et al., 2008] many focused on determining the packing arrangement of CO_2 molecules within the pores, the associated enthalpy of adsorption and the perturbation of these of the introduction of certain functionalities to the edge of the organic binders [Ghoufi et al., 2010].

4

LITERATURE REVIEW OF RECENT WORKS ON ADSORBENT MATERIALS FOR CO_2 CAPTURE AND SEPARATION

4.1. Introduction

Though various CO_2 capture technologies including physical and chemical absorption [Rochelle et al., 2009, Chiesa et al., 1999], adsorption [Chang et al., 2009], and membrane [Powell et al., 2006] exist, they are not matured technologies yet for post-combustion power plants. This is because that a huge amount of flue gas is needed to treat and significant mass transfer limitations exist in the processes. Because aqueous amine absorption processes exhibit some disadvantages such as low contact area between gas and liquid, low CO_2 loading, and severe absorbent corrosion, solid adsorption process may be an alternative to achieve the CO_2 capture purpose. Synthetic zeolites have served a prominent role in shaping the development of adsorptive process technologies for many of the separations and have been studied broadly from which a significant literature from both properties and applications [Ma et al., 2009; Bloch et al., 2010]. Though the rate-limiting step for adsorption as the diffusion of CO_2 from flue gas to the inside pore of a mesoporous adsorbent is about 3 orders of magnitude higher than that for aqueous amine absorption as the CO_2 mass transfer across the gas-liquid interface [Khatri et al., 2005], some existing problems including low CO_2 adsorption capacities at low pressures and influenced by water vapor and gases other than CO_2 still hinder the practical application of adsorption to capture CO_2.

The desirable characteristics for an adsorbent to separate CO_2 from N_2 and other gases includes *(i)* a high selectivity and good adsorption capacity for the target gas component, *(ii)* fast adsorption and desorption kinetics, *(iii)* good physical and chemical stability through the adsorption/desorption cycles, and *(iv)* be regenerable by modest pressure or temperatures leads to minimize operational energy costs. The selected adsorbent must also show robust performance in the presence of moisture and other contaminants that may be in the gas feed to the adsorption treating unit. The cost of the adsorbent and the bed packing density (which influences the adsorbent bed size) are further considerations. In several excellent reviews on CO_2 capture by adsorption [Xu et al., 2014; Sayari et al., 2011; Choi et al., 2009], it can be understood that to develop an appropriate CO_2 capture adsorbent should also satisfy (1) low-cost raw materials, and (2) low heat capacity.

There is a range of other physical, chemical, chemical engineering and solid mechanics criteria that must be fulfilled for a successful adsorbent/desorbent: composition, particle size, pore size and pore connectivity are all essential characteristics that affect the function of a CO_2 sorbent.

A typical combustion generates flue gas with a relatively low CO_2 concentration (15-16%), while the bulk of the effluent is composed of N_2 and other minor

components, such as H_2O, O_2, CO, NOx, and SOx [Rege et al., 2000]. Measurements at room (or slightly elevated) temperature and low pressure most resemble practical CO_2 capture, because of the low CO_2 component in the gas streams that need to be separated. Furthermore, the adsorption under room temperature and high pressure is directly related to the evaluation of the total CO_2 storage ability of an adsorbent material.

The preparation of a material that satisfies all of these requirements is currently a difficult synthetic challenge, although significant progress has been made in recent years. Quality is important in the manufacture of synthetic materials, and good product consistency is realistically attainable with modern production technology. Such reproducibility is important to attaining acceptable and sustainable levels of performance in gas separations [Plaza et al., 2007a].

Furthermore, the possibility of optimizing the parameters in each of the regeneration cycles (i.e., desorption temperature and pressure of inlet/outlet gas stream) and of combining multiple processes presents the option of tailoring the regeneration process to match the properties of a given adsorbent [Salles et al., 2008; Lee et al., 2008]. Above all, regeneration strategies must be designed to minimize the total cost of capturing CO_2, and as such, there will be a trade-off between maximizing the working capacity (the amount of CO_2 that can be captured in a given adsorption cycle) and minimizing the energy required for regeneration [Herm et al., 2011; Ishibashi et al., 1996; Mulgundmath et al., 2010]. While detailed analysis of the energy and economic optimization issues in CO_2 capture is beyond the scope of this dissertation, such efforts will be crucial in directing the optimization of real-world CO_2 capture processes.

4.2. Solid Porous Adsorbent Materials for CO_2 Capture

To achieve efficient adsorption-based CO_2 capture, the selection of an appropriate adsorbent is crucial. Commercial adsorbents being used to remove CO_2 from industrial gas streams include zeolites, activated carbons and titanosilicate molecular sieves. Another porous materials including metal oxides, alumino-phosphates, activated carbons, carbon nanotubes, silica gel, pillared clays and polymeric resins, among others, have been explored as adsorbents, and some of them have been implemented for various separations [Kulprathipanja, 2010; Loureiro and Kartel, 2006; Xu and Hedin, 2014].

Novel-structured materials developed over the past years that show potential for higher CO_2 capacities include adsorbents based on Metal-Organic Frameworks

(MOFs), Zeolitic Imidazolate Frameworks (ZIFs) surface functionalized silicas and porous carbons [Qiu et al., 2014]; Some of these materials are shown in Figure 4.1. Layered hydroxides and hydrotalcites have been studied extensively as sorbents for CO_2 capture from high temperature flue gases (600–700ºC) [Zhang et al., 2013]. These high temperature sorbents are not discussed further in this chapter because these temperatures are beyond the expected range of operating conditions for CO_2 removal units.

Zeolite

Activated Carbon
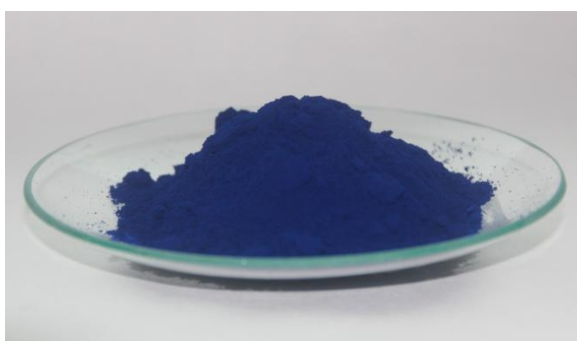
MOFs
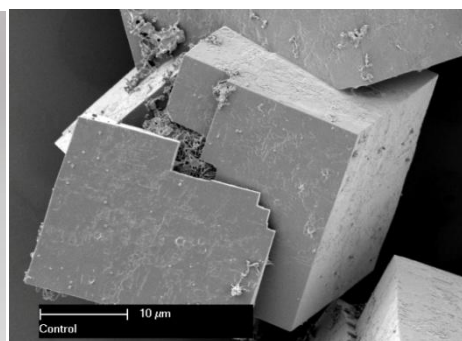
Aluminophosphate

Silica gel

Figure 4.1. Typical adsorbent materials.

The smaller kinetic diameter of CO_2 (3.3 Å) when compared to most other gases (except small molecules like H_2, He, Ne, H_2O, and NH_3) has established the method of

controlling the pore size of a material as a highly efficient way of achieving high CO_2 selectivity. This kinetic molecular sieving effect has been widely used in gas separations by using traditional porous materials [Duren et al., 2009]. Alternately, the advantage of the comparatively much higher quadrupole moment of CO_2 as compared to other gases can be taken to facilitate adsorptive separations, which usually leads to stronger adsorbate-adsorbent interactions and correspondingly higher uptake and selective adsorption [Li et al., 2012].

While initial experimental works in this area only tested general equilibrium adsorption isotherms, the more recent work has shifted its focus closer to practical application, including ultimate storage capacities, selective adsorption and separation of gases [Li et al., 2011].

Porous materials:

According to the IUPAC classification, porous materials are divided into three groups depending on the pore size: Materials with pores larger than 50nm are called macroporous materials. Mesoporous materials are the second group with pores from 2 to 50nm in diameter and microporous materials possess pores with diameters of less than 2nm.

Macroporous materials usually do not have a high specific surface area. The porous structure is rather used as carrier for other porous materials. The large pores enhance the performance as they allow high gas streams to pass through them with only minor pressure drops. Mesoporous materials possess high inner surface areas and are thus suitable for the adsorption of large molecules such as enzymes that cannot fit into micropores.

Until the late 1990[ies], two classes of microporous materials were dominating for separation and catalysis. Among them, inorganic materials and special microporous activated carbons. The class of inorganic porous materials can be subdivided into several groups, the most prominent of them being alumosilicates (zeolites) and aluminophosphates. Recently, the class of microporous materials was expanded by metal-organic frameworks (MOFs).

4.2.1. Activated Carbons

Activated carbons had attracted much interest as CO_2 adsorbents due to their wide availability, low cost and high thermal stability. These materials are amorphous porous forms of carbon that can be prepared by pyrolysis of various carbons containing resins, fly ash, or biomass [Sumida et al., 2012]. The relatively uniform

electric potential on the surfaces leads to a lower enthalpy of adsorption for CO_2, and hence lower capacities for CO_2 at lower pressures.

However, their significantly higher surface areas allow greater adsorption capacities at high pressures, which has resulted in activated carbons being considered for a variety of high pressure gas separation applications [Choi et al, 2009]. In the context of CO_2 capture, the high-pressure flue gas produced in pre-combustion CO_2 capture has been a major target application for these materials. Indeed, one study has shown that the upper limit for the CO_2 adsorption capacity within activated carbon materials is approximately 10-11wt% under post-combustion CO_2 capture conditions, while it reaches 60-70wt% under pre-combustion conditions [Martin et al., 2010]. A recent study has also demonstrated that careful selection of the material precursors and the reaction conditions employed can lead to carbon-based adsorbents that have a volumetric CO_2 adsorption capacity that is greater than some of the highest surface area MOFs at high pressure [Silvestre-Albero et al., 2011].

The weak CO_2 adsorption in the range of 50–120°C leads to high sensitivity in temperature and relatively low selectivity in operation. Moreover, consistent with the lower heat of adsorption, activated carbons require a lower temperature for regeneration. A further advantage is that their hydrophobic nature results in a reduced effect of the presence of water, and they consequently do not suffer from decomposition or decreased capacities under hydrated conditions [Plaza et al., 2010].

As a consequence, current research focuses on how to improve the CO_2 adsorption capacity and selectivity via two ways: (1) to improve surface area and pore structure of the carbonaceous adsorbents either using different precursors or fabricating different structures such as ordered mesoporous carbon [Saha et al., 2010], carbon nanotubes, graphene, etc.; or (2) to increase alkalinity by chemical modification on surface.

4.2.2. Zeolites

The lower heat capacities of solid porous adsorbents have led to investigation of new materials for CO_2 capture. In particular, as shown in Figure 4.2, zeolites are porous aluminosilicate materials that possess a high chemical and thermal stability [Cejka et al., 2010]. Zeolites have been studied especially in the context of upgrading of natural gas and CO_2 capture from post-combustion flue gas [Kusakabe et al., 1997; Cavenati et al., 2006; Himeno et al. 2007; Ghoufi et al., 2009].

Their packing structures allow the formation of regular cavities joint by the channels, where the molecules with an appropriate size such as carbon dioxide and the metallic exchangeable cations (Li^+, Na^+, K^+, Ca^{2+}, Ba^{2+}, Cu^{2+}, Zn^{2+}, Mg^{2+}, etc) can

penetrate and compensate for the negative charges created by the substitution of AlO_4 tetrahedron by SiO_4 tetrahedron [Bonenfant et al., 2008; Aguilar-Armenta et al., 2001].
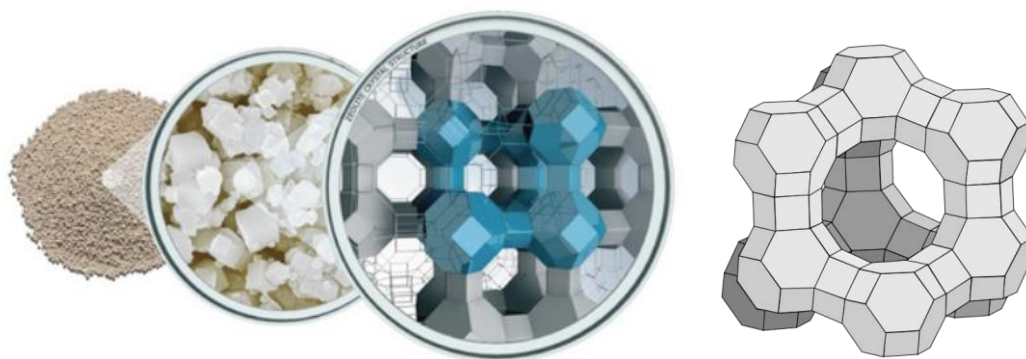
Figure 4.2. *Zeolite 13X.*

The adsorption efficiencies of zeolites are largely affected by their size, charge density, and chemical composition of cations in their porous structures [Wang et al., 2011]. Accordingly, a number of reports focus on zeolites with highly crystalline structure, high surface area and 3-dimensional pore structures by altering their composition as Si/Al ratio. Another research field focuses on the exchange with alkali and alkaline-earth cations in the structure of zeolites to enhance the CO₂ adsorption: highly charged species on the surfaces of porous solids can afford high affinities for CO₂ over other components of flue gas owing to the propensity for CO₂ to be polarized to a higher extent compared with N_2 (or other light gases like H_2) [Zhang et al., 2008].

Most of the known zeolites have a capacity of CO₂ adsorption at high pressures and low temperatures which varies from 0.15 to 5.5 mmol/g at 273–373K [Lee et al., 2002; Ko et al., 2003; Dunne et al., 1996; Khelifa et al., 2004; Pakeresht et al., 2002; Xu et al.; 2002]. For example, zeolite 13X, which has a relatively high surface area (S_{BET} = 726 m2/g) and micropore volume (0.25 cm³/g), has been shown to display promising capacities for CO₂ at room temperature (16.4wt% at 0.8bar and 298 K) [Wang and LeVan, 2009]. The large variety of structures [O'Keefe et al., 2008; Jiang et al.,2010] that have been reported to date present an opportunity for the study of the effect of composition, or certain structural or chemical features, on the adsorption performance.

As mentioned, the adsorption capacity depends on several factors including the size, polarizing power, distribution and the number of cations in their porous structure, Si/Al ratio, size, the form of their pores, the polarity and size of adsorbed molecules, the presence of water and other gas and presence of carbonates at their surface. Moreover, the distribution of exchangeable cations in the different sites of the structure causes the heterogeneous character of the CO₂ adsorption [Martin et al., 2010; Martra et al., 2002; Jacobs et al.; 1973].

It has also been shown that the adsorption capacity and selectivity of zeolites for the polar molecules increases when the Si/Al ratio decreases [Allan et al., 2010]. This effect is more important when the quadrupole moment of molecules is great. This phenomenon could be due to an increase of electric field in the zeolites pores induced by increasing number of charged sites present at the surface of zeolites, as shown in zeolite LTA, with crucial implications toward the adsorption selectivity and regeneration costs associated with the capture process [Duren et al., 2009].

In addition, the basicity of zeolites framework enhances with the content of Al^{3+} ions due to the presence of a greater amount of exchangeable cations [Laspèras et al., 1996]. Hence, at low pressure, the zeolites that possess the more small Si/Al ratios should have the best adsorption capacity and selectivity for the polar molecules such as CO_2.

Though CO_2 adsorption can be enhanced by these approaches, there exist several drawbacks: the CO_2 adsorption capacity greatly declines in the presence of moisture in gas because of their highly hydrophilic character, thus a high regeneration temperature is needed. Besides, since the CO_2 can also interact with the pore wall of zeolites, the CO_2 adsorption might be limited by the size of zeolites pores at high pressures because the CO_2–CO_2 interactions might prevent the adsorption of new molecules of CO_2 into the pore wall sites that are thus occupied by other molecules of CO_2 [Petit et al., 2012; Li et al., 2011; Karra et al., 2010]. Moreover, although natural zeolites are abundant and inexpensive, these attributes may not offset the effects of impurities and inconsistency of properties relative to the more uniform materials [Sand et al., 1978].

In the case of several cationic zeolites, the chemical adsorption of CO_2 is accompanied by the formation of carbonates at their surface, due to the interaction of CO_2 with the oxygen bridging aluminum and silicon atoms [Park et al., 2012; Wiersum et al., 2013; McEwen et al., 2013; Yang et al., 2013; Yu et al., 2013; Bastin et al., 2008], that might decrease the accessibility of carbon dioxide at a great part of the surface of zeolites and thereby contribute to limit its adsorption.

In comparison with post-combustion CO_2 capture, small-scale pilot plants using zeolites have demonstrated more rapid adsorption of CO_2 and lower energy penalty for the process than other traditional materials [Zhang et al., 2008]. However, compared to activated carbons, many of the zeolites studied to date become readily saturated with the water vapor present in the flue gas stream, and the CO_2 adsorption capacity is consequently reduced over time [Li et al., 2009a].

Furthermore, the large enthalpy of adsorption of CO_2 leads to relatively high CO_2 desorption temperatures (i.e. 135ºC) [Konduru et al., 2007]. This point highlights the importance of materials optimization for controlling the affinity of the pore surfaces, and while improved synthetic procedures that provide a greater degree of

control over the properties of the resulting zeolite have emerged, it still remains challenging to precisely tune the materials to the extent possible for MOFs [Li et al., 2011]. Nevertheless, the robust nature of zeolites coupled with their low cost and well-developed structural chemistry makes these materials an attractive target for use in CO_2 capture applications.

In addition to zeolites and carbon-based materials, other classes of porous materials are emerging as potential adsorbents in CO_2 capture applications, including amine-grafted silicas [Hicks et al., 2003; Xu et al., 2003; Jones et al., 2008] and covalent-organic frameworks (COFs) [El-Kaderi et al., 2007; Han et al., 2008; Glover et al., 2010; Dogru et al., 2011; Choi et al., 2011].

4.2.3. Amine-Impregnated/Grafted Adsorbents

Combining the high affinity of amines and the advantages of using a porous solid adsorbent holds tremendous promise for the development of new materials that exhibit appropriate properties for CO_2 capture applications (see Figure 4.3). Ordered mesoporous silica may be a candidate because of its high surface area, high pore volume, tunable pore size and good thermal and mechanical stability. So far mesoporous silicas including the families of M41S, Santa Barbara Amorphous type material (SBA-n), anionic surfactant-templated mesoporous silica (AMS), etc., have been reported [Sun et al., 2007].
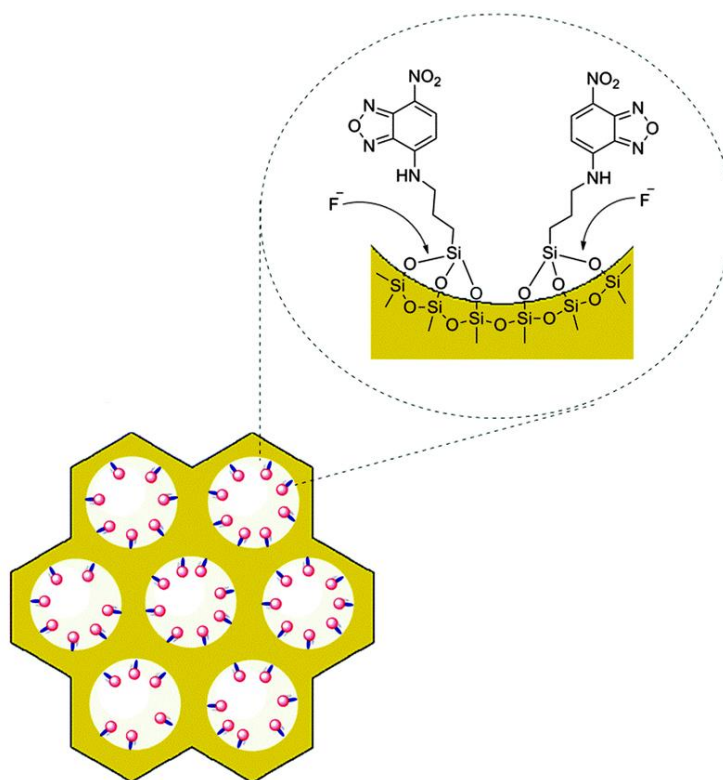
Figure 4.3. Mesoporous silica impregnated with amines.

According to the type of the interactions between amines and supports, the amine-based adsorbents can be categorized as amine-impregnated and amine-grafted materials via weak interactions and strong covalent bonding, respectively [Sayari et al., 2011]. Typically, the amine-grafted adsorbents exhibit comparatively higher adsorption rate and higher stability in cyclic runs than the amine-impregnated ones. However, the grafted amount of amine depends on surface silanol groups, sometimes leading to a comparatively lower amine loading as compared with the impregnated amount.

Impregnation or grafting of amines, alkanolamines, or alkylamines have been proposed to enhance the originally limited adsorption capacity and to promote the mass transfer rate of CO_2 into porous, or mesoporous adsorbents [Xu et al., 2002]. Besides, their use in the interior surfaces of activated carbons and zeolites are currently being surveyed experimentally [Plaza et al., 2009; Bezerra et al., 2011; Builes et al., 2012]: recently, activated carbons and zeolite 13X were loaded with MEA and TEA [Jadhav et al., 2007], founding that both materials exhibited selectivity for CO_2 over N_2, although the CO_2 capacity was decreased compared with the bare material owing to the lower surface area accessible to the gas molecules following installation of the amines.

The functionalization of pore surfaces, despite reducing the CO_2 capacity upon engrafting, shows strong interaction between CO_2 and framework with a higher CO_2/N_2 selectivity, especially at low pressure. The interaction between the acidic CO_2 molecules and modified basic active sites on the surface facilitates CO_2 adsorption through the formation of covalent bonding.

Amine-based adsorbents have widely been studied and exhibited the advantage as low heat of regeneration over aqueous amines due to the low heat capacity of solid supports [López-Aranguren et al., 2014]. However, the high cost and the CO_2 adsorption capacities are not high enough, especially at atmospheric pressure, to allow their practicability.

Leal and coworkers [Leal et al., 1995] firstly published the work on APS grafted silica gel for CO_2 capture. This APS grafted silica gel exhibited a CO_2 adsorption capacity as 0.41 and 0.89 mmol/g under an anhydrous and hydrous flow with pure CO_2 at 27°C, respectively. Huang and coworkers [Huang et al., 2007] studied CO_2 capture by the APS-grafted mesoporous silica MCM-48 and silica xerogel, obtained adsorption capacities at room temperature of 2.05 and 1.14 mmol/g under anhydrous condition. In a previous work [Leal et al., 1995a], APS, 2N-APS and 3N-APS were grafted onto MCM-41, SBA-15 and pore expanded-SBA- 15 [Chang et al., 2009], showing that SBA-15 was the most appropriate support because its pore size could accommodate more amines and avoid blocking during CO_2 adsorption. Besides, its high pore surface area providing large amount of silanol group was more beneficial for aminosilane grafting. Among the studied amines, 3N-APS exhibited the highest CO_2

adsorption capacity as 2.74 and 3.06 mmol/g at 40°C under anhydrous and hydrous (78%RH) flows containing 17%CO_2, respectively, followed by 2N-APS and APS.

The supports other than mesoporous materials to impregnate amines have also been reported in the literature. For instance, Song and coworkers reported the effects of polyethylenimine (PEI) loading, gas conditions, temperature, moisture and supports on CO_2 adsorption capacity for the PEI-impregnated mesoporous silica and carbonaceous materials [Wang et al., 2011; Jiang et al., 2011; Wang et al., 2009; Ma et al., 2009]. A higher PEI loading significantly enhanced CO_2 adsorption capacity together with the decreases of surface area, pore size and pore volume of the PEI impregnated supports. The highest CO_2 adsorption capacity of 3.02 mmol/g for the PEI-impregnated MCM-41 (PEI/MCM-41) with 75 wt% of PEI loading was observed under pure CO_2 at 75°C, while the highest amine efficiency (CO_2/N_2 molar ratio) occurred at 50 wt% PEI loading and was reduced with an increase of PEI loading. Thus, how to promote the performance of amine-impregnated adsorbent needs further studies.

4.2.4. Metal-Organic Frameworks (MOFs)

Metal-Organic Frameworks emerged approximately two decades ago and since then have allow a quickly development into a fruitful research field. MOFs are crystalline compounds consisting of metal ions or clusters (linker) coordinated to often rigid organic molecules to form one, two, or three-dimensional structures that can be porous. Figure 4.4 presents an schematic construction of these materials. In some cases, the pores are stable during elimination of the guest molecules (often solvents) and can be used for the storage of gases such as carbon dioxide.
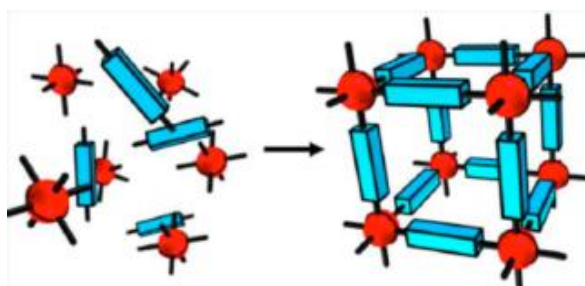
Figure 4.4. *Schematic construction of MOFs.*

The choice of metal and linker has significant effects on the structure and properties of the MOF. For example, the metal's coordination preference influences the size and shape of pores by dictating how many ligands can bind to the metal and in which orientation. The material selection has become a significant challenge because of

the large number of compounds reported each year. Some of the most typical structures are shown in Figure 4.5.

The high internal surface areas of MOFs provide an opportunity for large CO_2 adsorption capacities to be achieved, owes to the efficient packing and close approach of the guest molecules on the pore surface. Indeed, selected MOFs have recently been evaluated in detail for use in post-combustion CO_2 capture via TSA and a pre-combustion CO_2 capture via PSA [Plaza et al., 2009; Jadhav et al., 2007; Sayari et al., 2011]. For instance, at 35bar and 298K, the volumetric CO_2 adsorption capacity for MOF-177 reaches a storage density of 320 $cm^3(STP)/cm^3$ (e.g. 33.5 mol/L), which is approximately 9 times higher than the quantity stored at this pressure in a container without the MOF and is higher than conventional materials used for such an application, namely, zeolite 13X and MAXSORB [Jiang et al., 2007]. The authors ascribed this large CO_2 capacity to the large pore space enclosed in MOF-177.
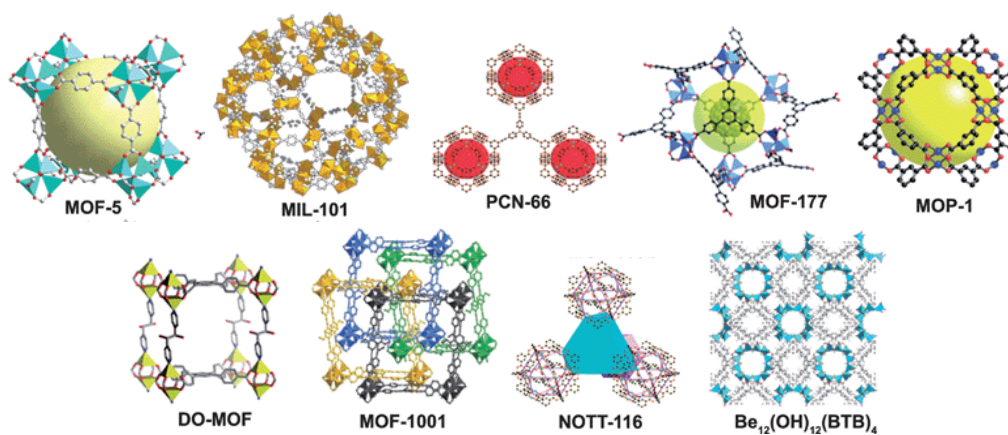
Figure 4.5. *Several MOFs structures.*

Millward and Yaghi [Millward and Yaghi, 2005] published a pioneering work in which CO_2 isotherms up to 42bar were reported for nine MOF materials, in order to examine a range of structural and pore attributes. Since then, several MOFs with high porosity and surface area have been examined for CO_2 storage, with the initial record capacity changing from MOF-177 to MIL-101 [Cooper et al., 2009]. MOF-210, synthesized again by Yaghi's group currently holds the CO_2 storage record with the saturated CO_2 uptake of 2400 mg/g at room temperature and up to 50bar [D'Alessandro et al., 2010]. This MOF has an estimated pore volume of 3.60 cm^3/g and a BET surface area of 6240 m^2/g, the highest reported for any crystalline material. It can be note that, as mentioned earlier, the volumetric adsorption capacity of activated carbon materials at high pressures has been demonstrated to be competitive with MOFs [Choi et al., 2009].

Usually, the CO_2 adsorption isotherms in rigid porous materials such as traditional zeolites and the majority of rigid MOFs present a normal type-I shape, but

in a few rigid MOFs stepwise isotherms have been observed. This can be related to the structural features of these MOFs, as for example, Zhang and coworkers reported a two-step CO_2 adsorption at low temperature in a highly connected MOF which has a biporous structure with cages and channels that co-exist [Llewellyn et al., 2008]. Conversely, several similar stepwise CO_2 adsorption behaviors, giving sigmoidal isotherms, have been observed in some ultrahigh pore MOFs, such as IRMOF-1 (MOF-5), MOF-177 and MOF-210 at near room temperature and high pressures [Jiang et al., 2007; D'Alessandro et al., 2010].

Several MOFs have been experimentally examined for single-component CO_2 adsorption and related gas separation. Zhou's group [Li et al., 2009; Zhou et al., 2011] reviewed the progress of MOFs for CO_2 capture from experimental to molecular simulation. In their review, MOFs exhibit exceptional CO_2 adsorption capacity to deal with pure CO_2 at high pressures. Their adsorption capacities are dramatically reduced when they are exposed to a gas mixture. Though MOFs have been shown to be the promising adsorbents for CO_2 capture in laboratory, more studies are required to verify their practical applications.

The concept of designing a MOF with a pore size between the kinetic diameters of CO_2 and other gases, thus allowing only CO_2 to pass, is easily understood, but designing and synthesizing such a pore in practice is tremendously challenging. In some cases, the actual pore size is larger than the sizes of all tested gases; however, only CO_2 adsorption is observed, which is usually attributed to a kinetic sieving effect. For example, Mn-$(HCO_2)_2$ has a porous framework structure containing cages with a diameter of about 5.5 Å connected to each other via small windows of about 4.5 Å [Banerjee et al., 2009]. This MOF showed almost no N_2 sorption at 78K but significant CO_2 uptake at 195K. This size-dependent and diffusion-controlled gas selective adsorption has been also systematically investigated in a series of ZIFs with incrementally tuned pore sizes [Mason et al., 2011].

Flexible MOFs have a different story in the selective adsorption of CO_2 over N_2. A "gate" phenomenon (see Figure 4.6) has been observed [Llewellyn et al., 2008; Furukawa et al., 2010; Banerjee et al., 2009; Zhang et al., 2009; Coudert et al., 2009; Kim et al., 2008]. An early example that clearly illustrates this "gate" effect is Cu(pyrdc)(bpp) reported by Kitagawa's group [Tanaka et al., 2008]. The CO_2 adsorption isotherm of this MOF shows a sudden increase at a relatively low pressure, referred to as the gate-opening pressure, and saturation at another pressure. Conversely, the desorption isotherm, does not retrace the adsorption isotherm and shows a hysteresis behavior.
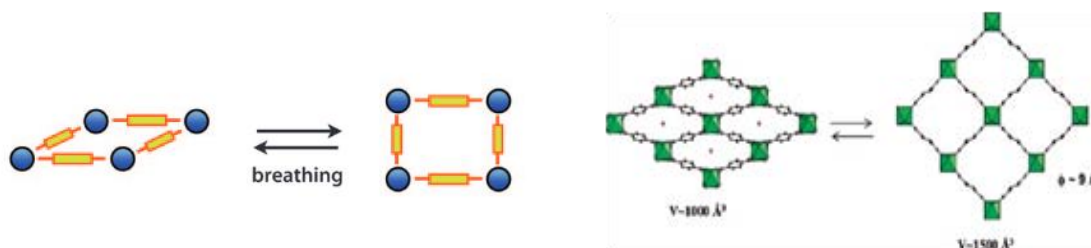
Figure 4.6. Example of gate opening in MOFs.

The impact on CO_2 adsorption in MOFs by various other factors has also been explored. Through the insertion of metal ions into a stable MOF, it was also observed the enhanced adsorption selectivity of CO_2 over N_2 in $(MOF-253)_3.0.97Cu(BF_4)_2$ as compared to MOF-253 [Ma et al., 2009]. Kajiro and coworkers [Maji et al., 2005] examined the effect of metal ions on the CO_2 adsorption in two isostructural structures, $M(4,4-bipy)_2(OTf)_2$ (M= Cu and Co). Although the difference in metal ions in these MOFs results in only slightly different structures, the gas adsorption properties, based on the expansion/shrinkage of these MOF structures, are largely dependent on the metal ions. As an alternative strategy, partial doping of MOF-5 with Co(II) by isomorphic substitution during synthesis has been investigated to explore the effect on CO_2 adsorption [Chun et al., 2009]. The adsorption result showed that the CO_2 uptake of these MOF-5-based materials systematically increases with the increase of Co(II) content at high pressure. Rosi and coworkers [An et al., 2010] recently demonstrated that post-synthetic exchange of extra-framework cations within an anionic MOF (bio-MOF-1) can be used as a means to systematically modify its pore dimensions, thereby, tuning the CO_2 adsorption capacity. In addition, Cao and coworkers [Xiang et al., 2011] recently showed that the incorporation of CNTs into MOFs can enhance the uptake of CO_2, which can be further improved by doping the CNT-modified MOFs with lithium.

4.2.5. Zeolitic Imidazolate Frameworks

Zeolitic Imidazolate Frameworks (ZIFs) are a class of Metal-Organic Frameworks that are topologically isomorphic with zeolites. ZIFs are composed of tetrahedrally-coordinated transition metal ions (e.g. Fe, Co, Cu, Zn) connected by organic imidazole linkers. Since the metal-imidazole-metal angle is similar to the 145° Si-O-Si angle in zeolites, ZIFs take on zeolite-like topologies, as shown in Figure 4.7.

ZIFs generally have high thermal and moister stability compared to other types of MOFs. Like zeolites and other porous materials, Zeolitic Imidazolate Framework membranes can be used for the separation of gases because of their highly porous structure, large accessible pore volume with fully exposed edges and faces of the organic links, pore apertures in the range of the kinetic diameter of several gas molecules and high CO_2 adsorption capacity. For instance, ZIF-8 crystals are non-toxic

and require little energy to be created, making them an attractive possibility for carbon capture and storage. The porous structures can be heated to high temperatures without decomposing and can be boiled in water or solvents for a week and remain stable, making them suitable for use in hot, energy-producing environments like power plants [An et al., 2010a].
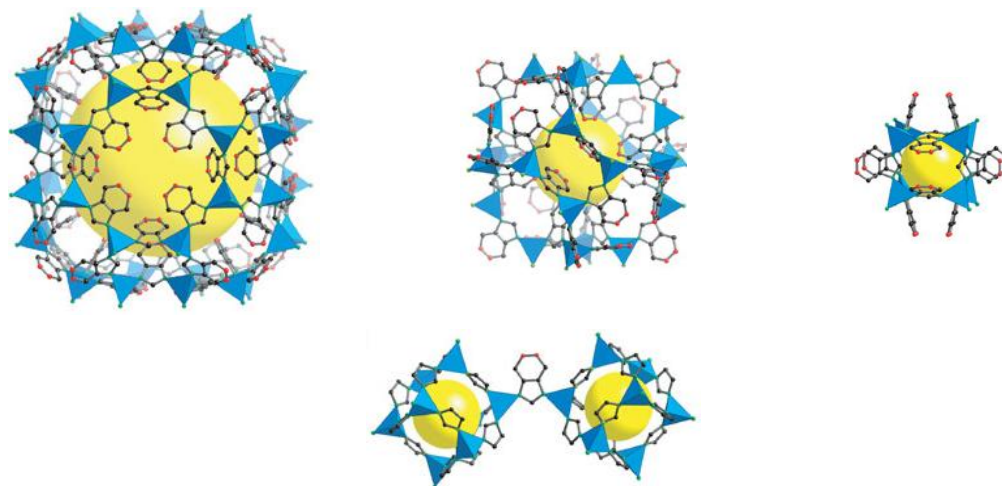
Figure 4.7. *Several ZIF topologies.*

Functionalized materials

MOFs functionalized with basic nitrogen-containing organic groups have been intensively studied for their CO_2 adsorption properties. The dispersion and electrostatic forces resulting from the interaction of the quadrupole moment of CO_2 with localized dipoles generated by heteroatom incorporation are typically responsible for the enhanced CO_2 adsorption. In some cases, acid-base type interactions between the lone-pair of nitrogen and CO_2 have been observed. For example, bio- MOF-11 was synthesized from adeninate and acetate linkers [Kondo et al., 2009]. Its CO_2 adsorption capacity is 5.8wt% at 298K and 0.15bar, with a corresponding isosteric heat of adsorption of 45 kJ/mol at zero-coverage. The large initial isosteric heat is likely partially attributable to the presence of an aromatic amine that also decorates the pore surface, however, the effects of the nitrogen heterocycle are considerable because the CO_2 capacity exceeds that of any other aromatic amine functionalized framework reported to date at 1bar, despite a surface area of only 1040 m^2/g. As for zeolites and amorphous silicas, the commercial availability of aromatic amine containing linkers, especially 2-aminoterephthalic acid (NH_2-BDC), and the expected affinity of amino groups toward CO_2 has generated significant interest in aromatic amine functionalized frameworks [Botas et al., 2010; Arstad et al., 2008; Vaidhyanathan et al., 2009], in particular, the IRMOF series. At 298K and 1.1bar, IRMOF-1 (or MOF-5) adsorbs approximately 4.6wt% CO_2, while the amine-functionalized variant, IRMOF-3, adsorbs 5.0wt% CO_2, despite a decrease in the BET surface area from 2833 to 2160m^2/g [Jiang et

al., 2007]. The reduced surface area of IRMOF-3 decreases the high-pressure CO_2 adsorption capacity, but the higher uptake observed within the material at lower pressures leads to it being a higher performance material compared with IRMOF-1 in the context of post-combustion CO_2 capture.

Amine functionalization has been shown to enhance CO_2 capacity in a number of other MOFs, including $Ni_2(NH_2\text{-}BDC)_2(DABCO)$, $NH_2\text{-}MIL\text{-}53(Al)$ and $In(OH)(NH_2\text{-}BDC)$, when their low-pressure capacities are compared with that of the parent material [Lee et al., 2008]. However, the amine may not always be directly responsible for the enhanced adsorption. It was recently shown for the well studied compound $NH_2\text{-}MIL\text{-}53(Al)$ that the aromatic amine has little direct interaction with adsorbed CO_2 at low pressures.

Nevertheless, significant work still needs to be performed to identify the most promising class of materials for CO_2 capture, although the rich and highly diverse nature of the materials discovered recently holds tremendous promise for the discovery of next-generation structures that are optimized for this application.

4.3. Simulation in selected systems for CO_2 adsorption and separation

Despite hundreds of activated carbons, zeolites, amine-silicas and MOFs have been explored experimentally to date in CO_2 adsorption and separation, far fewer structures regarding typical (or representative) structures has been studied by theoretical calculations based on molecular simulations. Computational modeling has been mainly used in the virtual screening for zeolites and Metal-Organic Frameworks, [Wilmer and Snurr, 2011] new hypothetical structures with high performance parameters, [Low et al., 2009] and predicting the stability of existing materials toward contaminants, such as H_2O [Yang et al., 2008]. While we do not provide a thorough coverage of the theoretical studies pertaining to CO_2 adsorption here, we introduce certain computational results as appropriate in the forthcoming sections. Zhong and coworkers systematically investigated nine typical MOFs with various pore sizes, topologies, organic linkers and electrostatic properties using molecular simulations [Zheng et al., 2009]. The results indicated that a suitable pore size for CO_2 storage is around 10-20Å. CO_2 uptake is governed by the strength of the CO_2–MOF interactions at low pressures. Other factors, such as accessible surface area and free volume, are also crucial to CO_2 adsorption capacity at high pressures. The electrostatic interactions between CO_2 and MOFs contribute up to 30% of the total adsorption capacity at low pressures, however, the contribution decreases rapidly with the increase of pressure and the percentage drops at high pressures. In general, MOFs have higher capacities

for CO_2 storage and comparable self-diffusivity in comparison to most zeolites and carbon materials.

In a further study, Zhong and coworkers [Zheng et al., 2009] examined 20 different MOFs. The results show that at low pressures CO_2 molecules preferentially adsorb around the polar centers in the framework and the electrostatic contribution is therefore large. The adsorption sites are saturated at high pressures and most CO_2 molecules are located far from the charge centers. The effect is more pronounced in large pores. Consequently, the electrostatic interaction decreases and can be neglected in many cases.

Babarao and Jiang [Babarao and Jiang, 2008] systematically evaluated the performance of various MOFs using Gibbs ensemble Monte Carlo (GEMC) simulations. Their work revealed that MOFs exhibit remarkably higher adsorption capacity than zeolites and single-wall nanotubes. The capacity is primarily determined by the strength of CO_2 adsorption at low pressures, while it is mainly dependent on the free volume and accessible surface area at high pressures. In 2007, Snurr and coworkers studied the adsorption sites of light gases in MOF-5 by using Monte Carlo (MC) simulations [Dubbeldam et al., 2007]. They reported that the positions and occupations of the binding sites can be correctly predicted when an appropriate force field was applied. Snurr and coworkers also compared the performance of 14 MOFs for CO_2 capture at low pressures using a combined experimental and computational approach. Their study aimed to develop a model for fast screening of MOFs for gas capture, leading to substantial savings in the experimental time and cost. CO_2 uptake correlates with the heat of adsorption at low pressures. The proposed model gave some successful predictions. For instance, MOFs with a high density of open metal sites has the highest efficiency for CO_2 uptake.

Recently, Sholl and coworkers [Keskin et al., 2009] proposed an efficient method to characterize the features which control gas diffusion in the MOFs. The method is based on the information from X-ray crystal structures and able to rapidly predict the Henry's constant for adsorption and diffusion activation energy for simple gases. The approach was used to screen more than 500 structures and has demonstrated to be effective in identifying suitable materials for kinetic separation of adsorbates. However, there are some limits which need to be overcome in the method: *(1)* the method is unable to examine non-spherical molecules; *(2)* the calculated Henry's constant for adsorption and diffusion activation energy are only applicable for non-polar adsorbates; and *(3)* the method may lead to large deviations at high pressures.

On the performance of zeolites and MOFs [Liu and Smit, 2009], a comparative study was carried out by Liu and Smit. They selected MFI-type for its arrangement with intersecting channels, DDR and LTA for their structures with open cages, and seven MOFs (CuBTC, MIL-47, IRMOF-1, -11, -12, -13 and -14) with a wide range of

chemical compositions, pore sizes and topologies. The simulation results show that although MOFs outperform over zeolites for gas storage, their separation performance is comparable to zeolites. The catenated IRMOFs exhibit a slightly higher selectivity than non-catenated counterparts. Also, they suggested that the difference in the quadrupole moments of sorbates should be considered in selecting a suitable material for separation. This indicates the important role of electrostatic interactions in the observed high selectivity in ionic MOFs. Together with early discussion, ionic MOFs with open metal sites show considerably larger selectivity and adsorption capacities, and have demonstrated to be good candidates for gas storage and CO_2 capture. However, experimental confirmation is required to further ascertain their performance.

Recently, a combined experimental and computational study on the adsorption of CO, N_2 and CO_2 on Mg-MOF-74, was conducted by Palomino and coworkers [Palomino et al., 2012]. The results showed that CO and N_2 form roughly linear 1:1 complexes with Mg^{2+} while CO_2 forms an angular complex. Remarkably, dispersion interactions contribute 1/2 gas-framework interaction energies in all the adsorption complexes and should be included in the calculations. The calculated adsorption enthalpy indicated that CO_2 has the strongest adsorption on Mg-MOF-74 among the 3 gases, in good agreement with the experimental values.

For ZIFs, Zhong and coworkers [Liu et al., 2009] studied the adsorption and diffusion behaviors of CO_2 in two typical structures, ZIF-68 and ZIF-69 using combined GCMC and MD techniques. They found that CO_2 molecules preferentially adsorb in the small pores encompassed by the nIM (nitroimidazole) linkers. With the increasing pressure, the molecules can also be adsorbed in the corners formed by the phenyl ring in the large pores and further occupy the pores. Similar to many other MOF systems, the contribution of framework charges cannot be ignored at low pressures. Their MD calculations indicated that the diffusion of CO_2 in ZIF-69 is slower than ZIF-68 due to the pore size and steric hindrance. Recently, Nieto-Draghi and coworkers [Perez-Pellitero et al., 2010] investigated the adsorption of CH_4, N_2, and CO_2 on ZIF-8 and ZIF-76 and ZIF-69. Their GCMC simulations showed that standard force fields were not reliable and failed to reproduce experimental data. A modified force field optimized by experimental data was adopted to examine the adsorption behavior. The simulated adsorption isotherms predicted the CO_2 uptake order (ZIF-69 < ZIF-8 < ZIF-76) at high pressures, which is partially verified by experiments. The simulations also indicated preferential adsorption sites of ZIF-8, located at the organic linkers. Furthermore, the charge–quadrupole contribution prevails in the interactions between the metal atoms and CO_2; whereas the vdW contribution is only <10% in the overall binding energy. According to the calculated Henry's constant and isosteric heats of adsorption, vdW interactions dominate the adsorption of N_2, while vdW and electrostatic interactions co-govern the adsorption of CO_2 in the ZIFs. Remarkably, the study indicated ZIFs possess some properties similar to zeolites.

MIL-53 has already triggered great interest due to its unusual microscopic adsorption behavior. Two interchanging configurations named the large pore (MIL-53lp(Al)) and narrow pore (MIL-53np(Al)) forms, were identified [Babarao and Jiang, 2010]. The two forms share the same chemical composition but differ in the pore width. Maurin and coworkers suggested that a structural transition occurs during the CO_2 adsorption process. Their GCMC simulation further provided evidence for the breathing effect (structural transition upon CO_2 adsorption) [Bourrelly et al., 2005]: the simulated isotherms for each MIL-53(Al) form are in good agreement with the corresponding region of the experimental isotherm. Furthermore, the calculated enthalpies of adsorption correspond to the experimental data at low pressures (<6bar) and at high pressures, respectively. The structural analysis showed that the breathing mechanism can only be induced by molecules with large dipole or quadrupole moments such as CO_2 and H_2O [Babarao and Jiang, 2010]. To further understand this breathing effect in MIL-53, Maurin and coworkers [Ramsahye et al., 2007b] compared adsorption of CO_2 in MIL-53(Al) and MIL-47(V). The breathing was found in MIL-53(Al) but not in MIL-47(V). They also successfully reproduced the breathing in the process of CO_2 adsorption for MIL-53(Cr) using a bonded force field [Ramsahye et al., 2007c].

To study the effect of small pockets on gas separation, Zhong and coworkers [Xue et al., 2009] perform simulations in IRMOFs and CuBTC (HKUST-1). Their simulation showed that gas separation was influenced by the geometry and pore size. MOF-5 possesses a simple channel structure and consequently exhibits simple selectivity properties; whereas CuBTC has a more complicated channel/pocket structure, leading to complex selectivity. More importantly, the strength of electrostatic interactions can tremendously alter the gas separation performance, particularly for the components with different dipoles/quadrupoles. Moreover, blocking of the side pockets results in large differences in their simulated selectivity curves at low-pressure range. The phenomenon was also noticed by Krishna and van Baten [Krishna and van Baten, 2010]. They pointed out that the experimentally inaccessible pockets of MOFs should be blocked appropriately in GCMC simulations or otherwise inaccurate and unrealistic results will be obtained.

Moreover, as well as in zeolites, introducing ions into MOF systems generally leads to enhanced adsorption and selectivity for CO_2. For example, the structure and separation properties of Li^+ exchanged MOFs (Li^+-MOFs) were examined by Babarao and Jiang [Babarao and Jiang, 2010]. Li^+-MOFs possess higher selectivity than non-ionic MOFs and most other porous materials. According to GCMC simulations, the high selectivity is originated from the charges of cations and frameworks.

Generally, in the simulation studies of nanoporous crystalline materials, the coordinates of framework atoms are usually adopted from experimental crystallographic data. Most studies use rigid frameworks with atomic positions fixed.

To date, only few simulation studies have been performed in the adsorption of flexible materials, in this case, MOFs [Lee and Sircar, 2008; Salles et al., 2008]. This has two advantages: first, there is no need to evaluate intra-framework interactions second, the interactions between framework and guest can be pre-tabulated and simulation can be accelerated. Such a simplified treatment is acceptable, particularly for small guest molecules like CO_2 and N_2. However, due to the large amount of time required it is not practical yet to perform this kind of simulations.

4.4. Literature review on materials for CO₂ capture

We present here a detailed comparison of CO_2 capacity of different materials, separated in high and low pressures. The review focused on publications in the last ten years.

It should be noted that different literature sources present their results in different units (as mmol/g, mol/mol, wt, kmol/m³, cm³/g, etc.). In order to make a more appropriate comparison between different materials and conditions employed, we made an effort and took all the values to the same unit of measurement focus our attention in volumetric capacity (in this case, kmol/m³); calculated data are distinguished by the asterisk on the value. Some materials are presented with their short or most common name, for aesthetic of the tables.

The gravimetric CO_2 uptake, which refers to the quantity of CO_2 adsorbed within a unit mass of the material, dictates the mass of the adsorbent material required to form the adsorbent bed. Meanwhile, the volumetric capacity refers to how densely the CO_2 can be stored within the material and is an equally crucial parameter, since it has a significant influence on the volume of the adsorbent bed (from an engineering point of view, the exchange between materials should not affect the dimensions of the adsorption unit). Both parameters also have an important role in determining the heating efficiency of the material, which directly impacts the energy penalty required for material regeneration and desorption.

4.4.1. CO₂ adsorption at high pressures

The high-pressure adsorption capacities for selected frameworks are tabulated in Table 4.1. Indeed, the greatest capacities at high pressures are observed for materials exhibiting large surface areas, although excellent adsorption properties have also been

demonstrated in a number of materials with modest surface areas that have a significant density of high-affinity adsorption sites, such as exposed metal cations.

Table 4.1. *List of materials for CO₂-capture at high pressures.*

MATERIAL	TEMP (K)	P (bar)	kmol/m³	%wt	EXP (E)/ SIM (S)	REFERENCE
MIL-101(Cr)	283	5.3	2.6	26	E+S	Chowdhuri et al (2009)
IRMOF-1 (MOF-5)	273	10	8.2*	58	E+S	Botas et al (2010)
DUT-4	303	10	4.6	26.4	E+S	Senkovska et al (2009)
SNU-M10	298	10	3.5*	15.2	E+S	Choi et al (2008)
IRMOF-1 (MOF-5)	298	14	6.8	11.0	E+S	Saha et al (2010)
MOF-177	298	14	3.8*	12	E+S	Saha et al (2010)
Zn₂(BDC)₂(DABCO)	298	15	7.4*	37.6	E+S	Liang et al (2009b)
CuBTC (HKUST-1)	298	15	7.2*	35.9	E+S	Liang et al (2009a)
MIL-53(Cr)	304	18	8.0	55	E	Llewellyn et al (2006)
UiO-66	303	18	7.3	24.3	E+S	Weirsum et al (2011)
MIL-47	298	20	10.8*	36	E	Bourrelly et al (2005)
NOTT-140	293	20	7.1*	46.2	E+S	Tan et al (2011)
MIL-96(Al)	303	20	5.2*	18.6	E+S	Surblé et al (2006b)
MIL-47(V)	304	20	0.0	55	E+S	Bourrelly et al (2005)
Ni-MOF-74	278	22	14.9*	54.2	E	Dietzel et al (2008)
MIL-53(Cr)	304	25	10.5*	44	E	Bourrelly et al (2005)
MIL-53(Al)	298	25	9.8*	45	E	Bourrelly et al (2005)
MIL-53(Al)	304	25	6.8	30.6	E	Bourrelly et al (2005)
USO-2-Ni	298	25	0.0	41	E+S	Arstad et al (2008)
Zn₄O(FMA)₃	300	28	12.7*	69	S	Xue et al (2009)
CuBTC (HKUST-1)	313	30	8.6*	42.8	E	Moellmer et al (2011)
MIL-101(Cr)	298	30	5.0*	50.2	S	Zhang et al (2011)
IRMOF-11	298	35	8.9	39.3	E	Millward and Yaghi (2005)
IRMOF-6	298	35	6.8*	46.2	E+S	Millward and Yaghi (2005)
MOF-505	298	35	6.5	31	S	Millward and Yaghi (2005)
PCN-61	298	35	6.5*	50.8	E	Yuan et al (2010)
IRMOF-3	298	35	6.5*	45.1	E	Millward and Yaghi (2005)
IRMOF-1 (MOF-5)	298	35	5.8	40.8	S	Millward and Yaghi (2005)
PCN-66	298	35	5.5	53.6	E+S	Yuan et al (2010)
PCN-68	298	35	4.9	57.2	E+S	Yuan et al (2010)
MOF-2	298	35	0.0	10.0	S	Millward and Yaghi (2005)
Mg-MOF-74	278	36	14.2	68.9	E	Dietzel et al (2008)
Co-BDP	313	40	9.4*	41.3	E	Helm et al (2011)

MATERIAL	TEMP (K)	P (bar)	kmol/m³	%wt	EXP (E)/ SIM (S)	REFERENCE
CuBTC (HKUST-1)	303	40	8.0*	40.1	S	Hamon et al (2010)
Cu-BTTri	313	40	7.3*	42.8	E	Helm et al (2011)
DUT-9	298	47	5.1*	62.1	S	Gedrich et al (2010)
MIL-100(Cr)	304	50	7.0*	44.2	E	Féreand et al (2004)
MOF-177	298	50	5.9*	60.8	E+S	Furukawa et al (2010)
MIL-101(Cr)	304	50	5.7	56.9	E	Llewellyn et al (2006)
MOF-205	298	50	5.4*	62.6	E	Furukawa et al (2010)
MOF-210	298	50	4.2*	74.2	E	Furukawa et al (2010)
MOF-200	298	50	3.7*	73.9	E	Furukawa et al (2010)

As inferred from the table, several MOFs have higher saturated CO_2 capacities than benchmark adsorbents such as zeolites NaX (or 13X) and activated carbon MAXSORB. Their results also showed that the saturated CO_2 capacities of the MOFs are qualitatively correlated with their surface areas.

4.4.2. CO₂ adsorption at sub-atmospheric pressures

The lower-pressure (<1.2bar) CO_2 uptake capacities for all materials collected at ambient temperatures (293-313 K) are listed in Table 4.2. At these conditions, the adsorptive properties are predominantly dictated by the chemical features of the pore surface, and most of the high-capacity materials are those bearing highly functionalized surfaces, or by electrostatic interactions. Many of them exhibit large CO_2 adsorption capacities at pressures at and above 1bar, owing to their high surface areas. However, these compounds are generally not well suited for post-combustion capture, since the adsorption capacity at lower pressures is a more relevant consideration due to the low partial pressure of CO_2 [Sayari et al., 2011]. However, the Mg-MOF-74 requires further investigation, given its high capacity at low pressure

Table 4.2. *List of materials for CO₂-capture at low pressures*

MATERIAL	TEMP (K)	P (bar)	kmol/m³	%wt	EXP (E)/ SIM (S)	REFERENCE
CuBTC (HKUST-1)	298	0.8	2.1*	10.6	E+S	Liu et al (2010)
Co-MOF-74	296	1	6.2*	23.4	S	Caskey et al (2008)
Mg-MOF-74	298	1	5.7*	27.5	E	Bao et al (2011)
Ni-MOF-74	296	1	5.6*	20.4	S	Caskey et al (2008)
Zn-MOF-74	298	1	5.5*	19.8	S	Millward and Yaghi

MATERIAL	TEMP (K)	P (bar)	kmol/m³	%wt	EXP (E)/ SIM (S)	REFERENCE
						(2005)
Cu-tdpat	298	1	4.6*	25.8	S	Li et al (2012)
Cu(bpy-1)$_2$(SiF$_6$)	298	1	4.5	23.1	E	Nugent et al (2013)
UTSA-16	298	1	4.3	19	E	Xiang et al (2011)
CuBTC (HKUST-1)	295	1	3.7	18.3	S	Yazaydin et al (2009)
USO-2-Ni-A	298	1	3.2*	14	E	Surblé et al (2006b)
PCN-6	298	1	3.1*	15.9	E	Kim et al (2011)
bio-MOF-11	298	1	2.8*	15.2	E	An et al (2010)
NH$_2$-MIL-53(Al)	298	1	2.7*	12	S	Arstad et al (2008)
UMCM-150(N$_2$)	298	1	2.5	10.8	S	Yazaydin et al (2009)
Cu-BTTri	298	1	2.4	14.3	E	Demesence et al (2009)
MIL-53(Al)	298	1	2.4*	10.6	E	Arstad et al (2008)
UMCM-150	298	1	2.3*	10.2	E	Yazaydin et al (2009)
USO-2-Ni	298	1	2.3*	10	E+S	Arstad et al (2008)
Cu-TATB-30	298	1	2.2*	13.4	E	Kim et al (2011)
ZIF-82	298	1	2.1*	9.1	E+S	Banerjee et al (2009)
ZIF-78	298	1	2.0	9.1	E+S	Banerjee et al (2009)
MIL-53(Al)	303	1	2.0	9.2	E	Rallapalli et al (2011)
SNU-50	298	1	2.0	13.7	E	Prasad et al (2010)
MIL-53(Cr)	304	1	2.0*	8.5	E	Llewellyn et al (2006)
ZIF-69	298	1	2.0*	8.6	E+S	Banerjee et al (2009)
USO-3-In-A	298	1	1.8	8	E	Arstad et al (2008)
MIL-47	298	1	1.8*	8.1	S	Yazaydin et al (2009b)
NOTT-140	298	1	1.8	11.7	E+S	Chen et al (2011b)
ZIF-81	298	1	1.6*	7.2	E+S	Banerjee et al (2009)
Zn-MOF-74	296	1	1.6	5.8	E	Caskey et al (2008)
Zn$_2$(BDC)$_2$(DABCO)	296	1	1.6*	8.1	E	Chen et al (2011b)
ZIF-68	298	1	1.5	6.7	E	Banerjee et al (2009)
ZIF-70	298	1	1.3*	5.7	E	Banerjee et al (2009)
en-CuBTTri	298	1	1.3*	5.5	E	Demesence et al (2009)
USO-3-In	298	1	1.3	5.5	E	Arstad et al (2008)
IRMOF-1 (MOF-5)	296	1	1.2*	8.5	E+S	Zhao et al (2009)
ZIF-8	298	1	1.1*	4.3	E+S	Yazaydin et al (2009)
bio-MOF-1	313	1	0.9*	5.2	S	An et al (2010)
UMCM-1	298	1	0.9	3.8	E	Yazaydin et al (2009)
UMCM-50	298	1	0.8	10.2	E	Yazaydin et al (2009b)
IRMOF-3	298	1	0.7*	4.7	S	Yazaydin et al (2009)

MATERIAL	TEMP (K)	P (bar)	kmol/m³	%wt	EXP (E)/ SIM (S)	REFERENCE
MOF-177	298	1	0.6*	6.5	E+S	Saha et al (2010)
Mg-MOF-1	298	1	0.6*	2.7	S	Mallick et al (2010)
MOF-2	298	1	0.5	2.4	S	Millward and Yaghi (2005)
SNU-30	298	1	0.4	4.9	S	Park et al (2010)
MIL-101(Cr)	319	1	0.4*	4.2	S	Chowdhuri et al (2009)
MOF-177	298	1	0.3*	3.6	E	Mason et al (2011), Yazaydin et al (2009)
SNU-31	298	1	0.3	2.6	E+S	Park et al (2010)
MOF-505	298	1.1	2.7*	12.6	E	Millward and Yaghi (2005)
IRMOF-11	298	1.1	1.7	7.3	E	Millward and Yaghi (2005)
ZIF-79	298	1.1	1.4*	6.2	S	Banerjee et al (2009)
IRMOF-6	298	1.2	0.7	4.6	E	Millward and Yaghi (2005)
SNU-50	296	0.15	4.28		E	Prasad et al (2010)
$Zn_2(atz)_2(ox)$	293	0.15	1.89		E	Vaidhyanathan et al (2009)
Zn-MOF-74	296	0.15	1.38		E	Caskey et al (2008)
USO-2-Ni-A	298	0.15	0.48		E	Arstad et al (2008)
MIL-53(Al)	298	0.15	0.38		E	Arstad et al (2008)
UMCM-1	298	0.15	0.11		E	Yazaydin et al (2009b)
IRMOF-3	298	0.15	0.09		E	Millward and Yaghi (2005)

Note that in Table 4.2, the adsorption capacities at 1bar (the most commonly reported value) are tabulated to facilitate a general comparison. However, the adsorption capacities for CO_2 (0.15bar) and N_2 (0.75bar) at pressures relevant to post-combustion CO_2 capture are often not directly reported, and these have been carefully estimated from the literature gas adsorption isotherms.

For post-combustion CO_2 capture, the pressure of the flue gas (aprox. 1bar) and the low partial pressure of CO_2 thereof (P_{CO2} 0.15bar) leads to the lower pressure region of the CO_2 adsorption isotherm being the area of interest. Thus, maximizing the adsorption capacity specifically around 0.15bar would be expected to lead to new materials with enhanced performance for post-combustion CO_2 capture. In this sense, Yazaydin and coworkers [Yazaydin et al., 2009], using both experiments and simulation to screen MOFs for the highest CO_2 capacities at about 0.1atm, found that

Mg-MOF-74 and Ni-MOF-74 have the highest CO_2 capacities (5.95 mol/1 and 4.07 mol/l) among the 14 MOFs that they considered. This corroborated the findings of Liu and coworkers [Li et al., 2013], who found that Ni-MOF-74 has a higher gravimetric CO_2 capacity than NaX and 5A zeolites at 0.1atm, and 25°C. In contrast to CO_2 adsorption in MOFs at high pressures, there is no correlation between the CO_2 capacity and the surface area or the free volume.

4.4.3. Selective adsorption of CO_2 (CO_2/N_2 Separation)

In the majority of reported literature, selective adsorption is the primary tool used to give the reader a guided view of a particular material's potential for separation. Table 4.3 provides a survey of the equilibrium CO_2 and N_2 capacities, and selectivities, of various commercial and novel adsorbents. CO_2 possesses the largest quadrupole in the mixtures and thus the strongest electrostatic interactions with the framework, while N_2 have smaller quadrupole moments and relatively weaker interaction. GCMC simulations have demonstrated that difference of electrostatic interactions enhanced the separation of gases. Remarkably, the gas selectivity also depend on temperature and gas composition: the selectivity decreases sharply with increasing temperature, and also significantly changes with the ratio of the components. These factors are important and need to be considered.

Table 4.3. Adsorbents for CO_2 capture from a CO_2/N_2 mixture.

MATERIAL	TYPE	TEMP (K)	P1/P2 (bar)	$S_{1/2}$	CO_2 uptake (kmol/m^3)	N_2 uptake (kmol/m^3)	REFERENCE
$Zn_4O(L3)_{1.5}$	MOF	298	0.15/0.75	580.8	0.92	0.5	Lan et al (2011)
UTSA-16	MOF	296	0.15/0.75	262	2.64*	3.2	Xiang et al (2012)
mmen-CUBTTri	MOF	298	0.15/0.75	165	2.16*	4.5	McDonald et al (2011)
$Zn_4O(L2)_{1.5}$	MOF	298	0.15/0.75	108	0.86	2.5	Bloch et al (2010)
$Zn_2(atz)_2(ox)$	MOF	273	0.15/0.75	80.8	3.07	12.3	Vaidhyanathan et al (2009)
NaX	ZEO	298	0.15/0.75	67.7	4.32*	20.0	Lee et al (2002)
NJU-Bai$_8$	MOF	298	0.15/0.75	60.5	0.62*	5.2	Du et al (2013)
NJU-Bai$_7$	MOF	298	0.15/0.75	58.3	0.95*	8.2	Du et al (2013)
Mg-MOF-74	MOF	313	0.15/0.75	52.3	3.90*	45.5	Mason et al (2011)
Mg-MOF-74	MOF	303	0.15/0.75	44	4.26	59.4	Mason et al (2011)
en-Cu-BTTri	MOF	298	0.15/0.75	44	0.52	3.9	Demessence et al (2009)
bio-MOF-11	MOF	298	0.15/0.75	36	0.98	8.0	Chen et al (2010)

MATERIAL	TYPE	TEMP (K)	P1/P2 (bar)	$S_{1/2}$	CO₂ uptake (kmol/m³)	N₂ uptake (kmol/m³)	REFERENCE
CuBTC (HKUST-1)	MOF	293	0.15/0.75	34.4	0.91*	13.2	Aprea et al (2010)
Ni-MOF-74	MOF	298	0.15/0.75	30	4.63	92.2	Dietzel et al (2009)
ZIF-78	MOF	298	0.15/0.75	30	0.74*	12.7	Phan et al (2010)
PCN-88	MOF	296	0.15/0.75	29.8	0.69	7.3	Li et al (2012)
CuTATB-60	MOF	298	0.15/0.75	24	0.95	21.1	Kim et al (2011)
Cu(bpy-1)₂(SiF₆)	MOF	298	0.15/0.75	22.5	0.60*	13.2	Burd et al (2012)
ZIF-100	MOF	298	0.15/0.75	22	0.23*	3.4	Wang et al (2008)
Cu-BTTri	MOF	298	0.15/0.75	19	0.49*	13.1	Demessence et al (2009)
CuTATB-60	MOF	298	0.15/0.75	18.1	0.53	9.3	Kim et al (2011)
Fe-BTT	MOF	298	0.15/0.75	18	1.20	21.6	Sumida et al (2010)
NOTT-202a	MOF	293	0.15/0.75	11.36	0.35	9.8	Yang et al (2007)
IRMOF-1 (MOF-5)	MOF	298	0.15/0.75	10.1	0.11*	5.3	Rao et al (2014)
MOF-253	MOF	298	0.15/0.75	9	0.23*	8.4	Bloch et al (2010)
MOF-177	MOF	298	0.15/0.75	4	0.06	5.9	Mason et al (2011)
NTU-105	MOF	273	0.15/0.75	2	0.15	23.9	Wang et al (2008)
MOF-508	MOF	323	0.1/0.9	2	0.10	0.60	Bastin et al (2008)
Activated Carbon	AC	298	0.1/0.9	1.2	0.34*	0.28	Na et al (2001)
ZIF-82	MOF	298	0.5/0.5	35.5	2.18*	0.2	Banerjee et al (2009)
ZIF-78	MOF	298	1	50	2.04*	0.2	Banerjee et al (2009)
bio-MOF-11	MOF	298	1	75	3.28	0.10	An et al (2010)
ZIF-81	MOF	298	1	23	1.57	0.1	Banerjee et al (2009)
ZIF-79	MOF	298	1	22.5	1.37	0.1	Banerjee et al (2009)
ZIF-69	MOF	298	1/1	20	9.18	119.6	Banerjee et al (2009)
ZIF-68	MOF	298	1	19.5	1.50	0.1	Banerjee et al (2009)
ZIF-70	MOF	298	1	18	1.29	0.1	Banerjee et al (2009)
MOF-253	MOF	298	1	2.8	1.41*	10.9	Bloch et al (2010)
MOF-508b	MOF	303	4.5/4.5	3	5.91	43.2	Bastin et al (2008)
NaX	ZEO	room	0.15/0.75		5.76	24.5	Bae et al (2013)
13X	ZEO	room	0.15/0.75		4.93	51.6	Rao et al (2014)
LiCHA	ZEO	room	0.15/0.75		4.88	40.2	Yang et al (2007)
Co-MOF-74	MOF	298	0.15/0.75		4.35		Mason et al (2011)
CaA	ZEO	room	0.15/0.75		4.19	26.8	Bae et al (2013)
NaCHA	ZEO	room	0.15/0.75		4.05	38.0	Yang et al (2007)
LTA-5A	ZEO	room	0.15/0.75		3.97	28.2	Rao et al (2014)
NaX(17.3)A	ZEO	room	0.15/0.75		3.84	1.3	Yang et al (2007)

MATERIAL	TYPE	TEMP (K)	P1/P2 (bar)	$S_{1/2}$	CO₂ uptake (kmol/m³)	N₂ uptake (kmol/m³)	REFERENCE
NaKA (17.4%)	ZEO	room	0.15/0.75		3.19	17.5	Liu et al (2010)
LiKFI	ZEO	room	0.15/0.75		3.18	22.0	Yang et al (2007)
CaCHA	ZEO	room	0.15/0.75		3.05	46.6	Yang et al (2007)
Zn₂(atz)₂(ox)	MOF	298	0.15/0.75		2.05		Vaidhyanathan et al (2009)
KCHA	ZEO	room	0.15/0.75		1.85	12.7	Cavenati et al (2004)
Cu-SSZ-13	AC	room	0.15/0.75		1.80	16.1	Hudson et al (2012)
H-SSZ-13	AC	room	0.15/0.75		1.79*	13.6	Hudson et al (2012)
NaA	ZEO	room	0.15/0.75		1.78*	4.1	Bae et al (2013)
DT-200	ZEO	room	0.15/0.75		0.56*	10.0	Bao et al (2011)
DT-100	ZEO	room	0.15/0.75		0.54*	10.2	Bao et al (2011)
DT-300	ZEO	room	0.15/0.75		0.49*	10.0	Bao et al (2011)
USO-2-Ni	MOF	298	0.15/0.75		0.35*		Arstad et al (2008)
USO-2-Ni-A	MOF	298	0.15/0.75		0.27*		Arstad et al (2008)
MIL-47	MOF	298	0.15/0.75		0.25*		Yazaydin et al (2009b)
NaX	ZEO	room	0.15/0.75		0.12*	12.3	McEwen et al (2013)
Mg-MOF-74	MOF	296	0.1/0.9		4.87		Britt et al (2009)
Co-MOF-74	MOF	296	0.1/0.9		3.28		Caskey et al (2008)
Ni-MOF-74	MOF	296	0.1/0.9		3.26		Caskey et al (2008)
LiX (Si/Al=1)	ZEO	303	0.1/0.9		3.10		Walton et al (2006)
SWCNT	SWNT	308	0.1/0.9		0.50		Cinke et al (2003)
5A (Sinopec)	ZEO	298	1/1		1.03*	12.7	Saha et al (2010)
Natural Chabazite	ZEO	303	1/1		0.75*	10.2	Jensen et al (2011)
PCB, Calgon Corp.	AC	296	1/1		0.55*		Ritter and Yang (1987)
Norit RB1 Extra	AC	298	1/1		0.50*	8.9	Dreisbach et al (1999)
Sutcliffe	AC	298	1/1		0.42*	6.1	Esteves et al (2008)
ZIF-100	MOF	298	1/1		0.24*		Wang et al (2008)
MOF-177	MOF	298	1/1		0.15*	0.2	Saha et al (2010)
IRMOF-1 (MOF-5)	MOF	298	1/1		0.13*	2.4	Saha et al (2010)
Sutcliffe	AC	298	10/10		1.82	41.4	Esteves et al (2008)
Norit RB1 Extra	AC	298	10/10		1.73	45.9	Dreisbach et al (1999)
PCB, Calgon Corp.	AC	296	10/10		1.64		Ritter and Yang (1987)
H-mordenite	ZEO	293	10/10		0.70		Delgado et al (2006)
Na-Mordenite	ZEO	293	10/10		0.68	34.1	Delgado et al (2006)

Calculated value from the data presented in each paper (framework densities in supporting information)

Liu and Smit compared the separation and storage efficiency of CO_2/N_2 mixture in three zeolites and seven MOFs using GCMC simulations [Liu and Smit, 2010]. Not surprisingly, CO_2 adsorption is more preferable for all the materials. Although the gas storage capacity of all the MOFs is substantially higher than that of zeolites at higher pressures, comparable separation selectivity of the two classes of materials was obtained. In the simulation, switching off the electrostatic interactions between gases and adsorbents resulted in lower selectivity, indicating the framework charges play a more significant role for CO_2 adsorption than for N_2 adsorption.

The charged zeolite-like MOF (rho-ZMOF), which contains an anionic framework and extraframework Na^+ ions, was investigated by Babarao and Jiang [Babarao and Jiang, 2009]., showing extraordinary CO_2 separation selectivities in CO_2/N_2 mixture (15:85), the selectivity reaches to 19000 at infinite dilution and drops 500 under ambient conditions, but so far, these results have not been experimentally confirmed. All of these selectivities are the highest predicted to our knowledge. In rho-ZMOF, Na^+ ions have larger mobility in the framework and can be acted as additional binding centers. This gives stronger charge–quadrupole interactions and accordingly, higher adsorption selectivity. However, the adsorption uptake is not as high as in other materials, and the simulations also showed that CO_2 adsorption drops sharply with only 0.1% of H_2O.

Some reports have approximated the adsorption selectivity factors by comparing the adsorption capacity of single-component adsorption isotherms. For instance, Chaffee and coworkers [Liang et al., 2009] calculated the adsorption selectivities of CO_2/N_2 in CuBTC (HKUST-1) from the single gas isotherms by dividing the CO_2 adsorption capacity by that of N_2 at each pressure point. Their results showed that the selectivity towards CO_2 at 25°C decreases slowly as pressure is increased. The similar method has also been used by Yaghi and coworker [Britt et al., 2008] in series of ZIFs for their selectivities, by Long and coworkers [Herm et al., 2012] in Fe-BTT, and by Rosi and coworkers [Li et al., 2013b] for bio-MOF-11.

Adsorption selectivities of CO_2 over other gases evaluated from experiments were recently reported. Deng and coworkers [Deng et al., 2010] reported the adsorption equilibrium selectivity of CO_2 over N_2 in MOF-5 and MOF-177, which were calculated from the ratio of Henrys constants. The results showed that the selectivity of CO_2 over N_2 is 17.48 for MOF-5 and 17.73 and MOF-177, both of which are lower than that of Zeolite 5A. In another example, Goj and coworkers reported the separation of CO_2/N_2 mixture in three siliceous zeolites with identical chemical composition but differing pore structures (MFI, ITQ-3 and ITQ-7) [Goj et al., 2002]. The predicted adsorption isotherms of pure CO_2 and N_2 agree well with available experimental data in MFI. CO_2/N_2 selectivities in the three zeolites vary strongly with the crystal structure. The study indicates that the electric fields of different strengths present in zeolites lead to the observed selectivities and suggests the appropriate selection of

zeolite structure is important for the separation of flue gas. Jiang and Sandler further simulated the adsorption of CO_2/N_2 mixture in Na^+-exchanged ZSM-5 [Jiang and Sandler, 2006]. With experimentally validated potentials, the predicted selectivity in Na-ZSM-5 is significantly higher than in siliceous ZSM-5 and increases with increasing density of Na^+ ions. As mentioned, similar behavior was also observed in cation-exchanged MOFs.

Selective adsorption, in most cases, uses single-component isotherms and the IAST method [Myers and Prausnitz, 1965] to calculate a material's selectivity factor. This approximate theory is known to work accurately in many porous materials [Kim et al., 2007; Murthi et al., 2004] (most of the reports on CO_2 selective adsorption in MOFs are based on simulated adsorption isotherms). However, as the name indicates, the calculation does not always account for all experimental variables, and should be viewed as a reference; gas mixture adsorption experiments should thus be conducted to complete the picture.

Using experimental single-component adsorption isotherms to calculate the adsorption selectivity of a multi-component mixture by IAST were pioneered by Snurr and Hupp in the MOF field. They studied the selective adsorption of CO_2 over N_2 in several modified MOFs based on the $ZN_2(bttb)(X)_2$ (X = pyridine substitutes) parent framework [Bae et al., 2009].

It should also be noted that the relevance of selectivity values calculated for flexible frameworks via the aforementioned method has not been fully established, although it is likely that the quantities calculated by this methodology would overestimate the true adsorptive selectivity. This is because flexible structures generally adsorb little N_2 at 0.75bar since the apertures of the framework are not opened by N_2 in single component gas adsorption experiments. However, if CO_2 affords the necessary gate opening pressure, the quantity of N_2 adsorbed is likely to be significantly higher than that observed during the single-component experiment. Since IAST cannot account for such effects, direct selectivity measurements of binary mixtures are likely the only accurate gauge of selectivity in flexible MOFs.

One of the most valuable techniques to evaluate the selective adsorption of CO_2 from a gas mixture is by directly measuring separation by *breakthrough experiments*. Some breakthrough experiments on CO_2 separation in MOFs have been performed and gave at least qualitative evaluations in most cases. An example of an efficient separation of CO_2 from a mixed CO_2/N_2 gas stream was demonstrated by a breakthrough measurement made by Chen and co-workers [Wang et al., 2006] who examined MOF-508 for its performance in the separation and removal of CO_2 from binary CO_2/N_2 and CO_2/CH_4, and ternary $CO_2/CH_4/N_2$ mixtures by fixed-bed adsorption. The separation efficiency was rationalized and compared in terms of the sorption selectivity. The results indicated that $S_{CO2/N2}$ of this MOF is moderate at 303K,

which is lower than the selectivity of activated carbon, and decreases with increasing temperature.

In addition, Yaghi and coworkers examined several ZIFs have also shown high CO_2 separation capacities as demonstrated by breakthrough experiments, including ZIF-68, -69, and -70 for CO_2/CO, [Rowsell et al., 2005] and ZIF-95 and -100 for CO_2/CH_4, CO_2/CO, and CO_2/N_2 separations [Deng et al., 2010]; these MOFs are feasible for the separation of CO_2 from other gases and have longer retention times for CO_2 than BPL Carbon under the same conditions. Besides these ZIFs, Dietzel and coworkers studied CPO-27-M (M= Ni, Mg), i.e. Ni-MOF-74 and Mg-MOF-74, for the separation of CO_2/N_2 mixtures by breakthrough experiments, giving similar results of preferential adsorption of CO_2 [Dietzel et al., 2008] and so on. Breakthrough experiments have also been performed on the MIL-53 series [Lee et al., 2008; Yu et al., 2011], and $Al_4(OH)_2(OCH_3)_4(2\text{-}NH_2\text{-}bdc)_3$ MOF [Caskey et al., 2008], to name a few.

In summary, although carbonaceous and MOFs materials exhibiting relatively higher CO_2 adsorption capacity seem to be as the promising CO_2 adsorbents, the operations at which they have been tested are at high pressures and low temperatures. Conversely, silica materials have lower adsorption capacity and selectivity toward CO_2, their abundant surface OH groups can facilitate chemical modification to improve their CO_2 adsorption capacity and selectivity and thus treat a flue gas with low CO_2 partial pressure. The materials displaying higher selectivities are generally those bearing functionalized pore surfaces. However, these materials do not show enough improvement of the adsorption uptake in comparison to the values found for some specific MOFs, but they are a good choice if they can be synthesized with lower cost, and are mechanically stable and more readily available materials. Moreover, although a variety of MOFs show good CO_2 adsorption capacity and excellent selectivity, at present their industrial application may be limited by their powder form, high cost and small available quantities, and poor chemical and thermal stability. In addition to the widely available synthetic zeolites such as 13X and 4A, maybe the new class of zeolitic materials known ZIFs can emerge as gas potential high capacity CO_2 adsorbents.

4.4.4. Studies at process conditions

On account of industrial application, an effective and less energy-consumed regeneration of the CO_2 captured adsorbents is definitely needed to be developed.

Yang's group studied the feasibility of the PSA process for the first time to concentrate and recover CO_2 from the flue gas using AC, carbon molecular sieve (CMS), and zeolite 13X as adsorbents [Kikkinides et al., 1993]. They compared zeolite 13X and AC by the heat of adsorption, working capacity, purge requirement, and equilibrium selectivity, and concluded that the former adsorbent was a better

adsorbent for bulk separation of CO_2 from the flue gas. Krishna and coworkers examined a variety of MOFs by PSA process due to the flexible framework exhibiting large pressure-dependent changes in pore volume [Krishna and Long, 2012; Krishna and van Baten, 2012]. Webley and coworkers presented an optimization methodology and results for the structure of adsorbents at a pore level by evaluating the effect of pore geometry, size and overall adsorbent porosity on ultimate working capacity of adsorbents applied in PSA process [Rezaei and Webley, 2012]. Dasgupta and coworkers [Dasgupta et al., 2012] studied PEI impregnated SBA-15 as an adsorbent used in a single column five-step PSA, which was found to be comparable with reported commercial zeolite adsorbents in literature. Rodrigues and coworkers investigated the integration of PSA process by altering the operation stages and steps. The performance parameters of each proposed process, such as CO_2 purity, CO_2 recovery, and power consumption, were evaluated and compared with those of other processes reported previously in the literature [Ribeiro et al., 2012; Lopes et al., 2012]. Ho and coworkers [Ho et al., 2008] examined the economic feasibility of CO_2 capture from power-plant flue gas by PSA process. Zhang and coworkers [Zhang et al., 2009] made a comparison between 6 and 9 step cyclic operations with their VSA systems, demonstrating that the power consumption and CO_2 capture cost are significantly influenced by adsorbent type, process configuration, and operating parameters such as feed gas pressure, vacuum pressure, temperature, and extents of purge.

In TSA, in contrast, the regeneration is achieved by hot air or steam, and the regeneration time is in general longer than PSA. Chuang and coworkers carried out the TSA process using solid amine in a dual column. One adsorbent bed column was expected to capture more than 90% of CO_2 from the flue gas at 30–40°C and the other one was regenerated at 120–135°C to produce more than 99% purity of CO_2. To achieve continuous removal of the CO_2 from the flue gas, a number of dual columns were necessary which depended on the time needed for CO_2 adsorption, sorbent regeneration, and cooling of the regenerated column as well as specific CO_2 adsorption capacity of adsorbents [Fisher et al., 2009]. Pirngruber and coworkers [Pirngruber et al., 2009] simulated the breakthrough curves to evaluate the diffusion rate of CO_2 and discussed the design of a potential adsorption process. They demonstrated that desorption by heating with water vapor (TSA) was not very favorable, due to the high vapor consumption needed for heating the column. Moreover, the time needed for regeneration was much longer than the adsorption step since the thermal inertia resulted in long heating and cooling times.

Therefore, the total number of columns in a regeneration mode for each column would be largely increased. Clausse and coworkers demonstrated the experimental and numerical parametric studies on the performance of zeolite (13X and 5A) in indirect TSA processes by means of an internal heat exchanger. They reported that a purity above 95% could be achieved with a CO_2 recovery of 81%, CO_2 adsorption

capacity of 1.31 mmol/g, and a specific energy consumption of 3.23 GJ/tonne CO_2. Their results showed that this process exhibited potential as compared with other adsorption processes [Merel et al., 2008; Clausse et al., 2011]. Kulkarni and Sholl [Kulkani and Sholl, 2012] estimated a specific TSA process and suggested the operating cost to be of the order 80–150 US/tonne CO_2. They also demonstrated the monetary cost as a function of increasing CO_2 adsorption capacity of the adsorbent. The cost of CO_2 capture can be decreased to 50–80 US/tonne CO_2 for different sources of electricity by maintaining the CO_2 adsorption capacity to 2 mmol/g.

Recently, some researchers have studied the use of a hybrid pressure (or vacuum)/temperature swing adsorption (PTSA or VTSA) process to improve CO_2 capture. Pugsley and coworkers [Both et al., 1994] studied the performance of PTSA theoretically, which could achieve 90% purity with 70% recovery. Ishibashi and coworkers [Ishibashi et al., 1996] investigated a VTSA to capture CO_2 from the flue gas in a pilot plant at 1000 Nm^3/h. Tlili and coworkers [Tlili et al., 2009] also studied the use of VTSA and could achieve 99% purity for both VSA and TSA processes. They concluded that the recovery depended on desorption temperature and purge flow rate.

In addition, for Electric Swing Adsorption (ESA) processes, heat is generated by Joule effect via electric current passing through the adsorbents. The in situ heating route can effectively deliver heat to adsorbents without heating the additional media, thus ESA offers several advantages including less heat demanded, fast heating rate, better desorption kinetics and dynamics and independent control of gas and heat flow rates as compared with PSA and TSA [An et al., 2011]. Grande and his coworkers have reported several works on ESA for CO_2 capture by monolith activated carbon, carbon molecular sieves, and zeolite-based adsorbents [Grande et al., 2009]. However, relatively low CO_2 adsorption capacity and selectivity at the CO_2 partial pressure below 10 kPa were observed as well.

4.4.5. Influence of impurities

4.4.5.1. Behavior with Water

Selectivity between H_2O and CO_2 is important for using adsorbent materials to separate CO_2 from flue gas. However, to our knowledge, little research has been published on CO_2/H_2O and $CO_2/N_2/H_2O$ mixtures adsorptions: Liu and coworkers [Liao et al., 2012] reported CO_2 isotherms for CuBTC (HKUST-1) and Ni-MOF-74 with different amounts of preloaded water. Although they found that water does not affect CO_2 adsorption as much as in traditional zeolites (NaX and 5A) and it is much easier to remove water by regeneration, those two MOFs strongly adsorbed water as indicated by their steep water isotherms. Moreover, neither CuBTC (HKUST-1) nor Ni-MOF-74

can adsorb any significant amount of CO_2 when water loadings are high. This is due to the strong interactions between water molecules and the Metal Centers in both materials.

Hydration of flexible MIL-53(Cr) has been demonstrated to enhance the CO_2 adsorption relative to CH_4 [Farha et al., 2008]. They found that the terminal water molecules in the hydrated MIL provide additional interaction sites and enhance gas adsorption at low pressures. This enhancement is more pronounced for CO_2, because the carbon dioxide molecule has a strong quadrupole. However, terminal water molecules reduce free volume and gas adsorption at high pressures. Liu and coworkers [Fernández et al., 2010] also reported that the DOBDC series of MOFs (MOF-74) are prone to lose their CO_2 capacities after water adsorption. In addition, Kizzie and coworkers [Kizzie et al., 2011] observed significant decreases in CO_2 capacities for the Mg-MOF-74 and Zn-MOF-74 which were regenerated after full hydration. The effect of humidity on the performance of the MOF-74 series (M= Zn, Ni, Co, or Mg) as adsorbents for CO_2 capture has also been explored by Matzger and co-workers [Kizzie et al., 2011a]. Mg-MOF-74 demonstrated an exceptional capacity for CO_2 under flow through conditions with dry flue gas ($5N_2 : 1CO_2$). The effect of humidity on the performance of these MOFs was investigated by $N_2/CO_2/H_2O$ breakthrough experiments at relative humidities (RHs) of 9%, 36%, and 70%. After exposure of the MOFs to the gas stream at 70%RH and subsequent thermal regeneration, only about 16% of the initial CO_2 uptake capacity was recovered for Mg-MOF-74. However, about 60% and 85% were recovered for Ni-MOF-74 and Co-MOF-74, respectively. These results indicated that although Mg-MOF-74 has the highest CO_2 uptake capacity, under the conditions used in this study, Co-MOF-74 may be a more desirable material for CO_2 capture in a practical environment where water exists in varying quantities in streams of flue gas.

The presence of trace H_2O in the mixtures considerably affects the selectivity. At low pressures, the selectivity slightly increases because the H_2O binding around trimers provides additional adsorption site for CO_2. At high pressures, however, the selectivity drops due to the competitive adsorption between CO_2 and H_2O.

For zeolites, as mentioned before, moisture content make them almost useless for separation applications: for instance, a bed dried is used in industry before separating CO_2 from N_2 for air purification. Brandani and Ruthven [Brandani and Ruthven, 2004] have observed that small amounts of water can inhibited the CO_2 adsorption on diverse cationic forms of type-X (NaLSX, LiLSX, CaX), at 35 and 70ºC. According to these authors, this can be due to a reduction of the strength and heterogeneity of the zeolites electric field caused by a high adsorption capacity of water on the exchangeable cations generated by its strong polarity. Also, in some cases the presence of water during the CO_2 adsorption on the zeolites surface seems also to

favor the formation of bicarbonates species via hydroxyl group formation, causing an increase of the CO_2 desorption temperature.

Song's group [Wang et al., 2009] studied the effect of moisture on CO_2 capture using the PEI/MCM-41 and showed that the CO_2 adsorption capacity was increased from 2.03 mmol/g for an anhydrous flow containing 15% of CO_2 to 2.84 mmol/g for a flow containing 10% of moisture and 13% of carbon dioxide. The uptake improvement was interpreted in terms of adsorption mechanisms, i.e., the formation of carbamate and bicarbonate under anhydrous and hydrous conditions, respectively [Zhang et al., 2010].

A straightforward approach to mitigate water effects on stability and CO_2 adsorption is to make materials that dislike water, in other words, to create hydrophobic surfaces. This can be done through hydrophobic surfaces or modifying hydrophilic materials after synthesis. For this, Yang and coworkers [Yang et al., 2007] synthesized some fluorous metal-organic frameworks (FMOFs), wherein hydrogen atoms were substituted by fluorine atoms in all ligands. Compared to their non-fluorous counterparts, FMOFs with fluoro-lined or fluoro-coated channels or cavities have enhanced thermal stability and hydrophobicity.

4.4.5.2. Other impurities

Another issue to consider when designing a process for post-combustion CO_2-capture are the impurities. The flue gas generally brings traces of other molecules that a priori would be removed, but to some extent, should be considered. The impurities discussed herein include sulfur and nitrogen compounds, not only for possible poisoning of the adsorbents but also for environmental considerations. A summary of the main results found are listed in Table 4.4. Most of these gases are released as waste gases from industrial processes into the environment. Effective capture of these is extremely important to avoid "poisoning" the capture-related materials and for the protection of the environment [DeCoste and Peterson, 2014].

As an example, Yaghi and co-workers [Britt et al., 2008] tested the adsorption and separation performances of six MOFs: IRMOF-1, Zn4O(2-NH2-bdc)3, Zn-MOF-74, MOF-177, CuBTC and IRMOF-62, for several harmful gases including SO_2, Cl_2, NH_3, CO, ethylene oxide and tetrahydrothiophene vapor. Kinetic breakthrough measurements revealed that pore functionality, in particular by active adsorption sites, such as functional groups (NH2-) and open metal sites (in MOF-74 and CuBTC), played a key role in determining the dynamic adsorption performance of these MOFs. For example, CuBTC revealed high efficacy equal to or greater than BPL carbon against all gases tested, except Cl_2. On the basis of experimental breakthrough data, it was found that MOFs like CuBTC and M-MOF-74 (M = Zn, Co, Ni or Mg) are capable of removing

toxic gases in dry environments, but failed to do so in humid conditions, where the competitive adsorption of water nearly eliminated the adsorption capacity. It was also confirmed that the identity of the metal atoms in this series of materials has a significant impact on the loading capability for all chemicals tested in both dry and humid conditions.

Table 4.4. Recent published studies related to the impurities capture in MOFs.

GAS	MATERIAL	CONDITIONS	VALUE	REFERENCE
Sulfur Dioxide (SO_2)	IRMOF-1 (MOF-5)	10.000 ppm	<0.1	Britt et al (2008)
	IRMOF-3		0.1	
	MOF-177		<0.1	
	CuBTC (HKUST-1)		0.5	
	IRMOF-62		<0.1	
	Zn-MOF-74		3.1	
		380 ppm, 293 K	0.3	Glover et al (2011)
	Ni-MOF-74		<0.1	
	Mg-MOF-74		1.6	
	Co-MOF-74		0.6	
	FMOF-2	0.25/0.5 bar	1.1/1.4	Fernández et al (2010)
Hydrogen Sulfide (H_2S)	MIL-47	5/30 kPa, 303 K	0.2/1.5	Hamon et al (2009)
	MIL-53(Cr)		1.2/2.5	
	MIL-53(Al)		0.2/2.7	
	MIL-53(Fe)		0.2/1.2	
	Ni-MOF-74	5 kPa	6.4	Allan et al (2012)
	CuBTC (HKUST-1)	1000 ppm, 70% RH	2.7	Petit et al (2010)
	IRMOF-1 (MOF-5)	100 ppm	0.5	Huang et al (2012)
Nitrogen Oxide (NO)	CuBTC	1 bar, 298 K	3.0	Xiao et al (2007)
	Cu-SIP-3	1 bar, 293 K	1.1	Allan et al (2010)
	Ni-MOF-74	10 mbar, 303 K	6.1	Bonino et al (2008)
	MIL-88	1 bar, 303 K	2.5	McKinlay et al (2013)
	MIL-88(B)		1.6	
Nitrogen Dioxide (NO_2)	CuBTC (HKUST-1)	1000 ppm	2.2	Levasseur et al (2010)
	UiO-66		1.6	Ebrahim et al (2012)
	UiO-67		1.7	
Carbon Monoxide (CO)	CuBTC (HKUST-1)	1 bar, 295 K	0.7	Wang et al (2002)
	MIL-100(Cr)	850 torr, 303 K	1.0	Munusamy et al (2012)
		20 kPa, 298 K	0.9	Wang et al (2012)
	Mil-100(Cr) TEM		0.1	

The removal of sulfur odorant components from natural gas was explored by Mueller and co-workers [Mueller et al., 2006]. Control experiments revealed that CuBTC has a higher volume specific uptake capacity for THT than two commercially available activated carbon materials, Norit (type RB4) and CarboTech (type C38/4). The adsorption of these polar molecules induced a color change of the CuBTC sample from a deep blue into a light green, which allows for visual detection of contaminants. Furthermore, after removal of the adsorbates by treatment under vacuum or heating, the original color reappeared, indicating practical regeneration of the adsorbent. A further example was demonstrated in flexible Zn(bchp), in which H_2S and SO_2 were selectively adsorbed over N_2, CO_2, and CH_4 at room temperature [Fernandez et al., 2010]. The adsorption of H_2S in MIL-53(Al, Cr, Fe), MIL-47, MIL-100(Cr), and MIL-101 also revealed that all of these MOFs are stable toward this corrosive gas and actually have high loading capacities and are easily regenerable, thus making them potential candidates in the purification of natural gas, or for a previous stage in a post-combustion process [Stephenson et al., 1999].

Recently, Sun and coworkers [Sun et al., 2014] used molecular simulations to study twelve representative porous materials, including six MOFs, two ZIFs and four zeolites to remove SO_2 and NOx from flue gases. CuBTC and MIL-47 were identified to perform best for the removal of SO_2, while considering the simultaneous removal of SO_2, NOx and CO_2 from flue gases, Mg-MOF-74 was recommended as the most promising due to its high density of open-metal sites which provides strong interactions with dipole and quadrupole molecules.

Sulfur compounds

Sulfur dioxide: SO_2 is a common toxic chemical used in industry and present as a combustion byproduct. Along with NOx emissions from industrial processes, lead to the formation of acid rain. Britt and coworkers investigated a variety of materials for the removal of several toxic chemicals, including sulfur dioxide [Britt et al., 2008]. Materials were evaluated under dry conditions, and breakthrough results show that Zn-MOF-74 provides excellent SO_2 removal while CuBTC provides similar SO_2 removal to activated carbon. All other MOFs studied show immediate breakthrough and negligible SO_2 loadings. Although this study shows the possibility of using MOF-74 and CuBTC in dry environments, the effect of moisture was not studied; therefore, it is unknown if H_2O is preferentially adsorbed over SO_2.

Glover and coworkers further investigated MOF-74 for SO_2 removal, this time looking at the effect of the metal in the SBU [Glover et al., 2011]. Four analogues were evaluated: Co, Mg, Ni, and Zn, for SO_2 dynamic breakthrough capacity at a concentration of 380ppm at 293K. In this study, moisture was added to determine both

dry (0%RH) and humid (80%RH) loadings. Under dry conditions, Mg-MOF-74 provided superior SO_2 removal, Co-MOF-74 provides about one-third of the loading, with the overall loadings decreasing according to the order Mg > Co > Zn > Ni. Under humid conditions, only the Mg-MOF-74 sample provided any appreciable SO_2 removal.

Additional work from a novel high temperature solid sorbent based on lithium orthosilicate (Li_4SiO_4) [Pacciani et al., 2011] has shown promises results for post-combustion CO_2 capture, however its performance in the presence of contaminants such as SO_2 drastically decreases capacity. Thus, industrial application would require desulfurization of flue gas prior to contacting the adsorbent.

In addition to experimental studies on sulfur dioxide sorption, a number of theoretical studies have been conducted: Fioretos and coworkers performed ab initio analyses of substituted benzenes, representing the linkers on the IRMOF series [Fioretos et al., 2011]. Calculations showed interaction energies between SO_2 and aniline, and it was found that molecules with larger dipole moments will interact more strongly with the amine group. The authors suggest that incorporating polar functional groups onto MOF linkers allows for better interaction, and thus separation, of polar compounds. Ding and Yazaydin performed DFT and GCMC calculations on the effects of flue gas on the CO_2 uptake of M-MOF-74 (M = Co, Mg, Ni) MOFs [Ding and Yazaydin., 2012]. Specifically, they found adsorption energies greater than 200 kJ/mol for the Co and Mg analogues, whereas the adsorption energy for the Ni analogue was approximately 50 kJ/mol. The former are representative of chemisorption and correspond to the experimental trend in SO_2 capacities reported by Glover and coworkers [Glover et al., 2011]. The study indicates that Ni-MOF-74 is actually preferred for CO_2 adsorption in flue gas applications, as SO_2 will have less impact on CO_2 adsorption; however, it also indicates that the Co and Mg analogues are better for SO_2 removal.

Most of these type materials do not provide the necessary chemistry for SO_2 reaction. Furthermore, moisture typically inhibits SO_2 removal on MOFs. However, some studies indicate that MOFs may be used as structures to hold nanoparticles or salts for SO_2 removal, and is a potential area for further study.

**Hydrogen sulfide:** H_2S is a toxic chemical commonly encountered as an impurity in the petroleum and natural gas industries and is also a byproduct of anaerobic decomposition, which gives it the commonly referred to name of sewer gas.

For this gas, Watanabe and Sholl used GCMC simulations to calculate adsorption in CuBTC [Watanabe and Sholl, 2010], founding that the material can adsorb at 50% of active copper sites at 300K, even at partial pressures less than 10bar. In addition, breakthrough experiments showed that H_2S reacts with the CuBTC,

causing the structure to breakdown and therefore may be promising for single-use filters.

Nitrogen oxides

Mononitrogen oxides: NOx are produced from the reaction of nitrogen and oxygen in the air during high-temperature combustion. NOx is composed of nitric oxide (NO) and nitrogen dioxide (NO_2).

As NO is a free radical, it strongly interacts with the metal centers of some MOFs, such as the CuBTC, MOF-74, and MIL- [Bordiga et al., 2007; Bonino et al., 2008; McKinlay et al., 2013] CuBTC shows a significant hysteresis observed in the NO isotherm, indicating the strong irreversible adsorption of many of the molecules on the coordinatively unsaturated copper sites. Furthermore, the binding energy for NO to the Cu^{2+} ion is much less than that for H_2O, meaning that NO likely cannot displace H_2O molecules that are preadsorbed onto CuBTC or found in the same streams as NO. Besides, there is no subsequent filling of the micropores at low partial pressures as the intermolecular forces between individual NO molecules are relatively weak. Ni-MOF-74 was also investigated, showing the highest reported capacity for any MOF [Allan et al., 2010]. Furthermore, NO is selective toward Ni(II), as there are minimal intermolecular interactions between NO molecules, whereas H_2O completely fills the pores after interacting with Ni(II). In contrast, Yu and coworkers [Yu et al., 2012] showed that NO has negligible loadings in Mg-MOF-74 through DFT studies, which they attribute to the absence of d-electrons in Mg.

Contrarily, NO_2 molecules do not make strong ligands for binding and rely heavily upon physical adsorption in MOFs or chemical reaction with the surface. The NO_2 dipole gives it the ability to interact with functional groups that may be incorporated onto the MOF linkers. Furthermore, it was shown that NO_2 molecules can react with carboxylate bonds to form species covalently bound to the MOF [Petit et al., 2012; Levasseur et al., 2010; Petit et al., 2012].

For instance, the adsorption capacity for CuBTC under dry (0%RH) conditions at room temperature for a 1000ppm NO_2 stream was calculated to be 2.21 mmol/g, however at conditions of 70%RH, the removal capacity is decreased to 1.13 mmol/g. The reduction in capacity under humid conditions is due to the competitive adsorption and coordination to Cu sites by water molecules. The structure of CuBTC is degraded when exposed to NO_2 as supported by FTIR and N_2 isotherm data.

Wang and coworkers have shown through GCMC simulations that both NO and NO_2 are weakly adsorbed on Zn_4O MOFs such as IRMOF-1 and MOF-177 [Wang et al., 2009]. Furthermore, the isotherms at 298K are fairly linear, indicating minimal interaction between the adsorbates and the inner surfaces.

**Nitrous oxide:** N_2O is present in air at concentrations of 300–350 ppb and represents an increasing problem in the separation of air [Khatri et al., 2006]. The presence of N_2O is most troublesome in facilities designed primarily to supply gaseous O_2, as well as in those plants equipped to additionally recover the rare gases Kr and Xe. CO_2 is generally the first primary contaminant to breakthrough a TSA pre-purifier. As a result, the adsorber effectiveness can be monitored continuously by sensing the CO_2 concentration of the effluent. Since N_2O breaks through the bed before CO_2 in conventional pre-purifiers, effective design for CO_2 does not guarantee the removal of N_2O to the desired efficiency. To reverse this effect, selective adsorbents for N_2O over CO_2 have been sought [Coudert et al., 2009]. The highest selectivity in zeolites, determined by the ratio of Henry's law constants was found for CaX, Na mordenite and BaX. These results suggest zeolites with high cation charge density and low Si/Al ratio for N_2O removal. The typical configuration is a three-layer adsorbent bed in which H_2O is removed in the first layer, CO_2 is removed in the second layer and the combination of CO_2 and N_2O are removed in the third layer [Plaza et al., 2007b].

Both CO_2 and N_2O have a kinetic diameter of 3.3Å. Adsorption studies of 5Å adsorbent with CO_2 and N_2O [Serna-Guerrero and Sayari, 2006] at relatively high concentrations (1800–24000ppm) suggest that CO_2 is the more strongly adsorbed molecule, although co-adsorption was significant. In view of these observations, it is doubtful that a selectivity of N_2O-over-CO_2 greater than 1.0 can be achieved in low Si/Al ratio zeolites.

Although adsorbent materials would be expected to selectively adsorb N_2O over N_2, such selectivity may be diminished by the large concentration advantage of N_2 (790 000 ppm) over N_2O (0.35 ppm) in the gas mixture. Thus, the problem becomes one of finding an appropriate adsorbent that has high N_2O/N_2 separation factor, high N_2O capacity and low N_2 loading.

Carbon Monoxide:

_CO_ is a colorless and odorless gas, resulting from the partial oxidation of carbon-containing compounds. Carbon monoxide separations have already been thoroughly reviewed [Li et al., 2009; Li et al., 2011a].

For this case, MOFs with unsaturated centers have the highest affinity for CO, but their capacities are still not very high. However, the removal of CO can be accomplished through catalytic oxidation to CO_2 in many instances. Sorbents MOFs such as CuBTC and MOF-74 have been studied for the removal of CO because of the ability of the metal ions to coordinate to CO, forming carbonyl complexes. The adsorption of CO on CuBTC was initially examined by Wang and coworkers [Wang et

al., 2002]. Karra and coworkers calculated through GCMC methods that the CO capacities are higher in CuBTC compared to Zn-based MOFs (IRMOF-1, IRMOF-3, and DMOF), largely due to the electrostatic interactions between the open copper sites and CO molecules [Karra et al., 2010; Zhou et al., 2011].

It has also been shown that amine groups can increase the adsorption capacity, as observed in IRMOF-3 or even serve as sites for the synthesis of Pd catalysts within the pores [Kleist et al., 2010]. Woo and coworkers [Prasad et al., 2010] carried out GCMC and MD studies of CO and CO_2 adsorption in ZIF-68 and ZIF-69. The GCMC simulation was performed at low pressures (0–1atm) at 273K. In the low-pressure range, the uptake of gas molecules is not determined by the geometric structure, but controlled by the properties of binding sites in the framework.

5

MOLECULAR MODELING OF MATERIALS FOR CO_2 CAPTURE AT TSA PROCESS CONDITIONS [1]

5.1. Background information

Traditionally, the industrial needs for high purity gases require several consecutive cycles of cryogenic fractional distillation [Parkes et al., 2013]; however the selective isolation of these gases near room temperature, known as Swing Adsorption Cycles, has reduced the dependence of the first less efficient energy processes in specialized applications, and represents a revolutionary advance in order to achieve a more dynamic production at industrial level.

For post-combustion CO_2 capture, the absorption with amines is the process used at demonstration and industrial scale. This has been the strategy further explored to date, since it can be easily adapted to existing plants. Nevertheless, although this process allows CO_2 capture with a high selectivity, the use of aqueous absorbent carries an energy penalty of about 30% of the energy produced in the central [Sumida et al., 2012], which reinforces the search for more efficient processes. In spite of the increasing interest for efficient materials for CO_2 separation for a gas stream at different conditions, most of the published work focused on adsorption isotherms and few to mixture measurements, providing limited data to be used for the industrial conditions.

The composition of a typical post-combustion flue gas has a relatively low CO_2 concentration (14-16% v/v), while the bulk of the effluent is composed of N_2 (73-78% v/v) and other minor components, such as H_2O (5-7% v/v), O_2 (3-4% v/v), CO, NOx, and SOx (ppm). In this sense, a high selectivity toward CO_2 is crucial, such that only pure carbon dioxide be captured and subjected to permanent storage or utilization. This is why these alternative adsorption processes (like PSA and TSA) advance in order to achieve a more dynamic production, but require very efficient sorbent materials to be practical. It should be noted that since the flue gas is released near ambient pressure, compressing or applying a vacuum to such a large volume of gas is expected to be more expensive than heating (that can even be supplied by the energy of the combustion gases), and therefore, TSA might represent a most viable process than PSA or VSA [Hedin et al., 2013]. The gas stream is released at a total pressure of approximately 1atm, and since SOx removal would precede CO_2 capture, the flue gas would be expected to enter the scrubber at temperatures between 40 and 60ºC. As outlined, an ideal adsorbent for CO_2 capture from a post-combustion stream should exhibit a high selectivity, but also high gravimetric and volumetric adsorption capacities, minimal energy penalty for regeneration, long-term stability under the operating conditions and rapid diffusion of the gas through the adsorbent material, to name the key ones. Traditional industrial sorbents, such as zeolites and porous carbons, usually have high surface areas and pore volumes, which generally promote uptake of weakly interacting gases [Krishna and van Baten, 2010]. In addition, Metal–Organic Frameworks (MOFs) have recently appeared with their synthetic versatility to enable a "materials by design" approach [O'Keeffe and Yaghi, 2012].

Regarding the characterization of materials for separation, molecular simulation has become a complementary tool to the experimental ones, and its value in this field has been proven through the intense interest in MOFs for storage of hydrogen, methane, and carbon dioxide [Duren et al., 2009; Meek et al., 2011]. Specifically, GCMC simulations can be used as a screening method for adsorption properties, providing valuable data such as adsorption isotherms, loadings, heats of adsorption and Henry's constants, all of which could have experimental counterparts that can be used for model validation. According to literature, using standard force fields can predict MOF adsorption trends and properties with reasonable accuracy, enabling both structural correlations and specific high-performing MOFs to be identified [Li et al., 2012]. With respect to the studied gases, both experimental measurements and computational simulations of low temperature adsorption are commonly used to determine pore volumes in MOFs and related frameworks [Walton et al., 2008]; however, only a few published studies have considered the room temperature adsorption (or process conditions) of other gases, and is what in part justifies this study [Huck et al., 2014].

Here, we present a systematic investigation of several types of families of MOFs found in literature (that has shown good preliminary results in the CO_2/N_2 separation type) vs. typically zeolites and materials used in industry for gas storage and CO_2 purification. GCMC simulations are used to identify features of these structures. The main objective is, by a fast screening using simulation, to find the most suitable adsorbent for a real Temperature Swing Adsorption process.

5.2. Force field and simulation details

Models for the zeolites and Metal–Organic Frameworks used in this work were taken from published single-crystal X-ray diffraction structures. Unit cells of non-orthogonal crystals were orthogonalized for later ease in simulation and analysis. Solvent molecules were deleted where appropriate, providing "activated" structures [Tagliabue et al., 2009]. All frameworks were treated as rigid structures with atoms fixed at their crystallographic positions. Using rigid crystallographic atom positions to model MOFs has been found to be appropriate for GCMC simulations when predicting adsorption of small gas molecules [Yan et al., 2009]. It should be noted that MOFs can be more flexible than zeolites, and several authors have explicitly considered the flexibility in their simulations [Coudert et al., 2011; Tan et al., 2010]. However, it is expected that their flexibility will have little influence on the adsorption, due to the range of pressures evaluated in this work (see, for instance the case of MIL-53(Al) in Figure 5.10). Hence, as considering flexibility increases the computational time and it should not affect our results, we have decided to simulate rigid frameworks.

The Lennard-Jones parameters for zeolites were taken from the force field of Watanabe and coworkers [Watanabe et al., 1995], while most of MOFs atoms were taken from the DREIDING force field [Mayo et al., 1990] with UFF [Rappé et al., 1992] parameters taken for structures with open metal sites. UFF force fields have been designed to be very generic, so that broad coverage of the periodic table, including metals, and transition metals, could be achieved. All van der Waals parameters are listed in Table 5.1, including the charges used for the frameworks atoms [Parkes et al., 2013; Dubbeldam et al., 2007; Xu et al., 2010; Martín-Calvo et al., 2008; Yazaydin et al., 2009; Ramsahye et al., 2007].

Table 5.1. *Lennard-Jones parameters for each atom used in the GCMC simulations.*

	ATOM	σ (Å)	ε/k_B (K)	q (e$^-$)	Force Field (REF)
Zeolites	Si	2.3	22	2.05	
	Al	2.3	22	1.75	[Watanabe et al., 1995]
	O_{Si-Si}	3.3	53	-1.025	
	O_{Al}	3.3	53	-1.2	
	Na	2.8	70	1	
MOFs	C	3.47	47.8	*	
	H	2.85	7.6	*	DREIDING [Mayo et al., 1990]
	O	3.03	48.2	*	
	N	3.26	34.7	*	
	Zn	2.46	62.4	*	
	Cu	3.114	2.52	*	UFF [Rappé et al., 1992]
	Zr	2.783	34.72	*	
	Mg	2.6914**	55.857	*	
GASES **Nitrogen**	N	3.31	36	-0.482	
	$COM_{(N2)}$	-	-	0.964	TraPPE [Potoff and Siepmann, 2001]
Carbon dioxide	C	2.8	27	0.7	
	O	3.05	79	-0.35	
Water	Hw	-	-	-	TIP-4P/2005 [Abascal and Vega, 2005]
	Ow	3.159	93	0.5564	
	q_{water}	-	-	-1.128	

Parameters for the gas atoms were taken from the literature in a transferable manner, as they accurately reproduce the condensed phase properties [Babarao and Jiang, 2009]. CO_2 and N_2 were modeled using the TraPPE force field [Potoff and

Siepmann, 2001]: the CO_2 molecules were modeled as rigid and linear with a partial charge of 0.35e- on the O atoms and a partial charge of +0.70e- on the C atom. A rigid, linear, three-site model was also used for the diatomic N_2 molecules, with partial charges of 0.482e- and +0.964e- on the N atoms and center of mass, respectively (with fixed bond lengths of 1.16 and 1.1 A for both molecules). The TIP-4P/2005 model, one of the most accurate models for water, was used to represent the H_2O molecule in order to evaluate the moisture effects in the mixture [Abascal and Vega, 2005]. A schematic representation of the molecules is shown in Figure 5.1.
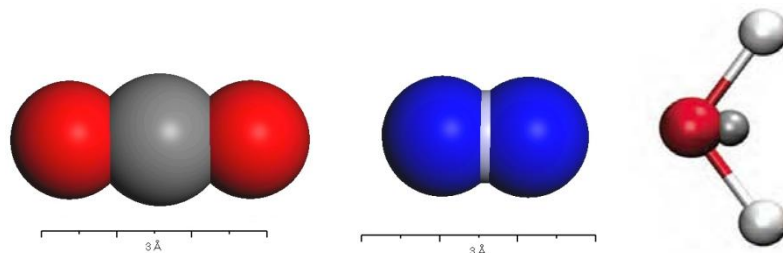
Figure 5.1. *Schematic representation of the molecules modeled (carbon dioxide, nitrogen, and water).*

GCMC simulations were performed using the *Sorption* code in Materials Studio 6.1 [*Accelrys M.S.*, 2013]. The GCMC movements included random translation, rotation and reinsertion of an existing molecule. The usual periodic boundary conditions were used. At each chemical potential, 10^7 moves were used to equilibrate the system and additional 10^7 MC moves were used for data collection. When necessary, multiple unit cells were used so that each cell parameter had a minimum dimension of 25 Å. A cutoff radius of 12.5Å was applied to the Lennard–Jones interactions, and the long-range electrostatic interactions were calculated using Ewald summation. The Lorentz–Berthelot combining rules were used to calculate the adsorbate/framework and adsorbate-adsorbate Lennard–Jones parameters. And in addition, the Peng-Robinson equation of state was used to relate the pressure with the chemical potential required in the GCMC simulations.

The selectivities were calculated as indicated in section 2, following equations (2.2) to (2.4)

Packed bed adsorber breakthrough simulations: We also performed

transient breakthrough calculations, following the methodologies described in Chapter 2 of this dissertation. Assuming plug flow of a gas mixture through a fixed bed maintained under isothermal conditions and negligible pressure drop, the partial pressures in the gas phase at any position and instant of time were obtained by solving the set of partial differential equations for each of the species *i*.

The equations were discretized using the finite differences scheme, while the molar loadings of the species i, q_i, at any position z and time t, were determined from correlations obtained GCMC calculations at different mixtures. Specifically, the calculations presented here were performed by taking the following parameter values: bed length, L = 0.1 m; voidage of bed, ε = 0.4; superficial gas velocity u = 0.1 m/s (at inlet).

5.3. Main results

Results concerning this study were divided in two parts: simulations for pure components and simulations for mixtures. Regarding the adsorption study of pure components, we focused on validating the force fields employed, the adsorption isotherms and the properties obtained for the substances at very low pressures (as Q_{ST} and K_H). In the mixture study the focus was on calculating selectivities for different materials (representative structures and those with the greatest potential for the process evaluated were selected). An additional analysis considering the breakthrough curves was also performed. Further analyses include the effect of water traces into the process in an attempt to assess behaviors under real operating conditions.

5.3.1. Validation of models

As mentioned, we have performed GCMC simulations to obtain adsorption isotherms of pure CO_2 and pure N_2 on eleven different types of materials and results were compared with available experimental data found in literature in order to assess the validity of the models for further predictions. The simulated isotherms were compared with experimental gas adsorption curves when available. This allowed us to quantify the accuracy of our predictions.

The materials were selected considering the results of the detailed review presented in chapter 4 of this dissertation. A crystallographic 2D representation of the evaluated structures is shown in Figure 5.2.
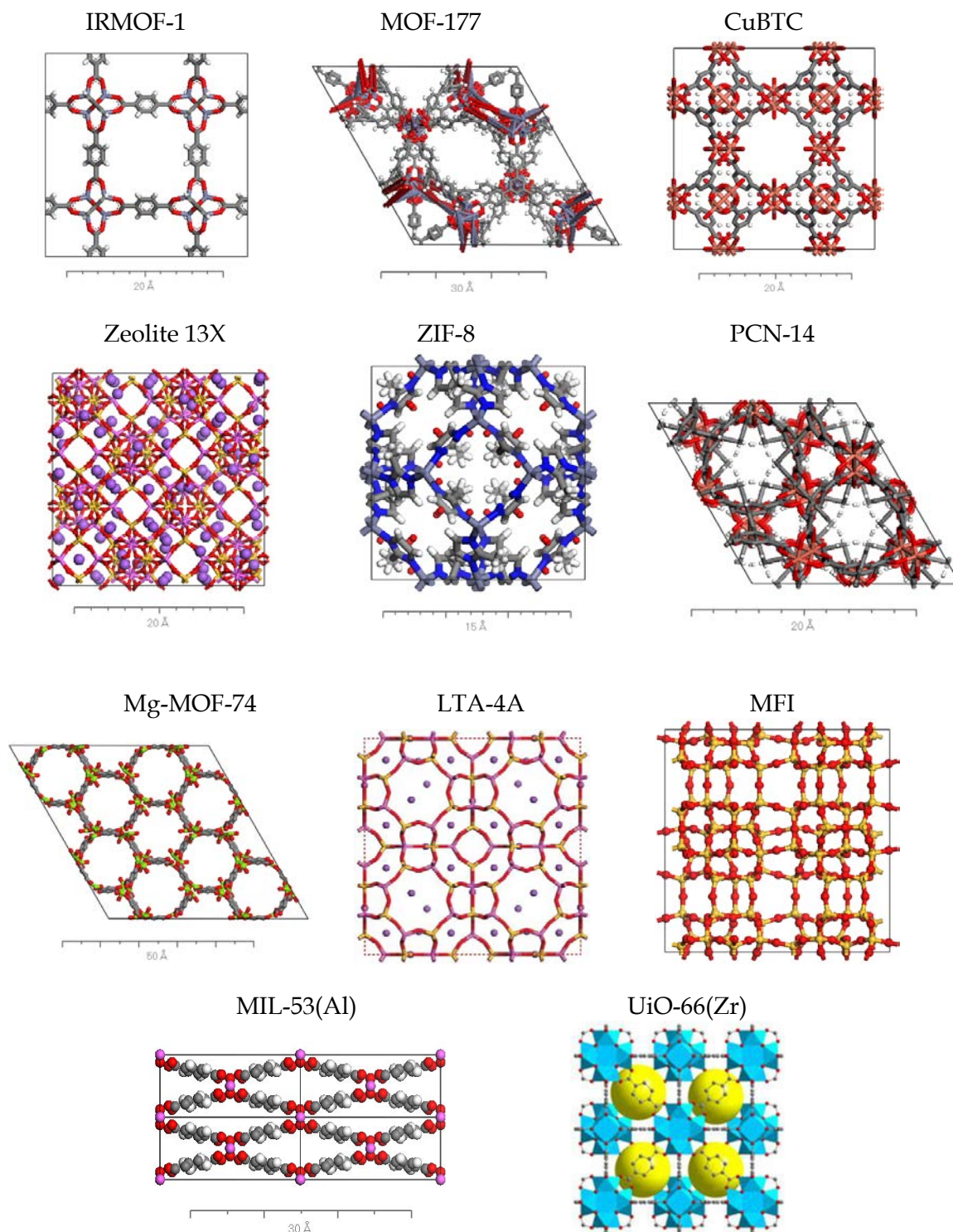
IRMOF-1

MOF-177

CuBTC

Zeolite 13X

ZIF-8

PCN-14

Mg-MOF-74

LTA-4A

MFI

MIL-53(Al)

UiO-66(Zr)

Figure 5.2. Adsorbents materials considered for CO_2 separation

For evaluating the performance of Mg-MOF-74 and MOF-177, the pure component CO_2 and N_2 adsorption isotherm data were obtained from the works of Dietzel et al. [Dietzel et al., 2009] and Mason et al. [Mason et al., 2011]. For evaluating the performance in MIL-53(Al) and PCN-14, the data were obtained from the works of

Boutin et al. [Boutin et al., 2010] and Parkes et al. [Parkes et al., 2013]. For CuBTC, the work from Wang et al. [Wang et al., 2002] was used. For evaluating the performance of UiO-66(Zr) and LTA-5A the adsorption isotherms reported by Wiersum et al. [Wiersum et al., 2013] were used, and for LTA-4A, the data from Bae et al. [Bae et al., 2013]; for IRMOF-1, the data by Furukawa et al. [Furukawa et al., 2010] at various temperatures, and for ZIF-8, the data by McEwen et al. [McEwen et al., 2013]. And finally, for evaluating the performance of zeolites NaX and MFI, the pure-component CO_2, and N_2 adsorption isotherms were taken by the reported data by Cavenati et al. [Cavenati et al., 2004] and Krishna et al. [Krishna et al., 2010], respectively.

Figure 5.3 depicts the pure adsorption isotherms calculated in this work and compared with the experimental data (the charges used for each atom of the MOFs structures are also presented).
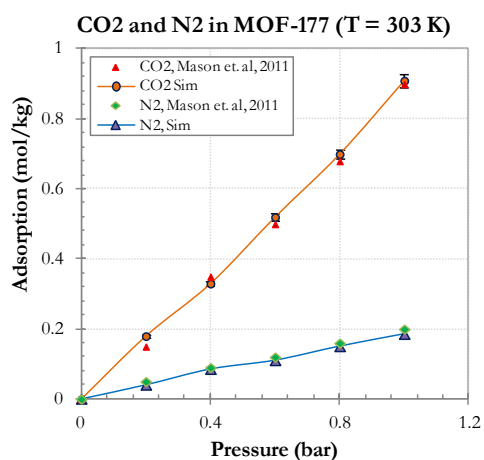
IRMOF-1 (MOF-5)
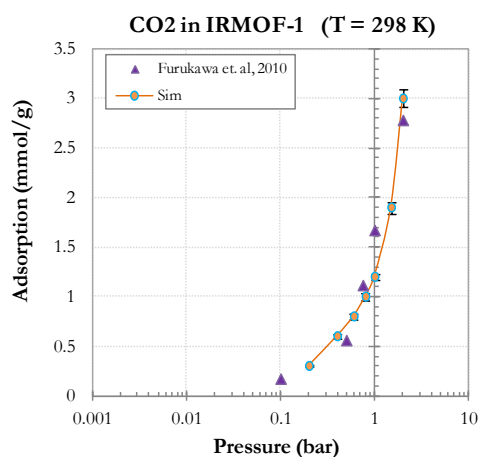
Element type	Charge (e⁻)
Zn [O,O,O,O]	1.275
O [Zn,Zn,Zn,Zn]	-1.50
O [C,Zn]	-0.60
C [C,O,O]	0.475
C [C,C,C]	0.125
C [C,C,H]	-0.15
H [C]	0.15

[Charges Ref: Dubbeldam et al. (2007)]

MOF-177

Element type	Charge (e⁻)
Zn	1.59
Oᵃ	-1.92
Oᵇ	-0.79
Cᵃ	0.80
Cᵇ	0.05
Cᶜ	-0.13
H	0.11

[Charges Ref: Xu and Zhong (2010)]

CuBTC (HKUST-1)

CO₂ and N₂ in Cu-BTC (T = 295 K)
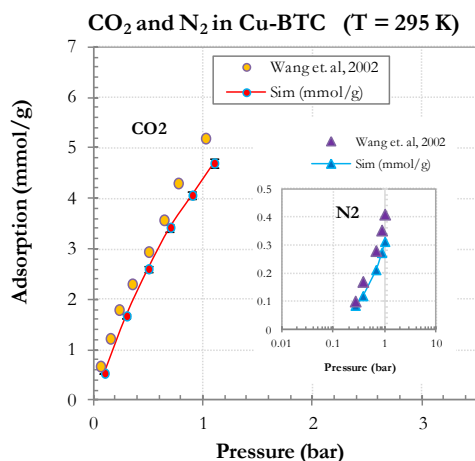
Element type	Charge (e⁻)
Cu [O,O,O,O]	1.098
O [C,Cu]	-0.665
C [C,O,O]	0.778
C [C,C,C]	-0.092
C [C,C,H]	-0.014
H [C]	0.109

[Charges Ref: Martín-Calvo et al (2008)]

MIL-53 (Al) - np

CO2 and N2 in MIL-53 (Al)
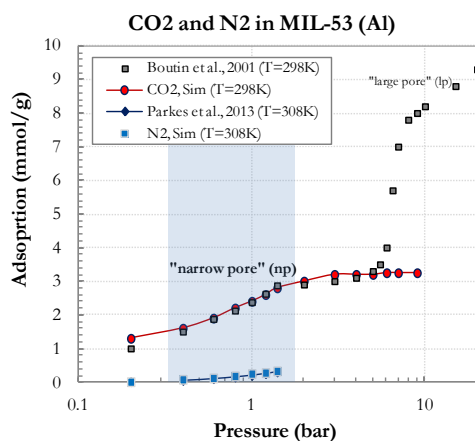
Element type	Charge (e-)
Al [O,O,O,O,O,O]	1.420
O [Al,Al,H]	-0.729
O [Al,C]	-0.564
C [C,O,O]	0.584
C [C,C,C]	-0.082
C [C,C,H]	-0.089
H [C]	0.145
H [O]	0.301

[Charges Ref: Ramsahye et al. (2007)]

Note: only the "narrow pore" structure was evaluated in this work due to the pressure range used for TSA (avoiding "breathing" effect; rigid structures)

ZIF-8

CO₂ and N₂ in ZIF-8 (T = 298 K)
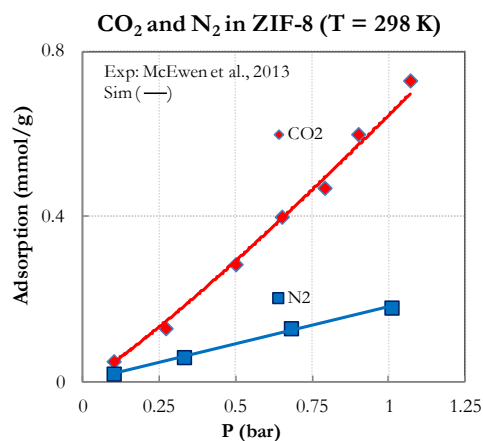
Element type	Charge (e-)
Zn [N,N,N,N]	0.749
C [C,N,N]	0.698
C [C,H,H,H]	-0.0093
C [C,H,N]	0.0117
N [C,C,Zn]	-0.387
H [C]	-0.139
H	0.0627

[Charges Ref: Xu and Zhong (2010)]

PCN-14

N₂ in PCN-14 (T = 308 K)
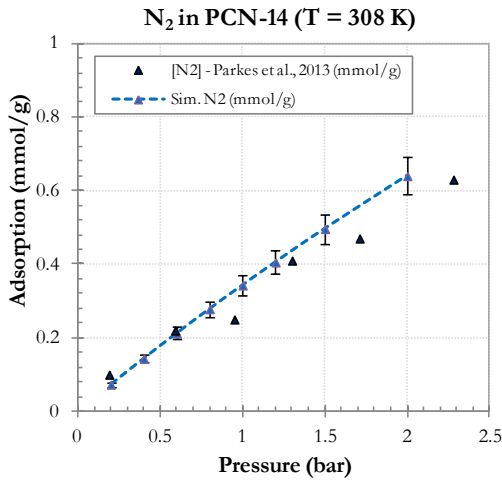
Element type	Charge (e-)
Cu [O,O,O,O]	1.05
O [C,Cu]	-0.65
C [C,O,O]	0.79
C [C,C,C]	0.04
C [C,C,H]	-0.14
H [C]	0.10

[Charges Ref: Parkes et al. (2013)]

Mg-MOF-74

CO₂ and N₂ in Mg-MOF-74 (T = 298 K)
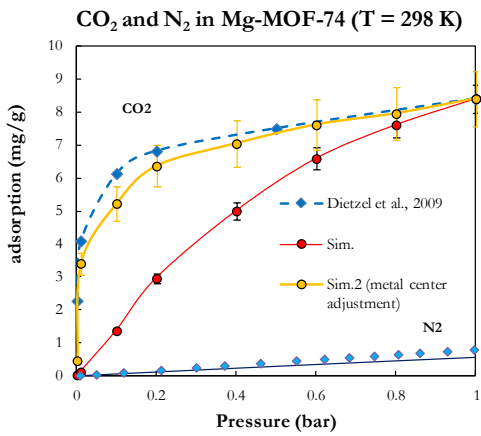
Element type	Charge (e-)
Mg	1.46 *
Oᵃ	-0.91
Oᵇ	-0.71
Oᶜ	-0.78
Cᵃ	0.80
Cᵇ	-0.26
Cᶜ	0.49
Cᵈ	-0.28
H	0.19

[Charges Ref: Yazaydin et al. (2009)]

Note: For Mg-MOF-74, the UFF sigma parameter assigned to the metal center (Mg) was adjusted (reduction to the half) as mentioned in literature, in order to reliably produce exp data and also to give a good agreement between the binding energy calculated with the force field and with DFT.

ZEOLITE 13X (NaX)

CO₂ and N₂ in NaX (T = 298 K)

LTA-4A

CO₂ and N₂ in LTA-4A (T = 298 K)
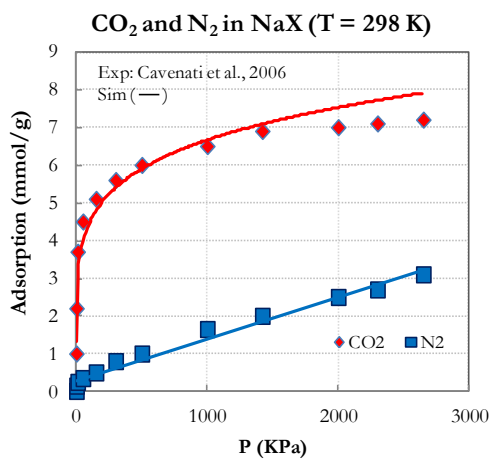
MFI

Figure 5.3. *Validation of adsorption isotherms obtained with GCMC (marked as "sim"), compared to experimental data.*

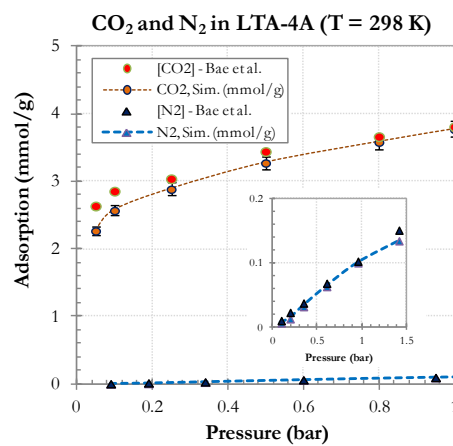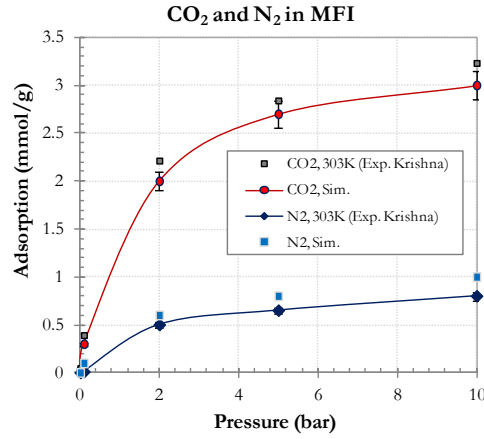The experimental and simulated gas uptake agree with each other well enough to feel confident in drawing conclusions on the adsorption trends obtained for the pressure range we are interested in, that is, close to atmospheric conditions (TSA process). Therefore, the parameters used in this work give good reproduction of the corresponding experimental adsorption isotherms, validating the use of these force fields for a fast screening procedure.

5.3.2. Calculated pure adsorption isotherms

The pure-component CO_2 and N_2 adsorption calculated isotherm data for zeolites and MOFs were fitted with the dual-site Langmuir–Freundlich (DSL-F) model for a range equivalent with operational conditions (close to ambient pressure and temperature, and with temperature rises above 400K). The parameters are provided in Table 5.2a and 5.2b.

For the obtained pure component isotherms, a dual-site Langmuir–Freundlich adjust was used:

$$q_i = \frac{q_{i,sat,A}b_{i,A}P_i^{v_{i,A}}}{1 + b_{i,A}P_i^{v_{i,A}}} + \frac{q_{i,satB}b_{i,B}P_i^{v_{i,B}}}{1 + b_{i,B}P_i^{v_{i,B}}} \tag{5.1}$$

with T-dependent parameters $b_{i,A}$ and $b_{i,B}$:

$$b_{i,A} = b_{0i,A}exp\left(\frac{E_A}{RT}\right) \quad ; \quad b_{i,B} = b_{0i,B}exp\left(\frac{E_B}{RT}\right); \tag{5.2}$$

Experimental gas isotherms are reported as excess adsorption, and simulated data is obtained as total adsorption. Note that at the low pressures considered here, excess and total gas adsorptions are nearly identical, so the difference can be ignored;

the situation will be different at high pressures, in this case, the simulation data should be converted to excess adsorption.

Table 5.2. *Temperature-dependent fit parameters for (a) CO_2 and (b) N_2 adsorption isotherms using a Langmuir-Freundlich Dual Site model (273 K < T < 450 K).*

(a) Carbon dioxide

MATERIAL	q_A (mmol/g)	b_{0A} (kPa^{-1})	E_A (kJ/mol)	v_A	q_B (mmol/g)	b_{0B} (kPa^{-1})	E_B (kJ/mol)	v_B
Activated Carbon	28.0	1.00x10^{-7}	5000	2.1	9.6	2.40x10^{-6}	16000	1
CuBTC (HKUST-1)	18.2	1.37x10^{-7}	25500	1	0	0	0	1
IRMOF-1	28.0	9.50x10^{-6}	10000	1	0	0	0	1
LTA-4A	1.75	4.19x10^{-4}	15500	1	2.5	1.07x10^{-5}	17500	1
MCM-41	14.0	1.50x10^{-7}	20000	0.9	20	2.20x10^{-7}	18000	1
MFI	2.0	3.48x10^{-7}	28000	1	1.9	1.80x10^{-5}	12000	1
MIL-53 (Al)	5.0	6.21x10^{-5}	12500	1	0.01	3.73x10^{-4}	35000	1
Mg-MOF-74	6.3	2.44x10^{-8}	40000	1	9.3	1.39x10^{-7}	24000	1
MOF-177	8.0	1.00x10^{-5}	12000	1	0	0	0	1
NaX	3.5	3.64x10^{-9}	35000	1	5.2	6.04x10^{-8}	35000	1
PCN-14	15.5	1.00x10^{-7}	25000	1	8.6	2.40x10^{-6}	16000	1
SWNT	3.0	1.00x10^{-5}	20000	1	2.0	2.40x10^{-9}	40000	1
UiO-66 (Zr)	23.5	1.00x10^{-10}	2000	2.1	8.6	2.40x10^{-6}	16000	1
ZIF-8	6.8	8.60x10^{-6}	12000	1	2	6.80x10^{-10}	35000	1

(b) Nitrogen

MATERIAL	qA (mmol/g)	b0A (kPa-1)	EA (kJ/mol)	vA	qB (mmol/g)	b0B (kPa-1)	EB (kJ/mol)	vB
Activated Carbon	2.0	1.00x10^{-6}	15000	1	0.8	2.04x10^{-6}	16000	1
CuBTC (HKUST-1)	2.2	1.37x10^{-7}	24000	1	0	0	0	1
IRMOF-1	60.0	1.20x10^{-8}	20000	1	0	0	0	1
LTA-4A	4.2	2.00x10^{-5}	6500	1	0	0	0	1
MFI	6.6	7.00x10^{-8}	20000	1	3.8	8.00x10^{-8}	20000	1
MIL-53 (Al)	8.6	6.20x10^{-7}	15000	1	1	5.00x10^{-8}	10000	1
Mg-MOF-74	14.0	4.96x10^{-7}	17500	1	0	0	0	1
MOF-177	4.0	1.40x10^{-6}	15000	1	0	0	0	1

MATERIAL	qA (mmol/g)	b0A (kPa-1)	EA (kJ/mol)	vA	qB (mmol/g)	b0B (kPa-1)	EB (kJ/mol)	vB
NaX	3.0	2.00×10^{-6}	12500	1	0.5	5.00×10^{-5}	12500	1
PCN-14	8.0	1.00×10^{-8}	25000	1	1.3	2.40×10^{-6}	16000	1
UiO-66 (Zr)	2.3	1.00×10^{-4}	2000	1	3.3	2.40×10^{-6}	15000	1
ZIF-8	4.0	1.60×10^{-6}	15000	1	0	0	0	1

In order to make a more realistic comparison for gas stream at temperatures slightly over ambient conditions, Figure 5.4 shows the simulated pure gas sorption isotherm of N_2 and CO_2 in the adsorbent materials as function of lower pressures and at a temperature of 318K (i.e. 45°C). Other simulated conditions can be found in Figure 5.5. In addition to the eleven materials simulated in this work we have included other representative materials such as activated carbon, mesoporous silica (MCM-41) and carbon nanotubes (SWCN) from the literature, obtained from Delgado et al. [Delgado et al., 2014], Builes et al. [Builes et al., 2011] and Cinke et al. [Cinke et al., 2003], respectively, and extrapolated when necessary by using the DSL-F model. In this study, the adsorption is given in units of kmol gas per cubic meter of adsorbent, taking into account that the different materials used in the adsorption column should not affect its dimensions. Gravimetric comparison of carbon dioxide between different materials over a wide range of pressures can be found elsewhere [Krishna and van Baten, 2012; Krishna and Long, 2011].

a) Nitrogen
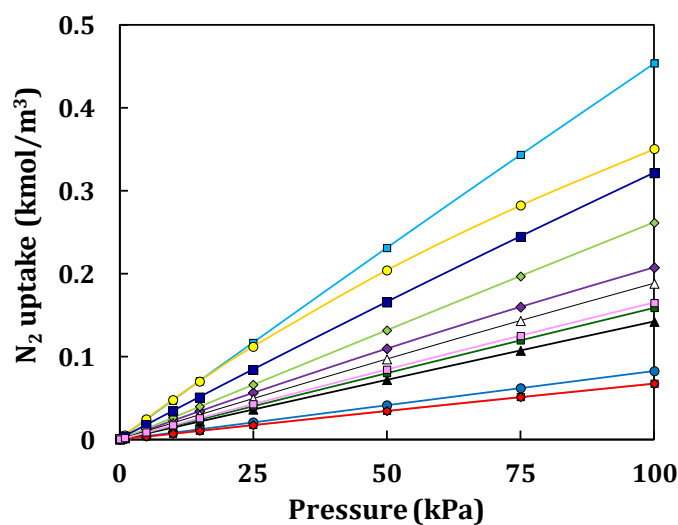
b) Carbon dioxide
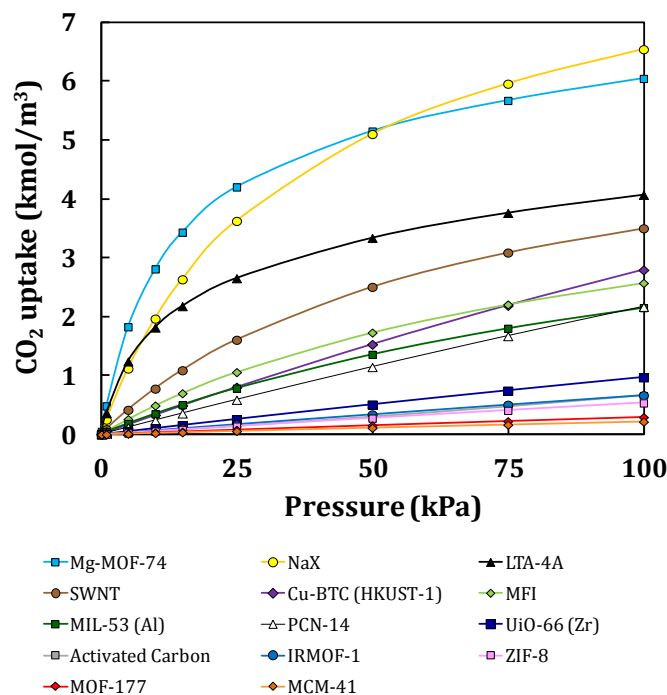
Figure 5.4. *Comparison of simulated adsorption isotherms for (a) nitrogen and (b) carbon dioxide in selected MOFs, zeolites and other adsorbent materials selected (T = 318 K). Symbols represent the GCMC results, and the lines are guides to the eyes, obtained by the DSL-F model (error bars are smaller than symbols).*

As shown in Figure 5.4, the uptake amount of CO_2 adsorbed is significantly higher than that of N_2 for all structures, with a type I isotherm shape in most of them, indicating that these are *a-priori* good candidate materials for CO_2/N_2 separation, being zeolite 13X (NaX) the highest carbon dioxide adsorbent, followed very closely by Mg-MOF-74. Specifically, for Mg-MOF-74 it was observed that CO_2 uptake capacity almost doubles that of any other MOF material; it was also noted that MOF-177 showed the lowest uptake capacity, mainly explained because of its low pore volume (Xu and Zhong, 2010).

It was also noted that, for N_2 isotherms comparison, most of the MOFs display roughly linear plots of adsorption vs. pressure, indicating that the frameworks are not saturated at these conditions. (Figure 5.5 shows simulated behaviors for higher pressures).
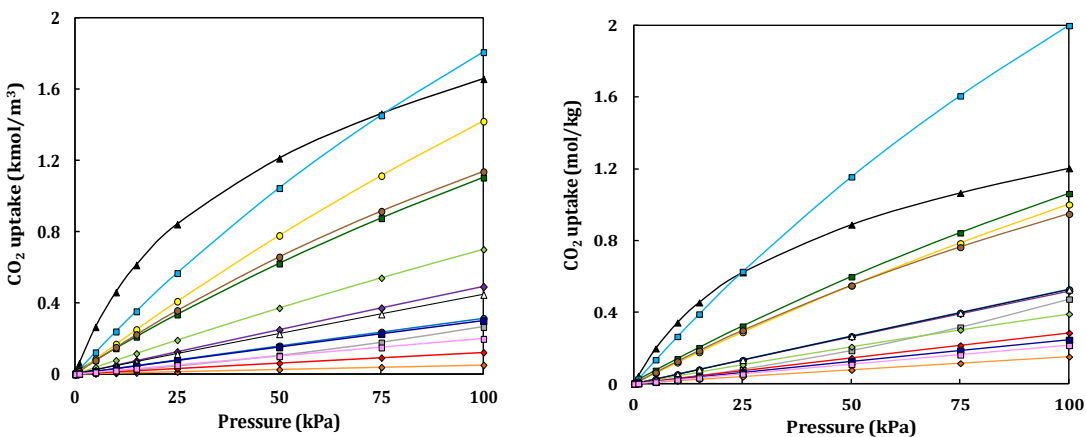
(a) Carbon dioxide (volumetric uptake) at higher (left) and lower (right) pressures (T=318K)
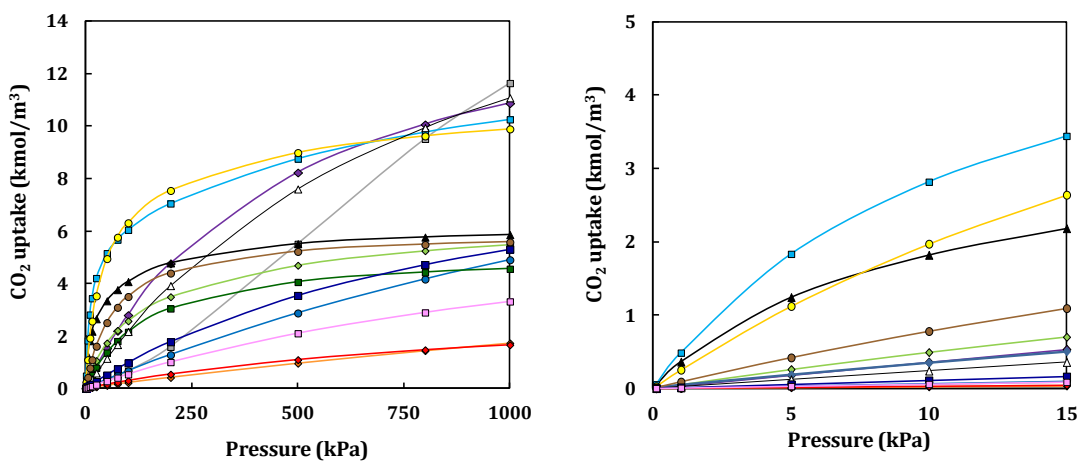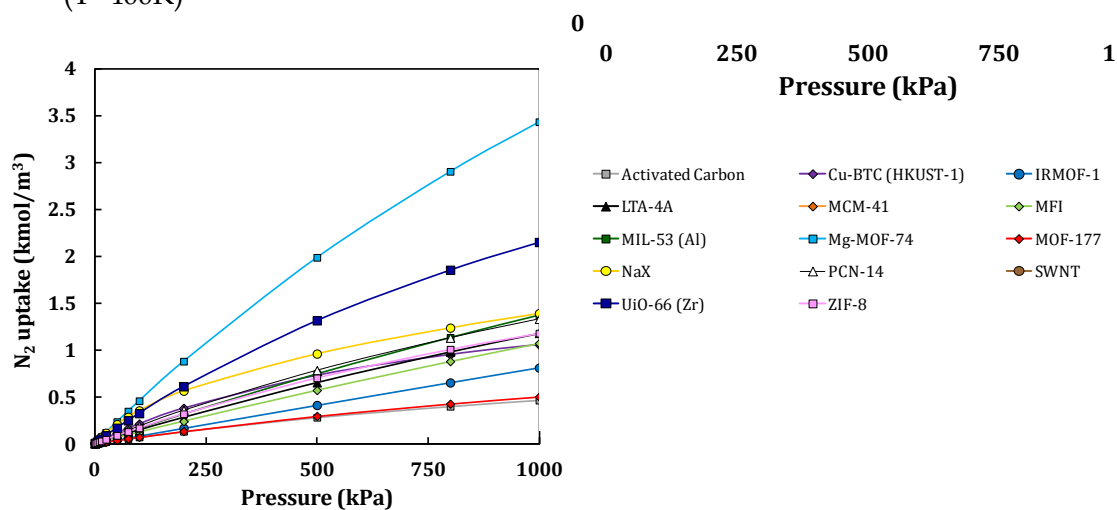

(b) Carbon dioxide (volumetric uptake) at higher (left) and lower (right) pressures (T=298K)
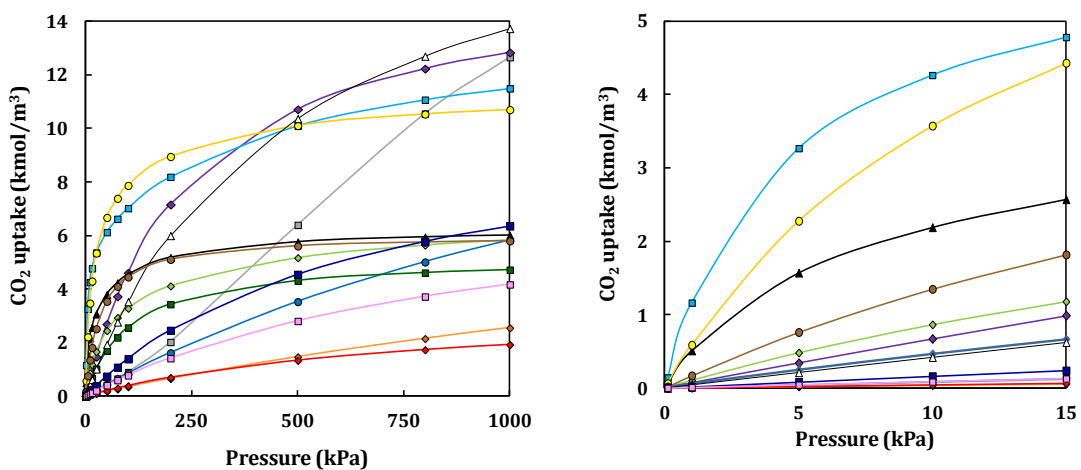
(c) Carbon dioxide (volumetric and gravimetric uptakes) at higher pressures (T=400K)

(d) Carbon dioxide (volumetric and gravimetric uptakes) at higher pressures (T=400K)

Figure 5.5. *Comparison of simulated adsorption isotherms for carbon dioxide and nitrogen, at different conditions of pressure and temperature for 14 selected materials.*

This pressure range is beneficial for zeolites like NaX and LTA-4A which more easily attract the quadrupole structure of CO_2. However, when the operating pressures -P_t - exceed atmospheric value (pressures above 500 kPa), zeolites have lower uptake capacities than some MOFs (see Figure 5.5). This can be rationalized as follows: the zeolites have pore volumes of 0.25 - 0.3 cm^3/g, significantly lower, for example, than Mg-MOF-74 (0.57 cm^3/g) and others. Therefore, the capacity of LTA-4A, MFI and NaX for CO_2 uptake becomes limiting for high-pressure operations. In other words, MOFs with "open" structures are especially attractive for high-pressure separations. Mg-MOF-74 is the most unusual MOF, because it has a combination of both high selectivities and high capacities. This explains why MOF-74 type has shown excellent separation performance in, for example, applications different than hydrogen separation [Sumida et al., 2012].

In screening materials for selective uptake at low pressures, two additional measures of adsorption must be considered: Henry's constant (K_H), a measure of the partitioning of a gas between the gas phase and gas adsorbed onto the surface of an adsorbent material at a constant temperature and very low pressure, and isosteric heat of adsorption (Q_{ST}), the energy released when the molecules of gas adsorb onto the surface of the material. In order to quantitatively compare the uptakes, both values are illustrated in Table 5.3, confirming the previous discussion and conclusions from the evaluation of the isotherms. I this case, K_H were calculated as the slope of the adsorption isotherm in the linear region at very low pressure (generally below 15 kPa). Although K_H and Q_{ST} measure two different processes, both can be thought of as the sorbent's affinity for gas adsorption [Vlugt et al., 2008].

Table 5.3. *Henry's constants (K_H) and isoteric heats of adsorption (Q_{ST}) from GCMC Simulations performed in this work (T = 318 K).*

MATERIAL	NITROGEN		CARBON DIOXIDE	
	K_H $x10^3$ (kmol/m^3-kPa)	Q_{ST} (kJ/mol)	K_H $x10^3$ (kmol/m^3-kPa)	Q_{ST} (kJ/mol)
Mg-MOF-74	4.70	17.5	370.65	38.9
NaX	4.07	12.5	355.11	34.9
CuBTC (HKUST-1)	2.31	23.9	39.28	25.4
PCN-14	2.02	20.8	24.10	22.1
MFI	2.65	20.0	52.63	22.0
LTA-4A	1.55	6.6	252.62	18.2
UiO-66(Zr)	3.40	12.3	10.76	16.1
ZIF-8	1.79	14.8	5.72	15.5
MIL-53(Al)	1.61	15.0	38.41	12.5
MOF-177	0.72	15.1	3.44	12.0
IRMOF-1	0.89	20.0	6.91	10.0

The loading dependence of Q_{ST} for CO_2 is compared in Figure 5.6 for the different types of simulated materials. The isosteric heats obtained for carbon dioxide, between 10 and 40 kJ/mol, indicate physisorption phenomenon. The values are comparable to that reported in literature [Sumida et al., 2012; Wang et al., 2002; Cavenati et al., 2004], but considering that in this study the conditions are slightly different.
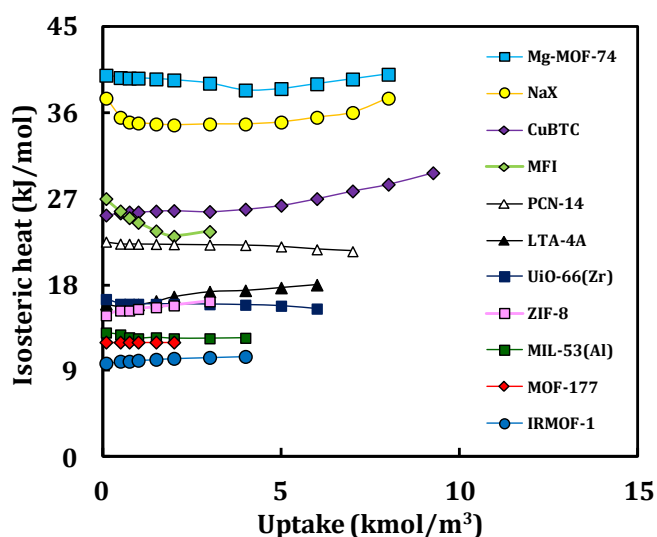

Figure 5.6: *Isosteric heat for CO_2 adsorption on the selected materials as a function of uptake. Symbols are obtained from the simulations (see text for details) while lines are a guide to the eye.*

A high similarity between NaX and Mg-MOF-74 with higher energy values is observed, while materials like MOF-177 and IRMOF-1 shown in the lower part of the

figure would be ideal materials when regeneration were needed because of their reduced energy requirement, however their adsorption capacity is negligible compared to the other mentioned materials. It should also be noted that the increase of the isosteric heat in most of the materials at higher loadings is due to the fact that at these high pressures the framework still has void regions, but there are no enough free spaces in the framework surface and the molecules condense and strongly interact among themselves.

In particular, it has been shown that MOFs with pore dimensions or cavities similar in size to a particular gas, show enhanced adsorption for that gas (detailed evaluation can be found in Babarao et al. [Babarao et al., 2011] and Liu et al. [Liu et al., 2009]). In this case, the effect of geometry on gas adsorption can be assessed by examining atomic density contour plots, showing the preferred location of adsorbed gas particles. Such plots are shown in Figure 5.7 for CO_2 and N_2 uptake.
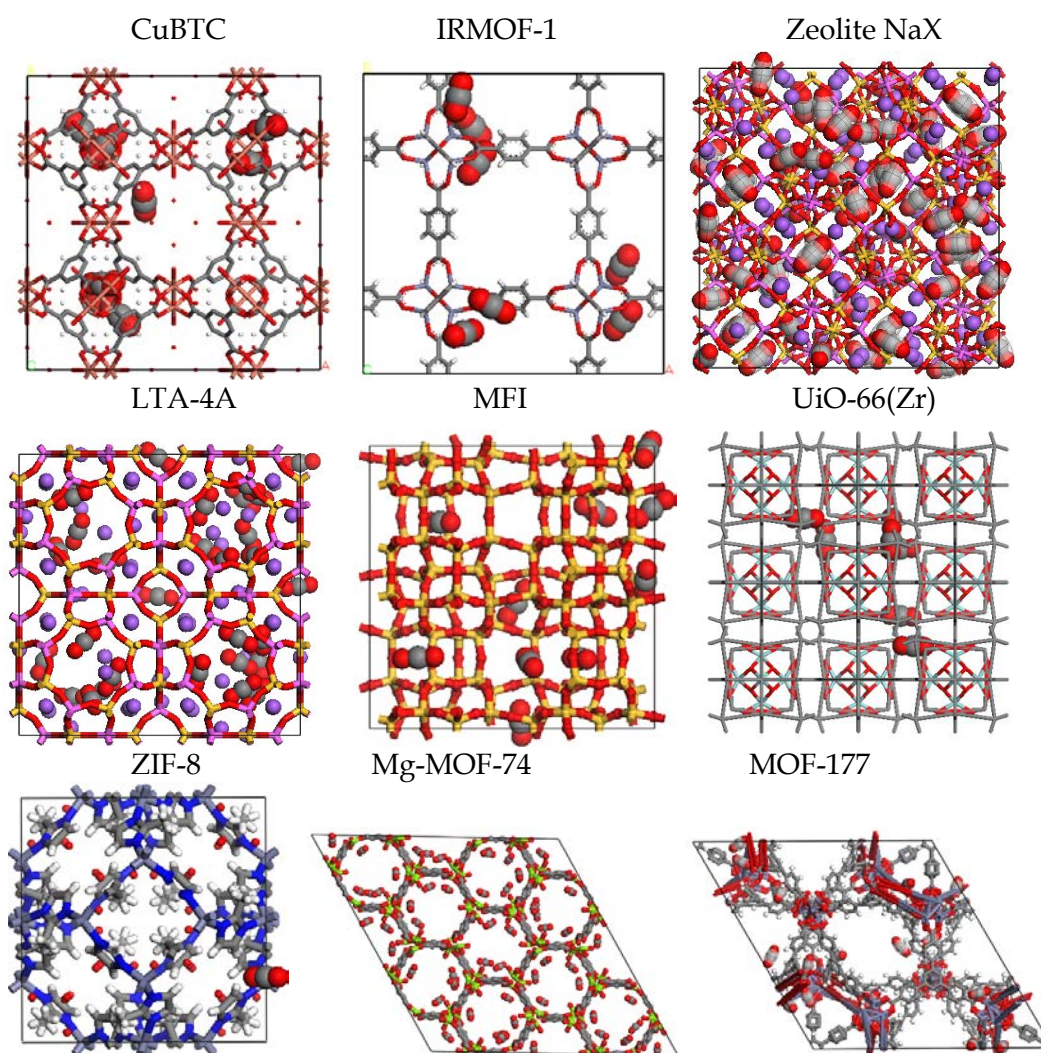

Figure 5.7. *Snapshots showing areas of high adsorbed CO_2 density for selected materials, from GCMC simulations at 318 K and 100 kPa.*

As seeing in the snapshots, CO_2 is preferably located close to the metals in MOFs, while N_2 occupies the larger portion of the pores, as can also be seen in zeolites with cations like NaX and LTA-4A; conversely, for MFI-type zeolite, there are no preferred locations found, so the competition does not depend on the difference of the nature of interaction forces between the material and gas molecules, neither on the different molecular diameters.

5.3.3. N_2/CO_2 separation selectivities

Turning now the attention on the selection of the most promising materials for separation at lower pressures, the selectivity of the sorbent material for the gas over the dominant component must be considered. Selectivities calculated for MOFs and zeolites are depicted in Figure 5.8. Binary adsorption was simulated at 318K and a total pressure of 100kPa, for a gas-phase molar composition of 14%CO_2 and 86%N_2.

As the gases considered here do not strongly interact with each other at low pressures, it is reasonable to assume that the selectivities can be estimated by considering the ratio of Henry's constants obtained from single-component isotherms [Dickey et al., 2012]. However, in order to determine if co-adsorption of the CO_2 and N_2 molecules has an impact on the amount adsorbed for the two species, we also compared the CO_2 and N_2 adsorption from the GCMC binary mixture simulations and with the adsorption from the single-component isotherms by using the equation 2.6 of IAST method [Myers and Prausnitz, 1965], previously explained in Chapter 2. Since using IAST to predict selectivity for a gas mixture requires accurate fits of the pure-component isotherms, selectivities are reported using the adsorption values provided in Tables 5.2.
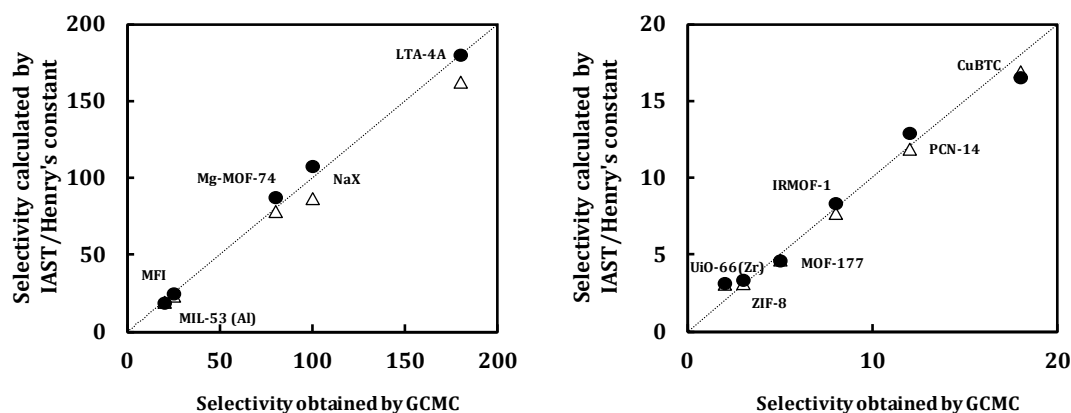
Figure 5.8. Comparison of the 14%/86% CO_2/N_2 selectivities (T = 318 K) calculated from the IAST method (closed circles) and from a ratio of the Henry coefficients, K_{CO2}/K_{N2}, (open triangles) with the selectivities from binary mixture GCMC simulations (x-axis).

As shown in Figure 5.8, the selectivities from IAST (closed circles) show a good agreement with those from the full mixture simulations for the large variety of structures examined in this study under flue gas conditions, being the most diverted the obtained for CuBTC. It can be noted that for MOFs with strongly polarizing sites, the selectivity likely underestimate the true adsorptive selectivity of the adsorbent. This is because in a realistic flue gas mixture, the strongest binding sites would be predominantly occupied by CO_2 owed to its greater polarizability and quadrupole moment. Thus, single-component isotherms overestimate the adsorption of N_2 and, consequently, reduce the calculated selectivity [Maurin et al., 2005]. This can be clearly observed in Figure 5.9.

Figure 5.8 also shows that the selectivities for different MOF materials vary by about one order of magnitude and it can also be inferred that in IRMOF-1, the CO_2 and N_2 adsorption in the mixture and single-component simulations are almost identical. Similar behavior was observed for all MOFs, except CuBTC, where the adsorption is slightly lower in the mixture than in the single component simulations, as previously mentioned. Among all the porous materials, zeolite LTA-4A shows the biggest selectivity, while NaX and Mg-MOF-74 have very similar values in the middle range, and the rest of the MOFs show very low affinity for CO_2 with respect to N_2, except for CuBTC, with a value close to 20. The specific orbital interactions of CO_2 molecules with the open Mg atoms accounts for the high selectivities offered by Mg-MOF-74 [Yazaydin et al., 2009]. Besides, one of the lowest adsorption selectivity is obtained for MOF-177, which has the most open structure of all MOF materials considered here, definitively not favorable for low-pressure CO_2 capture.
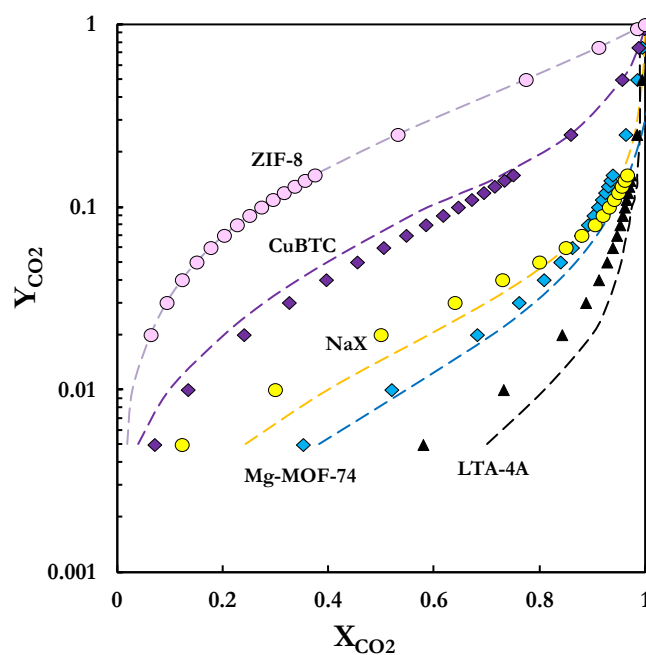
Figure 5.9. *Comparison between adsorbed CO_2 compositions in the different structures as a function of the gas stream, by using IAST (dotted lines) and GCMC simulations from this work (points).*

In order to evaluate the behavior of the selectivity with the increasing of the temperature, several IAST calculations were performed at different temperatures. The tendencies are shown in Figure 5.10, and as can be observed, zeolites present a decline in the selectivity due to the loss of CO_2 capacity. Instead, most of the MOFs do not show such a decrease and in some families there is even an increase in the parameter.
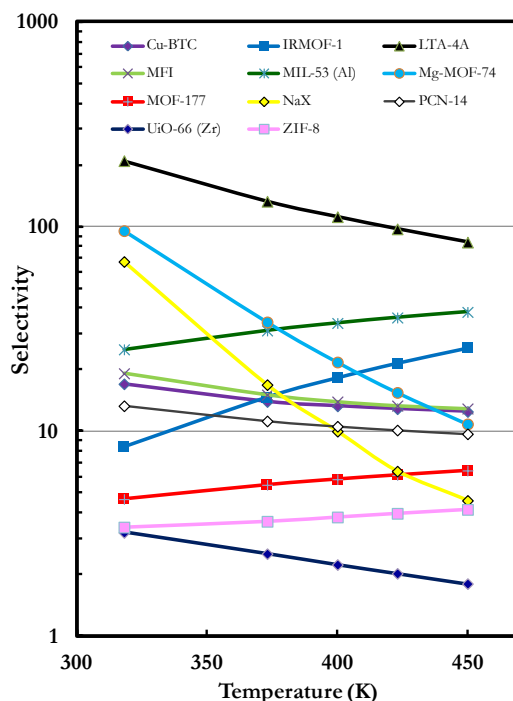
Figure 5.10. *CO_2/N_2 selectivity variation with temperature (P=100 kPa) for flue gas composition 14% CO_2/86% N_2.*

GCMC simulation also allow to identify the preferential adsorption sites for each molecule. Figure 5.11 presents snapshots of selected materials to show the cloud distribution of carbon dioxide (in red) and nitrogen (in blue) when a CO_2/N_2 binary mixture is imposed to these adsorbents.

CuBTC

IRMOF-1

Zeolite NaX

LTA-4A

MFI

UiO-66(Zr)

ZIF-8

Mg-MOF-74

MOF-177
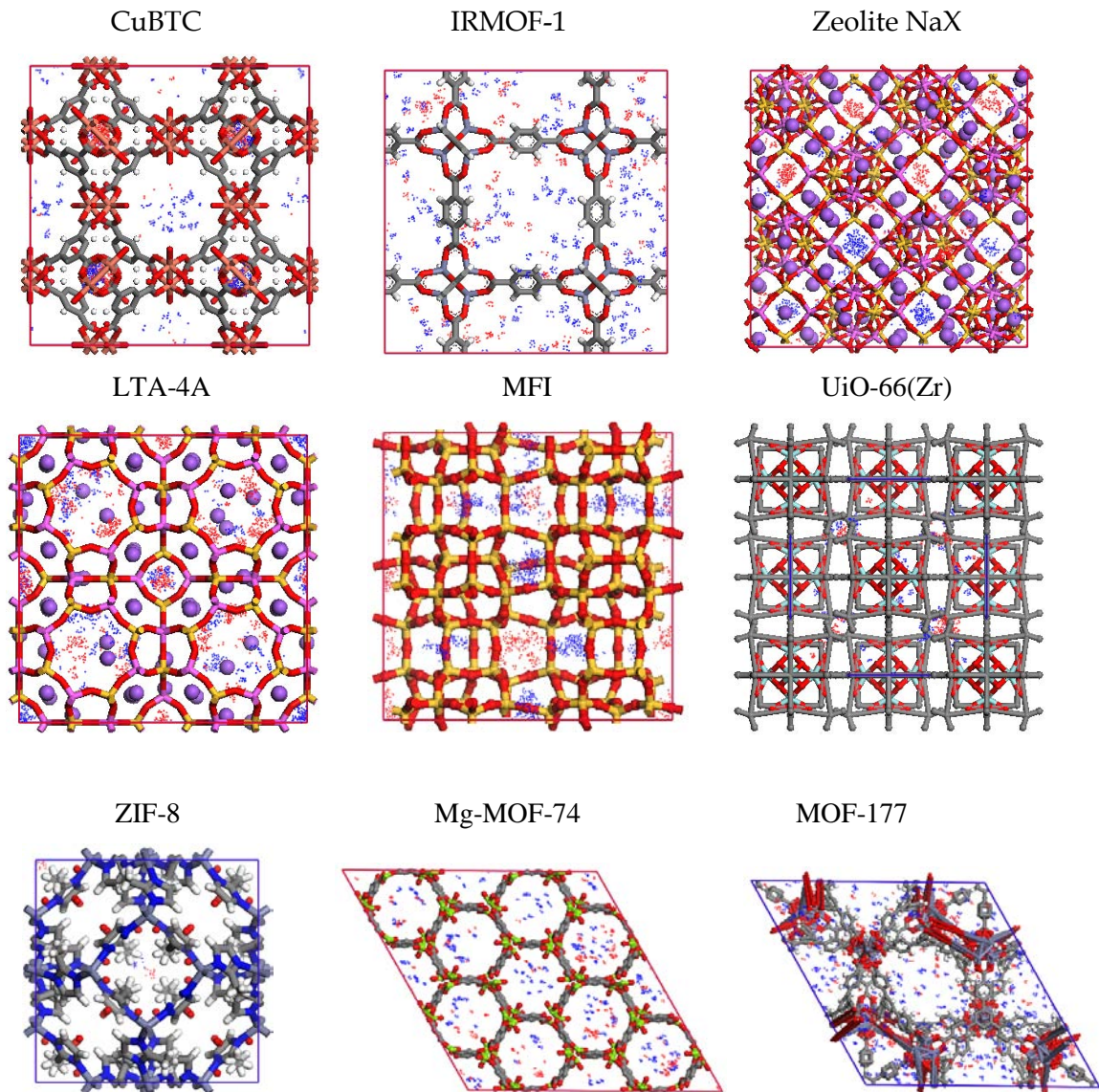
Figure 5.11. *Contour plots showing areas of adsorbed nitrogen and carbon dioxide, from GCMC simulations at 318 K and 14%/86% CO_2/N_2 mixture at a bulk pressure of 100kPa.*

5.3.4. Breakthrough calculations for TSA adsorber

Calculated breakthrough curves for a typical flue gas for coal fired power plant to be used in a TSA process must be evaluated by taking into account engineering and economic considerations. Based on this, a composition of 14%/86% CO_2/N_2, a total pressure of 100kPa and a temperature of 318K were investigated by using GCMC simulations, and shown in Figure 5.12. Additional different conditions (higher

temperatures and pressures), as well as differences between the adsorbed compositions of CO_2 obtained from IAST and GCMC, can be found in Figure 5.13.

Figure 5.12a presents a comparison of the typical breakthrough curves, where the molar concentrations of the gas phase (CO_2 is adsorbed and nitrogen pass though the packed bed) is shown exiting the adsorber packed and maintained under isothermal conditions at the inlet. Note that when comparing different materials, the fractional voidage is held constant; this implies the volume of adsorbents remains the same, so the total mass of the adsorbents used here is governed by the framework density. The x axis is a dimensionless time, τ, defined by dividing the actual time, t, by the characteristic time, $L.t/u$. On the basis of these calculations, the value of the breakthrough time, τ_{break}, can be determined for a specified purity of CO_2 in the outlet gas stream. When the composition in the exit gas reaches a certain desired purity level, the adsorption cycle needs to be terminated and the contents of the bed regenerated.

Figure 5.12a shows that Mg-MOF-74 has τ_{break} higher than CuBTC and other MOFs (for the combination of high selectivity and capacity), and it is even higher than the best zeolite, NaX. These values are comparable to those reported by Mason and coworkers [Mason et al., 2011] with a small difference in the operational conditions. Besides, the shortest breakthrough time is obtained with MOF-177, while IRMOF-1 and ZIF-8 have only slightly longer breakthrough times.

Additionally, a more visual comparison of the evaluated materials for the TSA CO_2/N_2 separation is presented in Figure 5.12b, where the breakthrough time (before saturation) is related to the CO_2 adsorption capacity of the adsorbents in the mixture, being the sphere diameter the selectivity of the material. As in the previous sections, Mg-MOF-74 stands as the best individual properties for a MOF; however, a systematic study on the cost of the regeneration as well as the influence of coexisting trace compounds in the mixtures on the adsorption properties of CO_2 is also needed before assessing that this is the best type material for this specific process. Therefore, in the following sections we study the effect of water traces in the behavior of the materials in the process.

(a)

b)
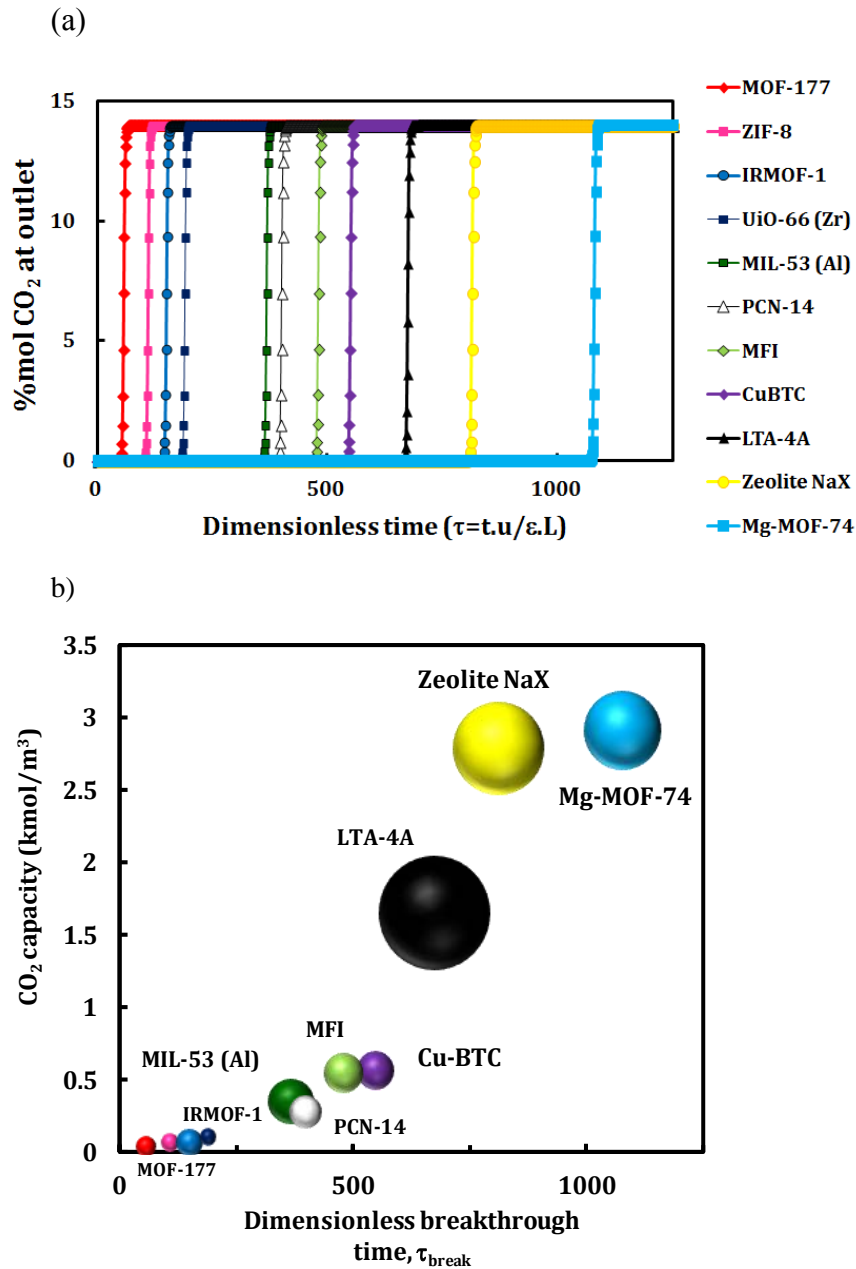
Figure 5.12. Breakthrough calculations for TSA adsorber. (a) Breakthrough characteristics of an adsorber packed maintained at isothermal conditions. In these calculations, the partial pressures of CO₂ and N₂ at the inlet were taken to be P_1 = 14 kPa and P_2 = 86 kPa. (b) Plot of the number of moles of CO₂ captured per m³ of adsorbent material (in the 14% CO₂/86% N₂ mixture) against the breakthrough time for a packed bed adsorber at 318 K and total pressures of 100kPa.

For the sake of the Figure 5.13, the name of the materials are not included in the graph. Hence, colors of the materials are as follows: MOF-177 (red), ZIF-8 (pink), UiO-66(Zr) (dark blue), IRMOF-1 (blue, circles), MIL-53(Al) (dark green), MFI (light green), PCN (white, triangles), LTA-4A (black), CuBTC (purple), NaX (yellow) and Mg-MOF-74 (light blue).

a)   T=298K, P=100kPa

b)   T=318K, P=100kPa

c)   T=400K, P=100kPa

d)   T=298K, P=1000kPa

e)   T=318K, P=1000kPa
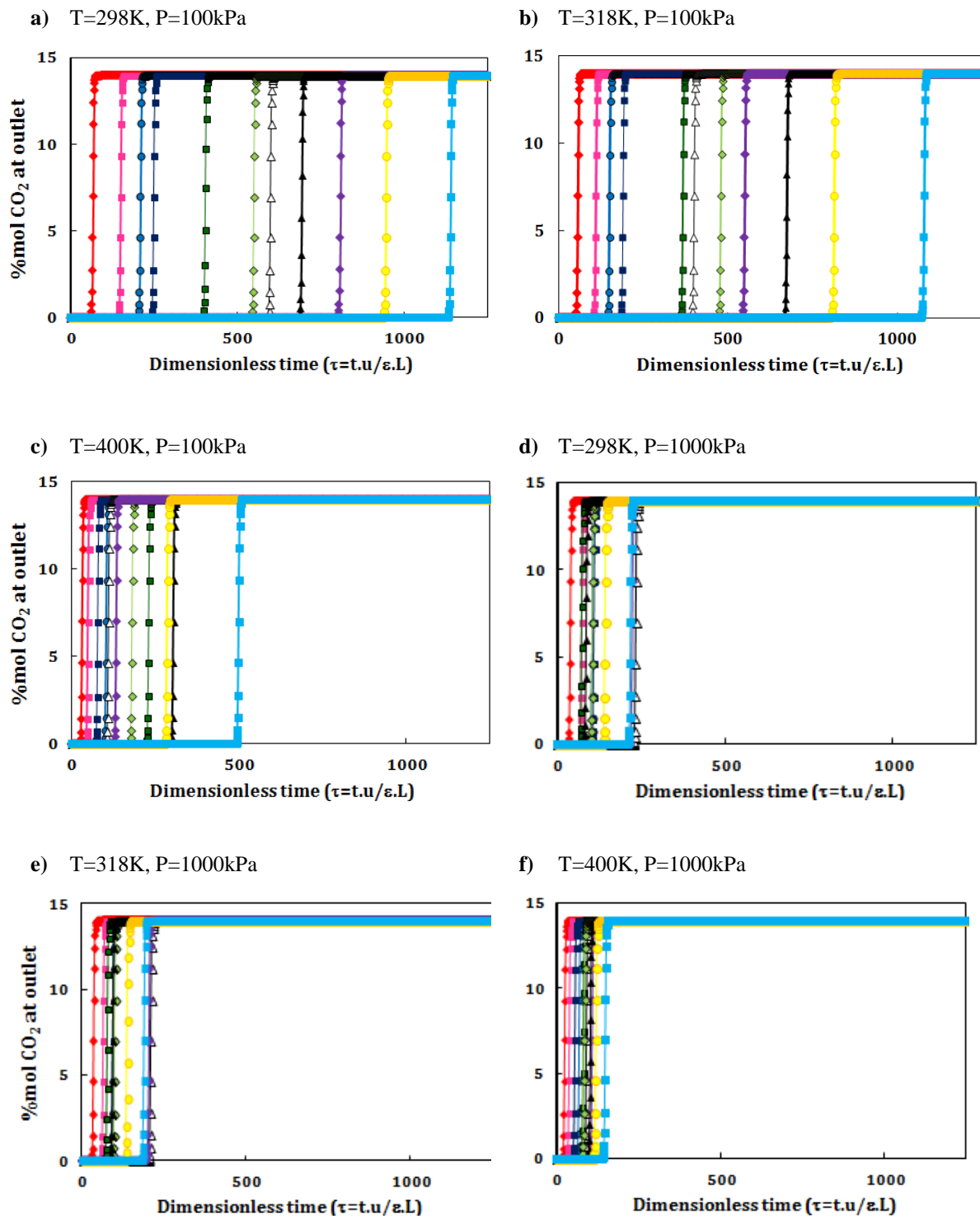
f)   T=400K, P=1000kPa

Figure 5.13. Breakthrough curves for selected materials at different conditions (molar composition: 14% CO_2 / 86% N_2).

5.3.4.1.   Regeneration of the bed adsorber

The economics of an adsorption unit for post-combustion CO_2 capture will be determined first and foremost by the amount of CO_2 captured during the adsorption cycle, that is, during the time interval $0-\tau_{break}$; this amount can be determined from a material balance of the discretized equations, and it is showed in Table 5.4. The CO_2 capture here is expressed both in gravimetric as in volumetric units adsorbent material. Again, we emphasize that the proper metric for comparing different crystal adsorbents for use in an adsorption unit is on the basis of kmol captured per cubic meter of adsorbent, because an existing adsorber will have a fixed volume. When considering the choice of the best MOF to replace the existing adsorbent, it should be compared the volumetric capture capacity should be compared. Thus, the relative costs of regeneration of the bed will be largely dictated by desorption of the CO_2 captured during the time interval, $0-\tau_{break}$.

Table 5.4. *Amount of CO_2 adsorbed per gravimetric and volumetric quantity of different materials, during the interval $0-\tau_{break}$ for the binary $14\%\,CO_2/86\%\,N_2$ mixture.*

MATERIAL	Cu-BTC	IRMOF-1	LTA-4A	MFI	MIL-53(Al)	Mg-MOF-74	MOF-177	NaX	PCN-14	UiO-66 (Zr)	ZIF-8
q (mol/kg)	0.63	0.13	1.11	0.30	0.33	3.11	0.10	1.96	0.32	0.08	0.09
q (kmol/m³)	0.55	0.08	1.64	0.54	0.34	2.82	0.04	2.78	0.27	0.10	0.08

In consequence, for a total pressure of 100 kPa and by doing a material balance on the adsorber, the amounts of CO_2 captured during the time interval present the following order (in terms of volumetric adsorption): Mg-MOF-74 > zeolite NaX > LTA-4A > CuBTC > MFI > MIL-53(Al) > PCN-14 > UiO-66(Zr) > IRMOF-1 > ZIF-8 > MOF-177. From the isosteric heats data, the values of Q_{ST} are determined at these CO_2 loadings to be 39.1, 34.7, 17.9, 25.6, 22.0, 12.5, 22.3, 16.2, 9.8, 15.1 and 12.0 kJ/mol, respectively. This implies that in this case, the regeneration requirement of Mg-MOF-74 will be around 15% higher than that of the traditionally used zeolite NaX for a desired production (besides the parasitic energies discussed by Huck and coworkers [Huck et al., 2014]).

5.3.5. Water Effect

Whereas CO_2 and N_2 account for more than 90% of the flue gas composition and can reach up to 99.9% before entering its final separation stage, understanding the effects of the gases present as traces or impurities is critical to properly evaluate any material for use in a realistic CO_2 capture process.

While the primary challenge of carbon dioxide capture is the separation of CO_2 and N_2, a detailed study of Metal-Organic Frameworks and other adsorbent materials - both novel and traditional- for post-combustion CO_2 capture must take into account the fact that flue gas is saturated with H_2O (5-7% by volume). Although partial dehydration of the effluent may be possible, completely drying the gas prior to extracting CO_2 is costly and most likely not feasible on such a large scale [Lee and Sircar, 2008]. Therefore, adsorbents used in CO_2 capture from flue gas must be stable in the presence of at least some water vapor. To the best of our knowledge, there are no direct experimental measurements of multi-component isotherms involving N_2, CO_2 and H_2O in MOFs to date.

Indeed, small amounts of water, or other contaminant [Pacciani et al., 2011], can significantly affect the CO_2 adsorption properties of many zeolites due to its strong adsorption on the highly hydrophilic surface, which prevents CO_2 from interacting with many of the strong adsorption sites in the material. Initial efforts at understanding the effect of water on CO_2/N_2 separations in Metal-Organic Frameworks have firstly focused on CuBTC [Li et al., 2007] and more recently in Mg-MOF-74 [Yu and Balbuena, 2013], with encouraging results.

To assess how the choice of the best material is affected with operating conditions, a series of GCMC simulation of ternary mixtures with different water composition were carried out. Although the pure adsorption isotherms obtained for water using the TIP-4P/2005 do not adjust as well as nitrogen and carbon dioxide to the experimental data in some of the available materials found in literature [Liang et al., 2009; DeCoste et al., 2013; Liu et al., 2010; Castillo et al., 2008; Wang et al., 2009; Jaramillo et al., 2004] (see Figure 5.14). It should be noted that the TIP-4P/2005 is, among the available models for water at this level of approximation, the one that best describes the liquid-vapor density curve and the critical water conditions, capturing what should be observed in adsorption processes when the material is saturated, and condensation becomes important. Hence, the comparison is good enough to provide more than qualitative trends in all cases, allowing elucidating the influence on the process under real operating conditions.
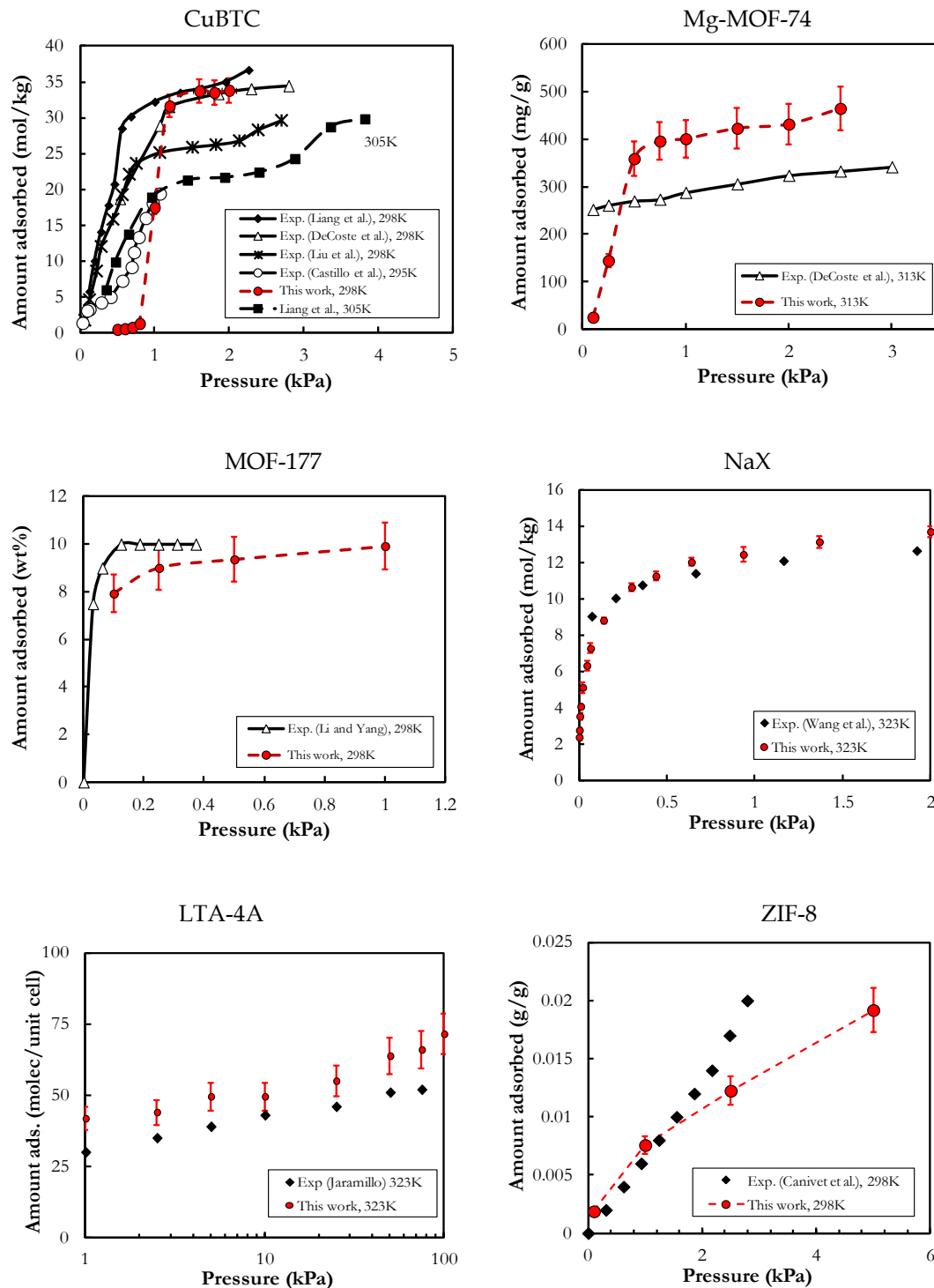
Figure 5.14. *Comparison of simulated adsorption isotherms for water with experimental data, for selected materials.*

In Figure 5.15 we present the variation of calculated breakthrough curves with the water content in the mixture. The value of τ_{break} mainly decreases for the materials with increasing water composition; this is due to limitations in the pore capacities, being more critical in zeolites, highly hydrophilic materials. In this case, it is well-known that the presence of water significantly decreases the adsorption of CO₂ because

water competitively adsorbs on the cations, blocking the access for CO_2. Moreover, as ZIF-8 is hydrophobic, its breakthrough time does not seem as affected as the other materials, resulting in one with the best performances when moisture is in the mixture.

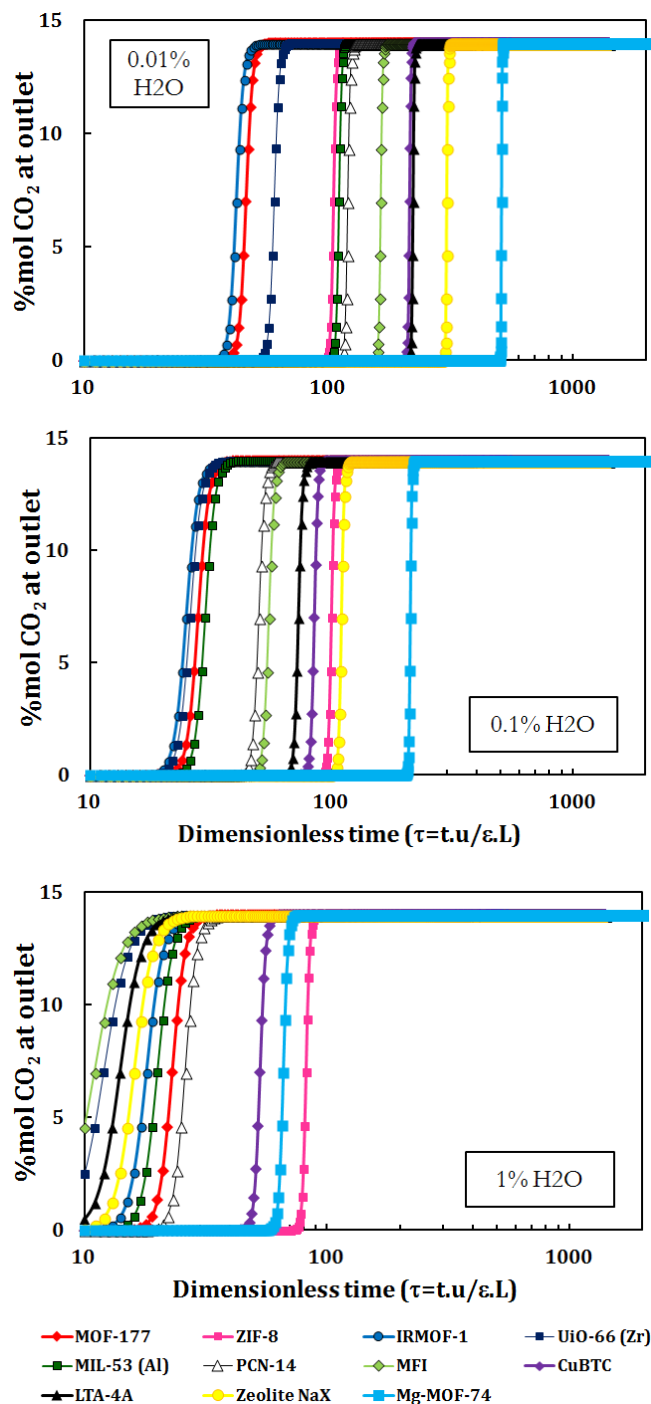***Figure 5.15.*** *Variation of breakthrough curves with the water content as an impurity, for compositions of 0.01%, 0.1% and 1% H_2O (P=100kPa, T=318 K).*

Some of the calculated isotherms for the mixtures $0.1\%H_2O/14\%CO_2/85.9\%N_2$ for the traditionally used zeolites NaX and LTA-4A, as well as the examined porous frameworks Mg-MOF-74, CuBTC, ZIF-8, IRMOF-1 and MOF-177 can be found in Figure 5.16.
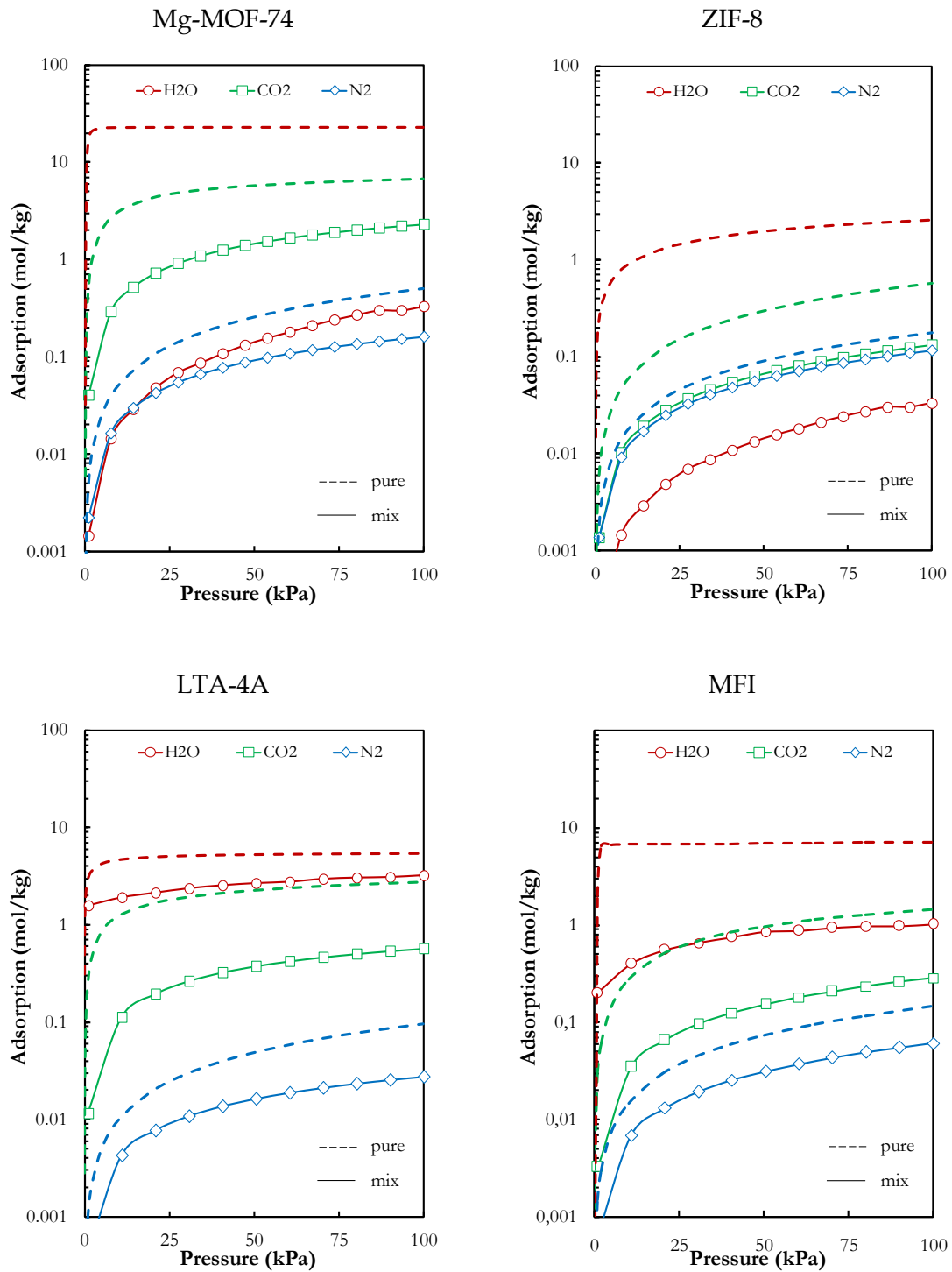
Figure 5.16. *Adsorption isotherms for pure components and in a ternary mixture with a composition of 0.1% H₂O, 14% CO₂, 85.9% N₂ (T=318K).*

To see the influence of the water content on the selectivity for the different materials, the reader is differed to the Figure 5.17, where the dimensionless breakthrough time, τ_{break} Is also presented. For example, at a pressure of 100kPa and a water composition

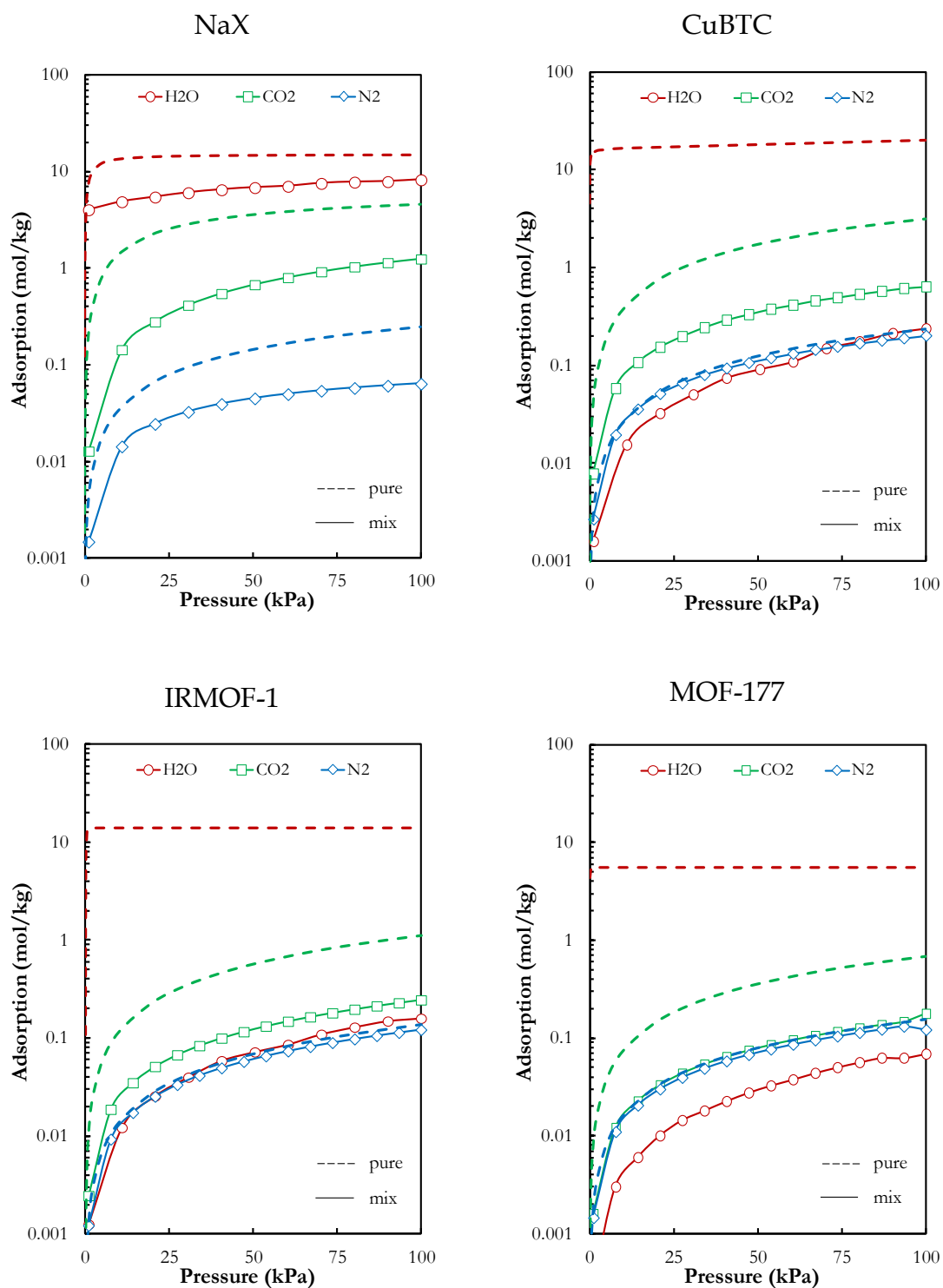of 0.1%, the breakthrough times, have the following hierarchy: Mg-MOF-74 > NaX > ZIF-8 > CuBTC > LTA-4A > MFI > MOF-177 > IRMOF-1. In other words, the decrease in τ_{break} is a reflection of the approach to pore saturation.
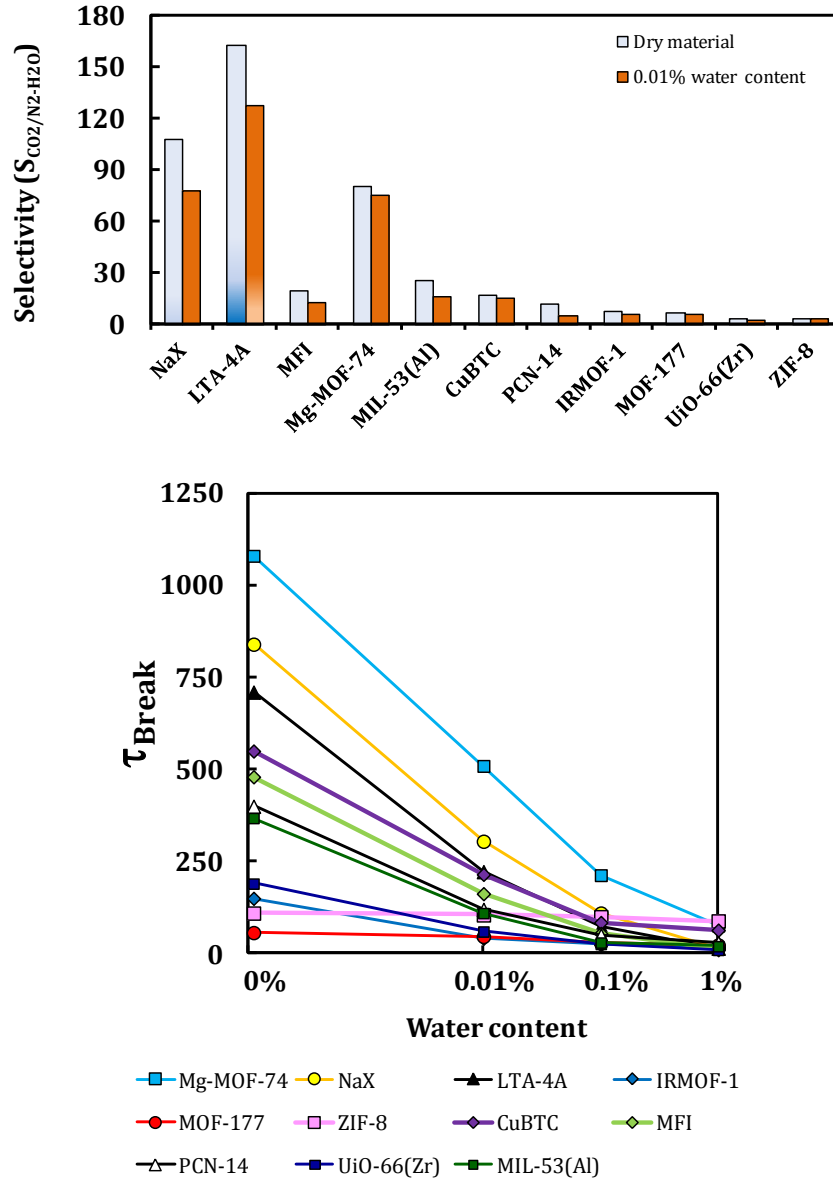
Figure 5.17. *(up) CO₂/N₂ selectivity behavior for flue gas (composition 14% CO₂/86% N₂), variation with water content (T=318K, P=100kPa). (down) Evaluation of breakthrough time as a function of water content in selected materials for CO₂ capture (T=318 K).*

5.3.6. Working Capacities

Finally, Table 5.5 summarizes different values of the working capacities for TSA processes, including all the mixtures evaluated in this work for flue gas composition.

The presented working capacity in TSA was calculated by the difference of CO_2 adsorption capacity between 400K and 318K, at a pressure of 100kPa. The parameter declines after water sorption in all cases, being more noticeable in zeolites as explained before for the adsorption capacity. Other working capacities at different desorption temperatures are provided in Figure 5.18.

Table 5.5. *Summary of the working capacity ($kmol/m^3$) of zeolites and MOF studied for TSA process under different conditions.*

MATERIAL	Pure CO_2	Binary (GCMC) 14%CO_2/86%N_2	0.1% H_2O	1% H_2O
Mg-MOF-74	4.24	2.13	1.05	0.47
MOF-177	0.17	0.02	0.01	0.01
CuBTC	1.54	0.33	0.25	0.18
LTA-4A	1.33	0.52	0.18	0.03
IRMOF-1	0.35	0.05	0.03	0.02
ZIF-8	0.34	0.03	0.03	0.02
NaX	5.12	1.95	0.81	0.12
MFI	1.87	0.28	0.20	0.03
MIL-53(Al)	1.05	0.19	---	---
PCN-14	1.72	0.18	---	---
UiO-66(Zr)	0.67	0.08	---	---

It can be observed that, although for pure-CO_2 adsorption under TSA conditions, the benchmark zeolite 13X (NaX) shows higher working capacity than Mg-MOF-74 and the rest of materials, when it comes to water traces in the CO_2/N_2 mixture, Mg-MOF-74 shows around 1.3 times higher working capacity values than NaX. This ratio is increased in the presence of more water, reaching a 3.9 ratio with 1% H_2O. This demonstrates that the Mg-MOF-74 is more appropriate for this process, in spite of presenting slightly higher energy requirement for regeneration, and also lower CO_2/N_2 selectivities.

a)

b)
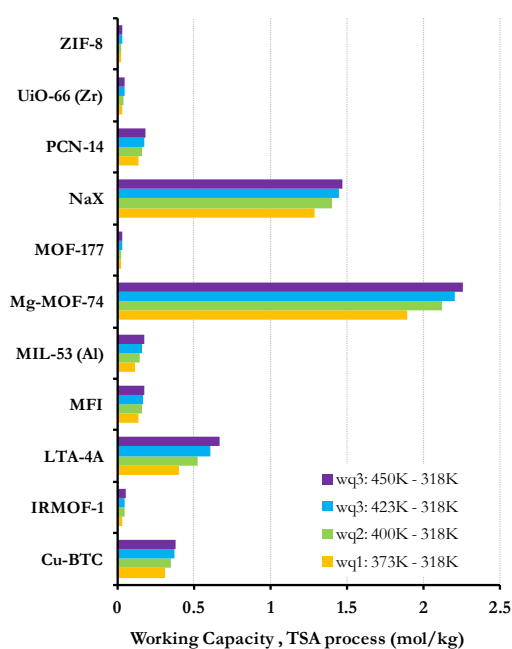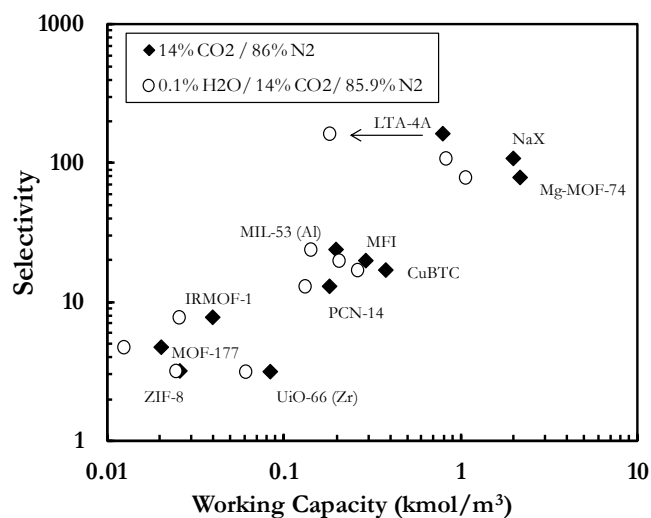
Figure 5.18. *values for working capacity in selected materials under different desorption temperatures (P=100kPa, composition: 14% CO_2/86% N_2); b) Variation of working capacity with moisture content as a function of material selectivity (P=100kPa, T_{ads}=318K).*

5.4. Conclusions

Eleven materials, including zeolites and several promising MOFs from different families, were screened for their adsorption and separation behavior toward gases like CO_2 and nitrogen. A throughout study was carried out by GCMC simulation for the

purpose of identifying key structural properties for selective adsorption from a post-combustion stream in a TSA process. The effect of the water content on the mixtures was also been explicitly evaluated.

After considering operating conditions and with respect to the results presented in this chapter, Mg-MOF-74 stands up as the most promising material to be used in such TSA processes; however, considering its current availability to large scale and from the economic point of view, the zeolite 13X (NaX) still remains, at present, as a the preferred candidate for the industrial process.

Besides, although CO_2, N_2, and H_2O (the three components considered in the current work) account for greater than 95% of the flue gas mixture, the other minor components (mostly O_2, SOx, NOx, and CO) cannot be ignored in assessing zeolites and Metal-Organic Frameworks for post-combustion CO_2 capture. Significantly, the effects of these trace gases on the CO_2/N_2 separation performance of MOFs is so far virtually unexplored. In the next chapter we address this issue for an specific MOFs, in order to see its potential to be implemented in a post-combustion CO_2 capture process.

6

EFFECT OF WATER AND IMPURITIES ON THE ADSORPTION OF CO_2 IN CUBTC AND ZEOLITE $13X$ [2]

6.1. Background information

Physical adsorption by microporous zeolite 13X has been reported to provide high CO_2 adsorption capacity at ambient temperature, but relatively high energy requirement for regeneration of the absorbents, especially in the presence of water [Franchi et al., 2005, Cavenati et al., 2004]. Due to the difficulty of modifying these materials to enhance selectivity and to regenerate them without significant heating [Ye et al., 2013], the design and preparation of high capacity adsorbents for CO_2 capture have attracted the interests of research in advanced material and in environmental areas.

A large number of studies have examined single-component adsorption of CO_2 in MOFs, but only a limited amount of multicomponent breakthrough simulations with MOFs have also been investigated [Krishna and Long., 2011]. It has clearly been demonstrated through these studies that MOFs can be used for the adsorptive separation of CO_2/N_2 and CO_2/CH_4, CH_4/CO_2 and CO_2/CO binary mixtures, as well as $CH_4/N_2/CO_2$ ternary mixtures. Several groups [Wang et al., 2002; Millward and Yaghi, 2005; Bourrelly, 2005] have reported MOFs with high CO_2 adsorption capacity. Among them, CuBTC [$Cu_3(BTC)_2(H_2O)_3$ (BTC: benzene-1,3,5-tricarboxylate)], first reported by Chui and coworkers [Chui et al., 1999], is one of the most studied for gas adsorption and storage. The CO_2 adsorption capacities reported are in the range of 8.0 mol/kg by Wang and coworkers [Wang et al., 2002] and 10.2 mol/kg by Millward and Yaghi at 25°C and 15 bar [Millward and Yaghi, 2005], the difference between the studies is mainly due to slightly different structural properties of CuBTC prepared by different methods [Yang et al., 2013]. In any case, the adsorption capacities at higher pressures are much higher than that of the benchmark zeolite 13X. Such a high performance for CO_2 capture is mainly attributed to the stronger interaction between exposed metal sites in the framework and CO_2 molecules [Yang et al., 2007; Liang et al., 2009]. In addition, the material could be completely regenerated under vacuum condition which may be employed for PSA processes.

CO_2 adsorption and separation processes over MOFs and zeolites have been intensely studied by means of experimental techniques and computational simulations in recent years, however, and in spite of the great importance from their final implementation, the investigation of the effect of coexisting components or impurities such as water, oxygen, sulfur compounds and other components in the flue gases has been less explored [Yazaydin et al., 2009; Yu et al., 2012; Cychosz and Matzger, 2010; Xiao et al., 2007]. Those impurities may significantly influence the stability and the performance of the materials [Babarao and Jiang, 2009]. Hence, a throughout understanding about the influence of the main components on the separation still needs further investigation, which is one of the main objectives of the present work.

As shown in Chapter 5, for practical applications, the adsorbents should not only possess a high adsorption capacity for CO_2 and high CO_2 selectivity over other species, but also exhibit good behavior under impurities and water presence. There are few examples of published works in this respect in the last years. For instance, Yazaydin and coworkers [Yazaydin et al., 2009] reported the CO_2 uptake and its selectivity over N_2 and CH_4 in the CuBTC, which significantly increased by the presence of water molecules coordinated to open-metal sites in the framework. Also, Liu and coworkers [Liu et al., 2010] studied adsorption equilibrium of CO_2/H_2O vapor and the rates of CO_2 adsorption in CuBTC and Ni/DOBDC. However, to our knowledge, a systematic study on the effect of co-existing impurities in the mixture behavior under operational conditions has not been performed yet. In addition, not only high CO_2 capacity, but also the resistance to flue gas components such as SO_2 is quite important for a good sorbent for industrial applications. Nevertheless, there are very few studies available on the influence of SO_2 in flue gas to MOFs structure and CO_2 adsorption performance [Xie et al., 2012; Sun et al., 2014; Liu et al., 2013].

In this chapter, we present results concerning adsorption potential for application in CO_2 adsorption separation from gas mixtures in MOF CuBTC and zeolite 13X, evaluated by using GCMC simulations. The influence of these coexisting species, i.e., water and SO_2 in flue gas on CO_2 separation was examined in detail in order to reach a better understanding of their adsorption capacity, selectivity, adsorption density location and isosteric heat distributions.

6.2. Methodology

6.2.1. Structures

Figure 6.1 shows the 2D projection structures for both CuBTC and 13X materials, generated for a similar box with dimensions ~25Å (size pores of the materials can also be seen). In the CuBTC framework, two octahedrally coordinated Cu atoms are connected to eight oxygen atoms of tetra-carboxylate units. Each BTC ligand holds three dimeric Cu paddle wheels that form two different microporous sites within the framework: a system of tetrahedral-shaped cages accessible through small windows (~3.5 Å in diameter) and large cavities connected through square shaped windows with a diameter of ~9 Å [Krungleviciute et al., 2007]. The crystal structure of CuBTC also includes axial oxygen atoms weakly bonded to the Cu atoms, which correspond to water ligands. Upon removal of the guest molecules, open metal sites (coordinatively unsaturated) are obtained. The partial positive charges on the metal sites in CuBTC have the potential to enhance adsorption properties, , as previously

discussed in literature for increasing hydrogen adsorption in MOFs [Prestipino et al., 2006].

| Pore size < 6 Å | 6 Å < Pore size < 8 Å | Pore size > 8 Å |

| Pore size ~3.5 Å | Pore size ~9 Å |
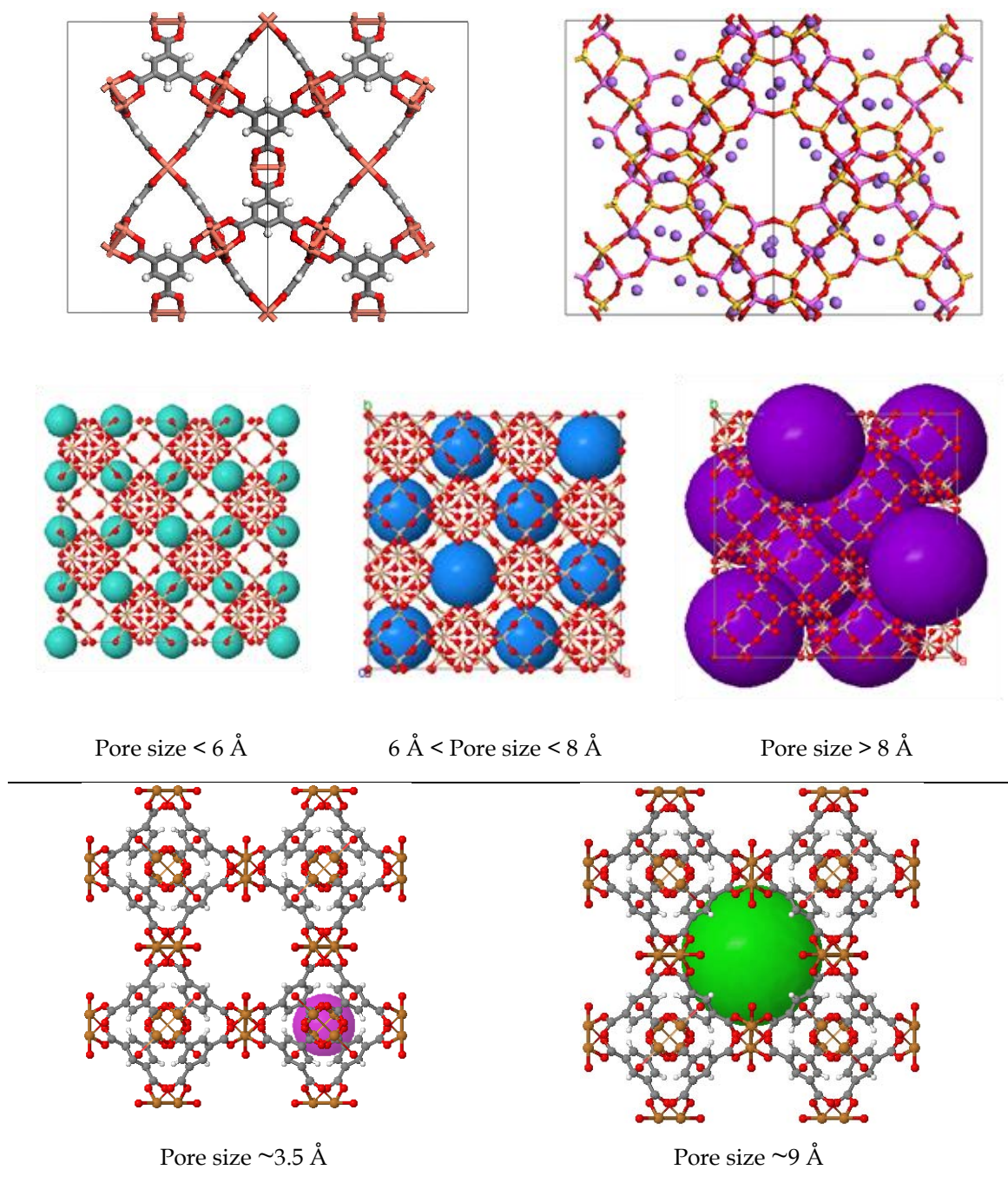
Figure 6.1. Image of crystallographic data and pore types for CuBTC and zeolite 13X.

Zeolite 13X (Na-Faujasite), with molecular formula $[Si_{104}Al_{88}O_{384}]^{-88}Na^{+88}$ is an aluminosilicate with a Si/Al ratio = 1.18. Since crystallographic Si/Al ratio is 1.0, 8

aluminium atoms have been replaced randomly by silicon atoms. Faujasites are classified as microporous materials, with pore diameters between 6 to 12 Å. It should be noted that most of the sodium atoms are located in pores with size diameter smaller than 6 Å, keeping available the small pores for adsorption.

6.2.2. Simulation Details

Molecular models for the zeolite and MOF were taken from the crystallographic data reported in literature: ccdc CuBTC reported by Chui [Chui et al., 1999], and zeolite 13X from Wang and coworkers [Wang et al., 2002]. The structures were orthogonalized to facilitate simulations and subsequent analysis. Solvent molecules were deleted, providing the so-called activated structures. It has been reported that only small structural changes were observed with the removal of coordinated water molecules after sample activation in CuBTC [Rowsell and Yaghi, 2005], so no further optimization was required. All frameworks were treated as rigid structures with atoms fixed at their crystallographic positions.

The Lennard-Jones parameters for zeolite 13X were taken from the force field of Watanabe and coworkers [Watanabe et al., 1995], while for CuBTC the parameters were taken from the DREIDING force field [Mayo et al., 1990] with UFF [Rappé et al., 1992] parameters taken for Cu open metal sites. The charges for the CuBTC and 13X atoms were obtained from the works of Castillo [Castillo et al., 2008] and Jaramillo [Jaramillo and Auerbach, 1999], respectively. Parameters for the gas molecules were taken from the literature in a transferable manner: CO_2, N_2 and O_2 were modeled using the TraPPE force field [Potoff et al., 2001]. Water was modeled with the TIP-4P/2005 model [Abascal and Vega, 2005], and SO_2 in a similar way to carbon dioxide [Ketko et al. 2011]. The full set of van der Waals parameters used is listed in Table 6.1 for completeness.

GCMC simulations were performed using the Sorption code in Materials Studio 6.1 [*Accelrys M.S.*, 2013]. The common movements and periodic boundary conditions were used. At each chemical potential, 10^7 MC moves were performed to equilibrate the system and then additional 10^7 MC moves were used for data collection. A cutoff radius of 12.5Å was applied to the Lennard–Jones interactions, and the long-range electrostatic interactions were calculated by using Ewald summation. The Lorentz–Berthelot combining rules were used to calculate the adsorbate/framework and the molecules Lennard–Jones crossed parameters, and the Peng-Robinson equation of state was used to relate pressure with chemical potential.

Table 6.1. *Force field parameters used in adsorption simulations.*

Type	$\varepsilon_0(K)$	$\sigma_0(\text{Å})$	q(e-)	Reference
Frameworks (CuBTC and Zeolite 13X) parameters				
C_a	47.86	3.47	0.5035	(Mayo et al., 1990) [Charges: Castillo et al., 2008]
C_b	47.86	3.47	0.1325	
C_c	47.86	3.47	-0.159	
H	7.65	2.85	0.159	
O	48.19	3.03	-0.636	
Cu	2.518	3.114	1.0	(Rappè *et al.*, 1992)
Al	22	2.3	1.75	(Watanabe et al., 1995) [Charges: Jaramillo and Aurebach, 1999]
Si	22	2.3	2.05	
O-$_{Al}$	58	3.6	-1.20	
O-$_{Si}$	53	3.3	-1.025	
Na	70	2.786	1.00	
Molecules parameters				
N	36	3.31	-0.482	(Potoff *et al.*, 2001)
COM $_{N2}$	-	-	0.964	
C $_{CO2}$	27	2.8	0.7	
O$_{CO2}$	79	3.05	-0.35	
O $_{O2}$	49	3.02	-0.113	
COM $_{O2}$	-	-	0.226	
S $_{SO2}$	73.8	3.39	0.59	(Ketko *et al.*, 2011)
O$_{SO2}$	79	3.05	-0.295	
O$_{water}$	93	3.159	0	(Abascal *et al.*, 2005)
H	-	-	0.5564	
COM $_{water}$	-	-	-1.128	

COM: Center of Mass

6.3. Results and discussion

In order to assess the accuracy of the force fields for multi-components mixtures, the simulated isotherms were first compared with experimental gas adsorption curves, when available. In addition, the isosteric heats of adsorption were

also evaluated, as well as the selectivity for CO_2. Besides post-combustion flue gas at ambient conditions, other different scenarios were evaluated such as: flue gas at a temperature of 400K, and air composition at 298K; both at an interval up to 10bar (i.e. 1000kPa). In order to study the structure behavior with the presence of SO_2 and some moisture, several mixtures were also evaluated.
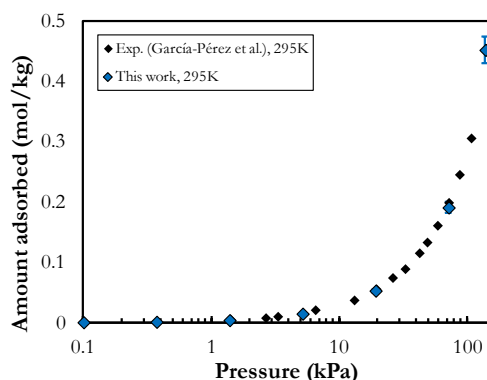
Results are divided into three parts: simulations for pure components, simulations for binary CO_2/N_2 mixtures, and evaluating the behavior of the adsorbents for CO_2 separation with the presence of impurities (either H_2O, SO_2, or multi-component mixtures)

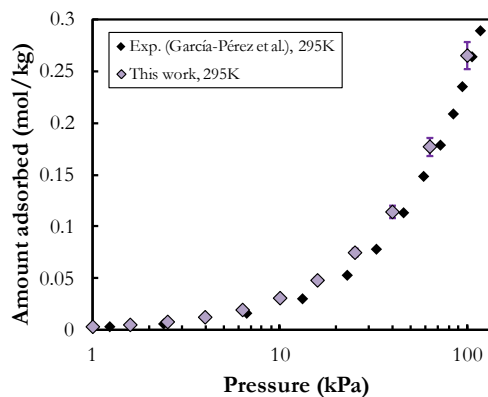## 6.3.1. Adsorption isotherms of pure gases

The first step was focused on validating the force fields employed by comparing GCMC simulation results with available experimental data at the same conditions [Cavenati et al., 2004; Castillo et al., 2008; Yang et al., 2013; Liang et al., 2009; Yazaydin et al., 2009; Liu et al., 2010; García-Pérez et al., 2009; Wang et al., 2009; DeCoste et al., 2013; Küsgens et al., 2009; Gutiérrez-Sevillano et al., 2015]. For this purpose isotherms of different gases (N_2, CO_2, H_2O, O_2 and SO_2) on zeolite 13X and CuBTC were obtained and compared with experimental data, showing good agreement in all cases, as provided in Figure 6.2. Two special cases for CuBTC are represented in Figure 6.3, where differences between experimental isotherms data regarding the type of synthetization of the material are showed.

a) CuBTC (Exp comparison)

Nitrogen

Oxygen

Figure 6.2. Validation of GCMC simulated adsorption isotherms in (a) CuBTC, and (b) Zeolite 13X (error bars included) versus experimental work.

However, there is some discrepancy between different sets of experimental data for the adsorption of CO_2 on CuBTC, depending on the material's synthesis procedure and the hydration stage. As can be observed in Figure 6.3, the simulated isotherm

obtained in this work for CO_2 is in agreement with the experimental data of Yang et al. [Yang et al., 2008] on the material synthesized using $CHCl_3$ at low pressures, and with Yazaydin's data for the dry-material [Yazaydin et al., 2009] at low-intermediate and high pressures, as expected, since coordinated water molecules were not included in the simulations.

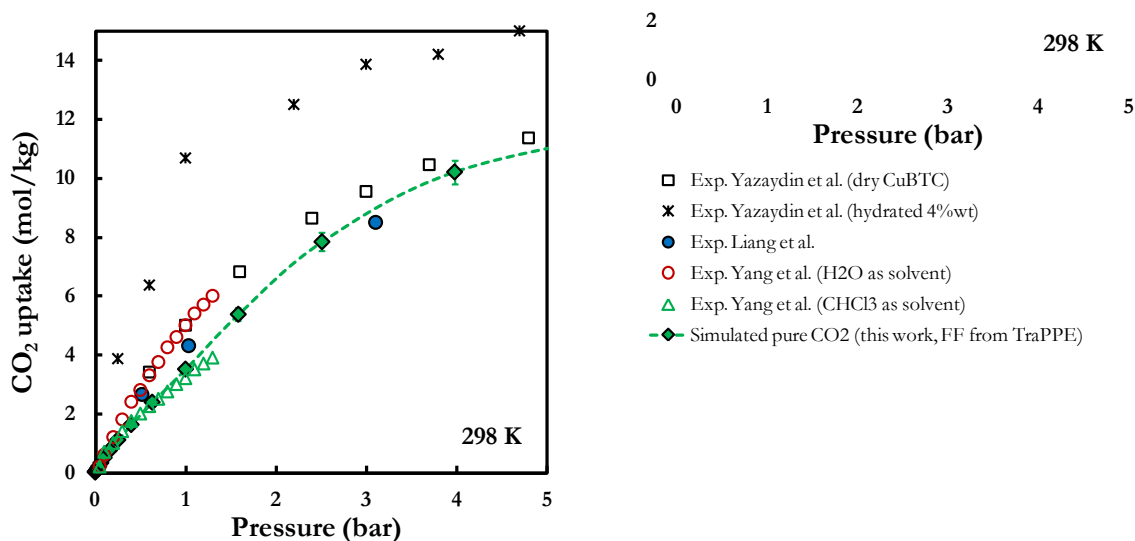***Figure 6.3.*** *Comparison of simulated and experimental isotherms for carbon dioxide in CuBTC.*

Individual adsorption isotherms simulated for the five selected compounds evaluated are provided in Figure 6.4 for both materials. The comparison of the adsorption behavior between CuBTC and 13X is done considering 13X a benchmark for CO_2 separation by adsorption, as currently used today in some industrial processes. Considerably different CO_2 adsorption isotherm shapes are obtained in both materials because of their different structure properties. The two materials have clear different adsorption behavior at the same pressure: for instance, the CO_2 adsorption capacity of the CuBTC at high pressures is much larger than in the case of zeolite 13X reported at 298K and 1000kPa; however the situation is reversed for pressures close to atmospheric conditions, where zeolite 13X shows best capacities.

It is remarkable that, even at the higher pressures evaluated, none of the isotherms appear to be completely at the saturation point in the CuBTC. This is directly related to the large surface area and pore volume of CuBTC accessible to the gas molecules. As shown in Figure 6.4a, the adsorption of CO_2 for CuBTC linearly increases with pressure up to ~500 kPa, while the CO_2 capacities reach saturation in the low pressure range for zeolite 13X. This fact can be explained by the strong guest-host interaction in zeolite 13X. However, in the MOF the CO_2 sorption rapidly increases with pressure above 100kPa due to the specific interactions between quadrupolar CO_2 molecules and partial positive charges on the uncoordinated metal sites in CuBTC. It is

known that N_2 and O_2 molecules present weak interactions with zeolites and MOFs, and this is why these structures have been extensively explored for the CO_2/N_2 separation, supported by their selectivity towards CO_2. For example, at 100kPa, CO_2 adsorbs 10-15 times more than N_2 and O_2 in 13X, while in CuBTC the adsorption is about 5 times higher.

a) CuBTC   b) Zeolite 13X
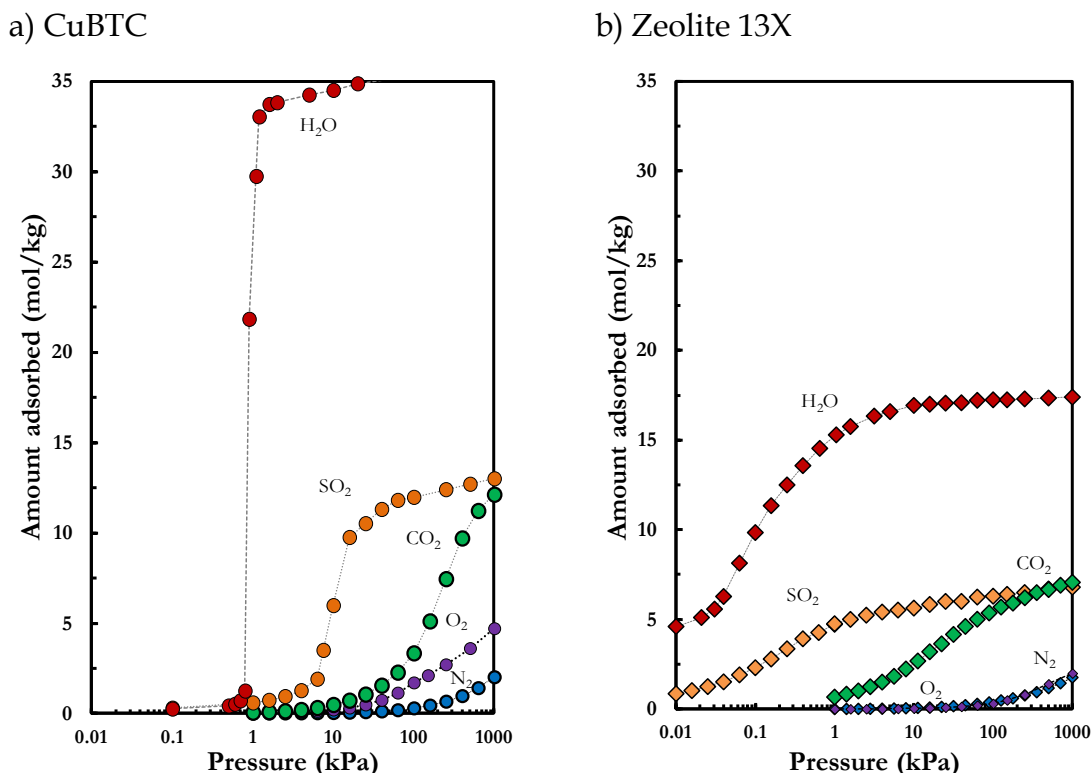
Figure 6.4. *Comparison of pure simulated adsorption isotherms of CO_2, N_2, SO_2, O_2, and H_2O in a) CuBTC and b) zeolite 13X frameworks (lines are guide to the eyes; error bars are smaller than symbols).*

Contrary to the previously discussed compounds, water has a very marked typical Type-I isotherm. In the low P/P_0 region, the adsorption of water vapor reaches saturation in both materials, indicating a strong guest-host interaction. It is observed that CuBTC has a very high H_2O adsorption capacity (e.g. 50 wt% at saturation sorption). The high H_2O capacities on CuBTC can be attributed to the high pore volumes and the metal–oxide clusters present in the frameworks of CuBTC. According to this, CuBTC and 13X are highly hydrophilic, because they retain high quantities of water under very little pressures. Moreover, it is also interesting to note that the materials have similar capacities for both SO_2 and CO_2 molecules, which originate a competition for adsorption sites into the structure between them, being *a–priori* the SO_2 molecules the favored ones because of the early saturation peak. This fact is of great importance for separating CO_2 from a flue gas in which traces of SO_2 [Pacciani et al., 2011] are also present.

6.3.2. Isosteric heat

Heats of adsorption of the compounds in CuBTC and zeolite 13X were also calculated in this work. The isosteric heat, Q_{ST}, is related to the energy released when a molecule of gas adsorbs onto the surface of the material. For multiple molecules adsorbed at different sites of the structure, relatively different energy values will be obtained.

Therefore, to identify features in the adsorption in both frameworks, histograms with the distribution profiles of the isosteric heats were calculated and are shown in Figure 6.5 for the different gas molecules.

a) CuBTC
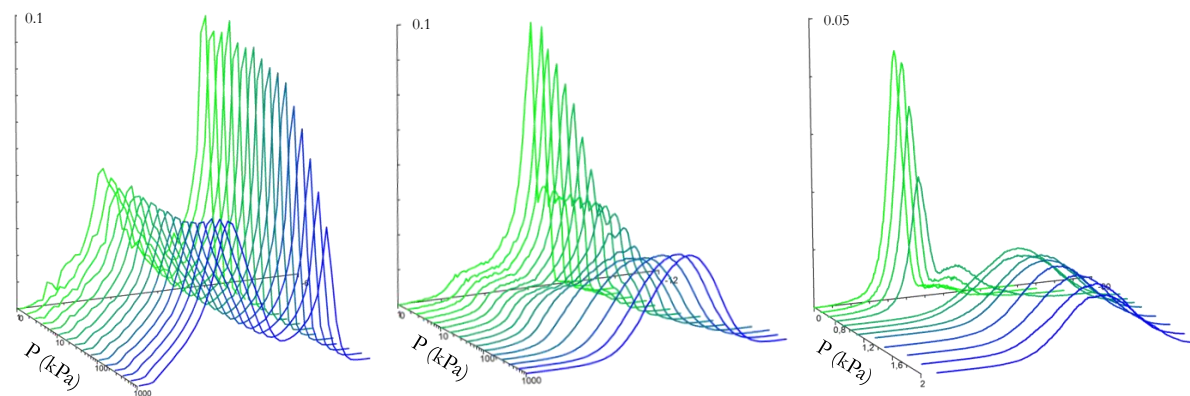
b) Zeolite 13X
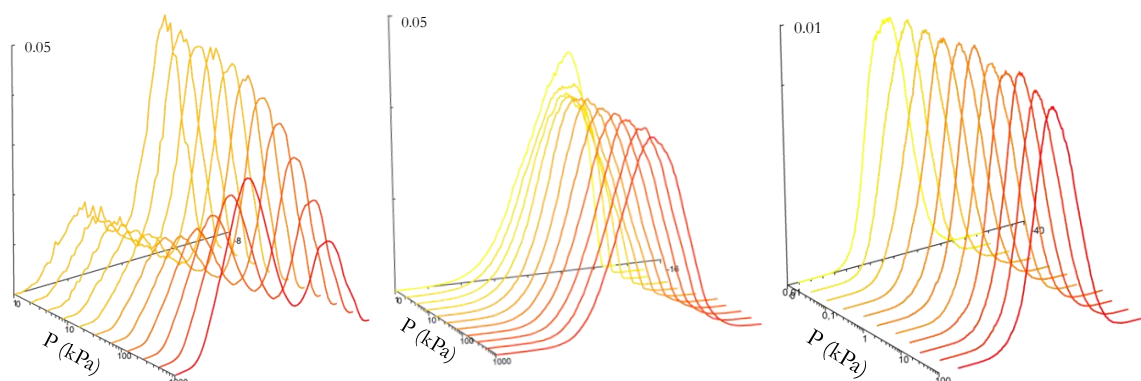
Figure 6.5. *Isosteric heat distribution profiles of pure components in (from left to right) nitrogen, carbon dioxide and water for a) CuBTC and b) zeolite 13X*

It can be observed that N_2 shows two different sites of adsorption in both structures, having more affinity for intermediate pore sizes: in zeolite 13X, the N_2 energy distribution plot has two peaks: the one closer to the y-axis corresponds to the

large pores and the second one to the intermediate pores, while in CuBTC, the two peaks correspond to the site II and III reported by Castillo and coworkers [Castillo et al., 2008], showing preferential adsorption at the octahedral side pockets.

For zeolite 13X, it is interesting to note that nitrogen changes the probability of the peaks as pressure increases: at very low pressures, N_2 prefers to be adsorbed in the interstices with intermediate diameter where has greater interaction with the material (and so more energy associated). However, when these intermediate pores are filled, nitrogen molecules tend to locate in the larger pores until full saturation. In contrast, CO_2 and H_2O have similar behavior, with nearly Gaussian curves meaning that there are not preferential sites and is indifferent for adsorption whether small, intermediate and large pores.

The behavior of the other gas components evaluated as well as snapshots reinforcing the preferred sites for all molecules can be seen in Figure. 6.6 and 6.7.

CuBTC: CO₂

CuBTC: H₂O
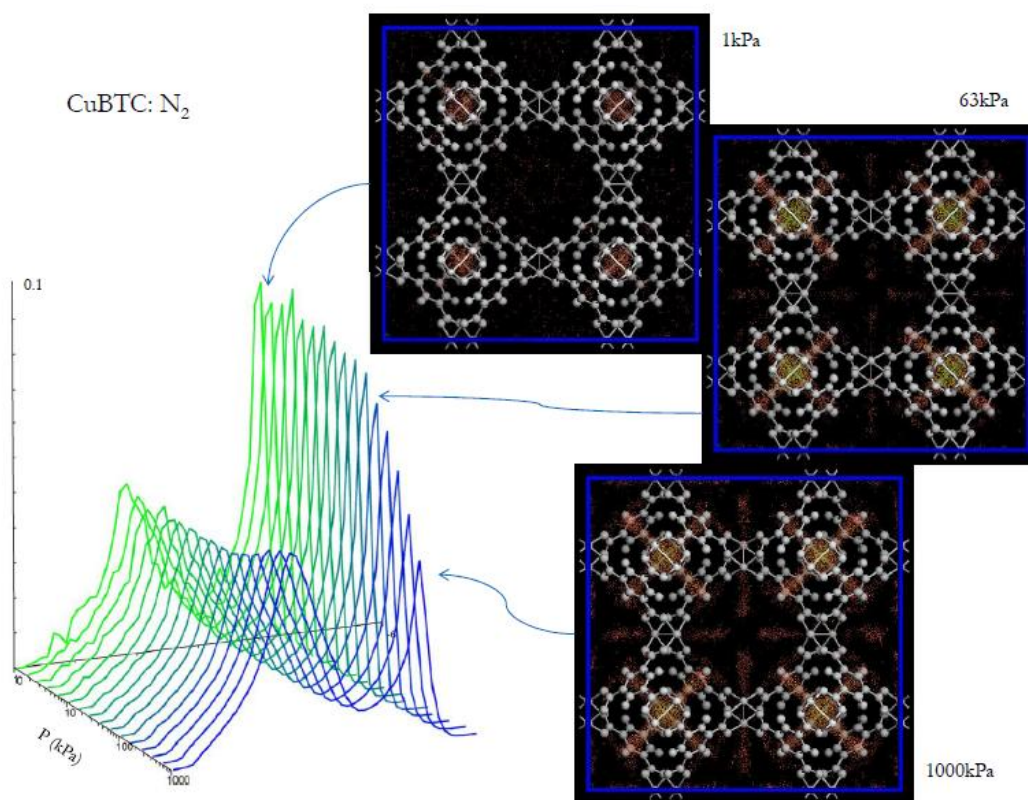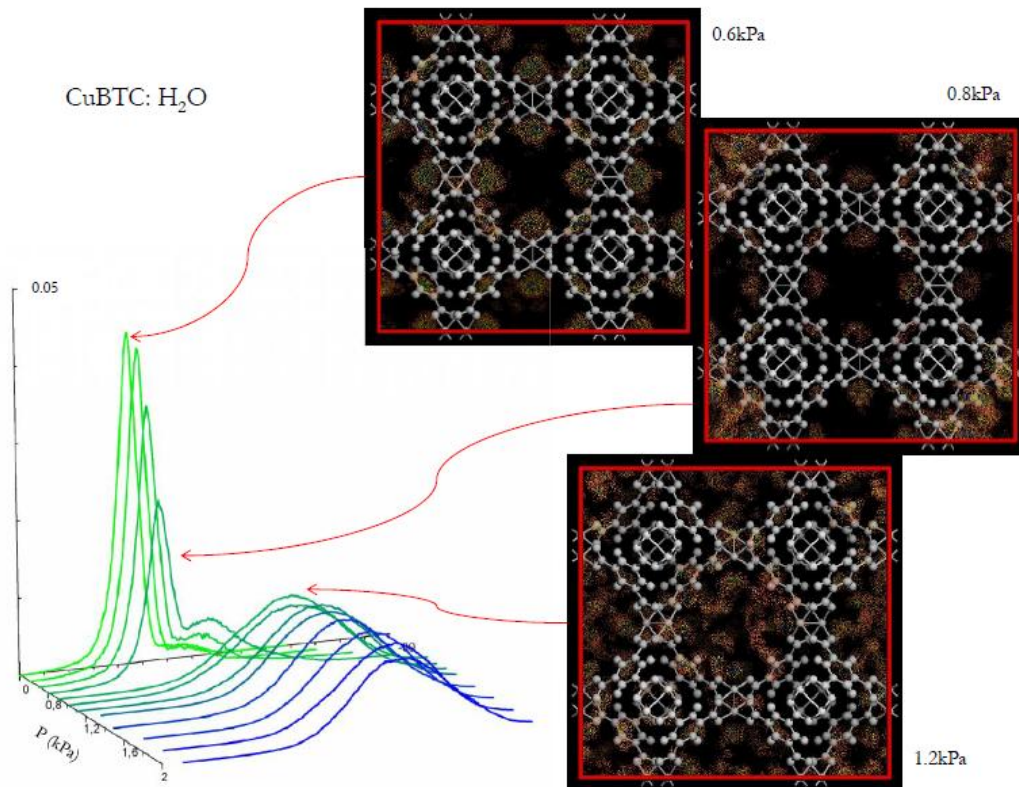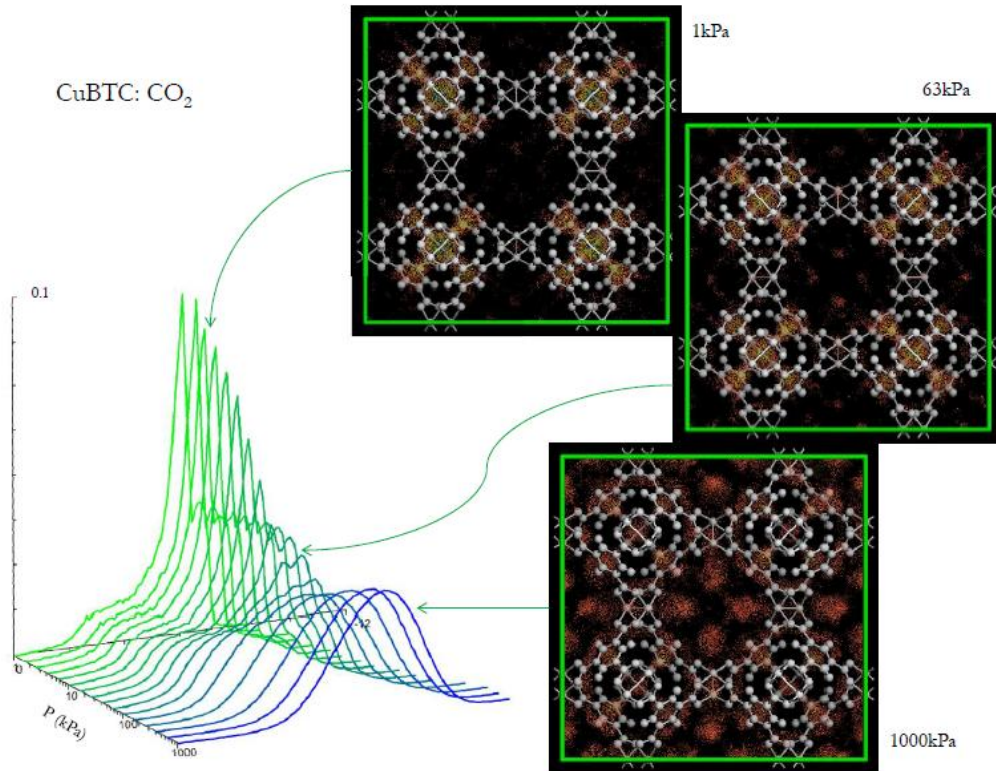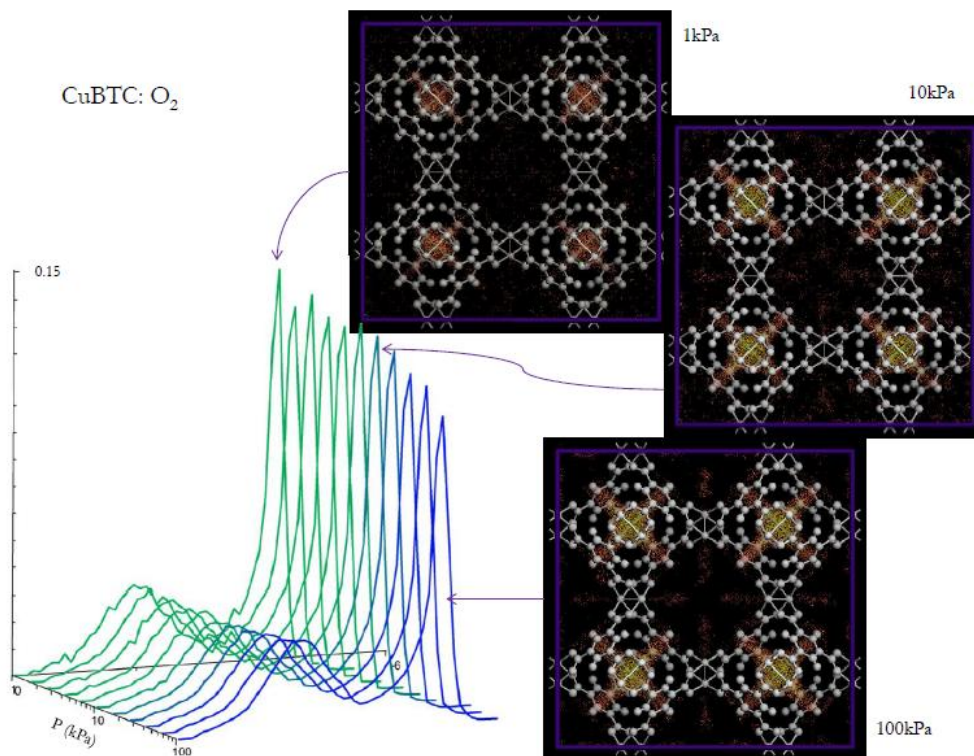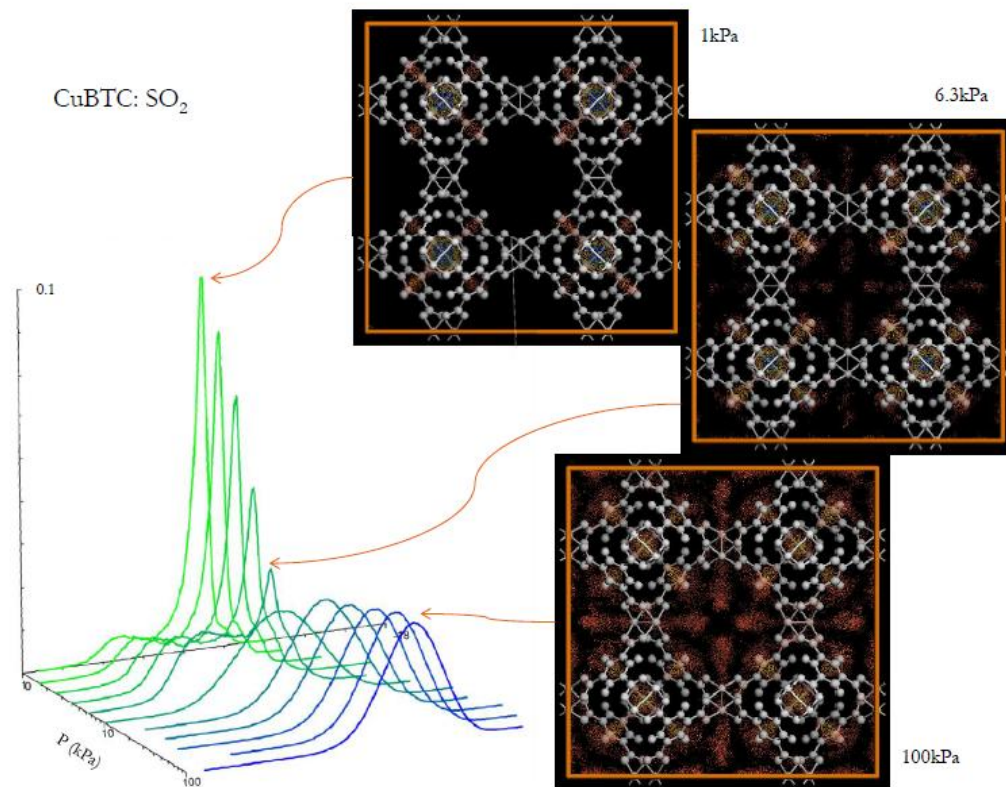
Figure 6.6. *Energy distribution probability as a function of pressure for adsorption of pure components in CuBTC.*

13X: H$_2$O

0.01kPa

0.1kPa

1kPa

13X: SO$_2$

0.01kPa

0.1kPa

1kPa
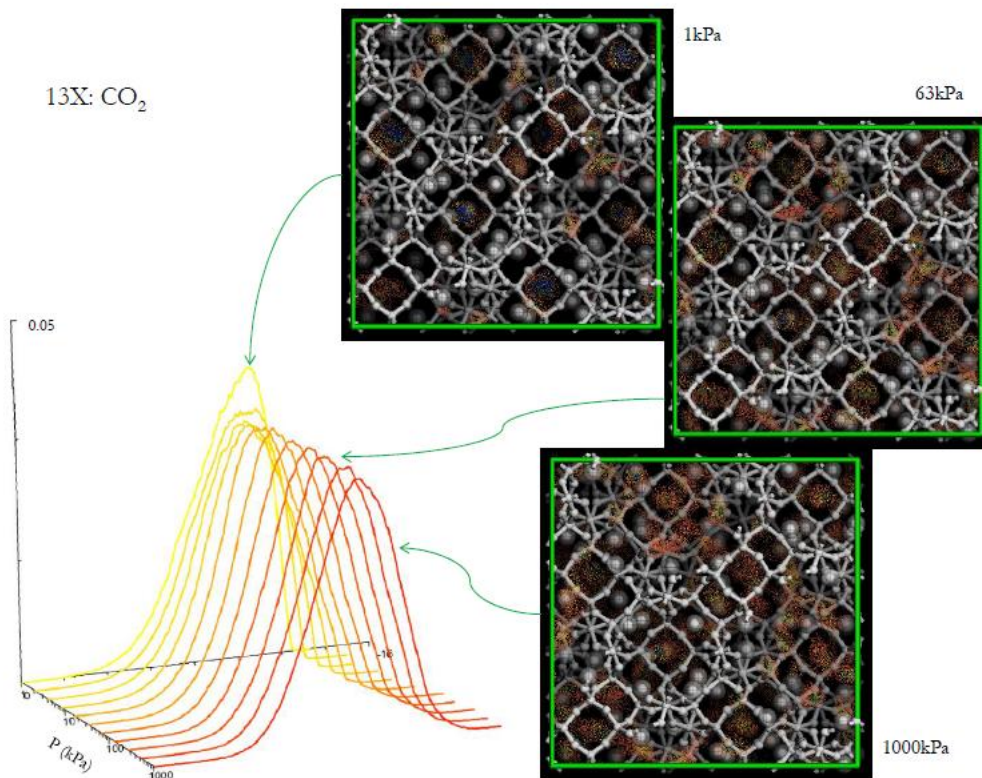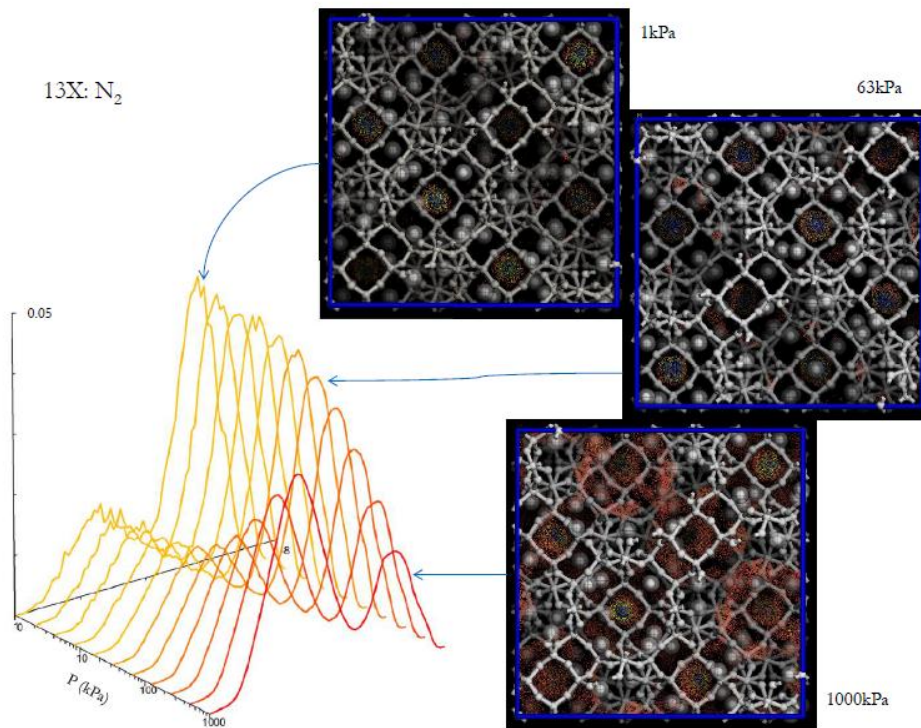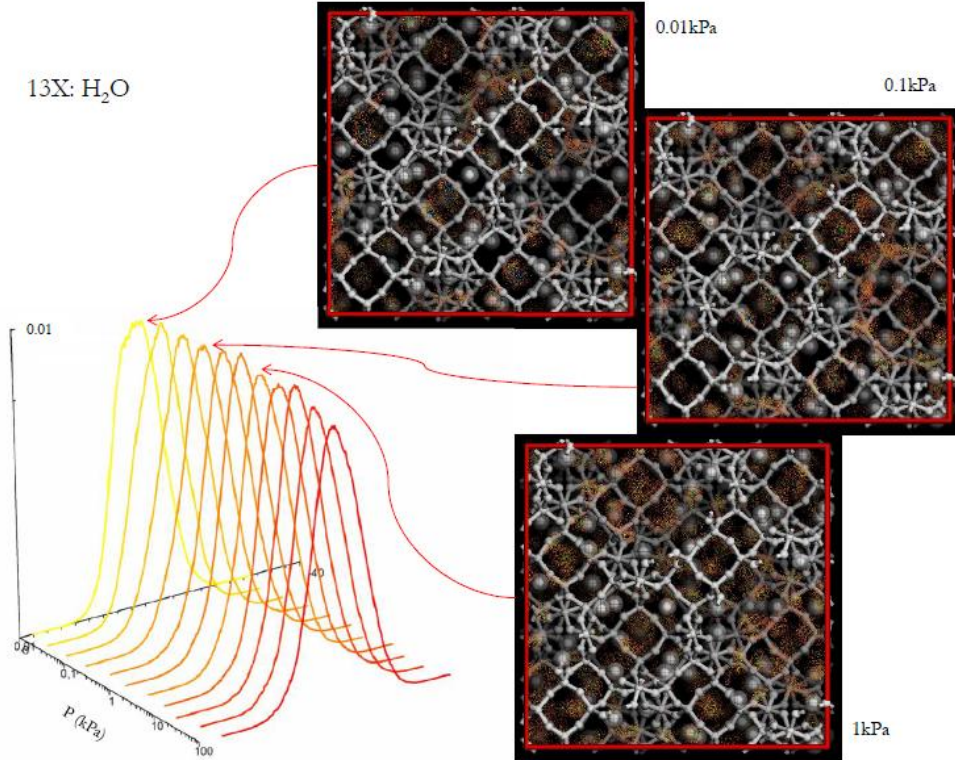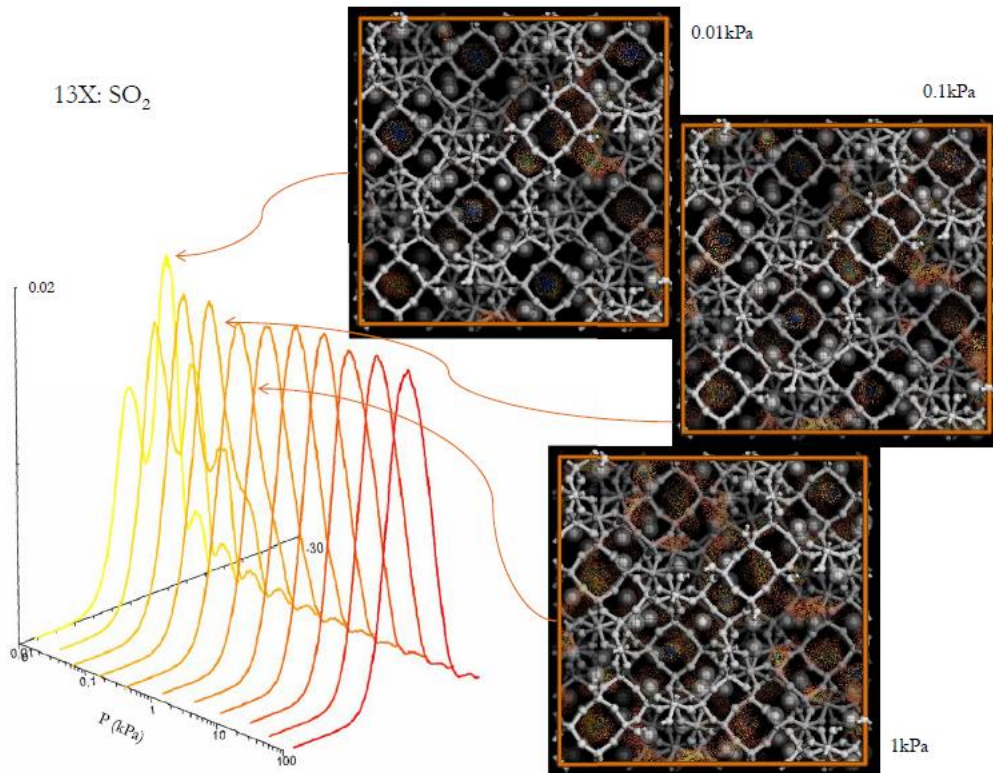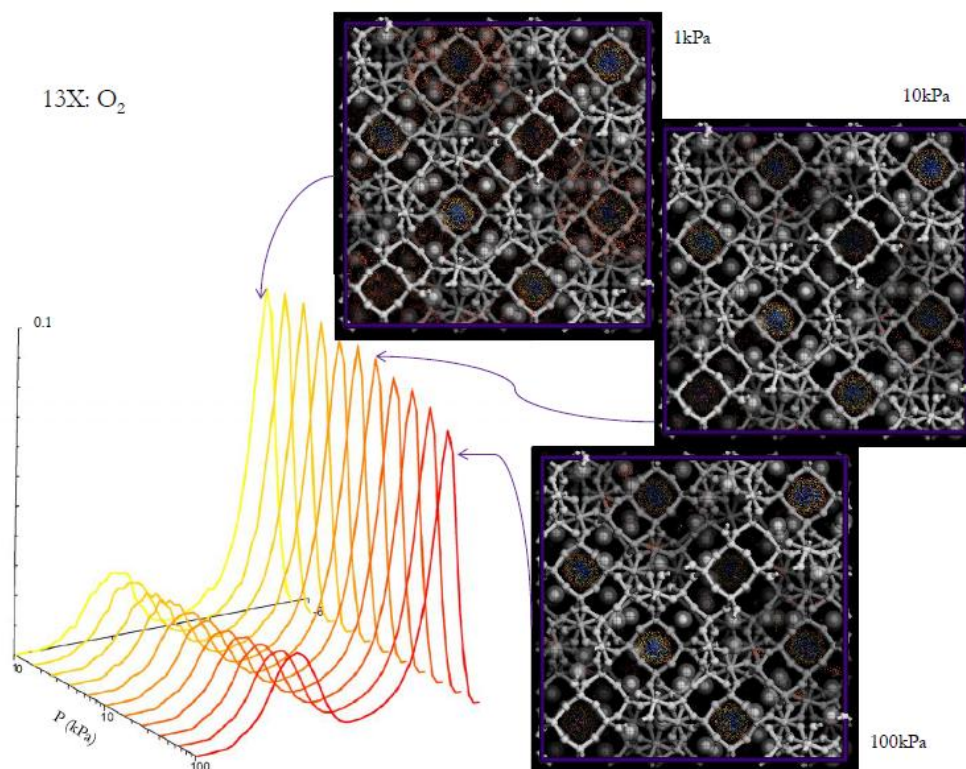
Figure 6.7. *Energy distribution probability as a function of pressure for adsorption of pure components in zeolite 13X.*

For CuBTC (see Figure 6.6), for example, more noticeable preference sites are observed: nitrogen adsorption shows two sites in the histogram that do not change substantially with increasing pressure. Meanwhile, carbon dioxide has a higher peak at low pressures related to the octahedral side pockets, and as the pressure is increased, the CO_2 tends to stay near the copper-clusters to further achieve the Gaussian behavior when saturation is reached. Similarly, water shows a marked tendency to adsorb initially near the framework metals (initial points in the adsorption isotherm before the sudden rise in capacity) and finally condenses and fills all pores.

As observed, GCMC simulations provide a series of distributions according to the likelihood that more or less molecules may adsorb in a specific site. Therefore, in Figure 6.8 we present the values corresponding to the highest peak of the histograms. For CuBTC, an isosteric heat of 28kJ/mol was obtained for carbon dioxide, a value that indicates a physisorption phenomenon. The value is comparable to that reported in literature [Wang et al., 2002], but slightly lower than the heat of adsorption obtained and/or reported for CO_2 with zeolite 13X (40 and 45kJ/mol respectively) [Franchi et al., 2005]. It is important to notice that the lower value for the MOF should be beneficial for the adsorbent regeneration from the perspective of a reduced energy requirement.

a) CuBTC
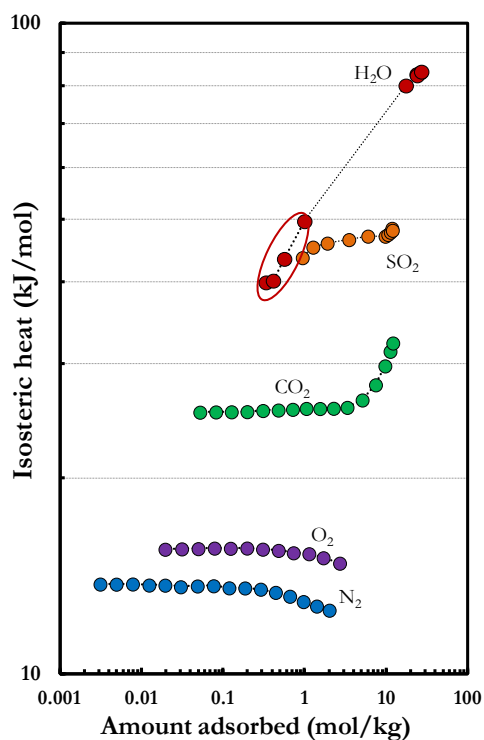
b) Zeolite 13X
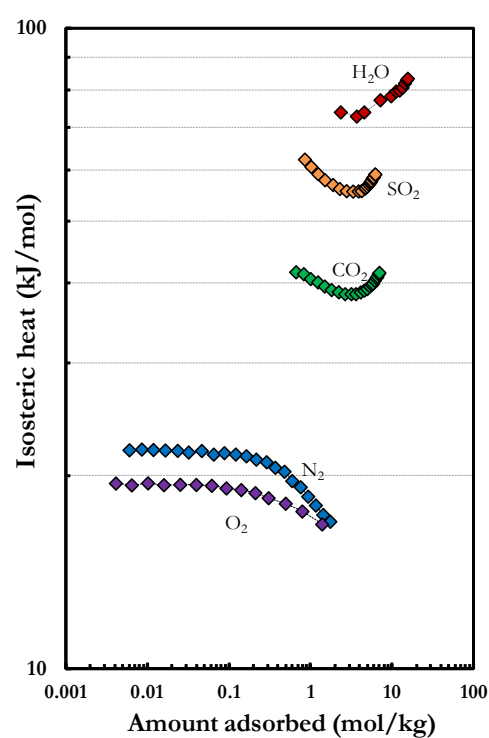
Figure 6.8. Isosteric heat patterns of (a) CuBTC and (b) zeolite 13X for the five pure components considered.

As observed in Figure 6.8, the isosteric heat for nitrogen and oxygen are lower than for CO_2, but water and SO_2 have stronger interactions with the frameworks. As mentioned before, the water isotherms show a very hydrophilic behavior typical for zeolites, and understandable for the Cu open sites in the MOF [Yazaydin et al., 2009]. Moreover, the obtained isosteric heats of water are about 2-4 higher than CO_2 and 4-6 than N_2. The Q_{ST} for water in CuBTC shows a peculiar behavior due to two different reasons: the first values, the lower ones (enclosed) correspond to conditions where the structure barely adsorbs water, while the higher ones are related to the sudden change in adsorption capacity, where the molecules condense and strongly interact among themselves. It should be noted that the values enclosed are in agreement with those reported in literature at very low pressures [Castillo et al., 2008]. And finally, the N_2 and O_2 values show a reduction with the amount adsorbed (more marked in zeolite 13X) because the molecules adsorb in non-preferential sites as mentioned already. The changing behaviors in isosteric heats and in adsorption isotherms regarding the mixtures evaluated will be explained in detail in the next sections.

6.3.3. CO_2/N_2 binary mixtures

Figure 6.9 depicts a comparison between the isosteric heat distributions of the molecules in both materials for the pure compounds and the adsorption behavior in a binary 15%CO_2/85%N_2 mixture (for flue gas composition at 298K). A close look at the binary mixtures in the zeolite 13X reveals that, when nitrogen molecules compete with CO_2 for the intermediate sites, carbon dioxide displaces the nitrogen molecules and adsorbs in large pores, leading to a decrease in the isosteric heat (as mentioned above, but for pressure increasing). On the contrary, CO_2 is not so affected by the presence of nitrogen and adsorbs on its preferred sites because of its higher interaction with the structure compared to N_2.

a) CuBTC   b) Zeolite 13X
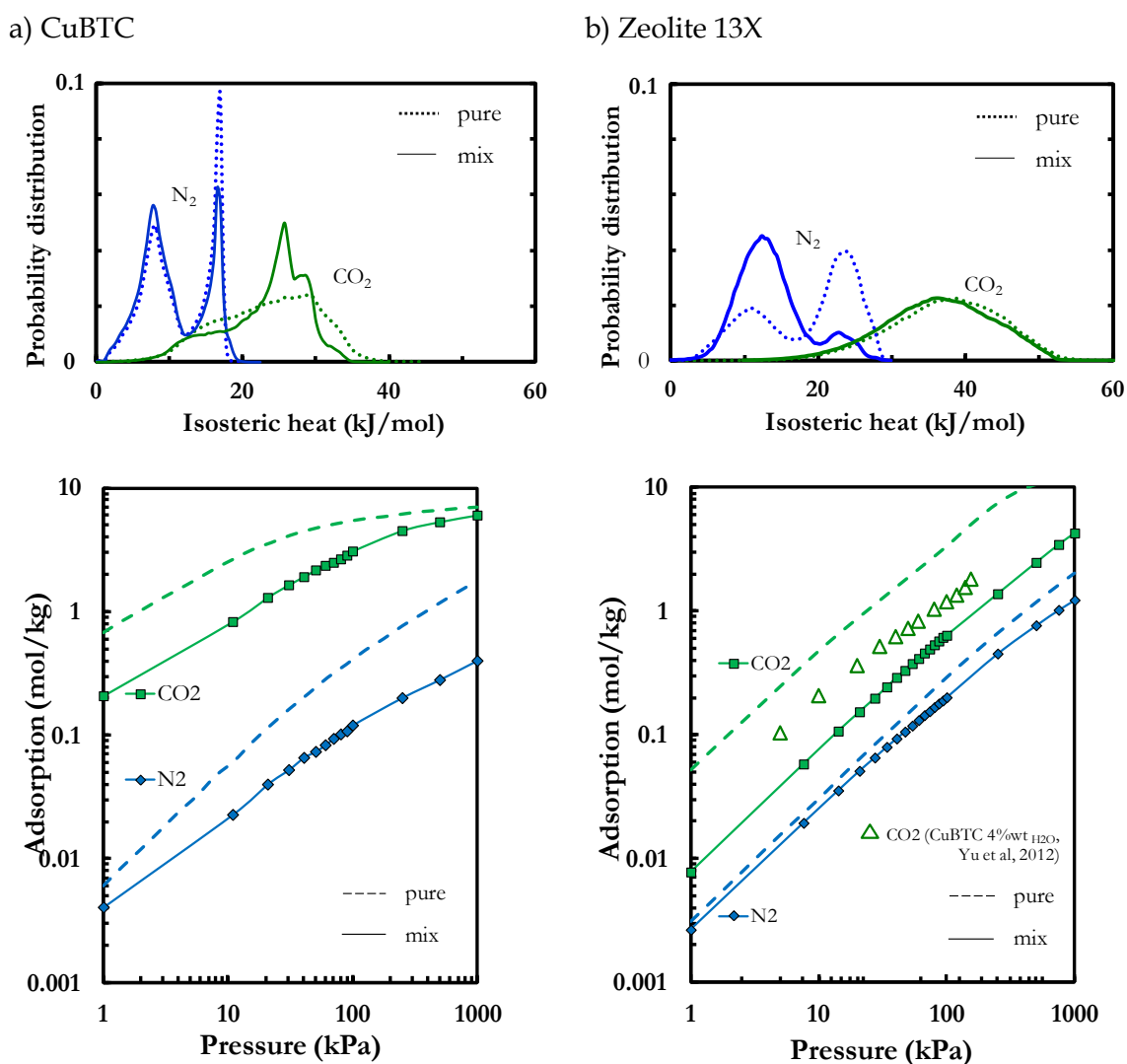
Figure 6.9. *Isosteric heat distribution profiles (top) and adsorption curves (bottom) for pure (dashed lines) and 15% CO_2/85%N_2 mixtures (full line and symbols) in a) CuBTC and b) zeolite 13X at 298K.*

A completely different behavior is shown by the CO_2 adsorption in CuBTC, where more targeted adsorption sites are observed: an initial plateau (close to the metals), within the middle size pores, corresponding to the highest peak at 25kJ/mol, and a second peak located at higher isosteric heat values corresponds to adsorption of CO_2 in the channels of small pores.

In order to assess differences in operating conditions, three conditions have been evaluated: the typical flue gas (i.e., 15/85 CO_2/N_2) at 298K, a high temperature flue gas, at 400K (i.e., the conditions at the chimney), and air gas at 298K with a concentration about 500 ppm of CO_2 (the results are provided in Figures 6.10 and 6.11). Although air and flue gas present more components, the first assessment for CO_2 separation will come from the CO_2/N_2 mixture study.

a) N_2/CO_2, 298K air condition (99.95%N_2/0.05%CO_2)

b) N_2/CO_2 400K flue gas (85%N_2/15%CO_2)

Figure 6.10. *Isosteric heat distribution profiles (P=100kPa) and adsorption isotherms for binary mixtures of N_2/CO_2 at different conditions in CuBTC.*

At air conditions, the percentage of adsorption of N_2 is higher than that obtained for CO_2, caused by the extremely low concentration of CO_2 in the modeled air (i.e., 0.05%). The opposite behavior was found in flue gas conditions at 400K, where the adsorbed percentages have reversed. It is also noted that when the temperature rises, the percentage of CO_2 decreases, showing a typical physisorption behavior; this is because CO_2 interactions become weaker and hence the material selectivity is reduced.

a) N_2/CO_2, 298K air condition (99.95%N_2/0.05%CO_2)

b) N_2/CO_2 400K flue gas (85%N_2/15%CO_2)

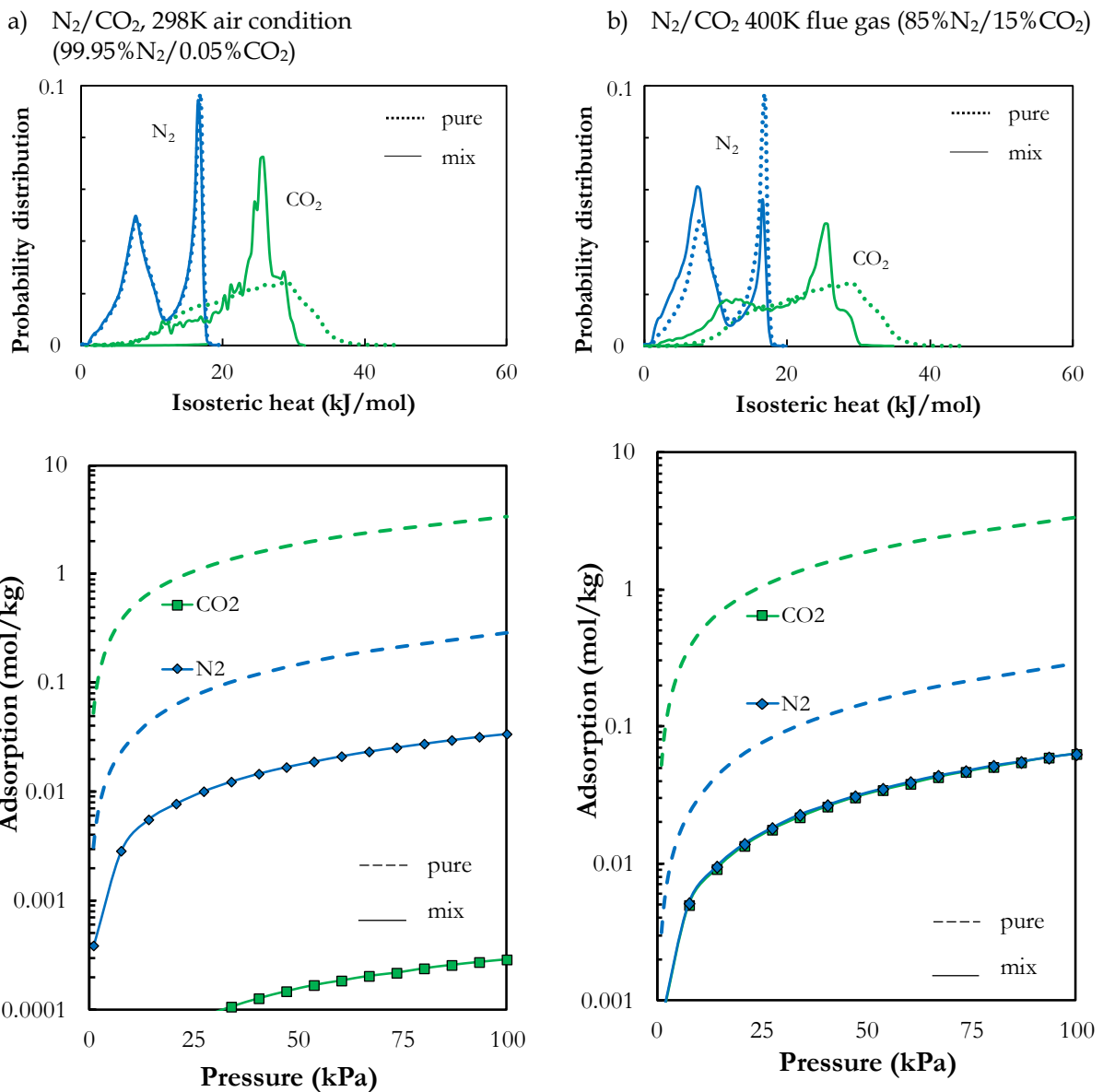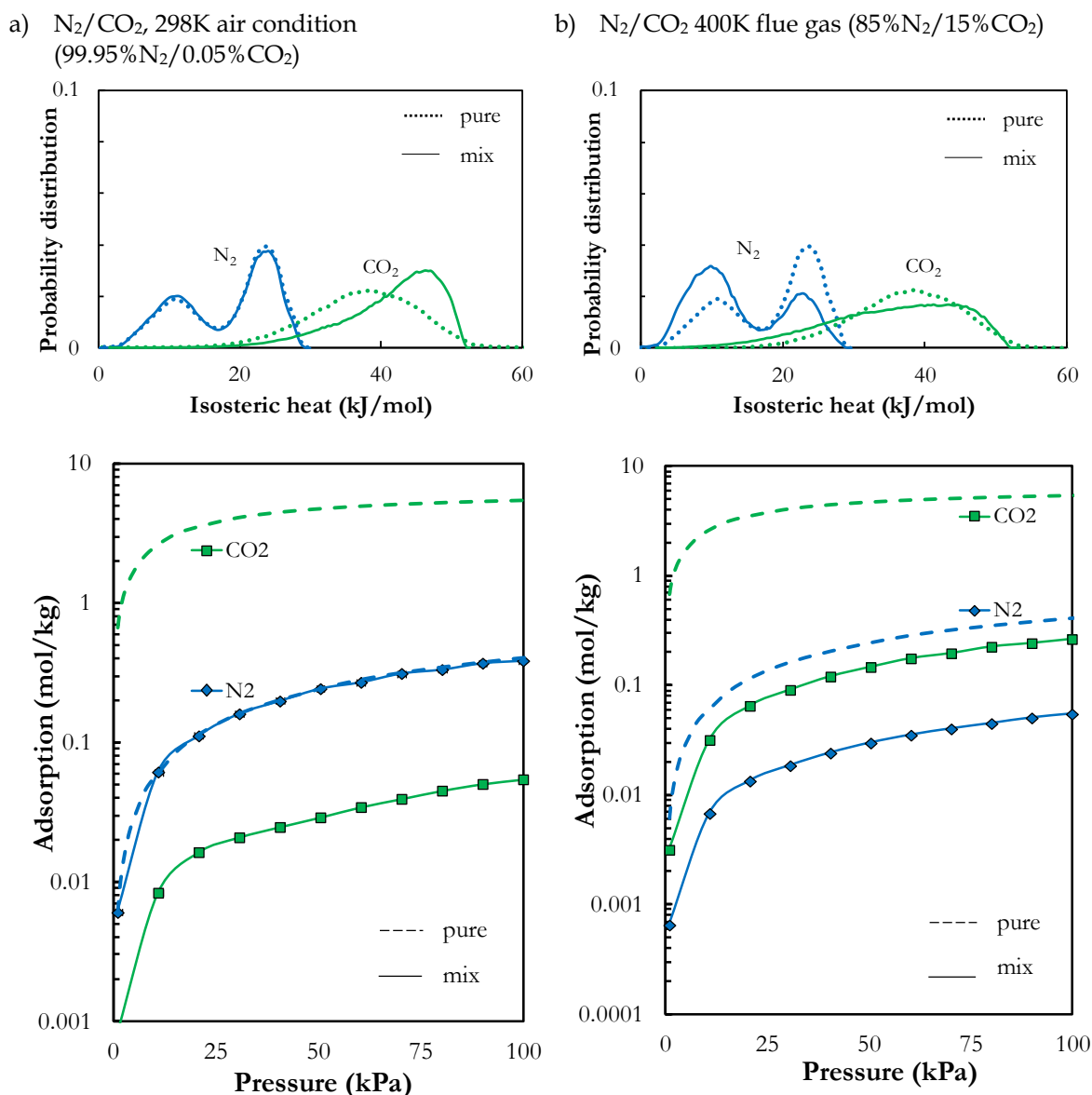**Figure 6.11.** *Isosteric heat distribution profiles (P=100kPa) and adsorption isotherms of binary mixtures N_2/CO_2 at different conditions in zeolite 13X.*

The selectivity of different mixtures in an interval of 1-100kPa was also calculated in order to assess the effect of the different conditions on the adsorption behavior. Results are depicted in Figure 6.12 where it can be observed that CuBTC

presents values one order of magnitude lower than zeolite 13X: CuBTC shows lower selectivity of CO_2 than zeolite 13X at the three explored conditions because of the relatively low heat of CO_2 adsorption. In addition, zeolite 13X selectivity towards CO_2 slightly decreases with increasing pressure whereas in the case of CuBTC is essentially unchanged. However, the presence of impurities dictates whether the material is appropriate or not for such separations. The lower selectivity for CO_2 from flue gas at 400K with respect to that obtained at 298K is observed in both materials.

a) CuBTC   b) Zeolite 13X
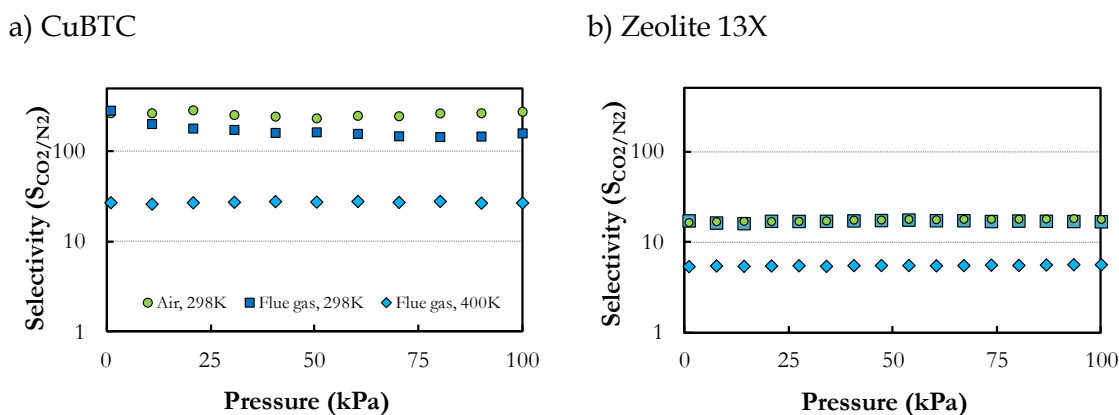
Figure 6.12. *Selectivity for different CO_2/N_2 conditions in a) CuBTC and b) zeolite 13X: circles (green) represent simplified air composition at 298K (N_2 with 500ppm of CO_2); squares (blue), flue gas composition (15%/85% CO_2/N_2) at 298K, and diamonds (light blue), flue gas composition (15%/85% CO_2/N_2) at 400K.*

For practical applications it is also necessary to investigate the CO_2 adsorption behavior in the presence of water and impurities, because flue gas contains water vapor and small amounts of other gases such as SO_2 which compete for the adsorption onto the material. Since the adsorption properties may be drastically affected by the presence of some compounds, studies on the adsorption behavior or possible "poisoning" of the material are important and they need to be assessed before the material reaches the final application. According to this, a systematic study on the influence of coexisting trace compounds in the mixtures on the adsorption properties of CO_2 in CuBTC and zeolite 13X is also presented here.

6.3.4. Influence of water on the adsorption behavior

Once the binary mixtures of gases were studied in detail, the effect of the presence of water (moisture) on the adsorption properties was evaluated for both structures at flue gas conditions; note that these simulations do not use coordinated

waters into the structures, as done in previous studies [Castillo et al., 2008; Krishna and Long, 2011]. Initial studies, not included in this work, revealed that the exclusion of these coordinated waters plays an important role at low pressures, while at atmospheric conditions these interactions are small, being more important those coming from uncoordinated waters. This fact should be a good approximation since when dealing with real processes, the structure would be completely dried after regeneration.

Figure 6.13 presents the adsorption sites preferences for the different components in the $CO_2/N_2/H_2O$ mixture compared to those in the pure state. In this case, simulations were carried out at 298K, and for different H_2O compositions: 1%, 0.1%, 0.01% and 0.001%. For the sake of clarity only those for 1% and 0.001% H_2O are provided.

a) CuBTC

1% H_2O (15% CO_2, 84% N_2):
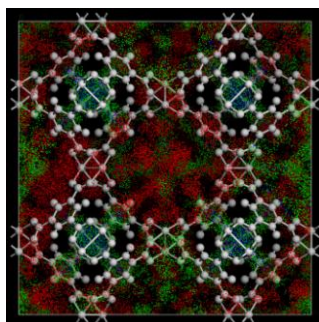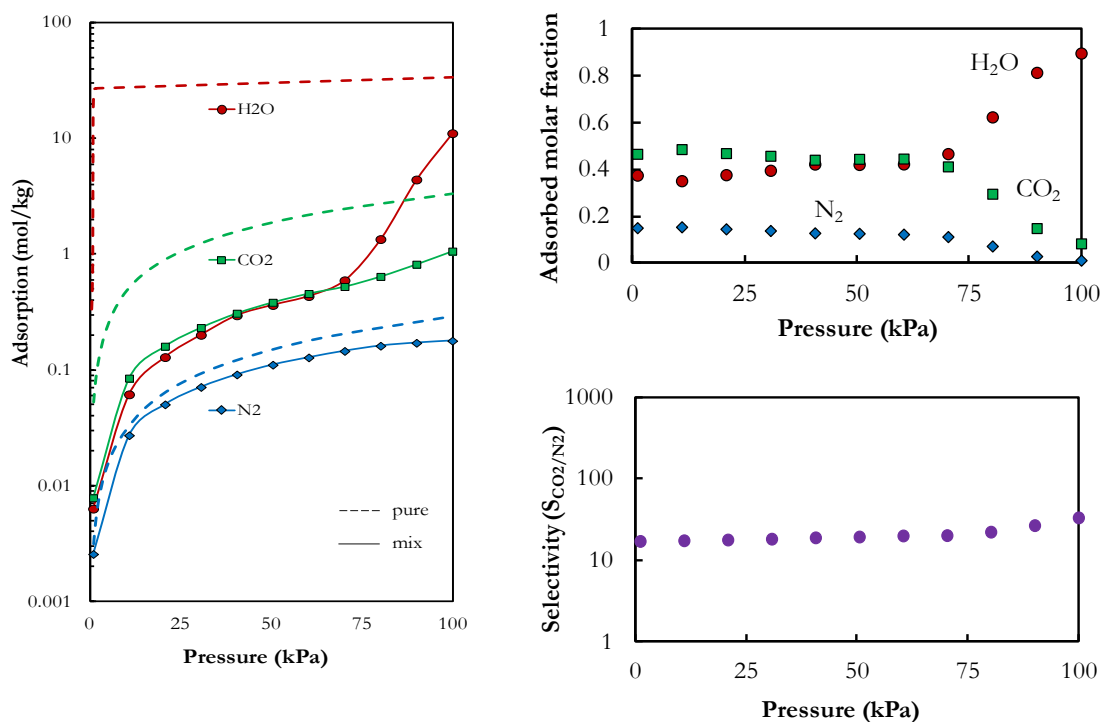
0.001% H_2O (15% CO_2, 84.999% N_2):
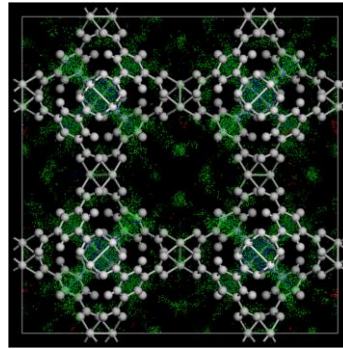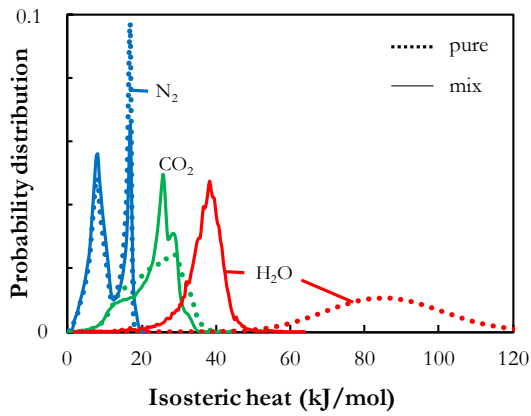
b) Zeolite 13X

1% H_2O (15% CO_2, 84% N_2):
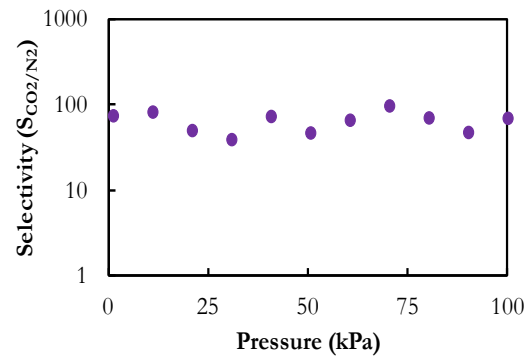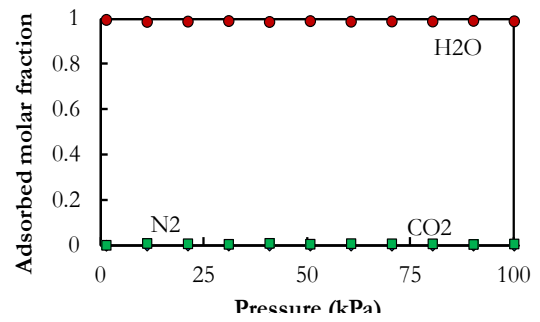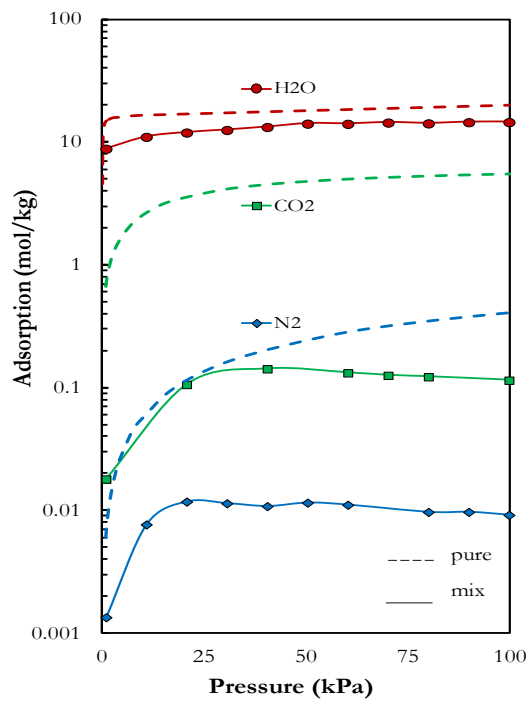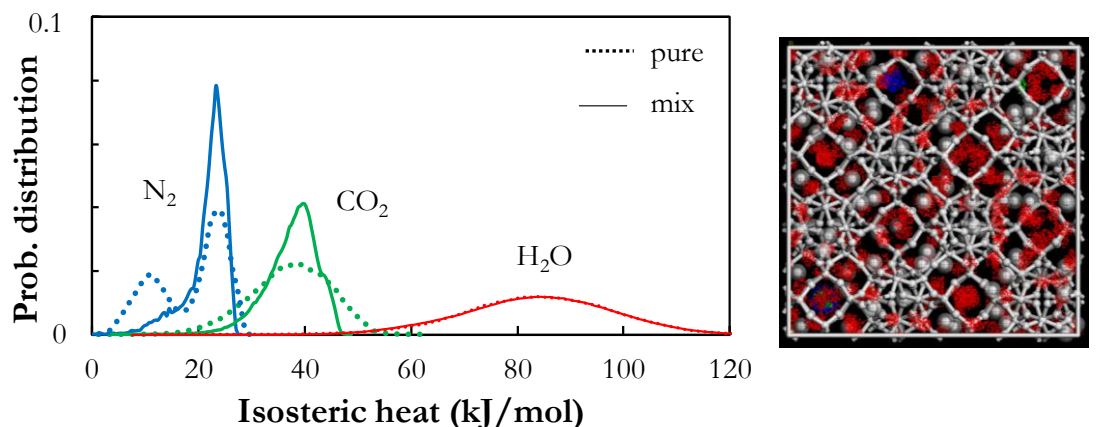
0.001% H_2O (15% CO_2, 84.999% N_2):
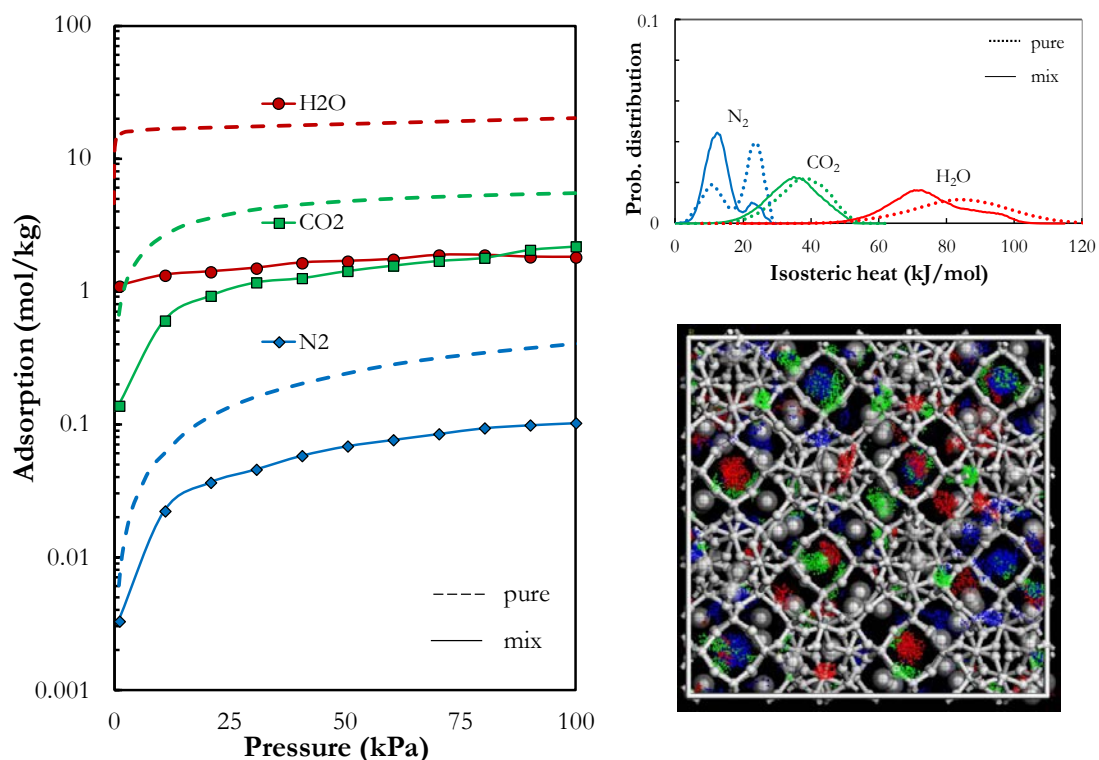
Figure 6.13. *Adsorption isotherms, isosteric heat distribution profiles and representative adsorption sites snapshots in the different mixtures at 100kPa, for pure and two ternary $CO_2/N_2/H_2O$ mixtures in a) CuBTC and b) zeolite 13X.*

For zeolites it is well-known that the presence of water significantly decreases the adsorption of CO_2 in these materials because water competitively adsorbs on the cations, blocking access for CO_2 (see Chapter 5 of this Thesis). In Figure 6.13, the first snapshot from 13X represents a mixture with 1% of water, and shows that the zeolite becomes fully filled with water. There is a small adsorption of CO_2 and N_2 in specific

zones, where the zeolite attraction strongest (also observed in the energy adsorption distribution plot where sharp distributions are obtained). As the amount of water is reduced, the adsorbed CO_2 increases. This fact allows that N_2 and CO_2 adsorb in lower energy zones since there is no more water available to fill them up. A displacement of the maximum respect the pure isotherms to lower energies is observed, and in the case of N_2, where the two sites of adsorption are differentiated, a shift in the maximum peak is also observed. At the lower water composition (0.001% H_2O) CO_2 can compete against water, then the CO_2 energy distribution is similar to the pure component and water molecules are displaced to occupy lower energy sites as N_2.

For CuBTC, very strong preference for site I (region close to the Cu metal centers) is found for water. As shown, CuBTC exposed to the mixture with 1% water content shows no significant peak change from snapshots patterns, which indicates that the CuBTC framework can be well maintained in the presence of moisture.

It is generally accepted that the presence of coordinatively unsaturated metal sites in MOFs can enhance the separation of CO_2 since it can coordinate to the metal clusters. But, in addition, such unsaturated sites can also coordinate with water and other molecules [Yu et al., 2012; Liu et al., 2010]. For instance, Yazaydin and coworkers showed that the presence of 4%wt coordinated water in the CuBTC framework can enhance CO_2 capture capacity and selectivity over N_2 [Yazaydin et al., 2009]. Initial studies (see Figure 6.14) revealed that the exclusion of these coordinated waters plays an important role at low pressures, while at atmospheric conditions these interactions are small, being more important those coming from uncoordinated waters.
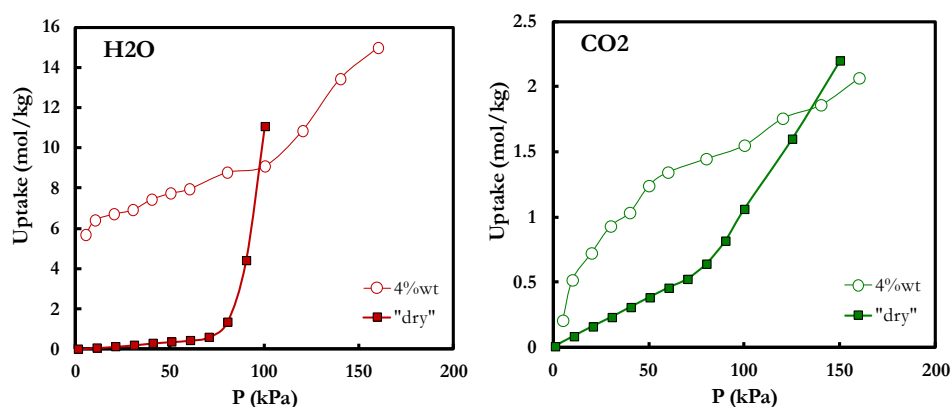
Figure 6.14. Adsorption isotherms for water and carbon dioxide in CuBTC, showing the difference between a dry framework and one with 4%wt of coordinated water.

It is interesting to see that for 1% H_2O in CuBTC, the adsorption isotherm of CO_2 shows a slightly increase after 80kPa, as depicted in Figure 6.15. As mentioned by Castillo and coworkers [Castillo et al., 2008], the strong interactions between the quadrupole moment of CO_2 and the electric field created by water molecules are

responsible for the enhanced CO_2 uptake. Nevertheless, the enhanced selectivity induced by uncoordinated water in the flue gas results in competition sites between water and CO_2: with more water molecules adsorbed at higher pressures, the competition would lead to the decrease of the CO_2 adsorption capacity.

From first look at the pure isotherms of water it may be inferred that there is higher free volume available at CuBTC, however, when the zeolite is exposed to 0.01%H_2O, its CO_2 adsorption capacity significantly decreases from 3 to 1.5 mol/kg at 100kPa (Figure 6.13b), and at a water composition of 0.1% the material is completely useless for CO_2 separation: water precludes any adsorption of CO_2 and N_2 on this type of zeolite. Only at a concentration of 0.001% of water, the molar composition of carbon dioxide inside the materials is greater than water at 100kPa, showing that adsorption of CO_2 can compete with H_2O. This is attributed to stronger interactions between water and zeolite 13X than those for the CuBTC. As H_2O molecules are pre-adsorbed in the pores, the CO_2 capacity decreases with the decrease of adsorption sites on the porous surface.
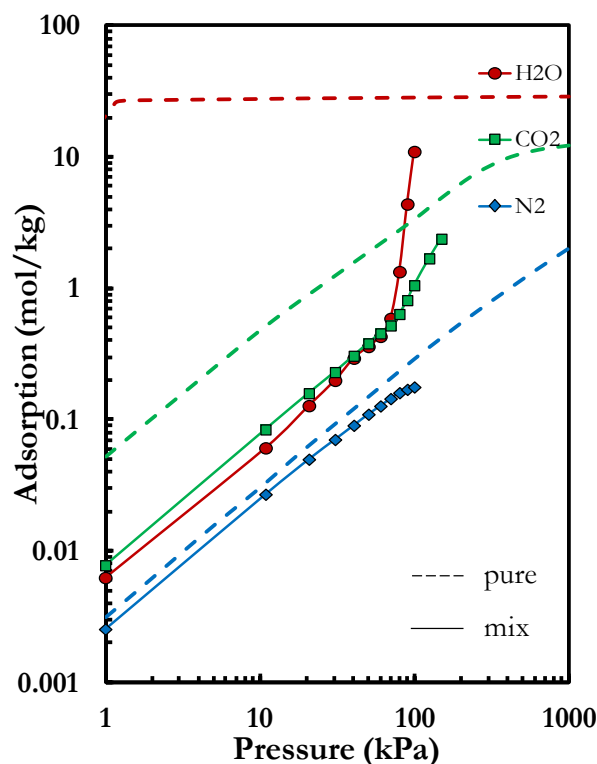
Figure 6.15. *Adsorption isotherms for pure and 15%CO_2/84%N_2/1%H_2O mixtures in CuBTC*

6.3.5. Other impurities

Moreover, the influence of flue gas components such as SO_2 and O_2 (besides water) on the CO_2 capacity of the adsorbent should be considered before the material is

designed for its final industrial applications. Therefore, the adsorbents should keep their CO_2 adsorption capacity (or similar) than in the absence of these impurities, indicating that they are adequate materials for these type of conditions.

Typically, in a flue gas the concentration of water, O_2 and SO_2 in volume are 5-8%, 3-5%, and 500-1500 ppm, respectively [Granite et al., 2002]. Therefore, we have studied the behavior of CuBTC compared to zeolite 13X upon CO_2 capture for ternary and 5-component mixtures, including impurities that can be found in a real typical operation conditions.

6.3.5.1.   Ternary mixtures $CO_2/N_2/SO_2$ (0.2% SO_2)

In these simulations, the behavior of CuBTC and 13X were first tested with SO_2. Figure 6.16 shows the behavior under a relatively large quantity of SO_2, 2000ppm, which rarely can be found in a real flue gas streams. We have used this high concentration to magnify the effect of this impurity for assessing its effect.

The results show that CuBTC and zeolite 13X maintain their adsorptive properties in the presence of small quantities of SO_2. In zeolite 13X, nitrogen changes the adsorption site location, while CO_2 competes with the SO_2 molecules for the same type of site. The adsorbed amount slightly decreases with respect to the binary original mixture, while almost an equimolar composition inside the framework is observed.

a) CuBTC
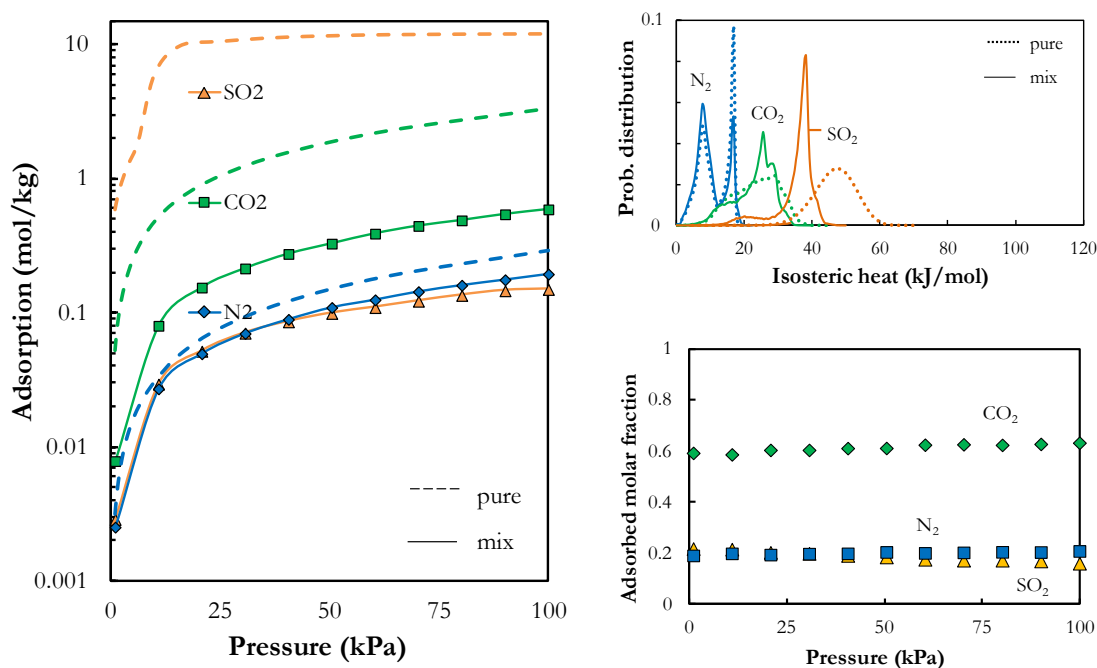
b) Zeolite 13X
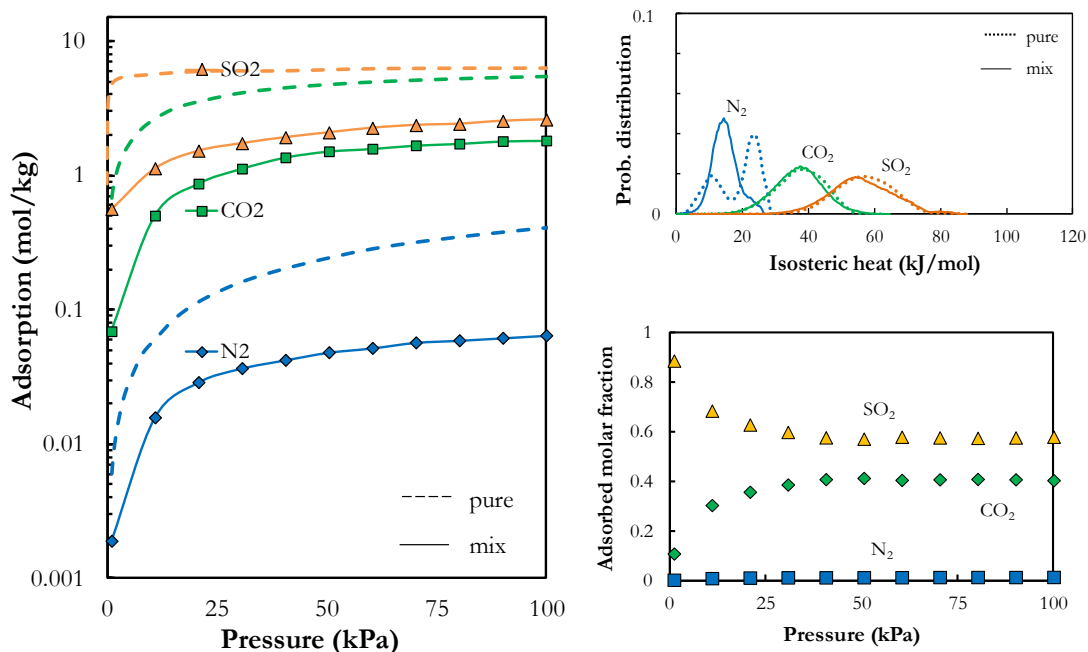
Figure 6.16. *Adsorption isotherms, isosteric heat distribution profiles and adsorbed molar fraction for pure and 15%CO_2/84.8%N_2/0.2%SO_2 mixtures at 298K in a) CuBTC and b) zeolite 13X.*

In CuBTC, the amount of SO_2 adsorbed is less than in zeolite 13X, and the molar fraction in the framework barely reaches 20%. In this material, SO_2 presents a radical change in energy distribution that can be explained for competition with CO_2, being the MOF more attractive to the latter; in fact, the CO_2 adsorption is similar than that obtained for binary mixtures (SO_2 molecules are placed in the small pores).

6.3.5.2.   5-component mixture

Finally, in order to explicitly quantify the computing effects on different gases in the preferential adsorption, we have performed a simulation study of multi-component system with the aim to elucidate the behavior in a real stream of post-combustion. Figure 6.17 represents the isosteric heat probability distribution of adsorption in a multi-component mixture (15%CO_2 / 78.8%N_2 / 5%O_2 / 0.2%SO_2 / 1%H_2O) and the molecules density/location snapshots in both materials.

Results obtained from the simulations allow a molecular explanation of the competing adsorption phenomena. In this case, it is obvious that water is the main component being adsorbed, especially in the zeolite 13X, with very similar behavior than those obtained for ternary CO_2/N_2/H_2O mixtures with 1% of water. The CO_2/N_2

selectivity does not change much even with relatively high concentrations of O_2 in the flue gas and it presents a similar behavior than nitrogen. These results are in agreement with those found by Yu and coworkers in a related study [Yu et al., 2012]. Hence, oxygen and SO_2 impurities do not play a main role in this separation, although in CuBTC, SO_2 tends to compete with CO_2 for adsorption sites, reducing the amount adsorbed of both components.

Moreover, it is interesting to note that the probability curve for CO_2 in CuBTC moves slightly to the right (to higher energy values), which means the improved adsorption by the presence of water, while in the zeolite the curve shifts to the left (i.e. lower isosteric heat values). Likewise, SO_2 presents a similar behavior but in the opposite directions: the peak value of the isosteric heat is increased for the zeolite while decreases for the MOF.

a) CuBTC
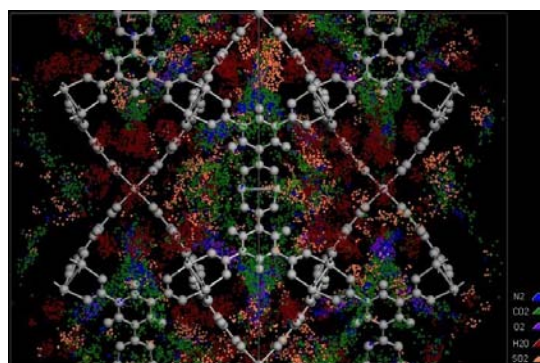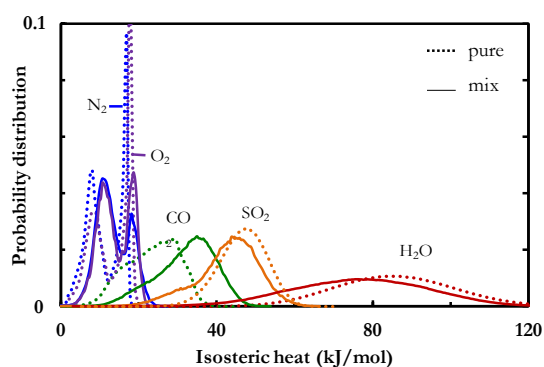
b) Zeolite 13X
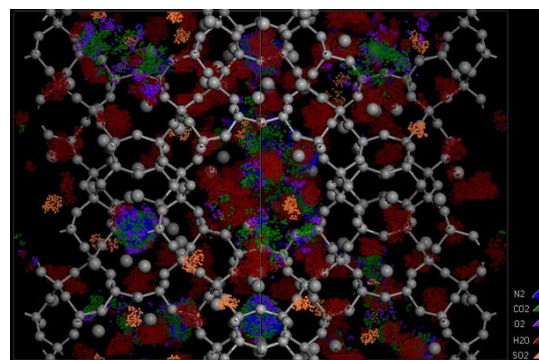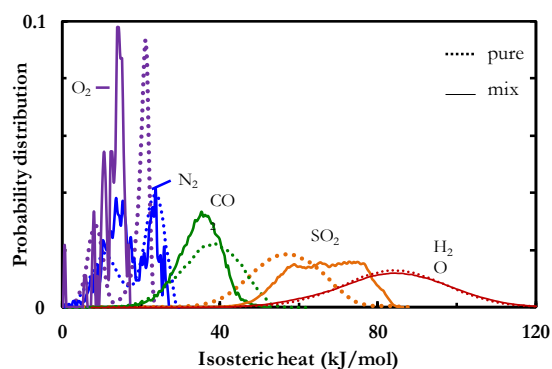
Figure 6.17. Isosteric heat distribution profiles of pure compounds and multi-component mixture (15% CO_2/78.8% N_2/5% O_2/1% H_2O/0.2% SO_2) in a) CuBTC and b) 13X; with snapshot showing the preferential location of the different molecules [P=100kPa, T=298K].

As a final point, the selectivity of the different mixtures was calculated in order to assess the effect of the different conditions on the adsorption behavior. Results are depicted in Figure 6.18 where it can be observed that CuBTC presents values one order of magnitude lower than zeolite 13X: CuBTC shows lower selectivity of CO_2 than zeolite 13X at the explored conditions because of the relatively low heat of CO_2 adsorption. However, the presence of impurities affects more forcefully the zeolite than the MOF CuBTC, being the mixture with 1% of water the closest to that in the faujasite.
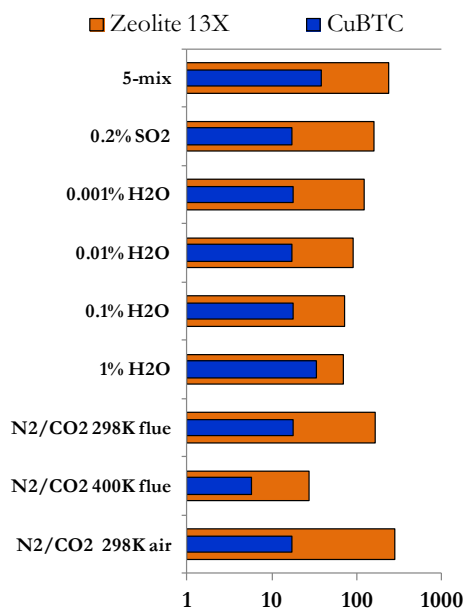
Figure 6.18. *CO_2/N_2 selectivity for different compositions in CuBTC and zeolite 13X [P=100KPa, T=298K].*

A slightly higher CO_2/N_2 selectivity of the ternary and 5-component mixtures were observed compared to that in a binary and ternary-water mixtures respectively, especially at high pressures, due to the strong SO_2 binding with the frameworks.

6.3.6. Implications for the application in a VSA, PSA or TSA process

As performed in Chapter 5, we calculate the working capacity of both materials at operating conditions Table 6.2 summarizes the different values for Vacuum Swing Adsorption (VSA), Pressure Swing Adsorption (PSA) or Temperature Swing Adsorption (TSA) processes, including all the mixtures evaluated in this work for flue gas composition. The working capacity in PSA and VSA cases was calculated by the

difference of CO_2 adsorption capacity between 1 and 10bar, and 1 and 0.15bar, respectively, at 298K, while in TSA case was calculated by the difference between 400K and 298K at 100kPa.

Table 6.2. Summary of the working capacity of zeolite 13X and CuBTC for VSA/PSA/PSA processes. See text for details.

Zeolite 13X:

Working capacity (mol/kg)	Pure	Binary	1% H_2O	0.001% H_2O	0.2% SO_2	5-mix
PSA	1.38	1.13	0.002	0.78	0.62	0.002
VSA	2.49	2.01	0.005	1.41	1.12	0.003
TSA	---	2.81	---	---	---	---

CuBTC:

Working capacity (mol/kg)	Pure	Binary	1% H_2O	0.001% H_2O	0.2% SO_2	5-mix
PSA	8.78	1.78	3.16	2.35	1.61	3.59
VSA	2.61	0.53	0.94	---	0.48	1.07
TSA	---	0.58	---	---	---	---

CuBTC shows much higher working capacity than the benchmark zeolite 13X in PSA in the presence of impurities, with lower energy requirement for regeneration, but also lower CO_2/N_2 selectivities. The CO_2 adsorption capacity declines after water sorption in both cases, being more noticeable in zeolite 13X. In addition, it is also clear that vacuum is inefficient for desorption of CO_2 from Cu active sites.

6.4. Conclusions

CuBTC and Zeolite 13X were evaluated in order to assess and compare their performance for CO_2 separation from N_2 in the presence of impurities, including SO_2 and H_2O, providing molecular insights into the competing adsorption phenomena.

Results reveal that a very little amount of uncoordinated water molecules induce an improvement on CO_2 capture in, while zeolite 13X became useless with less than 1% of water. As a consequence, zeolite 13X is not suitable for the adsorption of

CO_2 without a previous proper dehumidification process, because just a 0.01% of moisture in the adsorbent is able to significantly reduce the adsorption capacity of CO_2.

By comparing CO_2 selectivity for different mixtures, it was found that even with a concentration of SO_2 in the flue gas as high as 2000ppm, the selectivity in the flue gas mixtures remains essentially unaffected; there was only a slightly lower adsorption, attributed to the decrease of CO_2 adsorption with the introduction of SO_2 in flue gas (sites competition).

7

GCMC SIMULATIONS OF ADSORPTION ON KAOLINITE AND CHABAZITE[3]

7.1. Introduction

Clay minerals (aluminosilicates) are frequently used in many industrial and natural processes due to their interesting physico-chemical properties. Kaolinite (i.e., $Si_4Al_4O_{10}(OH)_8$), is a non-expansive phyllosilicate composed of plate-like structures. In Figure 7.1 is shown the kaolinite and chabazite natural minerals.

Chabazite   kaolinite

Figure 7.1. *Chabazite and kaolinite minerals*

As kaolinite is the main constituent of kaolin, is cheap and abundant in nature with external surfaces of octahedral alumina and tetrahedral silica faced and held together by hydrogen bonds. The important role played in industry is demonstrated by the increasing amount of kaolin produced per year. In the side of natural processes, the aerosolized mineral dust is another source of clay minerals directly expelled to the atmosphere. The dust is basically produced from arid zones (e.g., Sahara desert, Asian dust storms . . .) and it is formed by quartz and mineral clays and in a lower extent by feldspar, carbonates, sulfates and metal oxides.

Such a huge quantity of mineral dust present in the atmosphere along with the ability of clay minerals to take up water can influence atmospheric composition, cloud formation, visibility, climate as well as human health. A proof of this importance is the high number of theoretical studies for water interaction in zeolites at different pressures and mainly at 235 and 298 K. Moreover, experimental studies have reported adsorption isotherms of water adsorption on kaolinite at temperatures of 296 and 298 K by means of Horizontal ATR- or ATR-FTIR.

We have focused on reproducing the experimental adsorption isotherm at 298 K and obtain new isotherms at other temperatures since the problem we want to solve is mainly focused on outgoing gas flows that need to be processed by adsorbent materials to capture CO_2, but water presence can make useless the adsorbent material since they use to be highly hydrophilic. A previous treatment of gas flow with kaolinite could be enough to ensure the dehydration of the current flow and thus efficiently reach the CO_2 capture process increasing the efficiency of the entire process.

7.2. Methodology

Accelrys Materials Studio modeling package [*Accelrys M.S.*, 2013] was used to obtain crystallographic structures and the adsorption isotherms in a wide interval of pressures and at different temperatures via GCMC method. The force field used to simulate kaolinite structure was CLAYFF, a general Force Field developed by Cygan et al. suitable for the simulation of hydrated aluminosilicates and their interfaces with aqueous solutions. In addition, and as in previous chapters, the TIP4P- 2005 model was used to represent the water-water and water-lattice interactions since it is considered probably the best description of water that can be achieved with a single Lennard-Jones (LJ) site and three charges. This Force field proposes a dummy site as a carrier of the negative charge located on the H-O-H bisector at a distance of 0.1546 A from O atom. The angle H-O-H corresponds to 104.52°, and the O-H distances are 0.9572Å. In order to describe the crossed interactions, the Lorentz and Berthelot rules were used.

The bulk structure of kaolinite used corresponds to a triclinic P1 space group with cell parameters a=5.149Å, b=8.934Å and c=7.384Å, cell angles α=91.93°, β=105.04° and γ=89.79° and interlayer distance of 2.05Å. The interlayer distance points out the presence of hydrogen bonds between the hydroxyl groups on the Al-terminated surface and bridging oxygen atoms on the Si-terminated surface. This fact makes the layers practically inseparable and confers kaolinite nonexpanding or non-swelling properties. The charges, that ensure the neutrality of the simulation box, and the non-bonded interaction parameters used in this study are listed in Table 7.1. The study is performed on the hydroxylated surface since previous studies determined this termination as the most favorable energetically. The 3D simulation box (see Figure 7.2) contains a total of 1088 atoms and it is constructed stacking two pairs of kaolinite (001) layers separated by a vacuum of 30Å (in z direction) to avoid interactions between both pairs of layers and also to improve the statistics. The simulation box dimensions were 20.60Å, 17.87 Å and 160 Å, respectively. These values correspond to a 4x2x2 supercell in both top and bottom layers, plus an intermediate space of 30Å used for locating inside the water reservoir that interacts with both hydroxylated layers. The kaolinite

layers was periodic in x and y dimensions but truncated in z. In order to avoid unphysical fields originated from arbitrary truncation in z direction the top layers were exactly the mirror image of the bottom ones. Finally, the long-range interactions were calculated by means of 3D Ewald method leaving an empty space of 100Å enough to prevent interactions in the z direction between top and bottom layers. The LJ and real space interactions were cut off at half of the length of the x side of the simulation cell.

Table 7.1. Non-bond parameters for the CLAYFF and TIP4P/2005 FF.

CLAYFF (kaolinite)				
species	*symbol*	*charge(e)*	D_0 *(kcal/mol)*	$R_0(Å)$
Hydroxyl hydrogen	ho	0.4250		
Hydroxyl oxygen	oh	-0.950	0.1554	3.5532
Bridging oxygen	ob	-1.050	0.1554	3.5532
Tetrahedral silicon	st	2.100	1.8405e-6	3.7064
Octahedral aluminum	ao	1.5750	1.3298e-6	4.7943
TIP4P/2005 (water)				
species	symbol	charge(e)	D_0 (kcal/mol)	$R_0(Å)$
Water hydrogen	h*	0.5564		
Water oxygen	o*	0.0000	0.1852	3.5457
Dummy	M	-1.113		

Figure 7.3 shows the top view of a single Al-terminated layer of kaolinite highlighting the unit cell area. Since the different adsorption amount of water can be understood with the help of sites of adsorption it is convenient to separate this area in six small ones, namely A-F, that correspond to the different sites of adsorption characterized by the total surface area and charge associated to each one. Thus, the surface areas are 8.38, 6.88, 7.88, 8.02, 6.98 and 7.90 Å² for A-F sites and the total charge associated to each site corresponds to 0.1, -1.2, -1.4, 1.1, 0.4 and 0.1 e⁻ for A, B, C, D, E and F sites, respectively.
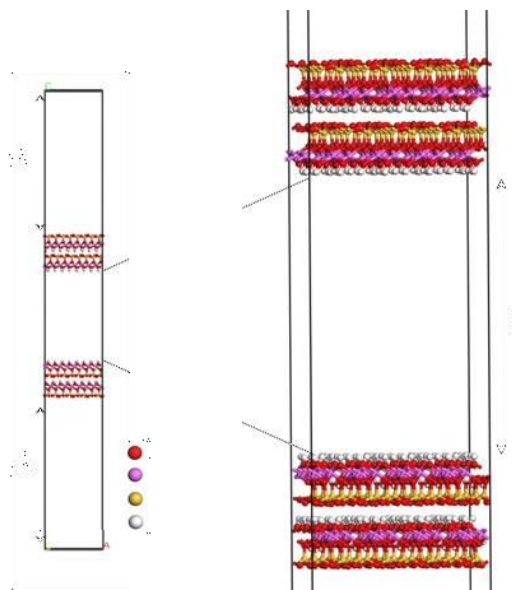
Figure 7.2. *Simulation cell used (left) and detail of the two kaolinite layers faced. The adsorption of water is restricted to the volume in between both pairs of layers.*
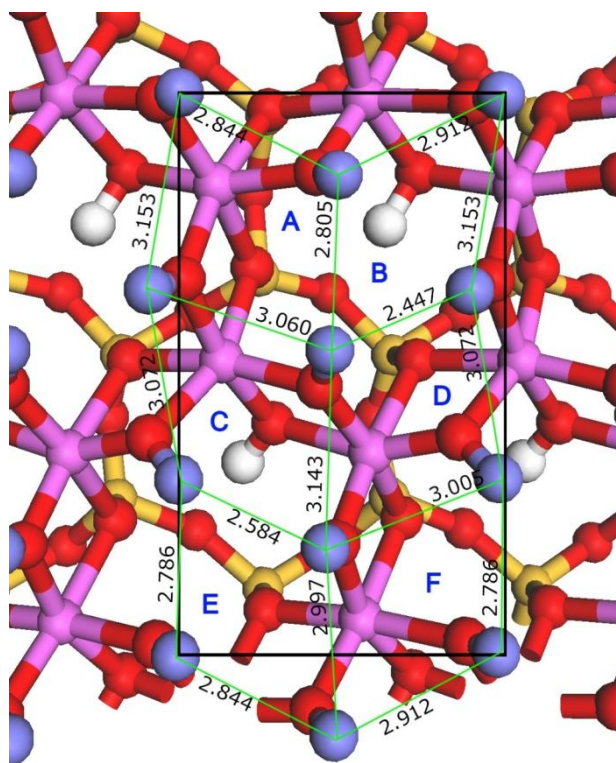
Figure 7.3. *Top view of a single layer of kaolinite surface. The black lines fence the unit cell and the different sites are labeled as A-F. Also the distances between outermost hydrogen atoms that belong to hydroxyl groups are indicated. Atoms color as labeled in Fig. 1 although the outermost hydrogen atoms are depicted in blue for convenience.*

The simulations were carried out employing the GCMC method. The acceptance rate for insertion and deletion steps was 0.01%, and the maximum size of the displacement steps was regulated to give an acceptance rate of 50%. The systems were firstly equilibrated during 5×10^7 MC steps. Hence, production stage was performed during 2×10^8 MC steps to obtain converged energy distributions, water content and density profiles. This procedure was repeated for a wide range of pressures and at different temperatures in order to get the adsorption isotherms.

7.3. Results and Discussion

From GCMC simulations we have obtained the loadings of water that were transformed conveniently into RH using vapor pressure of water at the temperatures explored through. Table 7.2 shows the saturation vapor pressures for water at the selected temperatures where the isotherm was simulated from Wagner equation (Eq. 3).

$$\ln\left(P_{vp} \big/ P_c \right) = (1 - t)^{-1} \left[at + bt^{1.5} + ct^3 + dt^6 \right]$$

$$(7.1)$$

with: $\quad t = 1 - \left(T \big/ T_c \right).$

Critical variables (i.e., Tc and Pc) are also listed in Table 7.2.

Table 7.2. *Saturation Vapor Pressure (P_{vp}) of Water from Wagner Equation.*

T(K)	P_{vp}(kPa)	Wagner constants		Critical values	
283.15	1.23	a	-7.7645	T_c (K)	647.3
298.15	3.17	b	1.4584	P_c (kPa)	22120
320.15	10.63	c	-2.7758		
360.15	62.53	d	-1.233		

Figs. 7.4 shows that the water content increases with increasing pressure and diminishes as temperature increases. These results are consistent with type II multilayer adsorption isotherms. Moreover, the quantity of adsorbed water increases continuously as pressure does, but with different slopes depending on the region of the pressures involved. Three zones are clearly noticeable: the first one at RH < 5% with a

low slope (i.e., 4.44×10^{-4}, 3.61×10^{-4} and 2.70×10^{-4} gH$_2$Ogkaolinite $^{-1}$%RH^{-1} for 283.15, 298.15 and 320.15K, respectively), the second one at 5% < RH < 15% with a higher slope (i.e., 2.05×10^{-3}, 2.61×10^{-3} and 3.48×10^{-3} gH$_2$Ogkaolinite $^{-1}$RH^{-1} for 283.15, 298.15 and 320.15K, respectively) and the last one at RH > 15% with a lower slope similar to that of the first region (i.e., 4.74×10^{-4}, 4.61×10^{-4} and 4.23×10^{-4} gH$_2$Ogkaolinite $^{-1}$%RH^{-1})
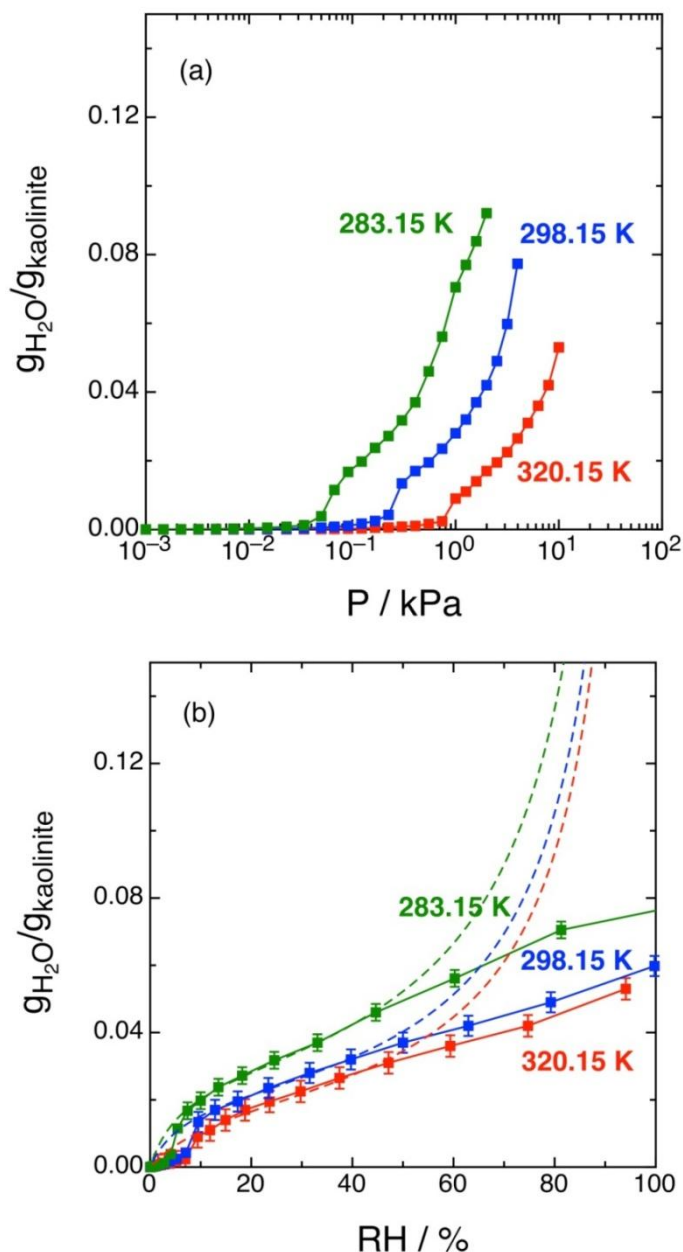
Figure 7.4. *Kaolinite water content at 10ºC (green), 25ºC (blue) and 47ºC (red) as a function of a) equilibrium pressure (kPa) and b) relative humidity, RH (%). The fitted BET isotherms (Eq. 4) are also showed with dashed lines.*

The results at 298.15 K were compared with experimental data in Figure 7.5. The experimental data were in agreement at RH values lower than 80%. However, at

higher values of RH the simulations underestimate the experimental results although the experimental errors associated to these values become important. Nevertheless, the range of interest for industry applications in outgoing flow gases is at RH values lower than 80%, so. In addition, the lack of experimental results in the interval 0 < RH < 10% makes impossible to confirm the shape observed in theoretical adsorption isotherms up to 10% of RH.
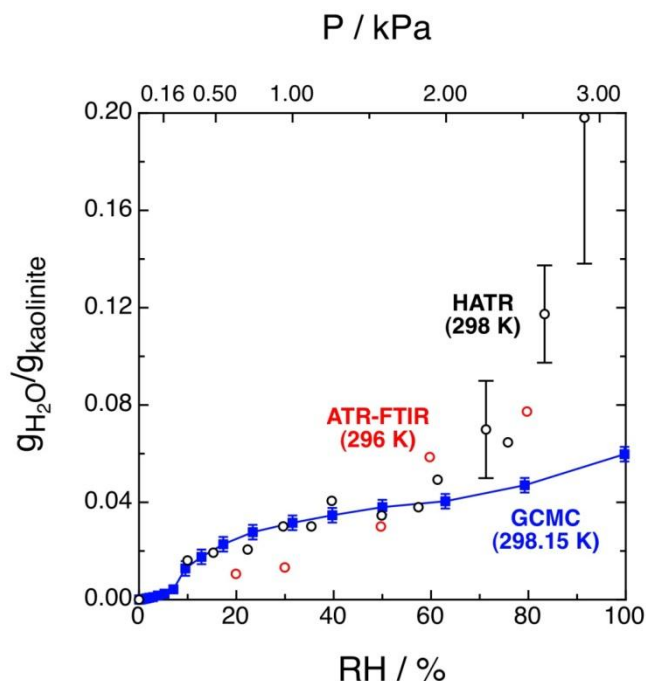
Figure 7.5. Kaolinite water content at 25ºC as a function of relative humidity (RH) or pressure (kPa) for GCMC simulations (blue) and experimental results at 23ºC and 25ºC, respectively.

In order to understand the shapes of adsorption isotherms we have studied the changes in water density of adsorption over kaolinite surface and in the isosteric heat of adsorption distributions at all the pressures studied (see Figure 7.6) at 298.15K. The first zone until 5% of RH (i.e., P=0.17 kPa) corresponds to a smooth increase of adsorption that comes from the adsorption of water molecules on site D as corroborated by the single peaked isosteric heat distribution centered at 12 kcal/mol in this range of pressure. As pressure is increased (i.e., from 5% < RH < 15%) the slope increases abruptly. This fact clearly indicates that within this range, site D is already fully occupied and that water molecules start to adsorb on site C. This new site of adsorption produces a double peak in the isosteric heat distribution with a new peak centered at 18 kcal/mol. At RH > 15% the adsorption isotherm increases again smoothly with RH. At this point, adsorption of water molecules starts at site A but regarding isosteric heat distributions, only a broadening of the peak centered at 18 kcal mol-1 is observed along with a nearly embedding of the peak centered at 12 kcal mol-1 due to adsorption on site D. At higher values of pressure the adsorption of water molecules reaches new available sites: first B sites and then F sites. The position of both

peaks is maintained, although the distributions become a bit narrower when the temperature is increased since the amount of adsorbed molecules is reduced
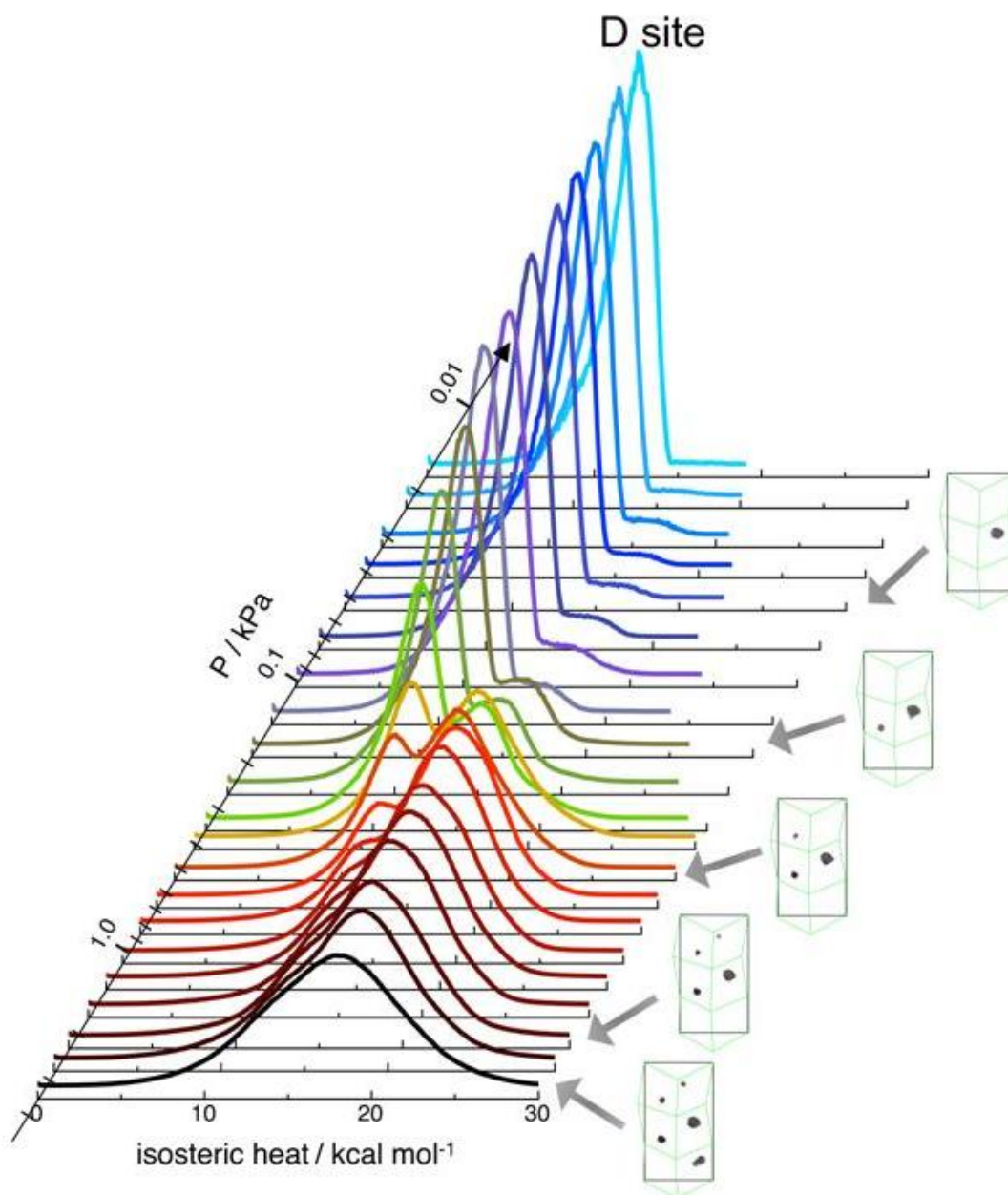
Figure 7.6. *Isosteric heat distributions and adsorption location density for water adsorption on kaolinite surface at 25ºC. The adsorption location densities corresponds to the following pressure (RH) values: a) 0.050 kPa (1.6%), b) 0.166 kPa (5.2%), c) 0.549 kPa (17.3%), d) 1.995 kPa (62.9%) and e) 3.162 kPa (99.7%).*

The sequence obtained for water adsorption on kaolinite (i.e., D, C, A, B, F) as a function of pressure can be also understood from the analysis of the accessible area per site and also from the charge located on each site of adsorption. At low pressures water molecules only adsorb on D site that presents an area of 8.02 A2 and a total charge of

1.05e. The other site with high area, site A (i.e., 8.38 A2), does not present adsorption because the total charge on it is 0.1e, a very low value that reduces drastically the coulomb term and avoids any adsorption. As pressure increases (at P 0.17 kPa, RH 5%) the adsorption starts on C site.

This site presents an effective area of 7.88 A² very close to the value of F site (i.e., 7.90 A2) but once again the first one is preferred for adsorption over the last one where no adsorption is observed at these pressures. As in the previous case, the coulombic term is decisive again; the C site has a net charge of -1.4e whereas the F site has the same value of A site (i.e., 0.1e). Obviously, the net charge on D and C sites has opposite sign, this fact indicates that adsorption of water molecules on D site comes from the interaction with negative dummy position on modeled water molecule and that adsorption on C site comes from the interaction with positive hydrogen atoms of water model. At P > 0.5 kPa (RH 16%) adsorption on A site starts and at P 1.5 kPa (47%) the adsorption on B site becomes also evident. At this point, once C and D sites are fully occupied the increasing pressure allows the occupation of other zones, for example A site is occupied before B site, that is, the available site that presents the highest area is occupied before the one that presents the lowest effective area (i.e., 8.38 and 6.88 A2 for A and B site, respectively). Such a reduced area for B site dilutes the high value of net charge on it (i.e., -1.2e) and adsorption on this site is only available when A site becomes fully occupied. The next location in the sequence is the F site that adsorbs water molecules at P 3.162 kPa (100%). In this case, the available area is 7.90 A2, a value higher than 6.98 A2 corresponding to site F. In this case, the area is the main contribution to adsorption since the net charge on both sites is really low (i.e., 0.4e and 0.1e for E and F sites, respectively).

Table 7.3. *BET adsorption model fitting for water over kaolinite as a function of temperature*

T (K)	c	V_m (cm³) $\times 10^2$	ML water content $\times 10^2$ $g_{H_2O} / g_{kaolinite}$	%RH at ML coverage	
273.15	17.21	2.76	2.76	19.3	*This work*
298.15	15.93	2.14	2.13	19.9	*This work*
298	16		2	20	Exp.
320.15	8.81	1.92	1.90	24.8	*This work*

Finally, following the idea of Hatch et al., we have fitted the adsorption isotherms to a Brunauer Emmett and Teller (BET) adsorption model. The fit of the GCMC isotherms obtained was performed at each temperature in the range 0.08 P/Pvp

0.45 obtaining the BET parameters reported in Table 7.3 with a good agreement with experimental values at 298 K. The results confirm a type II BET.

CHABAZITE

Effect of cations in chabazites

We have evaluated the adsorption in CHA type zeolites with different alkali cations exchange by molecular simulations in order to improve the CO_2/N_2 at a swing adsorption process.

Contrasting with the behavior in faujasite zeolites type, the Ca-CHA zeolite did not present the maximum adsorption capacity at a minimum Si/Al ratio. Instead, this maximum appeared at an intermediate Si/Al ratio. This unexpected behavior offers the possibility of performing a deep study of the behavior of this type of zeolites when other cations are added instead of calcium in order to use the best conditions for separation.

It is well known that CO_2 adsorption capacity and selectivity from a fue gas is strongly influenced by the composition and structural features of the adsorbents. Although there is a good amount of work on new porous structures like MOF's and ZIF's, it seems reasonable to evaluate other zeolite structures that could exhibit high selectivities at low partial pressures. Adsorption separation process using zeolites as adsorbents are still of great importance due their highly selective, energy efficient operation and high chemical stability at a wide range of temperature. A clear advantage of exploring zeolites is that the required pore sizes, densities, crush strengths, electrostatic interactions, ease of synthesis, etc. of them is already established.

In order to enhance the separation and purification processes, a good understanding of adsorption process is needed. Therefore, one of the key factors for improving the selectivity is to understand the interaction of the electric quadrupole moment of CO_2 with the electrostatic field gradient created by the extra-framework cations.

Hence, the goal was focused on evaluate the adsorption effect in CHA type zeolites with different alkali cations exchange using molecular modeling tools.

Among other adsorbents, chabazite zeolite is a promising but often ignored option: chabazite is a tectosilicate mineral of the zeolite group, closely related to gmelinite, with formula $(Ca,Na_2, K_2,Mg)Al_2Si_4O_{12} \cdot 6H_2O$. It was named chabasie in 1792 by Bosc d'Antic and later changed to the current spelling.

The published literature dealing with ion-exchange and its impact on adsorption properties of chabazites has grown in the past years. Previous studies

showed that cation siting and distribution in the framework are critical structural parameters for generating adsorption sites and enhancing the strength of the adsorption interaction (the thermal stability is largely dependent on the nature of the exchangeable cations). Further studies have shown that the Si/Al ratio controls the charge-balancing cation quantity and siting, which in turn controls the adsorption characteristics of the zeolite [Singh et. al., 2005].

Chabazite can be obtained as the naturally occurring mineral or synthesized. Natural chabazites, however are inherently variable in chemical composition [Ridha & Webley, 2009] and therefore in their adsorption capacities. Now, synthesis of chabazite with different Si/Al ratios is well known: Gaffney and Coe [1991] have reported synthesis of chabazite with Si/Al ratio in range 1.8 to 2.3 and have demonstrated that Ca and Sr exchanged chabazites are better for separation of N_2 and Ar.

Chabazites structures (raw CHA and CaCHA)

The structure of a zeolite chabazite in a typical unit cell is shown in Figure 7.7. (seen from different viewpoints).

Materials of this structural group (CHA) are crystalline microporous structures with uniformly sized pores of molecular dimensions and cavities of 8-ring windows. Exchangeable cations can be located within the cavities to balance the negative charge introduced into the framework by the aluminum atoms. Depending on their size and charge, the cations can effectively block the pore openings such that certain molecules are excluded in an adsorption process. However, it should be noted that the cation can also decrease the pore volume [Ridha & Webley, 2010].

For simplicity, a simulated synthetic material only includes Si and O. Therefore the unit cell in this case only includes 12 Silicon atoms (in yellow) and 24 Oxygen atoms (in red), in order to represent a complete ring and four quarters of rings.
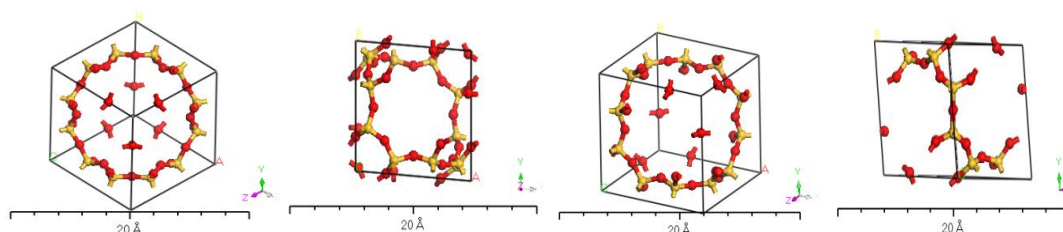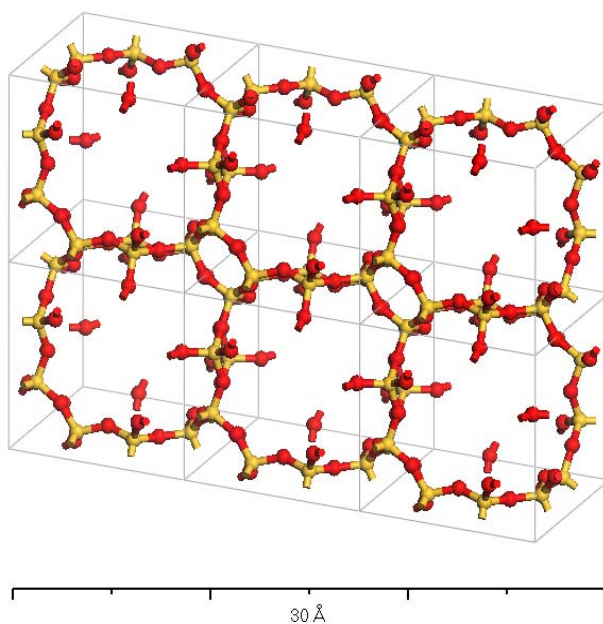
Figure 7.7. Chabazite structure framework

Carbon Dioxide   Nitrogen
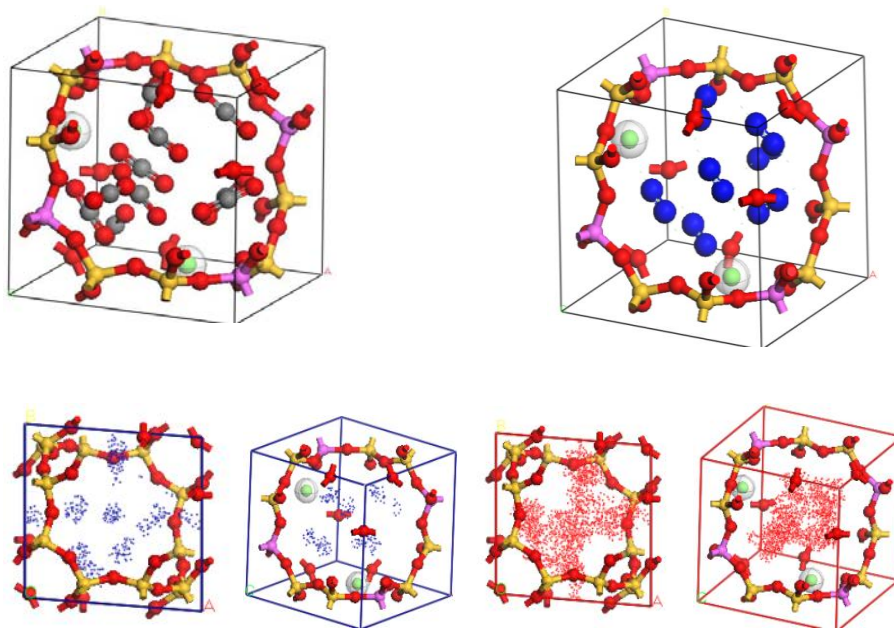
Figure 7.8. Probability cloud of nitrogen and carbon dioxide adsorption in raw chabazite and CaCHA.

Now, in a qualitatively way, we present the most likely locations for adsorption of different substances (at STP conditions). The probability cloud of adsorption (see Figure 7.8) shows the preference for nitrogen (blue) and carbon dioxide (red) in a raw

chabazite and a Ca-CHA material. It can be seen that the nitrogen adsorb in groups, tending to be located close to the oxygen atoms in the chabazite ring, while for the carbon dioxide we see a more compact cloud, with special preference for the center of the unit cell.

In the following sections we will describe preliminary results of adsorption isotherms for CO_2 and N_2 in raw chabazite and CaCHA.

CO2 adsorption

The first simulations in this subject were performed for adsorption of CO_2 in a raw chabazite (Figure 7.8). Here, it was possible to make a validation of the TraPPE force field, which showed good results for this type of interactions.
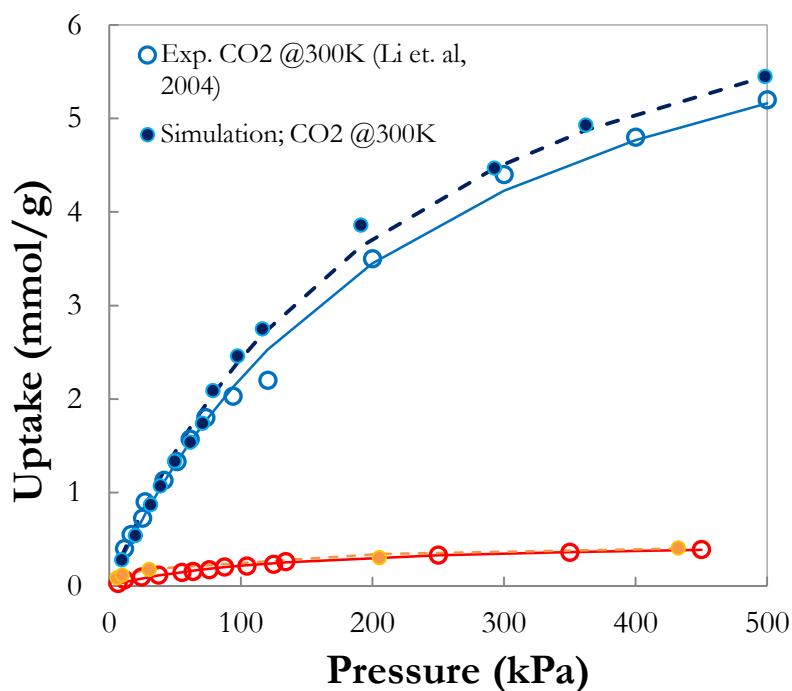
Figure 7.9. *Adsorption isotherm of CO₂ in CHA and Adsorption isotherms of CO2 in CaCHA materials with different number of exchanged-ions.*

And from these results, a purely computational evaluation was made for different chabazites, including different amounts of calcium (different Si/Al ratios in the unit cell). The adsorption isotherms obtained are shown in Figure 7.10. It can be seen that as Ca^{+2} ions were included, the amount of CO_2 adsorbed increased considerably, while a rise in the temperature decreases the adsorption (as logical).

In Figure 7.11 we present the main results of the adsorption isotherms. The experimental data are shown as points, the dashed lines stand for T=296K and the solid lines are for T=318K.
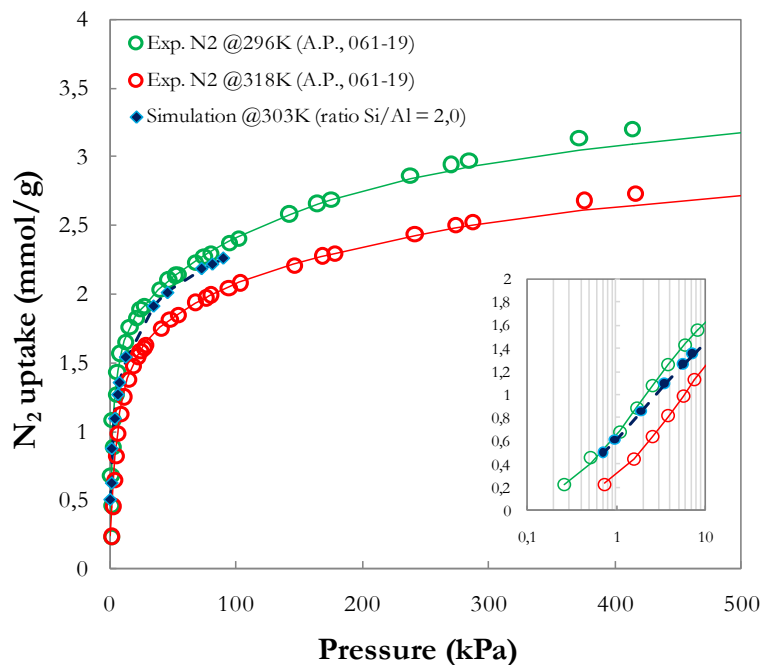
Figure 7.10. *Adsorption isotherms of nitrogen in different structures of CaCHA, according to the amount of ions exchanged (Ca^{+2} added)*
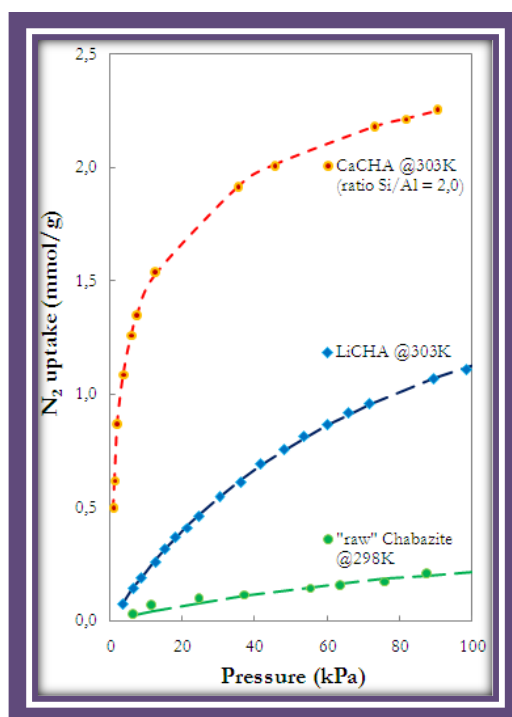
Figure 7.11. *Comparison of the amount adsorbed in different cation-exchanged chabazites*

7.4. Outlook

GCMC simulations of water adsorption on kaolinite surface, as well as carbon dioxide and nitrogen over chabazite, lead to a great agreement with experimental data (although for higher values of RH the simulated water results underestimate the experimental ones). The shape of the adsorption isotherms is explained in basis of isosteric heats and available surface per site of adsorption.

The adsorption isotherms obtained for kaolinite makes it a promising material for eliminating water from these currents in order to avoid poisoning of adsorbent materials used for CO_2 capture and separation. These results confirm that this kind of material can be used as a cheap treatment for drying the outgoing gases, so avoiding adsorbent poisoning and increasing the efficiency of CO_2 separation.

8

CONCLUSIONS AND FUTURE WORK

- Given the vast amount of work done in recent years regarding adsorbent for CO_2 capture through pre and post-combustion processes, in the chapter 3 we provide an overview of these recent literature results concerning structured adsorbents, including reference and advanced zeolites, carbon based materials, microporous polymers, amine-modified sorbents and Metal-Organic Frameworks (MOFs), among others.

- There are numerous different structural types of zeolites, MOFs and molecular sieves. Considering all possible cation, metals, linkers, etc. variations results in an unmanageable number of potential candidate adsorbents for any particular separation. Thus, efficient and effective methods for screening adsorbents are necessary. Conditions of the feed to be separated, the purity and value of the desired product, competing processes and other important constraints will vary widely across the many gas separations of interest.

- Methods for evaluating adsorbent effectiveness for a given separation vary from the measurement of a few isotherms to execution of detailed process models. Isotherms alone would confirm an adsorbent's ability to affect steric separations, but would not be sufficient to select the best adsorbent for either kinetic or equilibrium separations. Detailed process modeling requires accurate and extensive adsorbent characteristic input data. Obtaining such data for a large number of candidate adsorbents can be prohibitive. As a result, simple methods are required for ranking adsorbents for a particular separation by relating adsorbent characteristics to process performance.

- Although MOFs may provide elegant solutions for CO_2 sequestration and storage, they are not particularly suitable for post-combustion gas treatment (only the M-MOF-74 family shows good results for this type of application). Nevertheless, a continuous effort is being deployed to circumvent such drawbacks. The strategies being used include surface modification to enhance the interactions with CO_2, thus increasing the adsorption capacity at low pressure.

- Taking into account that an ideal adsorbent for a post-combustion stream should exhibit a high selectivity for CO_2 over the other flue gas components, high adsorption capacities under the operating conditions and minimal energy penalty for regeneration, results from chapter 4 show that among the 11 studied adsorbents, Mg-MOF-74 shows a great potential to become a material to be used for this separation under the TSA operating conditions, with even better performance than the most traditionally used zeolite 13X (NaX). This is a step forward in moving Mg-MOF-74 to industrial applications in an advantageous manner versus current used materials.

- On the basis of this advanced analysis of the most important studies about the post-combustion CO_2 capture, it appears that the basicity and size of pores of zeolites, as

well as the strength of electric field caused by the presence of exchangeable cations in their cavities are the essential factors for the CO_2 adsorption on zeolites. Thus, the consideration of all these factors seems to be necessary for the best choice of an appropriate material for CO_2 adsorption. Hence, the optimization of all these factors and experimental and simulating conditions may increase significantly the adsorption capacities and thus develops efficient technologies to capture the industrial emissions of CO_2.

- Material scientists and process engineers working together are likely to be more productive than either working alone. Cost and performance are always factors. Finding the match between a natural zeolite and a gas separation is a difficult challenge. Meeting this challenge requires a change in the way gas separations have been approached by all of us working in the field of natural zeolites.

- Although CO_2, N_2, and H_2O account for greater than 95% of the flue gas mixture, the other minor components (mostly O_2, SOx, NOx, and CO) present cannot be ignored in assessing zeolites and Metal-Organic Frameworks for CO_2 capture. Significantly, the effects of these trace gases on the CO_2/N_2 separation performance of MOFs is so far virtually unexplored. Future research must also address this issue.

- Regarding the CO_2 capture in MOF CuBTC, results reveal that a very little amount of uncoordinated water molecules induce a significant improvement on capture in due to the enhanced binding energy between CO_2 with the introduction of small amounts of water, while zeolite 13X became useless with less than 1% of water. As a consequence, zeolite 13X is not suitable for the adsorption of CO_2 without a previous proper dehumidification process, because just a 0.01% of moisture in the adsorbent is able to significantly reduce the adsorption capacity of CO_2.

- In addition to water, the effects of other impurities on CO_2 capture were also analyzed, including O_2 and SO_2. By comparing CO_2/N_2 selectivity for different $CO_2/N_2/SO_2$ mixtures, it is found that even with a concentration of SO_2 in the flue gas as high as 2000ppm, the CO_2/N_2 selectivity in the flue gas mixtures remains essentially unaffected; there was only a slightly lower adsorption, attributed to the decrease of CO_2 adsorption with the introduction of SO_2 in flue gas (sites competition).

Future work

The molecular simulation techniques used in this Thesis were demonstrated to be versatile tools for studying different parts and features of materials for capture and

separation. As we will see, a clear example of this versatility is demonstrated by the study presented in the appendix of this work.

Further investigation on the scale-up of the Metal-Organic Frameworks, the functionalization of mesoporous silica and other porous matrices will be necessary for the implementation of the process in a larger scale. Preliminary results have shown that … Hence, it would be useful to study the optimization of the processes at different conditions in order to reduce the process costs.

Bibliography

Abascal, J. L. F., and C. Vega. A general purpose model for the condensed phases of water: TIP4P/2005. *The Journal of Chemical Physics* 123, 23 (2005): 234505.

Accelrys Materials Studio. *Accelrys Materials Studio.*

Ackley, Mark W, Salil U Rege, and Himanshu Saxena. Application of natural zeolites in the purification and separation of gases. *Microporous and Mesoporous Materials* 61, 1-3 (2003): 25-42.

Adamson, A. W.; Gast, A. P., Physical chemistry of surfaces. 6th ed.; Wiley: New York, 1997; p 764.

Alaerts, Luc, Etienne Séguin, Hilde Poelman, Frédéric Thibault-Starzyk, Pierre A. Jacobs, and Dirk E. De Vos. Probing the Lewis Acidity and Catalytic Activity of the Metal-Organic Framework [Cu3(btc)2] (BTC=Benzene-1,3,5-tricarboxylate). *Chem. Eur. J.* 12, 28 (2006): 7353-7363.

Allen, M. P. and Tildesley, D. J. Computer simulation of liquids. (Clarendon, 1989).

Alvarez, Diego, and J. Carlos Abanades. Pore-Size and Shape Effects on the Recarbonation Performance of Calcium Oxide Submitted to Repeated Calcination/Recarbonation Cycles. *Energy Fuels* 19, 1 (2005): 270-278.

Allan, Phoebe K., Bo Xiao, Simon J. Teat, Jason W. Knight, and Russell E. Morris. In Situ Single-Crystal Diffraction Studies of the Structural Transition of Metal-Organic Framework Copper 5-Sulfoisophthalate, Cu-SIP-3. *J. Am. Chem. Soc.* 132, 10 (2010): 3605-3611.

Ammendola, Paola, Federica Raganati, and Riccardo Chirone. Effect of operating conditions on the CO2 recovery from a fine activated carbon by means of TSA in a fluidized bed assisted by acoustic fields. *Fuel Processing Technology* 134 (2015): 494-501.

An, Jihyun, and Nathaniel L. Rosi. Tuning MOF CO2 Adsorption Properties via Cation Exchange. *J. Am. Chem. Soc.* 132, 16 (2010): 5578-5579.

Angell, C. L., and M. V. Howell. Infrared spectroscopic investigations of zeolites and adsorbed molecules. Part V. Carbon dioxide. *Can. J. Chem.* 47, 20 (1969): 3831-3836.

Aprea, Paolo, Domenico Caputo, Nicola Gargiulo, Fabio Iucolano, and Francesco Pepe. Modeling Carbon Dioxide Adsorption on Microporous Substrates: Comparison between CuBTC Metal-Organic Framework and 13X Zeolitic Molecular Sieve. *J. Chem. Eng. Data* 55, 9 (2010): 3655-3661.

Arstad, Bjørnar, Helmer Fjellvåg, Kjell Ove Kongshaug, Ole Swang, and Richard Blom. Amine functionalised metal organic frameworks (MOFs) as adsorbents for carbon dioxide. *Adsorption* 14, 6 (2008): 755-762.

Atkins, P. W., Physical chemistry. 5 ed.; Oxford University Press: Oxford, 1998.

Attard, G.; Barnes, C., Surfaces. Oxford University press: Oxford, 2008; p 96.

Aukett, P. N., N. Quirke, S. Riddiford, and S. R. Tennison. Methane adsorption on microporous carbons: A comparison of experiment, theory, and simulation. *Carbon* 30, 6 (1992): 913-924.

Babarao, R., and J. W. Jiang. Cation Characterization and CO2 Capture in Li+-Exchanged Metal-Organic Frameworks: From First-Principles Modeling to Molecular Simulation. *Ind. Eng. Chem. Res.* 50, 1 (2011): 62-68.

Babarao, Ravichandar, Jianwen Jiang, and Stanley I. Sandler. Molecular Simulations for Adsorptive Separation of CO2/CH4 Mixture in Metal-Exposed, Catenated, and Charged Metal-Organic Frameworks. *Langmuir* 25, 9 (2009): 5239-5247.

Babarao, Ravichandar, Sheng Dai, and De-en Jiang. Effect of Pore Topology and Accessibility on Gas Adsorption Capacity in Zeolitic-Imidazolate Frameworks: Bringing Molecular Simulation Close to Experiment. *J. Phys. Chem. C* 115, 16 (2011): 8126-8135.

Babarao, Ravichandar, and Jianwen Jiang. Molecular Screening of Metal-Organic Frameworks for CO2 Storage. *Langmuir* 24, 12 (2008): 6270-6278.

Babarao, Ravichandar, and Jianwen Jiang. Unprecedentedly High Selective Adsorption of Gas Mixtures in rho Zeolite-like Metal-Organic Framework: A Molecular Simulation Study. *J. Am. Chem. Soc.* 131, 32 (2009): 11417-11425.

Bae, Youn-Sang, Brad G. Hauser, Omar K. Farha, Joseph T. Hupp, and Randall Q. Snurr. Enhancement of CO2/CH4 selectivity in metal-organic frameworks containing lithium cations. *Microporous and Mesoporous Materials* 141, 1-3 (2011): 231-235.

Bae, Youn-Sang, David Dubbeldam, Andrew Nelson, Krista S. Walton, Joseph T. Hupp, and Randall Q. Snurr. Strategies for Characterization of Large-Pore Metal-Organic Frameworks by Combined Experimental and Computational Methods. *Chem. Mater.* 21, 20 (2009): 4768-4777.

Banerjee, Rahul, Hiroyasu Furukawa, David Britt, Carolyn Knobler, Michael O'Keeffe, and Omar M. Yaghi. Control of Pore Size and Functionality in Isoreticular Zeolitic Imidazolate Frameworks and their Carbon Dioxide Selective Capture Properties. *J. Am. Chem. Soc.* 131, 11 (2009): 3875-3877.

Bastin, Laurent, Patrick S. Bárcia, Eric J. Hurtado, José A. C. Silva, Alírio E. Rodrigues, and Banglin Chen. A Microporous Metal-Organic Framework for Separation of CO2/N2 and CO2/CH4 by Fixed-Bed Adsorption. *J. Phys. Chem. C* 112, 5 (2008): 1575-1581.

Belmabkhout, Youssef, Rodrigo Serna-Guerrero, and Abdelhamid Sayari. Amine-bearing mesoporous silica for CO2 removal from dry and humid air. *Chemical Engineering Science* 65, 11 (2010): 3695-3698.

Berger, Adam Hughmanick, and Abhoyjit S. Bhown. Comparing physisorption and chemisorption solid sorbents for use separating CO2 from flue gas using temperature swing adsorption. *Energy Procedia* 4 (2011): 562-567.

Bezerra, Diôgo P., Ronan S. Oliveira, Rodrigo S. Vieira, Célio L. Cavalcante Jr, and Diana C. S. Azevedo. Adsorption of CO2 on nitrogen-enriched activated carbon and zeolite 13X. *Adsorption* 17, 1 (2011): 235-246.

Bonenfant, Danielle, Mourad Kharoune, Patrick Niquette, Murielle Mimeault, and Robert Hausler. Advances in principal factors influencing carbon dioxide adsorption on zeolites. *Sci. Technol. Adv. Mater.* 9, 1 (2008): 013007.

Botas, Juan A., Guillermo Calleja, Manuel Sánchez-Sánchez, and M. Gisela Orcajo. Cobalt Doping of the MOF-5 Framework and Its Effect on Gas-Adsorption Properties. *Langmuir* 26, 8 (2010): 5300-5303.

Both, K., D. W. Henderson, and D. R. Turner. Asbestos and erionite fibres can induce mutations in human lymphocytes that result in loss of heterozygosity. *Int. J. Cancer* 59, 4 (1994): 538-542.

Bourrelly, Sandrine, Philip L. Llewellyn, Christian Serre, Franck Millange, Thierry Loiseau, and Gérard Férey. Different Adsorption Behaviors of Methane and Carbon Dioxide in the Isotypic Nanoporous Metal Terephthalates MIL-53 and MIL-47. *J. Am. Chem. Soc.* 127, 39 (2005): 13519-13521.

Boutin, Anne, François-Xavier Coudert, Marie-Anne Springuel-Huet, Alexander V. Neimark, Gérard Férey, and Alain H. Fuchs. The Behavior of Flexible MIL-53(Al) upon CH4 and CO2 Adsorption. *J. Phys. Chem. C* 114, 50 (2010): 22237-22244.

Brandani, Federico, and Douglas M. Ruthven. The Effect of Water on the Adsorption of CO2 and C3H8 on Type X Zeolites. *Ind. Eng. Chem. Res.* 43, 26 (2004): 8339-8344.

Britt, David, David Tranchemontagne, and Omar M. Yaghi. Metal-organic frameworks with high capacity and selectivity for harmful gases. *PNAS* 105, 33 (2008): 11623-11627.

Britt, David, Hiroyasu Furukawa, Bo Wang, T. Grant Glover, and Omar M. Yaghi. Highly efficient separation of carbon dioxide by a metal-organic framework replete with open metal sites. *PNAS* 106, 49 (2009): 20637-20640.

Brunauer, S.; Deming, L. S.; Deming, W. S.; Teller, E., On a Theory of the van der Waals Adsorption of Gases. J. Am. Chem. Soc. 1940, 62, 1723 - 32.

Brunauer, Stephen, P. H. Emmett, and Edward Teller. Adsorption of Gases in Multimolecular Layers. *J. Am. Chem. Soc.* 60, 2 (1938): 309-319.

Builes S., Lórez-Aranguren, P.; Fraile, J.; Vega, L. F.; Domingo, C. Alkylsilane-functionalized microporous and mesoporous materials: molecular simulation and experimental analysis of gas adsorption. J. Phys. Chem. C. 2012, 116(18): 10150-10161.

Bukowski, R.; Szalewicz, K.; Groenenboom, G. C.; van der Avoird, A. Science 2007, 315, 1249.

Caskey, Stephen R., Antek G. Wong-Foy, and Adam J. Matzger. Dramatic Tuning of Carbon Dioxide Uptake via Metal Substitution in a Coordination Polymer with Cylindrical Pores. *J. Am. Chem. Soc.* 130, 33 (2008): 10870-10871.

Castillo, Juan Manuel, Thijs J. H. Vlugt, and Sofía Calero. Understanding Water Adsorption in CuBTC Metal-Organic Frameworks. *J. Phys. Chem. C* 112, 41 (2008): 15934-15939.

Cavenati, Simone, Carlos A. Grande, and Alírio E. Rodrigues. Adsorption Equilibrium of Methane, Carbon Dioxide, and Nitrogen on Zeolite 13X at High Pressures. *J. Chem. Eng. Data* 49, 4 (2004): 1095-1101.

Cavenati, Simone, Carlos A. Grande, and Alírio E. Rodrigues. Separation of mixtures by layered pressure swing adsorption for upgrade of natural gas. *Chemical Engineering Science* 61, 12 (2006): 3893-3906.

Cinke, Martin, Jing Li, Charles W. Bauschlicher Jr., Alessandra Ricca, and M. Meyyappan. CO2 adsorption in single-walled carbon nanotubes. *Chemical Physics Letters* 376, 5-6 (2003): 761-766.

Claquin, T., M. Schulz, and Y. J. Balkanski. Modeling the mineralogy of atmospheric dust sources. *J. Geophys. Res.* 104, D18 (1999): 22243-22256.

Clausse, Marc, Jérôme Merel, and Francis Meunier. Numerical parametric study on CO2 capture by indirect thermal swing adsorption. *International Journal of Greenhouse Gas Control* 5, 5 (2011): 1206-1213.

Cooper, Andrew I. Conjugated Microporous Polymers. *Adv. Mater.* 21, 12 (2009): 1291-1295.

Coudert, François-Xavier, Anne Boutin, Marie Jeffroy, Caroline Mellot-Draznieks, and Alain H. Fuchs. Thermodynamic Methods and Models to Study Flexible Metal-Organic Frameworks. *ChemPhysChem* 12, 2 (2011): 247-258.

Coughlan, Brendan, and Seán Kilmartin. Zeolites X, and Y. A enriched with trivalent cations: sorption of carbon dioxide and ammonia. Part 1. Isotherms and affinities. *J. Chem. Soc., Faraday Trans. 1* 71, 0 (1975): 1809-1817.

Croteau, T., A. K. Bertram, and G. N. Patey. Adsorption and Structure of Water on Kaolinite Surfaces: Possible Insight into Ice Nucleation from Grand Canonical Monte Carlo Calculations. *J. Phys. Chem. A* 112, 43 (2008): 10708-10712.

Croteau, T., A. K. Bertram, and G. N. Patey. Simulation of Water Adsorption on Kaolinite under Atmospheric Conditions. *J. Phys. Chem. A* 113, 27 (2009): 7826-7833.

Croteau, T., A. K. Bertram, and G. N. Patey. Water Adsorption on Kaolinite Surfaces Containing Trenches. *J. Phys. Chem. A* 114, 5 (2010): 2171-2178.

Cygan, Randall T., Jian-Jie Liang, and Andrey G. Kalinichev. Molecular Models of Hydroxide, Oxyhydroxide, and Clay Phases and the Development of a General Force Field. *J. Phys. Chem. B* 108, 4 (2004): 1255-1266.

Challa, Sivakumar R., David S. Sholl, and J. Karl Johnson. Adsorption and separation of hydrogen isotopes in carbon nanotubes: Multicomponent grand canonical Monte Carlo simulations. *The Journal of Chemical Physics* 116, 2 (2002): 814-824.

Chen, Y. F., J. Y. Lee, R. Babarao, J. Li, and J. W. Jiang. A Highly Hydrophobic Metal-Organic Framework Zn(BDC)(TED)0.5 for Adsorption and Separation of CH3OH/H2O and CO2/CH4: An Integrated Experimental and Simulation Study. *J. Phys. Chem. C* 114, 14 (2010): 6602-6609.

Chen, Y. F., R. Babarao, S. I. Sandler, and J. W. Jiang. Metal-Organic Framework MIL-101 for Adsorption and Effect of Terminal Water Molecules: From Quantum Mechanics to Molecular Simulation. *Langmuir* 26, 11 (2010): 8743-8750.

Cheon, Young Eun, Jungeun Park, and Myunghyun Paik Suh. Selective gas adsorption in a magnesium-based metal-organic framework. *Chem. Commun.*, 36 (2009): 5436-5438.

Choi, Sunho, Jeffrey, H. Drese, and Christopher, W. Jones. Adsorbent Materials for Carbon Dioxide Capture from Large Anthropogenic Point Sources. *ChemSusChem* 2, 9 (2009): 796-854.

Choi, Yoon Jeong, Jung Hoon Choi, Kyung Min Choi, and Jeung Ku Kang. Covalent organic frameworks for extremely high reversible CO2 uptake capacity: a theoretical approach. *J. Mater. Chem.* 21, 4 (2011): 1073-1078.

Chui, Stephen S.-Y., Samuel M.-F. Lo, Jonathan P. H. Charmant, A. Guy Orpen, and Ian D. Williams. A Chemically Functionalizable Nanoporous Material [Cu3(TMA)2(H2O)3]n. *Science* 283, 5405 (1999): 1148-1150.

Chun, Hyungphil, and Jinwoo Seo. Discrimination of Small Gas Molecules through Adsorption: Reverse Selectivity for Hydrogen in a Flexible Metal-Organic Framework. *Inorg. Chem.* 48, 21 (2009): 9980-9982.

D'Alessandro, Deanna, M., Berend Smit, and Jeffrey, R. Long. Carbon Dioxide Capture: Prospects for New Materials. *Angewandte Chemie International Edition* 49, 35 (2010): 6058-6082.

Dabrowski, A., Adsorption - from theory to practice. Adv. Colloid Interface Sci. 2001, 93, (1-3), 135-224.

DeCoste, Jared B., Gregory W. Peterson, Bryan J. Schindler, Kato L. Killops, Matthew A. Browe, and John J. Mahle. The effect of water adsorption on the structure of the carboxylate containing metal-organic frameworks CuBTC, Mg-MOF-74, and UiO-66. *J. Mater. Chem. A* 1, 38 (2013): 11922-11932.

DeCoste, Jared B., and Gregory W. Peterson. Metal-Organic Frameworks for Air Purification of Toxic Chemicals. *Chem. Rev.* 114, 11 (2014): 5695-5727.

Delgado, José A., V. I. Águeda, M. A. Uguina, J. L. Sotelo, P. Brea, and Carlos A. Grande. Adsorption and Diffusion of H2, CO, CH4, and CO2 in BPL Activated Carbon and 13X Zeolite: Evaluation of Performance in Pressure Swing Adsorption Hydrogen Purification by Simulation. *Ind. Eng. Chem. Res.* 53, 40 (2014): 15414-15426.

Demessence, Aude, Deanna M. D'Alessandro, Maw Lin Foo, and Jeffrey R. Long. Strong CO2 Binding in a Water-Stable, Triazolate-Bridged Metal-Organic Framework Functionalized with Ethylenediamine. *J. Am. Chem. Soc.* 131, 25 (2009): 8784-8786.

Deng, Wei-Qiao, Xin Xu, and William A. Goddard. New Alkali Doped Pillared Carbon Materials Designed to Achieve Practical Reversible Hydrogen Storage for Transportation. *Phys. Rev. Lett.* 92, 16 (2004): 166103.

De Pablo, J. J.; Laso, M.; Suter, U. W. Journal of Chemical Physics 1992, 96, 6157.

Dickey, Allison N., A. Özgür Yazaydin, Richard R. Willis, and Randall Q. Snurr. Screening CO2/N2 selectivity in metal-organic frameworks using Monte Carlo simulations and ideal adsorbed solution theory. *Can. J. Chem. Eng.* 90, 4 (2012): 825-832.

Dietzel, Pascal D. C., Vasileios Besikiotis, and Richard Blom. Application of metal-organic frameworks with coordinatively unsaturated metal sites in storage and separation of methane and carbon dioxide. *J. Mater. Chem.* 19, 39 (2009): 7362-7370.

Dietzel, Pascal D. C. Adsorption properties and structure of CO2 adsorbed on open coordination sites of metal-organic framework Ni2(dhtp) from gas adsorption, IR spectroscopy and X-ray diffraction. *Chem. Commun.*, 41 (2008): 5125-5127.

Ding, Lifeng, and A. Özgür Yazaydin. How Well Do Metal-Organic Frameworks Tolerate Flue Gas Impurities? *J. Phys. Chem. C* 116, 43 (2012): 22987-22991.

Dodd, L. R.; Boone, T. D.; Theodoru, D. N. Molecular Physics 1993, 78, 961.

Dogru, Mirjam, Andreas Sonnauer, Andrei Gavryushin, Paul Knochel, and Thomas Bein. A Covalent Organic Framework with 4 nm open pores. *Chem. Commun.* 47, 6 (2011): 1707-1709.

Doonan, Christian J., David J. Tranchemontagne, T. Grant Glover, Joseph R. Hunt, and Omar M. Yaghi. Exceptional ammonia uptake by a covalent organic framework. *Nat Chem* 2, 3 (2010): 235-238.

Doskocil, Eric J., and Robert J. Davis. Spectroscopic Characterization and Catalytic Activity of Zeolite X Containing Occluded Alkali Species. *Journal of Catalysis* 188, 2 (1999): 353-364.

Dubbeldam, David, Houston Frost, Krista S. Walton, and Randall Q. Snurr. Molecular simulation of adsorption sites of light gases in the metal-organic framework IRMOF-1. *Fluid Phase Equilibria* 261, 1-2 (2007): 152-161.

Dubbeldam, D.; Calero, S.; Vlugt, T.J.H.; Krishna, R.; Maesen, Th.L.M.; Smit, B. J. Phys. Chem. B 2004, 108, 12301–12313.

Dunne, J. A., M. Rao, S. Sircar, R. J. Gorte, and A. L. Myers. Calorimetric Heats of Adsorption and Adsorption Isotherms. 2. O2, N2, Ar, CO2, CH4, C2H6, and SF6 on NaX, H-ZSM-5, and Na-ZSM-5 Zeolites. *Langmuir* 12, 24 (1996): 5896-5904.

Düren, Tina, Youn-Sang Bae, and Randall Q. Snurr. Using molecular simulation to characterise metal-organic frameworks for adsorption applications. *Chem. Soc. Rev.* 38, 5 (2009): 1237-1247.

Ebrahim, Amani M., Benoit Levasseur, and Teresa J. Byosz. Interactions of NO2 with Zr-Based MOF: Effects of the Size of Organic Linkers on NO2 Adsorption at Ambient Conditions. *Langmuir* 29, 1 (2013): 168-174.

Bibliography

Eddaoudi, Mohamed. Systematic Design of Pore Size and Functionality in Isoreticular MOFs and Their Application in Methane Storage. *Science* 295, 5554 (2002): 469-472.

Erucar, Ilknur, and Seda Keskin. High CO2 Selectivity of an Amine-Functionalized Metal Organic Framework in Adsorption-Based and Membrane-Based Gas Separations. *Ind. Eng. Chem. Res.* 52, 9 (2013): 3462-3472.

Ewald, P.P. Annalen Der Physik 64, 253-287 (1921).

Farha, Omar K., Karen L. Mulfort, and Joseph T. Hupp. An Example of Node-Based Postassembly Elaboration of a Hydrogen-Sorbing, Metal-Organic Framework Material. *Inorg. Chem.* 47, 22 (2008): 10223-10225.

Farha, Omar K.. Metal-Organic Framework Materials with Ultrahigh Surface Areas: Is the Sky the Limit? *J. Am. Chem. Soc.* 134, 36 (2012): 15016-15021.

Férey, Gérard. Hybrid porous solids: past, present, future. *Chem. Soc. Rev.* 37, 1 (2007): 191-214.

Férey, Gérard, and Christian Serre. Large breathing effects in three-dimensional porous hybrid matter: facts, analyses, rules and consequences. *Chem. Soc. Rev.* 38, 5 (2009): 1380-1399.

Fioretos, Konstantinos A., George M. Psofogiannakis, and George E. Froudakis. Ab-Initio Study of the Adsorption and Separation of NOx and SOx Gases in Functionalized IRMOF Ligands. *J. Phys. Chem. C* 115, 50 (2011): 24906-24914.

Fischer, Michael, Frank Hoffmann, and Michael Fröba. Metal-organic frameworks and related materials for hydrogen purification: Interplay of pore size and pore wall polarity. *RSC Adv.* 2, 10 (2012): 4382-4396.

Formenti, P., W. Elbert, W. Maenhaut, J. Haywood, and M. O. Andreae. Chemical composition of mineral dust aerosol during the Saharan Dust Experiment (SHADE) airborne campaign in the Cape Verde region, September 2000. *J. Geophys. Res.* 108, D18 (2003): 8576.

Förster, Horst, and Monika Schumann. Infrared spectroscopic studies on carbon dioxide adsorption in alkali-metal and alkaline-earth-metal ion-exchanged A-type zeolites. Part 1. General features of CO2 interaction with A-type zeolites. *J. Chem. Soc., Faraday Trans. 1* 85, 5 (1989): 1149-1158.

Franchi, Robert S., Peter J. E. Harlick, and Abdelhamid Sayari. Applications of Pore-Expanded Mesoporous Silica. 2. Development of a High-Capacity, Water-Tolerant Adsorbent for CO2. *Ind. Eng. Chem. Res.* 44, 21 (2005): 8007-8013.

Frenkel, Daan, and Berend Smit. *Understanding Molecular Simulation: From Algorithms to Applications.* Academic Press, 2001.

Frenkel, D.; Mooij, G. C. A. M.; Smit, B. Journal of Physics - Condensed Matter 1992, 4, 3053.

Frost, Houston, Tina Düren, and Randall Q. Snurr. Effects of Surface Area, Free Volume, and Heat of Adsorption on Hydrogen Uptake in Metal-Organic Frameworks. *J. Phys. Chem. B* 110, 19 (2006): 9565-9570.

Furukawa, Hiroyasu. Ultrahigh Porosity in Metal-Organic Frameworks. *Science* 329, 5990 (2010): 424-428.

García, Edder J., John P. S. Mowat, Paul A. Wright, Javier Pérez-Pellitero, Christian Jallut, and Gerhard D. Pirngruber. Role of Structure and Chemistry in Controlling Separations of CO2/CH4 and CO2/CH4/CO Mixtures over Honeycomb MOFs with Coordinatively Unsaturated Metal Sites. *J. Phys. Chem. C* 116, 50 (2012): 26636-26648.

García-Pérez, Elena, Jorge Gascón, Víctor Morales-Flórez, Juan Manuel Castillo, Freek Kapteijn, and Sofía Calero. Identification of Adsorption Sites in CuBTC by Experimentation and Molecular Simulation. *Langmuir* 25, 3 (2009): 1725-1731.

Ghoufi, A., and G. Maurin. Hybrid Monte Carlo Simulations Combined with a Phase Mixture Model to Predict the Structural Transitions of a Porous Metal-Organic Framework Material upon Adsorption of Guest Molecules. *J. Phys. Chem. C* 114, 14 (2010): 6496-6502.

Goj, Anne, David S. Sholl, E. Demet Akten, and Daniela Kohen. Atomistic Simulations of CO2 and N2 Adsorption in Silica Zeolites: The Impact of Pore Size and Shape. *J. Phys. Chem. B* 106, 33 (2002): 8367-8375.

Grajciar, Lukáš, Andrew D. Wiersum, Philip L. Llewellyn, Jong-San Chang, and Petr Nachtigall. Understanding CO2 Adsorption in CuBTC MOF: Comparing Combined DFT-ab Initio Calculations with Microcalorimetry Experiments. *J. Phys. Chem. C* 115, 36 (2011): 17925-17933.

Grande, Carlos A., and Richard Blom. Dual Pressure Swing Adsorption Units for Gas Separation and Purification. *Ind. Eng. Chem. Res.* 51, 25 (2012): 8695-8699.

Granite, Evan J., and Henry W. Pennline. Photochemical Removal of Mercury from Flue Gas. *Ind. Eng. Chem. Res.* 41, 22 (2002): 5470-5476.

Grant Glover, T., Gregory W. Peterson, Bryan J. Schindler, David Britt, and Omar Yaghi. MOF-74 building unit has a direct impact on toxic gas adsorption. *Chemical Engineering Science* 66, 2 (2011): 163-170.

Greathouse, Jeffery A., Tiffany L. Kinnibrugh, and Mark D. Allendorf. Adsorption and Separation of Noble Gases by IRMOF-1: Grand Canonical Monte Carlo Simulations. *Ind. Eng. Chem. Res.* 48, 7 (2009): 3425-3431.

Greathouse, Jeffery A., and Mark D. Allendorf. The Interaction of Water with MOF-5 Simulated by Molecular Dynamics. *J. Am. Chem. Soc.* 128, 33 (2006): 10678-10679.

Gregg, J. S.; Sing, K. S. W., Adsorption, Surface Area and Porosity;. 2nd ed.; Academic Press: London, 1982; p 303.

Guillot, B. Journal of Molecular Liquids 2002, 101, 219.

Gutiérrez-Sevillano, Juan José, Sofia Calero, and Rajamani Krishna. Selective Adsorption of Water from Mixtures with 1-Alcohols by Exploitation of Molecular Packing Effects in CuBTC. *J. Phys. Chem. C* 119, 7 (2015): 3658-3666.

Haldoupis, Emmanuel, Sankar Nair, and David S. Sholl. Efficient Calculation of Diffusion Limitations in Metal Organic Framework Materials: A Tool for Identifying Materials for Kinetic Separations. *J. Am. Chem. Soc.* 132, 21 (2010): 7528-7539.

Hamon, Lomig. Comparative Study of Hydrogen Sulfide Adsorption in the MIL-53(Al, Cr, Fe), MIL-47(V), MIL-100(Cr), and MIL-101(Cr) Metal-Organic Frameworks at Room Temperature. *J. Am. Chem. Soc.* 131, 25 (2009): 8775-8777.

Han, Sang Soo, Hiroyasu Furukawa, Omar M. Yaghi, and William A. Goddard. Covalent Organic Frameworks as Exceptional Hydrogen Storage Materials. *J. Am. Chem. Soc.* 130, 35 (2008): 11580-11581.

Hao, Shiyou, Hong Chang, Qiang Xiao, Yijun Zhong, and Weidong Zhu. One-Pot Synthesis and CO_2 Adsorption Properties of Ordered Mesoporous SBA-15 Materials Functionalized with APTMS. *J. Phys. Chem. C* 115, 26 (2011): 12873-12882.

Harlick, Peter J. E., and Abdelhamid Sayari. Applications of Pore-Expanded Mesoporous Silicas. 3. Triamine Silane Grafting for Enhanced CO_2 Adsorption. *Ind. Eng. Chem. Res.* 45, 9 (2006): 3248-3255.

Hasegawa, Yasuhisa, Kaori Watanabe, Katsuki Kusakabe, and Shigeharu Morooka. The separation of CO_2 using Y-type zeolite membranes ion-exchanged with alkali metal cations. *Separation and Purification Technology* 22-23 (2001): 319-325.

Hatch, Courtney D., Jadon S. Wiese, Cameron C. Crane, Kenneth J. Harris, Hannah G. Kloss, and Jonas Baltrusaitis. Water Adsorption on Clay Minerals As a Function of Relative Humidity: Application of BET and Freundlich Adsorption Models. *Langmuir* 28, 3 (2012): 1790-1803.

Hedin, Niklas, Linnéa Andersson, Lennart Bergström, and Jinyue Yan. Adsorbents for the post-combustion capture of CO_2 using rapid temperature swing or vacuum swing adsorption. *Applied Energy* 104 (2013): 418-433.

Herm, Zoey R., Joseph A. Swisher, Berend Smit, Rajamani Krishna, and Jeffrey R. Long. Metal-Organic Frameworks as Adsorbents for Hydrogen Purification and Precombustion Carbon Dioxide Capture. *J. Am. Chem. Soc.* 133, 15 (2011): 5664-5667.

Heymans, N., S. Vaesen, and G. De Weireld. A complete procedure for acidic gas separation by adsorption on MIL-53 (Al). *Microporous and Mesoporous Materials* 154 (2012): 93-99.

Hicks, Jason C., Jeffrey H. Drese, Daniel J. Fauth, McMahan L. Gray, Genggeng Qi, and Christopher W. Jones. Designing Adsorbents for CO_2 Capture from Flue Gas-Hyperbranched Aminosilicas Capable of Capturing CO_2 Reversibly. *J. Am. Chem. Soc.* 130, 10 (2008): 2902-2903.

Himeno, Shuji, Toshihiro Tomita, Kenji Suzuki, and Shuichi Yoshida. Characterization and selectivity for methane and carbon dioxide adsorption on the all-silica DD3R zeolite. *Microporous and Mesoporous Materials* 98, 1-3 (2007): 62-69.

Ho, Minh T., Guy W. Allinson, and Dianne E. Wiley. Reducing the Cost of CO_2 Capture from Flue Gases Using Pressure Swing Adsorption. *Ind. Eng. Chem. Res.* 47, 14 (2008): 4883-4890.

House, Kurt Zenz, Charles F. Harvey, Michael J. Aziz, and Daniel P. Schrag. The energy penalty of post-combustion CO_2 capture \& storage and its implications for retrofitting the U.S. installed base. *Energy Environ. Sci.* 2, 2 (2009): 193-205.

Hu, Xiao Liang, and Angelos Michaelides. Water on the hydroxylated (0 0 1) surface of kaolinite: From monomer adsorption to a flat 2D wetting layer. *Surface Science* 602, 4 (2008): 960-974.

Huang, Chih-Hung, Kai-Ping Chang, Ching-Tsung Yu, Pen-Chi Chiang, and Chu-Fan Wang. Development of high-temperature CO2 sorbents made of CaO-based mesoporous silica. *Chemical Engineering Journal* 161, 1-2 (2010): 129-135.

Huck, Johanna M.. Evaluating different classes of porous materials for carbon capture. *Energy Environ. Sci.* 7, 12 (2014): 4132-4146.

Jacobs, Peter A., Franz H. van Cauwelaert, and Etienne F. Vansant. Surface probing of synthetic faujasites by adsorption of carbon dioxide. Part 2. Infra-red study of carbon dioxide adsorbed on x zeolites exchanged with mono- and bi-valent ions. *J. Chem. Soc., Faraday Trans. 1* 69, 0 (1973): 2130-2139.

Jaramillo, E., and M. Chandross. Adsorption of Small Molecules in LTA Zeolites. 1. NH3, CO2, and H2O in Zeolite 4A. *J. Phys. Chem. B* 108, 52 (2004): 20155-20159.

Jaramillo, Eugenio, and Scott M. Auerbach. New Force Field for Na Cations in Faujasite-Type Zeolites. *J. Phys. Chem. B* 103, 44 (1999): 9589-9594.

Jiang, Hai-Long, and Qiang Xu. Porous metal-organic frameworks as platforms for functional applications. *Chem. Commun.* 47, 12 (2011): 3351-3370.

Jiang, Jianwen, Ravichandar Babarao, and Zhongqiao Hu. Molecular simulations for energy, environmental and pharmaceutical applications of nanoporous materials: from zeolites, metal-organic frameworks to protein crystals. *Chem. Soc. Rev.* 40, 7 (2011): 3599-3612.

Jiang, Jianwen, and Stanley I. Sandler. Monte Carlo Simulation for the Adsorption and Separation of Linear and Branched Alkanes in IRMOF-1. *Langmuir* 22, 13 (2006): 5702-5707.

Jobic, Hervé, and Doros N. Theodorou. Quasi-elastic neutron scattering and molecular dynamics simulation as complementary techniques for studying diffusion in zeolites. *Microporous and Mesoporous Materials* 102, 1-3 (2007): 21-50.

Karra, Jagadeswara R., and Krista S. Walton. Effect of Open Metal Sites on Adsorption of Polar and Nonpolar Molecules in Metal-Organic Framework CuBTC. *Langmuir* 24, 16 (2008): 8620-8626.

Karra, Jagadeswara R., and Krista S. Walton. Molecular Simulations and Experimental Studies of CO2, CO, and N2 Adsorption in Metal-Organic Frameworks. *J. Phys. Chem. C* 114, 37 (2010): 15735-15740.

Keskin, Seda, Jinchen Liu, J. Karl Johnson, and David S. Sholl. Atomically detailed models of gas mixture diffusion through CuBTC membranes. *Microporous and Mesoporous Materials* 125, 1-2 (2009): 101-106.

Ketko, MaryBeth H., Ganesh Kamath, and Jeffrey J. Potoff. Development of an Optimized Intermolecular Potential for Sulfur Dioxide. *J. Phys. Chem. B* 115, 17 (2011): 4949-4954.

Khelifa, Amine, Leila Benchehida, and Zoubir Derriche. Adsorption of carbon dioxide by X zeolites exchanged with Ni2+ and Cr3+: isotherms and isosteric heat. *Journal of Colloid and Interface Science* 278, 1 (2004): 9-17.

Kikkinides, E. S., R. T. Yang, and S. H. Cho. Concentration and recovery of carbon dioxide from flue gas by pressure swing adsorption. *Ind. Eng. Chem. Res.* 32, 11 (1993): 2714-2720.

Kim, Se-Na, Won-Jin Son, Jung-Sik Choi, and Wha-Seung Ahn. CO2 adsorption using amine-functionalized mesoporous silica prepared via anionic surfactant-mediated synthesis. *Microporous and Mesoporous Materials* 115, 3 (2008): 497-503.

Kiselev, A. V. Lopatkin, A. A. and Shulga, A. A.. Zeolites 5, 261-267 (1985).

Kitagawa, Susumu, Ryo Kitaura, and Shin-ichiro Noro. Functional Porous Coordination Polymers. *Angewandte Chemie International Edition* 43, 18 (2004): 2334-2375.

Ko, Daeho, Ranjani Siriwardane, and Lorenz T. Biegler. Optimization of a Pressure-Swing Adsorption Process Using Zeolite 13X for CO2 Sequestration. *Ind. Eng. Chem. Res.* 42, 2 (2003): 339-348.

Koehler, K. A., S. M. Kreidenweis, P. J. DeMott, M. D. Petters, A. J. Prenni, and C. M. Carrico. Hygroscopicity and cloud droplet activation of mineral dust aerosol. *Geophys. Res. Lett.* 36, 8 (2009): L08805.

Kohl, Arthur L., and Richard Nielsen. *Gas Purification, Fifth Edition.* 5 edition. Houston, Tex: Gulf Professional Publishing, 1997.

Konduru, Naveen, Peter Lindner, and Nada Marie Assaf-Anid. Curbing the greenhouse effect by carbon dioxide adsorption with Zeolite 13X. *AIChE J.* 53, 12 (2007): 3137-3143.

Krishna, Rajamani, and Jasper M. van Baten. A comparison of the CO2 capture characteristics of zeolites and metal-organic frameworks. *Separation and Purification Technology* 87 (2012): 120-126.

Krishna, Rajamani, and Jasper M. van Baten. Comment on Comparative Molecular Simulation Study of CO2/N2 and CH4/N2 Separation in Zeolites and Metal-Organic Frameworks. *Langmuir* 26, 4 (2010): 2975-2978.

Krishna, Rajamani, and Jasper M. van Baten. In silico screening of zeolite membranes for CO2 capture. *Journal of Membrane Science* 360, 1-2 (2010): 323-333.

Krishna, Rajamani, and Jeffrey R. Long. Screening Metal-Organic Frameworks by Analysis of Transient Breakthrough of Gas Mixtures in a Fixed Bed Adsorber. *J. Phys. Chem. C* 115, 26 (2011): 12941-12950.

Krungleviciute, V. Argon Adsorption on Cu3(Benzene-1,3,5-tricarboxylate)2(H2O)3 Metal-Organic Framework. *Langmuir* 23, 6 (2007): 3106-3109.

Kulkarni, Ambarish R., and David S. Sholl. Analysis of Equilibrium-Based TSA Processes for Direct Capture of CO2 from Air. *Ind. Eng. Chem. Res.* 51, 25 (2012): 8631-8645.

Kusakabe, Katsuki, Takahiro Kuroda, Atsushi Murata, and Shigeharu Morooka. Formation of a Y-Type Zeolite Membrane on a Porous ?-Alumina Tube for Gas Separation. *Ind. Eng. Chem. Res.* 36, 3 (1997): 649-655.

Küsgens, Pia. Characterization of metal-organic frameworks by water adsorption. *Microporous and Mesoporous Materials* 120, 3 (2009): 325-330.

Landau, D. P.; Binder, K. A guide to Monte Carlo simulations in statistical physics; Cambridge University Press: New York, 2002.

Langmuir,I. J. Am. Chem. Soc. 38, 2221 (1916)

Laspéras, Monique, Hélène Cambon, Daniel Brunel, Isabel Rodriguez, and Patrick Geneste. Cesium oxide encapsulation in faujasite zeolites effect of framework composition on the nature and basicity of intrazeolitic species. *Microporous Materials* 7, 2-3 (1996): 61-72.

Leach, A.R. Molecular Modelling: Principles and Application, 2nd ed., Prentice-Hall, Englewood Cliffs, NJ, (2001).

Leal, Orlyo, Carmelo Bolívar, César Ovalles, Juan José García, and Youssef Espidel. Reversible adsorption of carbon dioxide on amine surface-bonded silica gel. *Inorganica Chimica Acta* 240, 1-2 (1995): 183-189.

Lee, K. B., and S. Sircar. Removal and recovery of compressed CO2 from flue gas by a novel thermal swing chemisorption process. *AIChE J.* 54, 9 (2008): 2293-2302.

Lee, Yong-Gon, Hoi Ri Moon, Young Eun Cheon, and Myunghyun Paik Suh. A Comparison of the H2 Sorption Capacities of Isostructural Metal-Organic Frameworks With and Without Accessible Metal Sites: [\Zn2(abtc)(dmf)2\3] and [\Cu2(abtc)(dmf)2\3] versus [\Cu2(abtc)\3]. *Angewandte Chemie International Edition* 47, 40 (2008): 7741-7745.

Levasseur, Benoit, Camille Petit, and Teresa J. Byosz. Reactive Adsorption of NO2 on Copper-Based Metal-Organic Framework and Graphite Oxide/Metal-Organic Framework Composites. *ACS Appl. Mater. Interfaces* 2, 12 (2010): 3606-3613.

Li, Gang, Penny Xiao, Paul A. Webley, Jun Zhang, and Ranjeet Singh. Competition of CO2/H2O in adsorption based CO2 capture. *Energy Procedia* 1, 1 (2009): 1123-1130.

Li, Gang, Penny Xiao, Paul Webley, Jun Zhang, Ranjeet Singh, and Marc Marshall. Capture of CO2 from high humidity flue gas by vacuum swing adsorption with zeolite 13X. *Adsorption* 14, 2-3 (2008): 415-422.

Li, Hailian, Mohamed Eddaoudi, M. O'Keeffe, and O. M. Yaghi. Design and synthesis of an exceptionally stable and highly porous metal-organic framework. *Nature* 402, 6759 (1999): 276-279.

Li, Jian-Rong, Julian Sculley, and Hong-Cai Zhou. Metal-Organic Frameworks for Separations. *Chem. Rev.* 112, 2 (2012): 869-932.

Li, Jian-Rong, Ryan J. Kuppler, and Hong-Cai Zhou. Selective gas adsorption and separation in metal-organic frameworks. *Chem. Soc. Rev.* 38, 5 (2009): 1477-1504.

Li, Yingwei, and Ralph T. Yang. Gas Adsorption and Storage in Metal-Organic Framework MOF-177. *Langmuir* 23, 26 (2007): 12937-12944.

Liang, Zhijian, Marc Marshall, and Alan L. Chaffee. CO2 Adsorption-Based Separation by Metal Organic Framework (CuBTC) versus Zeolite (13X). *Energy Fuels* 23, 5 (2009): 2785-2789.

Liu, Bei, and Berend Smit. Molecular Simulation Studies of Separation of CO2/N2, CO2/CH4, and CH4/N2 by ZIFs. *J. Phys. Chem. C* 114, 18 (2010): 8515-8522.

Liu, Dahuan, Chengcheng Zheng, Qingyuan Yang, and Chongli Zhong. Understanding the Adsorption and Diffusion of Carbon Dioxide in Zeolitic Imidazolate Frameworks: A Molecular Simulation Study. *J. Phys. Chem. C* 113, 12 (2009): 5004-5009.

Liu, Jian, Yu Wang, Annabelle I. Benin, Paulina Jakubczak, Richard R. Willis, and M. Douglas LeVan. CO2/H2O Adsorption Equilibrium and Rates on Metal-Organic Frameworks: HKUST-1 and Ni/DOBDC. *Langmuir* 26, 17 (2010): 14301-14307.

Liu, Qing, Liqi Ning, Shudong Zheng, Mengna Tao, Yao Shi, and Yi He. Adsorption of Carbon Dioxide by MIL-101(Cr): Regeneration Conditions and Influence of Flue Gas Contaminants. *Sci. Rep.* 3 (2013).

Liu, Yunhua, Dahuan Liu, Qingyuan Yang, Chongli Zhong, and Jianguo Mi. Comparative Study of Separation Performance of COFs and MOFs for CH4/CO2/H2 Mixtures. *Ind. Eng. Chem. Res.* 49, 6 (2010): 2902-2906.

Lopes, Filipe V. S., Carlos A. Grande, and Alírio E. Rodrigues. Fast-cycling VPSA for hydrogen purification. *Fuel* 93 (2012): 510-523.

López-Aranguren, P.; Builes, S.; Fraile, J., Vega, L. F.; Domingo, C. Understanding the performance of new amine-functionalized mesoporous silica materials for CO2 adsorption. *Ind. Eng. Chem. Res*. 2014, 53(40): 15611-15619.

Loureiro, José Miguel, and Mykola T. Kartel, . *Combined and Hybrid Adsorbents.* Springer Netherlands, 2006.

Low, John J., Annabelle I. Benin, Paulina Jakubczak, Jennifer F. Abrahamian, Syed A. Faheem, and Richard R. Willis. Virtual High Throughput Screening Confirmed Experimentally: Porous Coordination Polymer Hydration. *J. Am. Chem. Soc.* 131, 43 (2009): 15834-15842.

Llewellyn, Philip L., Sandrine Bourrelly, Christian Serre, Yaroslav Filinchuk, and Gérard Férey. How Hydration Drastically Improves Adsorption Selectivity for CO2 over CH4 in the Flexible Chromium Terephthalate MIL-53. *Angewandte Chemie International Edition* 45, 46 (2006): 7751-7754.

Llewellyn, Philip L. High Uptakes of CO2 and CH4 in Mesoporous Metal-Organic Frameworks MIL-100 and MIL-101. *Langmuir* 24, 14 (2008): 7245-7250.

Ma, Shengqian, Daofeng Sun, Daqiang Yuan, Xi-Sen Wang, and Hong-Cai Zhou. Preparation and Gas Adsorption Studies of Three Mesh-Adjustable Molecular Sieves with a Common Structure. *J. Am. Chem. Soc.* 131, 18 (2009): 6445-6451.

Mahoney, M. W.; Jorgensen, W. L. Journal of Chemical Physics 2000, 112, 8910.

Martin, M.G.; Siepmann, J.I. J. Am. Chem. Soc. 1997, 119, 8921-8924.

Martín, C. F., M. G. Plaza, J. J. Pis, F. Rubiera, C. Pevida, and T. A. Centeno. On the limits of CO2 capture capacity of carbons. *Separation and Purification Technology* 74, 2 (2010): 225-229.

Martín-Calvo, Ana, Elena García-Pérez, Juan Manuel Castillo, and Sofia Calero. Molecular simulations for adsorption and separation of natural gas in IRMOF-1 and CuBTC metal-organic frameworks. *Phys. Chem. Chem. Phys.* 10, 47 (2008): 7085-7091.

Mason, Jarad A., Kenji Sumida, Zoey R. Herm, Rajamani Krishna, and Jeffrey R. Long. Evaluating metal-organic frameworks for post-combustion carbon dioxide capture via temperature swing adsorption. *Energy Environ. Sci.* 4, 8 (2011): 3030-3040.

Maurin, G., P. L. Llewellyn, and R. G. Bell. Adsorption Mechanism of Carbon Dioxide in Faujasites: Grand Canonical Monte Carlo Simulations and Microcalorimetry Measurements. *J. Phys. Chem. B* 109, 33 (2005): 16084-16091.

Mayo, Stephen L., Barry D. Olafson, and William A. Goddard. DREIDING: a generic force field for molecular simulations. *J. Phys. Chem.* 94, 26 (1990): 8897-8909.

McCash., E. M., Surface chemistry. Oxford University Press: Oxford 2001; p 177.

McEwen, Joe, Jim-Dario Hayman, and A. Özgür Yazaydin. A comparative study of CO2, CH4 and N2 adsorption in ZIF-8, Zeolite-13X and BPL activated carbon. *Chemical Physics* 412 (2013): 72-76.

Meek, Scott T., Jeffery A. Greathouse, and Mark D. Allendorf. Metal-Organic Frameworks: Metal-Organic Frameworks: A Rapidly Growing Class of Versatile Nanoporous Materials. *Adv. Mater.* 23, 2 (2011): 141-141.

Merel, Jérôme, Marc Clausse, and Francis Meunier. Experimental Investigation on CO2 Post-Combustion Capture by Indirect Thermal Swing Adsorption Using 13X and 5A Zeolites. *Ind. Eng. Chem. Res.* 47, 1 (2008): 209-215.

Metropolis, N.; Rosenbluth, A.W.; Rosenbluth, M.N.; Teller, A.N.; Teller, E. J. Chem. Phys. 1953, 21, 1087–1092.

Metropolis, N. Los Alamos Science 1987, 12, 125–130.

Millward, Andrew R., and Omar M. Yaghi. Metal-Organic Frameworks with Exceptionally High Capacity for Storage of Carbon Dioxide at Room Temperature. *J. Am. Chem. Soc.* 127, 51 (2005): 17998-17999.

Moellmer, J. Insights on Adsorption Characterization of Metal-Organic Frameworks: A Benchmark Study on the Novel soc-MOF. *Microporous and Mesoporous Materials* 129, 3 (2010): 345-353.

Mueller, U., M. Schubert, F. Teich, H. Puetter, K. Schierle-Arndt, and J. Pastré. Metal-organic frameworks prospective industrial applications. *J. Mater. Chem.* 16, 7 (2006): 626-636.

Murray, B. J., S. L. Broadley, T. W. Wilson, J. D. Atkinson, and R. H. Wills. Heterogeneous freezing of water droplets containing kaolinite particles. *Atmos. Chem. Phys.* 11, 9 (2011): 4191-4207.

Myers, A. L., and J. M. Prausnitz. Thermodynamics of mixed-gas adsorption. *AIChE J.* 11, 1 (1965): 121-127.

Neumann, M. Molecular Physics 1983, 50, 841.

Niu, Ji-Nan, and Ying-Huai Qiang. Molecular Dynamics Simulation on Structure of Water Molecules in a Kaolinite-Water System. *Acta Physico-Chimica Sinica* 25, 6 (2009): 1-3.

Norman, G. E.; Filinov, V. S. High Temperature 1969, 7, 216.

O'Keeffe, Michael, and Omar M. Yaghi. Deconstructing the Crystal Structures of Metal-Organic Frameworks and Related Materials into Their Underlying Nets. *Chem. Rev.* 112, 2 (2012): 675-702.

Olajire, Abass A. CO_2 capture and separation technologies for end-of-pipe applications: A review. *Energy* 35, 6 (2010): 2610-2628.

Pacciani, R.. Influence of the Concentration of CO_2 and SO_2 on the Absorption of CO_2 by a Lithium Orthosilicate-Based Absorbent. *Environ. Sci. Technol.* 45, 16 (2011): 7083-7088.

Palomino, Miguel, Avelino Corma, Jose L. Jordá, Fernando Rey, and Susana Valencia. Zeolite Rho: a highly selective adsorbent for CO_2/CH_4 separation induced by a structural phase modification. *Chem. Commun.* 48, 2 (2011): 215-217.

Panagiotopoulos, A. Z.. Molecular Physics 61(4), 813-826 (1987).

Papadopoulos, George K., Hervé Jobic, and Doros N. Theodorou. Transport Diffusivity of N_2 and CO_2 in Silicalite: Coherent Quasielastic Neutron Scattering Measurements and Molecular Dynamics Simulations. *J. Phys. Chem. B* 108, 34 (2004): 12748-12756.

Park, Jinhee, Daqiang Yuan, Khanh T. Pham, Jian-Rong Li, Andrey Yakovenko, and Hong-Cai Zhou. Reversible Alteration of CO_2 Adsorption upon Photochemical or Thermal Treatment in a Metal-Organic Framework. *J. Am. Chem. Soc.* 134, 1 (2012): 99-102.

Parkes, Marie V., Chad L. Staiger, John J. Perry Iv, Mark D. Allendorf, and Jeffery A. Greathouse. Screening metal-organic frameworks for selective noble gas adsorption in air: effect of pore size and framework topology. *Phys. Chem. Chem. Phys.* 15, 23 (2013): 9093-9106.

Pathria, R. K. Statistical Mechanics, Second ed.; Butterworth-Heinemann: Oxford, 1996; Vol. 1.

Patra, M.; Karttunen, M.; Hyvonen, M. T.; Falck, E.; Lindqvist, P.; Vattulainen, I. Biophysics Journal 2003, 84, 3636.

Petit, Camille, and Teresa J. Byosz. Exploring the coordination chemistry of MOF/graphite oxide composites and their applications as adsorbents. *Dalton Trans.* 41, 14 (2012): 4027-4035.

Pirngruber, Gerhard D., Stefania Cassiano-Gaspar, Sylvain Louret, Alexandra Chaumonnot, and Bruno Delfort. Amines immobilized on a solid support for postcombustion CO_2 capture: A preliminary analysis of the performance in a VSA or TSA process based on the adsorption isotherms and kinetic data. *Energy Procedia* 1, 1 (2009): 1335-1342.

Plaza, M. G., C. Pevida, A. Arenillas, F. Rubiera, and J. J. Pis. CO_2 capture by adsorption with nitrogen enriched carbons. *Fuel* 86, 14 (2007): 2204-2212.

Plaza, M. G., S. García, F. Rubiera, J. J. Pis, and C. Pevida. Post-combustion CO_2 capture with a commercial activated carbon: Comparison of different regeneration strategies. *Chemical Engineering Journal* 163, 1-2 (2010): 41-47.

Poling, Bruce, John Prausnitz, and John O. Connell. *The Properties of Gases and Liquids.* McGraw Hill Professional, 2000.

Potoff, Jeffrey J., and J. Ilja Siepmann. Vapor-liquid equilibria of mixtures containing alkanes, carbon dioxide, and nitrogen. *AIChE J.* 47, 7 (2001): 1676-1682.

Powell, Clem E., and Greg G. Qiao. Polymeric CO2/N2 gas separation membranes for the capture of carbon dioxide from power plant flue gases. *Journal of Membrane Science* 279, 1-2 (2006): 1-49.

Prasad, Thazhe Kootteri, Dae Ho Hong, and Myunghyun Paik Suh. High Gas Sorption and Metal-Ion Exchange of Microporous Metal-Organic Frameworks with Incorporated Imide Groups. *Chem. Eur. J.* 16, 47 (2010): 14043-14050.

Prausnitz, J.M., Lichtenthaler, R.N, Gomes, E. Termodinámica Molecular de los equilibrios de fases.3rd edición. Prentice Hall. España. 2000.

Prestipino, C.. Local Structure of Framework Cu(II) in HKUST-1 Metallorganic Framework: Spectroscopic Characterization upon Activation and Interaction with Adsorbates. *Chem. Mater.* 18, 5 (2006): 1337-1346.

Qiu, Shilun, Ming Xue, and Guangshan Zhu. Metal-organic framework membranes: from synthesis to separation application. *Chem. Soc. Rev.* 43, 16 (2014): 6116-6140.

Ramsahye, N. A., G. Maurin, S. Bourrelly, P. Llewellyn, T. Loiseau, and G. Ferey. Charge distribution in metal organic framework materials: transferability to a preliminary molecular simulation study of the CO2 adsorption in the MIL-53 (Al) system. *Phys. Chem. Chem. Phys.* 9, 9 (2007): 1059-1063.

Rankin, Rees B., Jinchen Liu, Anant D. Kulkarni, and J. Karl Johnson. Adsorption and Diffusion of Light Gases in ZIF-68 and ZIF-70: A Simulation Study. *J. Phys. Chem. C* 113, 39 (2009): 16906-16914.

Rappe, A. K., C. J. Casewit, K. S. Colwell, W. A. Goddard, and W. M. Skiff. UFF, a full periodic table force field for molecular mechanics and molecular dynamics simulations. *J. Am. Chem. Soc.* 114, 25 (1992): 10024-10035.

Rege, Salil U., and Ralph T. Yang. Kinetic Separation of Oxygen and Argon Using Molecular Sieve Carbon. *Adsorption* 6, 1 (2000): 15-22.

Ribeiro, Ana M., João C. Santos, Alírio E. Rodrigues, and Sébastien Rifflart. Pressure Swing Adsorption Process in Coal to Fischer-Tropsch Fuels with CO2 Capture. *Energy Fuels* 26, 2 (2012): 1246-1253.

Rosenbluth, A. W., Metropolis, N. and Teller, A. H.. Journal of Chemical Physics 21, 1087–1092 (1953).

Rouquerol, F., Roquerol, J., Sing, K., Adsorption by Powders and Porous Solids, 1998, Academic Press, San Diego

Rowsell, Jesse L. C., Elinor C. Spencer, Juergen Eckert, Judith A. K. Howard, and Omar M. Yaghi. Gas Adsorption Sites in a Large-Pore Metal-Organic Framework. *Science* 309, 5739 (2005): 1350-1354.

Rowsell, Jesse L. C., and Omar M. Yaghi. Metal-organic frameworks: a new class of porous materials. *Microporous and Mesoporous Materials* 73, 1-2 (2004): 3-14.

Rowsell, Jesse L. C., and Omar M. Yaghi. Strategies for Hydrogen Storage in Metal-Organic Frameworks. *Angewandte Chemie International Edition* 44, 30 (2005): 4670-4679.

Safarifard, Vahid, and Ali Morsali. Influence of an amine group on the highly efficient reversible adsorption of iodine in two novel isoreticular interpenetrated pillared-layer microporous metal-organic frameworks. *CrystEngComm* 16, 37 (2014): 8660-8663.

Saha, Dipendu, and Shuguang Deng. Adsorption equilibrium and kinetics of CO_2, CH_4, N_2O, and NH_3 on ordered mesoporous carbon. *Journal of Colloid and Interface Science* 345, 2 (2010): 402-409.

Saha, Dipendu, Zongbi Bao, Feng Jia, and Shuguang Deng. Adsorption of CO_2, CH_4, N_2O, and N_2 on MOF-5, MOF-177, and Zeolite 5A. *Environ. Sci. Technol.* 44, 5 (2010): 1820-1826.

Salles, Fabrice, Aziz Ghoufi, Guillaume Maurin, Robert, G. Bell, Caroline Mellot-Draznieks, and Gérard Férey. Molecular Dynamics Simulations of Breathing MOFs: Structural Transformations of MIL-53(Cr) upon Thermal Activation and CO_2 Adsorption. *Angewandte Chemie International Edition* 47, 44 (2008): 8487-8491.

Sayari, Abdelhamid, and Youssef Belmabkhout. Stabilization of Amine-Containing CO_2 Adsorbents: Dramatic Effect of Water Vapor. *J. Am. Chem. Soc.* 132, 18 (2010): 6312-6314.

Sayari, Abdelhamid, Youssef Belmabkhout, and Rodrigo Serna-Guerrero. Flue gas treatment via CO_2 adsorption. *Chemical Engineering Journal* 171, 3 (2011): 760-774.

Schuttlefield, Jennifer D., David Cox, and Vicki H. Grassian. An investigation of water uptake on clays minerals using ATR-FTIR spectroscopy coupled with quartz crystal microbalance measurements. *J. Geophys. Res.* 112, D21 (2007): D21303.

Serna-Guerrero, Rodrigo, and Abdelhamid Sayari. Modeling adsorption of CO_2 on amine-functionalized mesoporous silica. 2: Kinetics and breakthrough curves. *Chemical Engineering Journal* 161, 1-2 (2010): 182-190.

Serna-Guerrero, Rodrigo, Youssef Belmabkhout, and Abdelhamid Sayari. Influence of regeneration conditions on the cyclic performance of amine-grafted mesoporous silica for CO_2 capture: An experimental and statistical study. *Chemical Engineering Science* 65, 14 (2010): 4166-4172.

Shaw, D. J., Introduction to colloid and surface chemistry. 3rd ed.; Butterworths: London, 1980; p 273.

Shelley, J. C., and G. N. Patey. A configuration bias Monte Carlo method for water. *The Journal of Chemical Physics* 102, 19 (1995): 7656-7663.

Siepmann, J. I. Computer simulation of biomolecular systems: theoretical and experimental applications; Escom Science Publisher: Leiden, 1993.

Siepmann, J. I.; Frenkel, D. Molecular Physics 1992, 75, 59.

Silvestre-Albero, Joaquín, Anass Wahby, Antonio Sepúlveda-Escribano, Manuel Martínez-Escandell, Katsumi Kaneko, and Francisco Rodríguez-Reinoso. Ultrahigh CO_2 adsorption

capacity on carbon molecular sieves at room temperature. *Chem. Commun.* 47, 24 (2011): 6840-6842.

Simmons, Jason M., Hui Wu, Wei Zhou, and Taner Yildirim. Carbon capture in metal-organic frameworks: a comparative study. *Energy Environ. Sci.* 4, 6 (2011): 2177-2185.

Sing, K. W.; Everett, D. H.; Haul, R. A. W.; Moscou, L.; Pierotti, R. A.; Rouquerol, J.; Siemieniewska, T., Reporting physisorption data for gas/solid systems with special reference to the determination of surface area and porosity. Pure Appl. Chem. 1985, 57, (4), 603-19.

Siriwardane, Ranjani V., Ming-Shing Shen, and Edward P. Fisher. Adsorption of CO2, N2, and O2 on Natural Zeolites. *Energy Fuels* 17, 3 (2003): 571-576.

Smirnov, Konstantin S., and Daniel Bougeard. A Molecular Dynamics Study of Structure and Short-time Dynamics of Water in Kaolinite. *J. Phys. Chem. B* 103, 25 (1999): 5266-5273.

Snurr, Randall Q., Joseph T. Hupp, and SonBinh T. Nguyen. Prospects for nanoporous metal-organic materials in advanced separations processes. *AIChE J.* 50, 6 (2004): 1090-1095.

Sokolik, F., Y. Guissani, and B. Guillot. Molecular dynamics simulations of thermodynamic and structural properties of liquid SO2. *Molecular Physics* 56, 2 (1985): 239-253.

Steinbach, P. J.; Brooks, B. R. Journal of Computational Chemistry 1994, 15, 667.

Stephenson, Dale J., Charles I. Fairchild, Roy M. Buchan, and Maxine E. Dakins. A Fiber Characterization of the Natural Zeolite, Mordenite: A Potential Inhalation Health Hazard. *Aerosol Science and Technology* 30, 5 (1999): 467-476.

Stern, H. A.; Rittner, F.; Berne, B. J.; Friesner, R. A. Journal of Chemical Physics 2001, 115, 2237.

Sullivan, R. C., M. J. K. Moore, M. D. Petters, S. M. Kreidenweis, G. C. Roberts, and K. A. Prather. Effect of chemical mixing state on the hygroscopicity and cloud nucleation properties of calcium mineral dust particles. *Atmos. Chem. Phys.* 9, 10 (2009): 3303-3316.

Sumida, Kenji. Carbon Dioxide Capture in Metal-Organic Frameworks. *Chem. Rev.* 112, 2 (2012): 724-781.

Sun, Weizhen, Li-Chiang Lin, Xuan Peng, and Berend Smit. Computational screening of porous metal-organic frameworks and zeolites for the removal of SO2 and NOx from flue gases. *AIChE J.* 60, 6 (2014): 2314-2323.

Sun, Yan, Xiu-Wu Liu, Wei Su, Yaping Zhou, and Li Zhou. Studies on ordered mesoporous materials for potential environmental and clean energy applications. *Applied Surface Science* 253, 13 (2007): 5650-5655.

Svensson, E. A., C. Delval, P. von Hessberg, M. S. Johnson, and J. B. C. Pettersson. Freezing of water droplets colliding with kaolinite particles. *Atmos. Chem. Phys.* 9, 13 (2009): 4295-4300.

Tagliabue, Marco. Natural gas treating by selective adsorption: Material science and chemical engineering interplay. *Chemical Engineering Journal* 155, 3 (2009): 553-566.

Tan, Jin Chong, Thomas D. Bennett, and Anthony K. Cheetham. Chemical structure, network topology, and porosity effects on the mechanical properties of Zeolitic Imidazolate Frameworks. *PNAS* 107, 22 (2010): 9938-9943.

Bibliography

Tlili, Nabil, Georges Grévillot, and Cécile Vallières. Carbon dioxide capture and recovery by means of TSA and/or VSA. *International Journal of Greenhouse Gas Control* 3, 5 (2009): 519-527.

Tokarský, Jonáš, Pavla Rapková, and Jaroslav V. Burda. Structure and stability of kaolinite/TiO2 nanocomposite: DFT and MM computations. *J Mol Model* 18, 6 (2011): 2689-2698.

Torrisi, Antonio, Caroline Mellot-Draznieks, and Robert G. Bell. Impact of ligands on CO2 adsorption in metal-organic frameworks: First principles study of the interaction of CO2 with functionalized benzenes. II. Effect of polar and acidic substituents. *The Journal of Chemical Physics* 132, 4 (2010): 044705.

Torrisi, Antonio, Robert G. Bell, and Caroline Mellot-Draznieks. Functionalized MOFs for Enhanced CO2 Capture. *Crystal Growth \& Design* 10, 7 (2010): 2839-2841.

Tunega, Daniel, Martin H. Gerzabek, and Hans Lischka. Ab Initio Molecular Dynamics Study of a Monomolecular Water Layer on Octahedral and Tetrahedral Kaolinite Surfaces. *J. Phys. Chem. B* 108, 19 (2004): 5930-5936.

Ungerer, P.; Tavitian, B.; Boutin, A., Applications of molecular simulation in the oil andgas industry IFP publications; Paris, 2005.

Vaidhyanathan, Ramanathan, Simon S. Iremonger, Karl W. Dawson, and George K. H. Shimizu. An amine-functionalized metal organic framework for preferential CO2adsorption at low pressures. *Chem. Commun.*, 35 (2009): 5230-5232.

Valderrama, J. O.; Vargas, D. A. Applied Thermal Engineering 2003, 23, 1417.

Valenzano, L., B. Civalleri, S. Chavan, G. T. Palomino, C. O. Areán, and S. Bordiga. Computational and Experimental Studies on the Adsorption of CO, N2, and CO2 on Mg-MOF-74. *J. Phys. Chem. C* 114, 25 (2010): 11185-11191.

Vega, L.F. El CO$_2$ como recurso: de la captura a los usos industriales, (2010) Guías Técnicas y de Medio Ambiente, 19, Fundación Gas Natural, ISBN: 978-84-614-1195-5. Second edition, 2011.

Vlugt, T. J. H., E. García-Pérez, D. Dubbeldam, S. Ban, and S. Calero. Computing the Heat of Adsorption using Molecular Simulations: The Effect of Strong Coulombic Interactions. *J. Chem. Theory Comput.* 4, 7 (2008): 1107-1118.

Vlugt, T.J.H.; Zhu, W.; Kapteijn, F.; Moulijn, J.A.; Smit, B.; Krishna, R. J. Am. Chem. Soc. 1998, 120, 5599–5600.

Vlugt, T. J. H.; Krishna, R.; Smit, B. Journal of Physical Chemistry B 1999, 103, 1102-1118.

Wagner, W.; Pruss, A. Journal of Physical and Chemical Reference Data 2002, 31, 387.

Walton, Krista S. Understanding Inflections and Steps in Carbon Dioxide Adsorption Isotherms in Metal-Organic Frameworks. *J. Am. Chem. Soc.* 130, 2 (2008): 406-407.

Wang, Bo, Adrien P. Côté, Hiroyasu Furukawa, Michael O'Keeffe, and Omar M. Yaghi. Colossal cages in zeolitic imidazolate frameworks as selective carbon dioxide reservoirs. *Nature* 453, 7192 (2008): 207-211.

Wang, Qiang, Jizhong Luo, Ziyi Zhong, and Armando Borgna. CO2 capture by solid adsorbents and their applications: current status and new trends. *Energy Environ. Sci.* 4, 1 (2010): 42-55.

Wang, Xueguang, Jerry C. C. Chan, Yao-Hung Tseng, and Soofin Cheng. Synthesis, characterization and catalytic activity of ordered SBA-15 materials containing high loading of diamine functional groups. *Microporous and Mesoporous Materials* 95, 1-3 (2006): 57-65.

Wang, Yu, and M. Douglas LeVan. Adsorption Equilibrium of Carbon Dioxide and Water Vapor on Zeolites 5A and 13X and Silica Gel: Pure Components. *J. Chem. Eng. Data* 54, 10 (2009): 2839-2844.

Wang, Zhenqiang, and Seth M. Cohen. Postsynthetic modification of metal-organic frameworks. *Chem. Soc. Rev.* 38, 5 (2009): 1315-1329.

Warne, M. R., N. L. Allan, and T. Cosgrove. Computer simulation of water molecules at kaolinite and silica surfaces. *Phys. Chem. Chem. Phys.* 2, 16 (2000): 3663-3668.

Watanabe, K., N. Austin, and M. R. Stapleton. Investigation of the Air Separation Properties of Zeolites Types A, X and Y by Monte Carlo Simulations. *Molecular Simulation* 15, 4 (1995): 197-221.

Watanabe, Taku, and David S. Sholl. Molecular chemisorption on open metal sites in Cu[sub 3](benzenetricarboxylate)[sub 2]: A spatially periodic density functional theory study. *The Journal of Chemical Physics* 133, 9 (2010): 094509.

Wells, Brad A., Zhijian Liang, Marc Marshall, and Alan L. Chaffee. Modeling gas adsorption in metal organic frameworks. *Energy Procedia* 1, 1 (2009): 1273-1280.

Wiersum, Andrew D., Jong-San Chang, Christian Serre, and Philip L. Llewellyn. An Adsorbent Performance Indicator as a First Step Evaluation of Novel Sorbents for Gas Separations: Application to Metal-Organic Frameworks. *Langmuir* 29, 10 (2013): 3301-3309.

Widom, B. Journal of Chemical Physics 1963, 39, 2808.

Wilmer, Christopher E., and Randall Q. Snurr. Towards rapid computational screening of metal-organic frameworks for carbon dioxide capture: Calculation of framework charges via charge equilibration. *Chemical Engineering Journal* 171, 3 (2011): 775-781.

Wolf, D.; Keblinski, P.; Phillpot, S. R.; Eggebrecht, J. Journal of Chemical Physics 1999, 110, 8254-8282.

Wu, Dong, Qing Xu, Dahuan Liu, and Chongli Zhong. Exceptional CO2 Capture Capability and Molecular-Level Segregation in a Li-Modified Metal-Organic Framework. *J. Phys. Chem. C* 114, 39 (2010): 16611-16617.

Xie, Jiangkun, Naiqiang Yan, Zan Qu, and Shijian Yang. Synthesis, characterization and experimental investigation of CuBTC as CO2 adsorbent from flue gas. *Journal of Environmental Sciences* 24, 4 (2012): 640-644.

Xu, Bo, and Larry Kevan. Formation of alkali metal particles in alkali metal cation exchanged X zeolite exposed to alkali metal vapor: control of metal particle identity. *J. Phys. Chem.* 96, 6 (1992): 2642-2645.

Xu, Qing, and Chongli Zhong. A General Approach for Estimating Framework Charges in Metal-Organic Frameworks. *J. Phys. Chem. C* 114, 11 (2010): 5035-5042.

Xue, Chunyu, Qingyuan Yang, and Chongli Zhong. Effects of the side pockets on gas separation in metal-organic framework CuBTC: a molecular simulation study. *Molecular Simulation* 35, 15 (2009): 1249-1255.

Yaghi, Omar M., Michael O'Keeffe, Nathan W. Ockwig, Hee K. Chae, Mohamed Eddaoudi, and Jaheon Kim. Reticular synthesis and the design of new materials. *Nature* 423, 6941 (2003): 705-714.

Yamazaki, Tatsuya, Masahiro Katoh, Sentaro Ozawa, and Yoshisada Ogino. Adsorption of CO2 over univalent cation-exchanged ZSM-5 zeolites. *Molecular Physics* 80, 2 (1993): 313-324.

Yang, Chi, Xiaoping Wang, and Mohammad A. Omary. Fluorous Metal-Organic Frameworks for High-Density Gas Adsorption. *J. Am. Chem. Soc.* 129, 50 (2007): 15454-15455.

Yang, Qingyuan, Chongli Zhong, and Jian-Feng Chen. Computational Study of CO2 Storage in Metal-Organic Frameworks. *J. Phys. Chem. C* 112, 5 (2008): 1562-1569.

Yang, Qingyuan, Chunyu Xue, Chongli Zhong, and Jian-Feng Chen. Molecular simulation of separation of CO2 from flue gases in CuBTC metal-organic framework. *AIChE J.* 53, 11 (2007): 2832-2840.

Yang, Ying, Pradeep Shukla, Shaobin Wang, Victor Rudolph, Xiao-Ming Chen, and Zhonghua Zhu. Significant improvement of surface area and CO2 adsorption of CuBTC via solvent exchange activation. *RSC Adv.* 3, 38 (2013): 17065-17072.

Yazaydin, A. Özgür. Enhanced CO2 Adsorption in Metal-Organic Frameworks via Occupation of Open-Metal Sites by Coordinated Water Molecules. *Chem. Mater.* 21, 8 (2009): 1425-1430.

Yazaydin, A. Özgür. Screening of Metal-Organic Frameworks for Carbon Dioxide Capture from Flue Gas Using a Combined Experimental and Modeling Approach. *J. Am. Chem. Soc.* 131, 51 (2009): 18198-18199.

Ye, Sheng. Post-combustion CO2 capture with the HKUST-1 and MIL-101(Cr) metal-organic frameworks: Adsorption, separation and regeneration investigations. *Microporous and Mesoporous Materials* 179 (2013): 191-197.

Yin, Yan, Sabine Wurzler, Zev Levin, and Tamir G. Reisin. Interactions of mineral dust particles and clouds: Effects on precipitation and cloud optical properties. *J.-Geophys.-Res.* 107, D23 (2002): 4724.

Yu, Cheng-Hsiu. A Review of CO2 Capture by Absorption and Adsorption. *Aerosol and Air Quality Research*, 2012.

Yu, Jiamei, and Perla B. Balbuena. Water Effects on Postcombustion CO2 Capture in Mg-MOF-74. *J. Phys. Chem. C* 117, 7 (2013): 3383-3388.

Yu, Jiamei, Yuguang Ma, and Perla B. Balbuena. Evaluation of the Impact of H2O, O2, and SO2 on Postcombustion CO2 Capture in Metal-Organic Frameworks. *Langmuir* 28, 21 (2012): 8064-8071.

Yu, Kuang, Kalin Kiesling, and J. R. Schmidt. Trace Flue Gas Contaminants Poison Coordinatively Unsaturated Metal-Organic Frameworks: Implications for CO2 Adsorption and Separation. *J. Phys. Chem. C* 116, 38 (2012): 20480-20488.

Yue, Ming Bo, Lin Bing Sun, Yi Cao, Ying Wang, Zhu Ji Wang, and Jian Hua Zhu. Efficient CO2 Capturer Derived from As-Synthesized MCM-41 Modified with Amine. *Chem. Eur. J.* 14, 11 (2008): 3442-3451.

Zelenák, V., Z. Vargová, M. Almáši, A. Zelenáková, and J. Kuchár. Layer-pillared zinc(II) metal-organic framework built from 4,4'-azo(bis)pyridine and 1,4-BDC. *Microporous and Mesoporous Materials* 129, 3 (2010): 354-359.

Zhang, Jun, Paul A. Webley, and Penny Xiao. Effect of process parameters on power requirements of vacuum swing adsorption technology for CO2 capture from flue gas. *Energy Conversion and Management* 49, 2 (2008): 346-356.

Zhang, Jun, Penny Xiao, Gang Li, and Paul A. Webley. Effect of flue gas impurities on CO2 capture performance from flue gas at coal-fired power stations by vacuum swing adsorption. *Energy Procedia* 1, 1 (2009): 1115-1122.

Zhang, Jun, Ranjeet Singh, and Paul A. Webley. Alkali and alkaline-earth cation exchanged chabazite zeolites for adsorption based CO2 capture. *Microporous and Mesoporous Materials* 111, 1-3 (2008): 478-487.

Zhang, Zhijuan, Yonggang Zhao, Qihan Gong, Zhong Li, and Jing Li. MOFs for CO2 capture and separation from flue gas mixtures: the effect of multifunctional sites on their adsorption capacity and selectivity. *Chem. Commun.* 49, 7 (2012): 653-661.

Zhao, Xuebo, Bo Xiao, Ashleigh J. Fletcher, K. Mark Thomas, Darren Bradshaw, and Matthew J. Rosseinsky. Hysteretic Adsorption and Desorption of Hydrogen by Nanoporous Metal-Organic Frameworks. *Science* 306, 5698 (2004): 1012-1015.

Zheng, Baishu, Junfeng Bai, Jingui Duan, Lukasz Wojtas, and Michael J. Zaworotko. Enhanced CO2 Binding Affinity of a High-Uptake rht-Type Metal-Organic Framework Decorated with Acylamide Groups. *J. Am. Chem. Soc.* 133, 4 (2011): 748-751.

Zhou, Chenggang, Lujie Cao, Shihao Wei, Qiuju Zhang, and Liang Chen. A first principles study of gas adsorption on charged CuBTC. *Computational and Theoretical Chemistry* 976, 1-3 (2011): 153-160.

A

REMOVAL OF POLLUTANTS (IBUPROFEN) IN WATER BY ADSORPTION IN ACTIVATED CARBONS

Molecular simulations have been performed in order to understand, at the molecular level, the interaction between the pollutants and the activated carbon. Models and methods, as well as the most relevant results are detailed below, related to the simulation of ibuprofen dissolved in water at the presence of different activated carbons.

A.1. Introduction

The presence of emerging contaminants in water has become a serious concern. Typical water treatment facilities are not designed to remove pharmaceuticals from drinking water. These drugs, both prescription and over-the-counter, can end up in water supplies. There are many concerns that this is a result of flushing drugs, but many drugs are not completely metabolized by the body, and enter the environment after passing through wastewater treatment facilities [FDA, 2011]. The effluents from such treatment facilities are discharged into bodies of water that can end up in water supplies, from which drinking water is taken.

Removing ibuprofen from water is an important issue to address through research and the development of effective technologies for removal. Ibuprofen is a nonsteroidal anti-inflammatory drug (NSAID). The drug's wide usage is why it is being found in waterways. Despite current research in ibuprofen removal, little has been done to look at the effectiveness of adsorption methods.

The purpose of this work was to investigate, by molecular simulations, the use of different activated carbon materials to adsorb ibuprofen contented in drinking water, in order to reach a better understanding towards the adsorption process. Materials included carbon sheets and carbon nanotubes of different diameters.

These structures were first optimized by an energy minimization method, and afterwards the most stable configuration of ibuprofen (IBP) were found for each surface with and without water traces, leading to a final study of the adsorption capacities at different compositions of IBP.

A.2. Structures and models

Ibuprofen molecule

With a molecular mass of 206.3 g/mol, IBP contains a chiral carbon in the propionic acid chain which generates two enantiomers of the molecule, being the S-enantiomer of the analgesic and anti-inflammatory activity (the R is inert). With this in mind, the most stable form of the active molecule can be obtained from an energy minimization [Vueba et al., 2008]. The structure is shown in Figure A.1.

$C_{13}H_{18}O_2$

10 Å
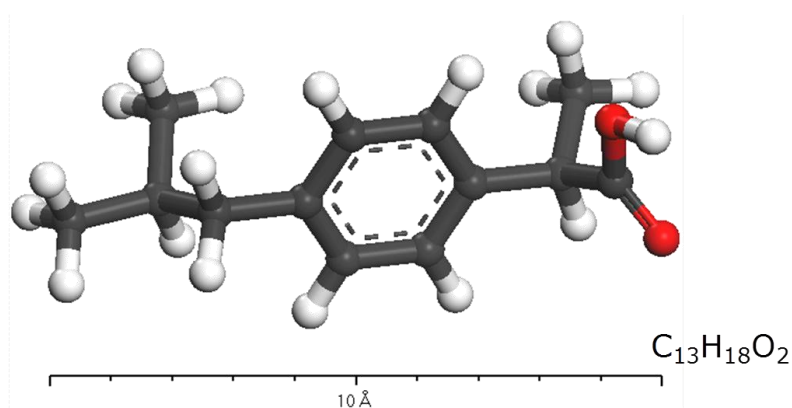
Figure A.1. Ibuprofen structure (gray: carbon; white: hydrogen; red: oxygen).

Activated carbons

The arrangement and shape of the activated carbon, the defective crystals which may contain, the capacity and other properties vary according to how the starting material is transformed into graphite by the heat treatment used. Currently, the shape and the microstructure of porous carbons cannot be determined from experiments, since it is very complex. Therefore, a suitable model for the internal structure of carbon for predicting the properties of adsorption and diffusion is required [Jain et al., 2005; Striolo et al., 2006].

A morphological model presents rigid aromatic sp2 carbon plates randomly located in a three-dimensional simulation cubic cell [Lastokie and Gubbins, 1997]. A typical carbon plate has the structure shown in Figure A.2, and for this case, the plates are roughly aligned but with variations in their inclination angles. Additionally, some carbon atoms have been "lost" to create imperfections on the surface.

50 Å
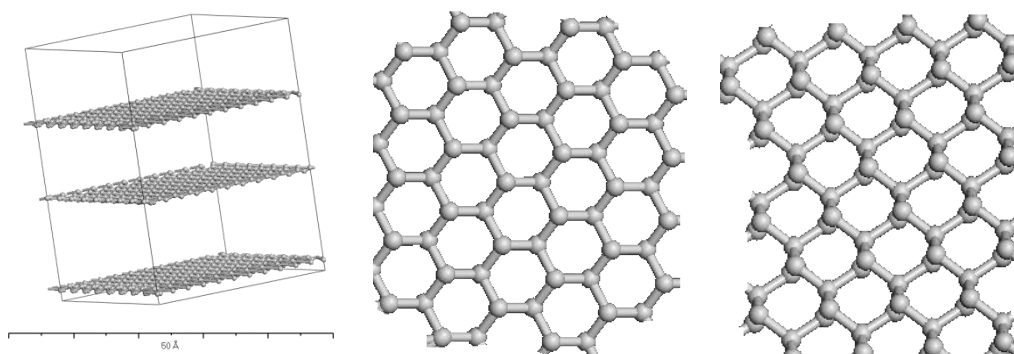
Figure A.2. Schematic representation of the interconnected carbon pore model.

Here we have used a model consisting of three layers of graphitic carbon, comparing the rhombohedral and hexagonal structures (see center and right images in Figure A.2), with a layer separation of 15Å. The dimensions of the simulation box were 27 x 20 x 40 Å. The unit cell was simulated with periodic boundary conditions in all three axes for an effectively infinite plate in these directions, allowing represent what happens at the macroscopic level in these materials.

A.3. Simulation details

An energy minimization of structures was made in order to calculate the adsorption properties, by using the commercial software Materials Studio® [*Accelrys M.S.*, 2013].

Models and force fields used for molecules and structures were taken from the literature. Once the structures were optimized in terms of the minimum energy, they were simulated rigid, based on the Universal Force Field (UFF) [Rappé et al., 1992]. Each carbon atom in the structure was simulated as a Lennard-Jones sphere. The behavior of water molecules was modeled by TIP4P/2005 [Abascal and Vega, 2005] model, as shown in Chapters 5 and 6..

The ibuprofen-ibuprofen and ibuprofen-structure interactions were calculated from the parameters of Lennard-Jones + Coulomb potential with mixing rules Lorentz-Berthelot for cross-terms (see Table A.1); LJ interactions beyond 12.5 Å were obviated, to be far-reaching. The coulombic interactions were calculated by partial charges on the atoms while electrostatic interactions were calculated by the Ewald summation method. The GCMC simulations consisted in 10^6 Monte Carlo cycles for phase equilibration and 10^6 additional production cycles to calculate the equilibrium properties. To balance the system and for an efficient production, the following MC movements were used for both water and ibuprofen molecules: translation, rotation, insertion, removal and reinsertion.

Table A.1. *Lennard-Jones and Coulomb interaction parameters for ibuprofen and water.*

Atom	ε/k_B (K)	σ (Å)	Charge (e-)
C_ring (C)	74.5	3.617	-0.2220
C_ring (CH)	74.5	3.617	-0.0420
C_CH$_1$ (quiral)	19.6	3.875	-0.3420
C_CH$_2$_ib	19.6	3.875	-0.4710

Atom	ε/k_B (K)	σ (Å)	Charge (e⁻)
C_CH₃_ib	19.6	3.875	-0.6730
C_COOH	90.6	3.617	0.7550
O_COOH	114.7	2.859	-0.6180
H_CH	19.1	2.449	0.2400
H_OH	0	0	0.5430
H_water	--	--	-1.1128
O_water	106.1	3.554	+0.5564 *

Charge at the center of mass, slightly offset from the oxygen atom.

*** O-H distance: 0.957 Å, H-O-H angle: 104.52º.*

Positioning of lower energy

In this study we have evaluated different types of carbon plates surfaces (surfaces C (1 1 1) and C (-1 0 0)), and in addition, calculations were made using carbon nanotubes -SWNT by the acronym *Single Wall Nano Tubes*- to determine the relationship between the diameter and the adsorption uptake obtained (SWNT of 7.5 Å and 15 Å were evaluated).

Figure A.3 presents some of the tested molecules to isolated IBP (not including water in the mixture) configurations, with the drug molecule with less energy locked in the green circle. It can be seen that the most stable configuration in carbon sheets is related to the quiral carbon close to the surface, while for the carbon nanotubes a higher energy is obtained when the molecule is inside the cavity.

Furthermore, the potential energy of a molecule within a material is related with the isosteric heat which is often considered as an indication of the heterogeneity of the adsorbent, due that is more sensitive to microstructure than the same adsorption isotherm. This energy can be divided into individual components, such as the chemical affinity of the activated carbon for the molecules, and the adsorbate-adsorbate interactions, among others components.

The isosteric heats obtained for the C(1 1 1), C (-1 0 0), SWNT (7.5 Å) and SWNT (15 Å) surfaces were, respectively, 46, 35, 33 and 31 kJ/mol.
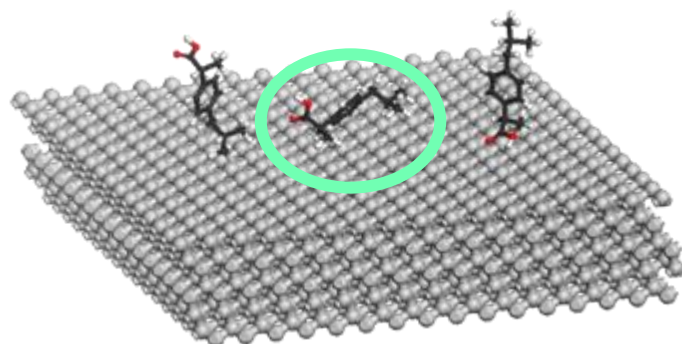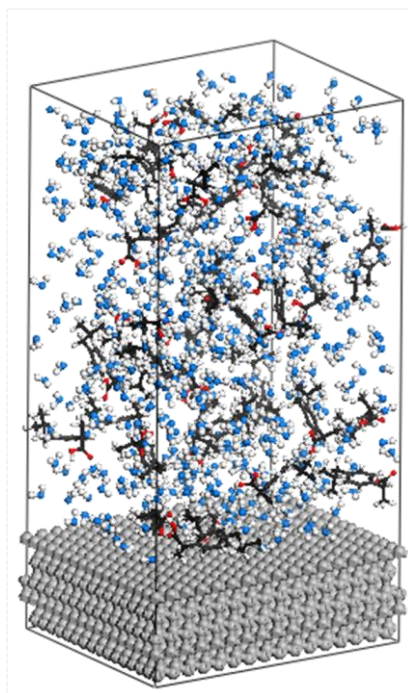
C(1 1 1) surface
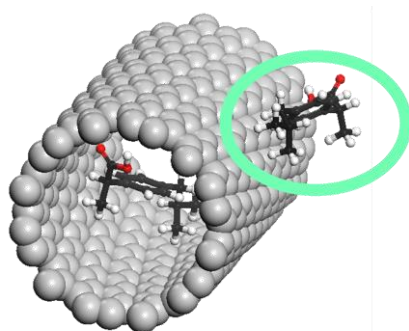
Carbon nanotube, 15Å diameter

Figure A.3. lower energy position of an IBP adsorbed on a porous carbon material (excluding water).

After delving into the IBP-activated carbon interaction, the energy change by the presence of water was studied. The aim was to deepen the system behavior to improve the efficiency of water treatment with activated carbon to remove the ibuprofen molecule by adsorption. Figure A.4 shows a typical configuration for a mixture of 1000 ppm of ibuprofen dissolved in water, and its interaction with a C (1 1 1) surface. A high concentration was chosen in order to obtain representative amount of IBP molecules inside the simulation box.

Figure A.4. *Representation of the equilibrium position of water molecules (in blue) and ibuprofen on a C (1 1 1) carbon surface obtained by CMCG simulations [IBP concentration: 1000ppm]*

A.4. Results of molecular adsorption simulations

The selective adsorption of the activated carbon for ibuprofen as a function of water was calculated in liquid phase (a liquid phase in the context of this work relates to aqueous IBP solutions). Complete adsorption isotherms were not performed, but different molar fractions of solute/solvent were evaluated, between 0.01 and 10%wt (10 ppm - 10,000ppm) under ambient conditions, since this is the range of interest for experimental measurements. The fugacity of the gas phase needed for the simulations was calculated from the saturated vapor pressures of the components and the activity coefficients in the liquid phase.

Table A.2 shows the summary of the results obtained by adsorption evaluated at different scenarios. Figures A.5 and A.6 represent visually the adsorption of ibuprofen in an aqueous mixture of 10 ppm, as a representative example of the study, both for flat surfaces as for carbon nanotubes.

It should be noted that the capacities of all structures are very similar for the different concentrations tested, confirming that the activated carbon is highly selective for ibuprofen. In general, the molar composition in the different materials was in the

range of 30% IBP/70% H_2O, and even at low concentrations, the activated carbon is capable of removing traces of the drug that can lead water wastes after the primary and secondary treatments.

Table A.2. Adsorption Capacity of different structures, as a function of the amount of ibuprofen in the initial aqueous mixture and of the material structure.

Uptake (molecules/unit cell)	10 ppm	100 ppm	1,000 ppm	10,000 Ppm	Pure components
C(1 1 1)	10.8	11.9	13.7	19.2	20.4 (IBP) 140.6 (H_2O)
C(-1 0 0)	13.0	13.2	15.8	18.2	21.1 (IBP) 120.1 (H_2O)
SWNT 7.5Å	11.1	---	13.9	18.7	19.0 (IBP) 12.2 (H_2O)
SWNT 15Å*	22.3	---	27.8	34.9	37.4 (IBP) 61.3 (H_2O)

* This unit cell contains 380 carbon atoms, while the other structures are in the range of 700 to 750 carbon atoms.

(C -1 0 0)   C (1 1 1)
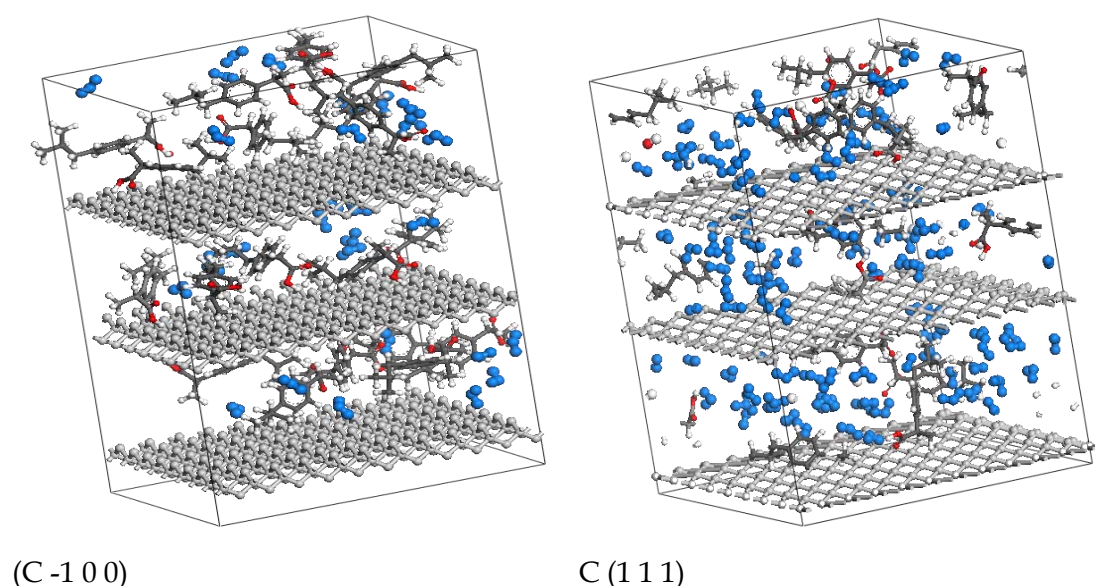
Figure A.5. Adsorption of Ibuprofen in a microporous carbon from an aqueous mixture of 10ppm.

SWNT (15Å)   SWNT(7.5Å)
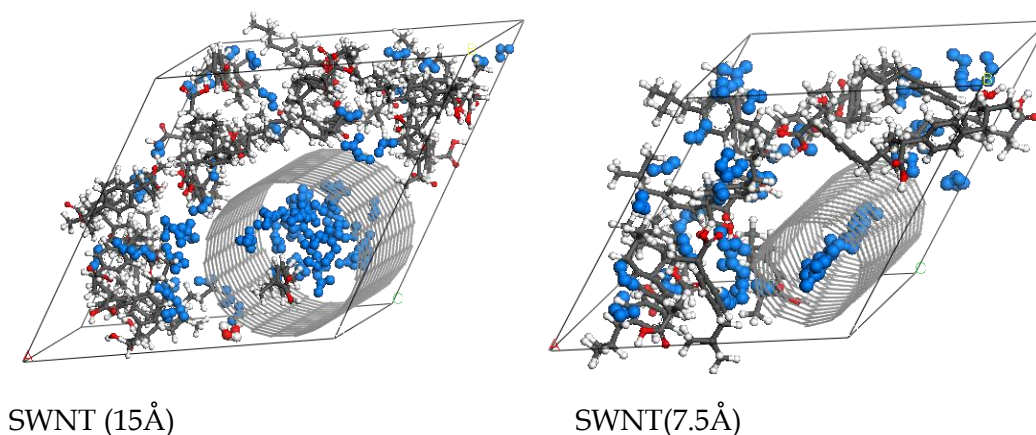
Figure A.6. Adsorption in SWNTs from an aqueous solution of 10 ppm IBP.

Finally, an interest feature was observed in SWNT: the ibuprofen molecules are not capable of adsorbing within the smaller carbon nanotube (diameter of 7.5Å); at the molecular level it can be seen that this is due mainly to the very narrow pore structure: it does not allow free movement of the IBP molecules inside the cavity and the water molecules (smaller) inside the nanotube displace the pharmaceutical molecule. Therefore, this fact must be taken into account for application in the process of treating water contaminated with ibuprofen.

A.5. Conclusions

Molecular simulations have been carried out in order to understand, at the molecular level, the interaction between ibuprofen -content in a stream of water- and activated carbon. For this, molecular simulation methods were used allowing the calculation of adsorption and configurations of the liquid phase at low contaminant concentrations, ranging from 10 to 10000 ppm.

Different structures for the carbonaceous adsorbent have been evaluated, including sp2 flat plates morphological models and carbon nanotubes, to determine the relationship between the diameter of the material and the adsorption obtained. The results show that the capacities of all structures are very similar to each other for the different concentrations tested, confirming that the activated carbon is highly selective for ibuprofen.

A.6. References

Abascal, J. L. F.; Vega, C. A general purpose model for the condensed phases of water: TIP4P/2005, *Journal of Chemical Physics*, **2005**, 123 234505.

Jain, S.K.; Pikunic, J.P.; Pellenq, R.J.M.; Gubbins, K.E. Effects of Activation on the Structure and Adsorption Properties of a Nanoporous Carbon Using Molecular Simulation. *Adsorption*, **2005**, 11, 355–360.

Lastoskie. C.M.; Gubbins, K.E. Characterization of porous materials using molecular theory and simulation. Book chapter (Molecular Modeling and Theory in Chemical Engineering).

Striolo, A.; Chialvo, A.A.; Cummings, P.T.; Gubbins, K.E. Simulated water adsorption in chemically heterogeneous carbon nanotubes. *The Journal of Chemical Physics*, **2006**, 124.

Vueba, M.L.; Pina, M.E.; Batista de Carvalho, L.A.E. Conformational Stability of Ibuprofen: Assessed by DFT Calculations and Optical Vibrational Spectroscopy. *Journal of Pharmaceutical Sciences*, **2008**, 97 (2).

Curriculum Vitae

Daniel Bahamón García was born in Medellín, Colombia in 1987. He received his B.Sc. in Chemical Engineering from the Universidad Pontificia Bolivariana in 2009 and his M.Sc. in Engineering in 2012 from the same university. In 2012, he was admitted to the Ph.D. program at the Universitat Autònoma de Barcelona and joined Dr. Lourdes Vega's Molecular Simulation research group in MATGAS 2000 AIE. His research interests are mainly focused on the rational development of energy/environmental processes by optimization with simulation tools. During the time as PhD student, he has coauthored 3 publications in peer-review journals (with some more under final writing) and also contributed with oral presentations at regional, national and international conferences.

He has been involved in several European and Spanish funded projects such as SOFCOM and BioQuim_Rescue, as well as some industrial projects. He is amember of the Xarxa de Referencia en Quimica Teòrica I Computationnal (XRQTC) and of the MOLSIMAP group, recognized as a Group of Excellence by the Generaolitat of Catalonia, 2014SGR-1582).

List of publications

Referred journal papers

[1] D. Bahamón and L. F. Vega, Systematic evaluation of materials for post-combustion CO2 capture in a Temperature Swing Adsorption process, Chemical Engineering Journal, 2015. doi:10.1016/j.cej.2015.08.098

[2] D. Bahamon, A. Díaz-Márquez, P. Gamallo and L. F. Vega, Effect of water and coexisting impurities on the adsorption of CO_2 in CuBTC and zeolite 13X, Separation and Purification Technology Journal, Submitted 2015.

[3] P. Gamallo, A. D. Márquez, D. Bahamon and L. F. Vega, Grand canonical Monte Carlo simulations of water adsorption on kaolinite, Langmuir, Submitted 2015.

[4] D. Bahamon, L. Carro, S. Guri, L.F. Vega, Removal of ibuprofen in water by activated carbons – a molecular simulation insight, to be submitted to International Journal of Environmental Science and Technology, 2015.

[5] D. Bahamon, L.F. Vega, Propective materials for CO_2 capture in a post-combustion process: a review on recent advances and opportunities, to be submitted to Energy, 2015.

Conference contributions

S. Builes, D. Bahamón and L. F. Vega, Modeling novel adsorbent materials for gas separation and CO_2 capture, In XRQTC, Poster contribution, Barcelona (Spain), May 13th, 2013.

A. García-Sánchez; F. Llovell; D. Bahamón; O. Vilaseca; R. M. Marcos; L. F. Vega , A combined approach for the modelling of thermophysical properties: molecular simulations and soft-SAFT. Oral Contribution. In XXIX Annual Meeting of Theoretical and Computational Chemistry, Barcelona (Spain), July 10–11th, 2013.

D. Bahamón and L. F. Vega, Modeling Novel Adsorbent Materials For Application In Carbon Dioxide Separation, In FLUCOMP, Poster contribution, Barcelona (Spain), June 12-13th, 2014.

D. Bahamón and L.F. Vega. Evaluation of materials for application in CO_2 capture. Workshop Aportando Valor al CO_2, organized by The Spanish Technological Platform for CO_2 (PTECO2) and the Spanish Technological Platform for Sustainable Chemistry (SusChem). Madrid (Spain). February 17-18th, 2015.

A. Díaz-Márquez, P. Gamallo, D. Bahamón and L. F. Vega. Influence of impurities in CO_2 capture over a zeolitic material. Workshop Aportando Valor al CO_2, organized by The Spanish Technological Platform for CO_2 (PTECO2) and the Spanish Technological Platform for Sustainable Chemistry (SusChem). Madrid (Spain). February 17-18th, 2015.

D. Bahamón, A. Díaz-Márquez, P. Gamallo and L. F. Vega, Effect of water and coexisting impurities on the adsorption of CO_2 in CuBTC and zeolite 13X, In XRQTC Workshop 2015, Poster contribution, Girona (Spain), June 25-26th, 2015.

D. Bahamón and L. F. Vega, Comparison between different materials for CO_2 capture in a post-combustion stream, In EQUIFASE, Oral contribution, Alicante (Spain), June 28- July 01, 2015.

D. Bahamón, A. Díaz-Márquez, P. Gamallo and L. F. Vega, CO_2 separation from multi-component mixtures by adsorption in MOF CuBTC and zeolite 13X , In RICI-6, Oral contribution, Guimaräes (Portugal), July 08-10th, 2015.